Hydroxyl in mantle minerals

Thesis by

David Ronald Bell

In partial fulfillment of the requirements

for the degree of

Doctor of Philosophy

California Institute of Technology
Pasadena, California.

1993

(submitted November 17, 1992)

Acknowledgments

The scientific ideas and philosophical approach expressed in this thesis result from interactions with many people, whose educational influence has been profound and will always be deeply appreciated.

George Rossman, my thesis advisor, has been a constant source of enthusiasm, encouragement, and active support. The independent style of research he has encouraged combined with an ever-ready willingness to discuss and help with technical or scientific problems have made graduate work a pleasure. It has been a privilege to witness and benefit from his example as a scientist, teacher and human being.

The 3rd floor of the Arms Laboratory provided a unique growth environment, in which valuable discussions on matters of hydrogen took place with Michael Baker, John Beckett, Jennifer Blank, Michael Carroll, Huw Davies, Jackie Dixon, Andy Gaynor, Phil Ihinger, Glen Mattioli, Greg Miller, Oded Navon, Sally Newman, Henrik Skogby, John Stone, Dimitri Vlassopoulos and Laurie Watson. Interactions with Joel Blum, Cheryl Brigham, Laurinda Chamberlin, Diane Clemens Knott, Pat Dobson, Yigal Erel, Charlie Rubin, Jack Sheng, Stephen Wickham and Michael Wolf have been a pleasure and an education. That mensch Phil Ihinger shared his technical knowledge of the cold-seal and H-isotope laboratories and his boundless enthusiasm and curiosity.

For other technical instruction I am indebted to John Armstrong, John Beckett, Paul Carpenter, Dana Johnston, Allen Kennedy, Glen Mattioli and, especially, George Rossman. I would like to thank Professors Epstein, Stolper, Wyllie and Wasserburg for access to the facilities in their laboratories. Collaborations with Henrik Skogby (Uppsala University), Joe Smyth (University of Colorado), Denis Endisch and Friedel Rauch (University of Frankfurt) and Charles Geiger (Technical University of Berlin, University of Kiel) have been stimulating and productive.

Formal and informal discussions with T. J. Ahrens, D. L. Anderson, J. T. Armstrong, C. R. Bacon, J. R. Holloway, G. R. Rossman, R. P. Sharp, L. T. Silver, E. M. Stolper, H. P. Taylor Jr., G. J. Wasserburg and P. J. Wyllie have been an important component of my education, reflected in this thesis. My academic advisor and scientific conscience, Ed Stolper, has been a philosophical beacon throughout this endeavor. His surgical dissections and personal interest have been formative and invaluable. No-one has influenced my scientific thinking more.

Material support during my tenure as a student was provided by G. R. Rossman, H. P. Taylor, Jr. and P. J. Wyllie, to whom I am most grateful. Additional fellowships from the Harry Crossley Foundation, the American Federation of Mineralogical Societies and the F. Beach Leighton Foundation are gratefully acknowledged. Roger Clement, John Bristow, Jock Robey and Mike Skinner of the Anglo American Corporation of S. A. (Ltd) maintained a $\frac{p}{m}$aternal interest, providing critical support at the right time. I appreciate their freedom with samples and access to xenolith-rich real estate. George Read was a soul-mate in the field and a Trojan in the post-office. Wys my die lang pad weg van die skare...

At the University of Cape Town, John Gurney first introduced me to mantle rocks, and has been a generous supplier of important samples and source of encouragement in this study. Rory Moore shared his samples, unpublished data and interpretations selflessly. Our friendship, discussions about and trips to the Monastery Mine have been important.

The Division staff, especially Dorothy Coy McDougall, Fran Barnard, Jean Grinols and Priscilla Piano, created a new home for me which will be difficult to leave. Jim O'Donnell and Pat Kelly were ever helpful and maintained an excellent lab. Vicky Gray kept it all in order and was always unbelievably cheerful way too early in the morning.

Throughout this time I have enjoyed the love, support and interest of my parents, who got me into earth science some twenty-five years ago, and who've seen it through.

Above all I thank Kathy who gave up so much of her life for mine.

Abstract.

This thesis is an investigation of the infrared spectroscopic characteristics, abundance, stability and partitioning behavior of hydroxyl (OH) in minerals from the Earth's upper mantle. Using manometric and nuclear reaction analysis techniques to calibrate intensities of OH bands in the mineral IR spectra, the following ranges in OH concentration (expressed as ppm H_2O by weight) were determined for natural samples: clinopyroxene 150 - 1080; orthopyroxene 50 - 460; olivine <1 - 245; garnet < 0.1 - 330; kyanite 55 - 222; zircon 28 - 74.

Systematics of OH distribution in garnets from various mantle rock types indicate a connection with petrogenetic environment, illustrating qualitative use of OH as an indicator of the activity of hydrous components (e.g., water) in the mantle. Applications to specific mantle assemblages are discussed. Heterogeneous distribution of H in the mantle on local and regional scales is indicated.

Trace structural OH in mantle rocks ranges from 30 to 600 ppm H_2O in samples examined, implying that nominally anhydrous minerals in peridotite could store all the water (about 100 - 200 ppm) in the depleted upper mantle (MORB source). These minerals also provide a mechanism to recycle water into the mantle in subduction zones.

Partitioning behavior of H was investigated in a suite of co-magmatic kimberlite megacryst minerals. Fugacities of water calculated from OH in olivine are compatible with mantle conditions and yield an estimate of ~1 wt.% H_2O in the parental megacryst magma. OH concentrations in garnet, pyroxenes and olivine are influenced by water activity, crystal chemistry (particularly Ti substitution) and possibly temperature, resulting in substantial variations in inter-mineral D_{H_2O} involving garnet, but relatively constant D_{H_2O} among pyroxenes and olivine and illustrating the complications of quantitative hydrobarometry in nature.

Experiments on the thermal stability of OH in garnet and other minerals were conducted at atmospheric, crustal and mantle pressures. These demonstrate slow equilibration of OH in synthetic pyrope. Rapid mobility of H, redox processes and necessity for structural changes in the host crystal are important factors in determining the behavior of H in natural mineral systems.

Relatively deuterium-depleted isotopic compositions are indicated for this form of H.

Table of Contents:

Introduction.

It has been a relatively recent discovery that hydrogen is incorporated in trace amounts in the crystal structure of most terrestrial minerals, where it is bound as hydroxyl, OH. The hydrous component has attracted attention, because of the changes in physical behavior which it induces, or might be thought to induce, in the host mineral, in a manner analogous to the well studied and geologically important effects of hydrous components in magmas. It was realized at an early stage in these studies that OH in nominally anhydrous minerals might have important geochemical consequences for the distribution of hydrogen (commonly referred to as "water") in rocky planetary interiors and that measurements of the OH contents of minerals might be used to place constraints on conditions of their formation, with respect to the role of hydrous volatiles (Fyfe 1970; Martin and Donnay 1972). This thesis is concerned with these geochemical and petrological consequences.

Systematic surveys of OH in specific minerals (Aines and Rossman 1984a,b; Beran and Götzinger 1987; Miller *et al.* 1987) revealed that samples of these minerals derived from the upper mantle often contained relatively high OH concentrations. Because of this observation and the fact that vastly more H-rich phases (hydrous minerals and liquid water) are known to dominate the crustal reservoir of H, structurally-bound trace OH is likely to play a more important role in the geochemistry of H in the mantle than in the crust. The potential value of nominally anhydrous, but trace OH-bearing minerals as probes into the petrogenetic role of hydrous volatiles is similarly enhanced for the mantle regime because of the lack of alternatives; few hydrous minerals are stable to dehydration at typical subsolidus mantle temperatures, and none are known to be stable at the liquidi of water-poor mantle melts. This study was undertaken to investigate the role of OH-bearing, nominally anhydrous minerals as reservoirs of H in the Earth's mantle, to examine their

potential use as petrogenetic indicators in certain mantle settings and to elucidate selected aspects of the geochemical principles governing H incorporation in these phases.

The study was designed to proceed in three parallel efforts: (i) a systematic and wide-ranging analysis of the OH content of mantle-derived materials of known petrologic setting in order to establish a representative sample of the range in OH concentrations, to describe inter-mineral partitioning of H, and to demonstrate, where applicable, the use of these minerals as petrogenetic indicators, (ii) the development of the quantitative analytical techniques necessary for the accurate analysis of OH in mantle minerals and (iii) experimental studies aimed at understanding some of the factors which dictate the behavior of H in these minerals and which impact their applicability in solving geochemical and petrologic problems.

Chapter 1 reports the results of a survey of the OH contents of a large sample of garnets from the upper mantle beneath southern Africa. The receptivity of the garnet structure to a variety of cation substitutions makes it a powerful indicator of host rock paragenesis. Garnet has been previously well studied from the perspective of hydrogarnet and a study of mantle garnets had revealed interesting variations in OH content from samples of different geographic origins (Aines and Rossman 1984b). The principle aims of the research reported in Chapter 1 were to define the OH spectroscopic characteristics and the range of OH concentrations encountered, with particular attention to how these observables were linked to the petrologic character and geologic history of the sample, as far as the latter could be determined. An effort was made in this study to select samples which had been previously characterized, or were representative of xenolith suites which had been previously studied petrologically. This chapter was published, in coauthorship with Gr. R.

Rossman as an article in *Contributions to Mineralogy and Petrology*, and is reproduced here without change.

Chapter 2 presents an overview of the abundance of OH in mantle minerals and discusses the implications of these observations for the geochemistry of H in the mantle. This chapter includes data from a literature survey in addition to new analyses of OH in garnet, pyroxenes, olivine, kyanite and zircon. The chapter was published, in co-authorship with G. R. Rossman, as a general article in *Science*, and is reproduced without alteration.

Chapter 3 is a detailed study of the OH, major and trace element contents of garnet, olivine, orthopyroxene, clinopyroxene and zircon samples from a single petrological association, namely the megacryst suite of minerals from the Monastery kimberlite, South Africa. This is an extensively studied suite, for which a generally accepted petrologic model exists. This provides a well-defined context in which to examine the partitioning of OH between minerals thought to be in chemical equilibrium with one another, and to examine the way in which OH behaves in minerals in high-pressure igneous processes. It also offers the opportunity to examine the case for preservation of source OH concentrations in these minerals and provides a counterpoint in the natural system to laboratory studies aiming to describe behavior of OH in nominally anhydrous minerals. This chapter has been the result of a collaboration with Dr. R. O. Moore, from whose collection and mineral analyses the appropriate samples were selected. The four ion microprobe analyses reported were done with, but mostly by, Allen Kennedy.

The above three chapters constitute much of the work done under activity (i) above. Additional published results from this work are presented in the appendices. Other work conducted under this banner, but reported here in the form of data tables only, consisted of

a systematic study of the OH and trace element content of kyanite (mantle data reported) and a suite of garnets from Garnet Ridge, Arizona.

Chapter 4 documents the results of a calibration study aimed at refining the quantitative analysis of OH in minerals by IR spectroscopy. It represents one of several efforts in this area by the Rossman "group," another being our collaboration with D. Endisch and F. Rauch in Frankfurt on nuclear reaction analysis of H in a more extensive suite of mantle minerals, including the samples analyzed in Chapter 4. Analysis of the small amounts of OH in nominally anhydrous minerals is problematic because of severe H contamination. In this chapter I describe the analysis of H in spectroscopically characterized samples of augitic clinopyroxene, enstatite and pyrope garnet by manometry after extraction by heating highly pure mineral separates under vacuum. The extraction of H was done together with P. D. Ihinger who provided instruction in use of the line, and in reality performed many of the critical steps in the measurements, as well as the mass spectrometric measurements reported in Appendix 1. It is intended that this chapter will be submitted for publication to the *American Mineralogist,* in co-authorship with Ihinger, G. R. Rossman and S. Epstein.

Chapter 5 is a summary of the experiments that were conducted on natural mantle minerals and synthetic pyrope compositions in order to understand aspects of the behavior of the hydrous components in these phases. These include simple heating experiments at atmospheric pressure, hydrothermal treatment in rapid-quench cold seal apparatus and piston cylinder syntheses of OH-bearing pyrope. Aspects of this work were published together with the results of a study by C. A. Geiger and co-workers in the *American Mineralogist* (Appendix 5), as described in the introduction to this chapter.

Chapter 6 is an overview of some of the broader principles and concerns emerging from the study, and reviews the geochemical importance of trace OH in mantle minerals.

Appendix 1 is a study with P. D. Ihinger on the isotopic composition of H measured after the extraction from nominally anhydrous minerals described in Chapter 4. Appendix 2 is a commentary on the issue of OH in mantle minerals which was published in *Nature*. Appendices 3-5 are published papers resulting from collaborations with other individuals which arose directly out of the work reported in the thesis. Appendices 6-9 are published meeting abstracts and Appendix 10 consists of additional data. All writing, with the exception of appendices 3-5, is the work of the author. Analytical work performed by others is indicated above and in the text.

References

Aines, R.D. and Rossman, G. R. 1984a. The hydrous component in garnets: Pyralspites. *Amer Mineral* **69,** 1116-1126.

Aines, R.D. and Rossman, G. R. 1984b. Water content of mantle garnets. *Geology* **12,** 720-723.

Beran, A. and Götzinger, M. A. 1987. The quantitative IR spectroscopic determination of structural OH groups in kyanites. *Mineral. Petrol.* **36,** 41-49.

Fyfe, W. S. 1970 Lattice energies, phase transformations and volatiles in the mantle. *Phys. Earth planet. Int.* **3**, 196-200.

Martin R. F and Donnay, G. 1972. Hydroxyl in the mantle. *Amer. Mineral*. **57**, 554-570

Miller, G. H., Rossman, G. R. & Harlow, G. E. 1987. The natural occurrence of hydroxide in olivine. *Phys. Chem. Minerals* **14,** 461-472.

Chapter 1. The distribution of hydroxyl in garnets from the subcontinental mantle of southern Africa.

Abstract

166 garnets of dominantly mantle origin were analyzed for OH content by infrared (IR) spectroscopy. IR spectra in the 3400 - 3700 cm^{-1} region display consistent absorption patterns attributable to OH structurally bound within the garnet crystal, occasionally contaminated by low intensity OH absorptions from microscopic inclusions. The principal structural OH absorption occurs near 3570 cm^{-1}, with the appearance of additional absorptions near 3512 cm^{-1} and 3650 cm^{-1} dependent on garnet composition or paragenesis. Samples derive from a wide variety of rock types occurring as xenoliths in kimberlites of southern Africa. OH abundances, using the best currently available calibration, range from less than 1 up to 135 ppm H_2O, and increase in the general order as follows : on-craton eclogites < coarse-granular peridotites < Ti-rich deformed peridotites < some off-craton eclogites < Cr-poor megacrysts. OH abundances in garnet are closely linked to host rock paragenesis and cannot be explained purely by any crystal chemical factors which we have investigated. Cr-poor garnet megacryst nodules display striking inverse correlations between OH contents and Mg/(Mg+Fe) ratios, which we interpret to reflect the progressively increasing water content of the differentiating parental megacryst magmas. OH abundances in garnet megacrysts decrease in the host rock order Group 2 (micaceous) kimberlite > Group 1 (basaltic) kimberlite > alnöite > alkali basalt. The OH contents of common lithospheric garnets from coarse peridotites, including several phlogopite-bearing samples are typically less than 20 ppm H_2O, for tectonic settings of kimberlites both on and off the Archaean Kaapvaal craton. Ti-rich garnets from deformed peridotites are richer in OH, supporting previous suggestions of associaton of these xenoliths with putative megacryst magmas. Subcalcic Cr-rich xenocrysts, diamond inclusion garnets and garnets from diamondiferous eclogites have very low OH contents,

similar to eclogites and depleted peridotites without macroscopic diamonds. The OH content of southern African peridotite and eclogite garnets are significantly lower on average than those previously examined from the Colorado Plateau diatremes. While details of emplacement-related H mobility in garnets remain to be established, our results suggest that garnets record useful information on the role of water or other hydrous volatile species in petrological processes at their source regions in the mantle. Although garnets do not appear to constitute a large reservoir of mantle hydrogen, the large stability range of OH-bearing garnet in the crust and mantle implies wide applicability as a qualitative hydrobarometer.

Introduction

In recent years, numerous studies have demonstrated that many nominally anhydrous minerals incorporate limited amounts of structurally-bound hydroxyl. Such OH has been observed in variable concentrations in compositionally diverse natural garnets that are conventionally regarded as anhydrous (Wilkins and Sabine 1973, Aines and Rossman 1984a). Aines and Rossman (1984a,b) found that OH-bearing garnets occur in a variety of geological environments, including the Earth's upper mantle. These observations lent some support to earlier speculation by Fyfe (1970), later revived by Ackermann et al. (1983), that OH-bearing garnet might be a significant reservoir of hydrogen in the Earth's mantle.

While Aines and Rossman (1984a) were unable to identify the specific location of OH within the garnet crystal structure, they did note that the data were consistent with OH incorporation via the hydrogarnet substitution. This mechanism, in which four OH^- groups, linked in a tetrahedral configuration, are substituted for an SiO_4^{4-} group, is operative in natural hydrogrossular garnets, which form a complete solid-solution series from grossular ($Ca_3Al_2[SiO_4]_3$) to katoite, ($Ca_3Al_2[H_4O_4]_3$). The hydrogarnet substitutional mechanism is also claimed to be responsible for the hydrous component in synthetic OH-bearing pyropes (Ackermann et al. 1983). Although this type of substitution in mantle minerals was supported by the existence of a stable hydrogarnet species in the crustal regime, its viability in the mantle has been questioned on crystal chemical grounds by Martin and Donnay (1972) and Lager et al. (1989). Regardless of conjecture on the precise structural location, the occurrence of OH-bearing pyrope garnets from high pressure natural and synthetic environments is now well established.

Furthermore, it was envisioned by Martin and Donnay (1972) that determination of a crystal / fluid distribution coefficient for OH might allow direct estimation of water activity during the mineral-forming event at depth. Thus several important questions emerge in the study of high pressure hydrous garnets, notably: What is the structure of the hydrous component, what is the abundance of this form of "water" in the mantle and what can be learned from this phenomenon about the role of hydrous volatiles in mantle petrology? Answering the first question is severely hampered by the concentration of hydroxyl in garnets of high pressure origin, which is typically so low as to prevent direct determination of the crystallographic sites where such OH is located. In this paper, we take some initial steps in addressing the issues of abundance and petrological importance of structural OH in garnet from the upper mantle.

Knowledge of the "water" content of the Earth's mantle and its exact chemical form are of particular importance in geochemical, petrological and geophysical studies, since volatile elements are well known for their profound effect on physical and chemical properties of rocks, such as melting relations, rheology, and transport properties. Martin and Donnay (1972) have summarized some estimates of mantle water contents and possible mechanisms of storage. Proposed modes include fluid and melt phases, stoichiometrically hydrous minerals such as amphiboles, micas and various synthetic candidates (see Liu 1987, Finger and Prewitt 1989) and the nominally anhydrous minerals containing OH. The importance of the nominally anhydrous mineral reservoir of water is presently virtually unknown, but of great interest to evaluate, since the petrological and geophysical effects of water in this form are likely to differ significantly from those of a fluid phase. In addition, the stability ranges of these minerals are often quite different from those of the commonly observed hydrous minerals, such as amphiboles and micas.

A previous study on the OH content of natural mantle-derived garnets (Aines and Rossman 1984b) noted a variability in OH concentration, with some indication of a

geographic correlation. Garnet samples studied in that work were often single crystals of unknown paragenesis, and the issue of possible systematic petrological correlations could not be addressed. In this study, we aimed to investigate the petrological aspects of OH in mantle garnets by analysis of samples from well characterized petrological environments within the upper mantle. Our objectives were to document the variability in hydroxyl concentration of mantle garnets from the well-studied kimberlites of southern Africa, and to determine if these variations are linked to factors of petrological importance such as host rock lithology, tectonic setting, crystallization history, pressure, temperature and water activity. More specifically, we wished to investigate whether garnets record information on the concentration and geochemical behaviour of water in their source regions in the upper mantle.

Samples

All our samples, with the exception of four garnet megacrysts, are from xenoliths erupted in kimberlites of southern Africa. This area was chosen for study due to ready sample availability and the large amount of background information in the form of previous detailed studies of kimberlites and their xenolith suites from this region. Where possible, we have examined garnets from previously studied suites or localities. Our collection includes garnets from peridotites and eclogites, garnet megacrysts and xenocrysts, and covers kimberlites which sample mantle material below the Archaean Kaapvaal Craton, as well as those erupted through the surrounding younger Namaqua Province (Hartnady et al. 1985). These are referred to as "on-craton" and "off-craton" tectonic settings respectively. In all cases, we have tried to attain as wide a coverage of regularly encountered mantle lithologies and garnet compositions as possible.

Since this study attempts to focus on the petrological significance of hydroxyl in mantle garnets, it is important that the paragenesis of the garnet samples be unambiguously defined. Many of the most striking features involving OH occur in the so-called "megacrysts," which in the sense used throughout this paper are specifically the chemically distinctive (Fe,Ti-rich and Cr-poor) and often large, monomineralic garnets referred to by Nixon & Boyd (1973b) as discrete nodules and by Eggler et al. (1979) as Cr-poor megacrysts. These megacrysts are believed by the above and many other authors, e.g. Gurney et al. (1979), Schulze (1984), Jones (1987) to be crystallization products of a liquid in the mantle and are a specific subset of the host of diverse garnets that happen to exceed a millimeter or so in diameter, occurring in the heavy-mineral concentrates of kimberlites and related rocks (the sense used by Aines and Rossman 1984b).

Where possible, garnet megacrysts for infrared spectroscopic analysis were selected from large suites, previously analyzed by electron microprobe. This enabled coverage of the entire range of compositions recorded for certain suites. Megacrysts were analyzed from the following kimberlites : Monastery, Kaalvallei, Jagersfontein (on-craton, group I), Lace (also known as Crown), (on-craton, group II) and Koherab (off-craton, group I). Peridotites were analyzed from the Premier and Jagersfontein localities, where large variations in pressure and temperature of origin, generally well correlated with texture and bulk composition, exist (Danchin 1979, Winterburn et al. 1990), and from the off-craton Louwrensia kimberlite, where sheared peridotites also tend to record higher equilibration temperatures (MacGregor 1975, Mitchell 1984). Single garnet xenocryst grains, believed to be peridotite-derived, were analyzed from the Lace kimberlite. These include lilac coloured subcalcic Cr-rich garnets of the type that have been linked to diamond occurrence in the mantle (Gurney 1984).

Eclogites from the classic on-craton Roberts Victor locality were selected to cover as much as possible of the compositional range of this suite. Most of the samples have been

previously studied by Hatton (1978). Eclogites have also been analyzed from the off-craton Rietfontein kimberlite (Gurney et al. 1971, Gurney 1984)) and others of the Karoo Province (Robey 1981). Diamond-bearing eclogitic lithologies from the Lace, Star, Orapa and Kaalvallei kimberlites and a garnet of eclogitic paragenesis, included in diamond, from the Premier kimberlite, were examined. A list of all samples studied, together with paragenesis and compositional information is presented in Table 1. The geographic location of the host kimberlites of our samples, the petrological affinities of the kimberlites, and their relationship to major tectonic boundaries are illustrated in Fig.1.

Methods

Infrared spectroscopy

Garnets were extracted from xenoliths by crushing or sawing and were then handpicked under a low power binocular microscope to select the purest looking grains. For the peridotites and most eclogites, a selection of grains from each xenolith was mounted in acrylic resin or epoxy and doubly polished. Thicknesses varied from ~ 150 μm to 2 mm, depending on sample quality. The polished grains were examined under a binocular microscope, using large area illumination from below, which highlighted imperfections, particularly under crossed polarizers. This examination was used to select volumes of garnet that were free of inclusions or cracks for analysis. A second examination at 100X to 400X magnification in transmitted light using a petrographic microscope was performed as a cross check, or where spectroscopic data suggested the presence of foreign material, such as cracks or inclusions. Intersection of the infrared beam with cracks commonly resulted in

strong absorptions which are, however, often readily distinguishable from the intrinsic garnet OH component.

The absorption spectrum of a clear region of each sample was then recorded for unpolarized light in the interval 11,000 to 1800 cm^{-1} using a Nicolet 60SX Fourier transform infrared spectrophotometer equipped with an InSb detector. A large number (250-2000) of scans were averaged for each analysis point in order to yield the desired signal-to-noise ratio. Resolution for the averaged scans was 2 cm^{-1}. Thickness of the sample was measured with a micrometer gauge and all spectra were normalized to a thickness of one millimeter. Because the OH absorption bands are perched on the tail of a broad absorption due to Fe^{2+} (see Fig. 2), it is necessary to know the form of the baseline in order to calculate the OH absorption intensity. Although the specific baseline varies with the Fe^{2+} content of each sample, the general baseline shape was gauged from the spectra of a selection of naturally anhydrous garnets (e.g., Fig. 2i), and a few originally hydrous samples that were dehydrated by heating in a bench furnace in air. A hand-drawn baseline, matched to the characteristics of the Fe^{2+} absorption of each spectrum, was subtracted and the net integrated absorbance between 3700 cm^{-1} and 3400 cm^{-1} was calculated. This absorbance was related to OH concentration (expressed as ppm H_2O by weight) using the expression (discussed in the calibration section below):

$$\text{ppm } H_2O = 0.7194 \times \text{Integrated absorbance per cm sample thickness.} \quad (1)$$

The detection limit depends on the thickness of the sample, which is dictated by the extent to which the garnet must be thinned down to yield a window for transmission that is free of cracks and contaminating phases. For typical samples (on the order of 0.5 mm thick), detection limit is about 1 ppm H_2O, and is lower for many megacrysts with large gem-quality regions. Homogeneity was checked in a number of (but not all) samples by

analyzing two or more grains from the same xenolith. This practice commonly yielded identical spectra, but occasionally a small degree of heterogeneity was observed, similar to that reported by Aines and Rossman (1984b). Analysis of more than one area of the same garnet grain also typically indicated homogeneity, with occasional exceptions of small magnitude.

Calibration of IR analysis

In principle, infrared spectroscopy is capable of sensitive and accurate quantitative analysis of OH if the relationship between absorption intensity per unit thickness and concentration is known by independent calibration. Because the proportionality constant in this relationship (the molar absorption coefficient, ε) is dependent on composition and structure of the host phase, the calibration should be performed on material as closely allied as possible to the unknown (in this case, pyrope-rich garnet). The low levels of hydroxyl in nominally anhydrous silicates are a continuing obstacle to accurate calibration of the extremely sensitive IR technique by independent methods. Over the years, several estimates for molar absorption coefficient of OH in garnet have been made (e.g., Wilkins and Sabine 1973, Aines and Rossman 1984a, Rossman et al. 1988) and the area is one of current active research.

The pyrope-rich garnets encountered in this study exhibit fairly simple IR spectra between 3500 and 3700 cm^{-1}, usually comprised of one dominant and one or two subordinate absorption bands, although the dominant band is probably a composite one. The band occurring near 3570 cm^{-1} is commonly the most intense. The frequency of this band is relatively constant, although we have observed some minor composition-dependent variation. Skogby and Rossman (1991) showed that the molar absorption coefficient of the

OH stretching vibration in amphibole increases with decreasing frequency of absorption, consistent with the observation of Paterson (1982) for silicate glasses and other materials, and it is therefore possible that garnets with different OH spectra may have varying molar absorption coefficients. However, the orders-of-magnitude variation in OH absorption intensity for the samples studied is much greater than that which would be predicted if the observed variation were due to variable molar absorption coefficient alone. Where a band of different frequency dominates the spectrum (e.g., the 3660 cm^{-1} band in samples RFT-1 and RFT-2), the effect of varying molar absorption coefficient may be more pronounced.

The calibration used in this study for quantitative estimation of OH concentration is based on a determination of the H content of a garnet megacryst (MON-9) by high temperature vacuum extraction and gas manometry . Details of this calibration are described elsewhere (Bell et al., in prep). In this study, the integrated molar absorption coefficient was determined to be 6700 ± 670 $l \cdot mol^{-1} \cdot cm^{-2}$. This calibration is in good agreement with recent ^{15}N nuclear reaction analysis of pyrope garnets (D. Endisch, F. Rauch, D. Bell and G. Rossman, in prep.). It is indistinguishable from the integrated molar absorption coefficient for hydrous grossular garnets of 7070 ± 1030, calculated from the data in Table 3 of Rossman and Aines (1991). The pyrope calibration has been simplified to the equation (1), by the assumption of constant garnet density. This introduces a small degree of uncertainty (about ± 5%) into the analysis. Other uncertainties in the calculation of OH content from the IR spectra arise from the measurement of sample thickness (+/- 2 μm), integrated absorbance and minor sample heterogeneity. While very careful sample preparation, spectroscopy and baseline fittting can achieve analytical precision down to the order of ±1% (Bell et al., in prep), the less stringent procedures were adopted in the present study. Uncertainties in integrated absorbance are due to errors in the baseline fitting routine, contamination by small amounts of atmospheric water vapor and detector ice during analysis and scattering effects resulting from poor surface polishing.

This uncertainty is estimated at ± 10% for OH-rich samples and up to ±30% for samples with very low OH concentrations, but varies according to the conditions of analysis.

The concentrations determined using the present calibration are dramatically lower (by a factor of 20 to 30) than, and supersede earlier estimates by Aines and Rossman (1984a) on pyrope garnets with similar absorption intensities. While the absolute concentrations reported here may require some adjustment as more precise and accurate calibrations become available, the relative amounts of OH are better established and are in all probability a good reflection of the natural variability.

Electron microprobe analysis

Compositions of the spectroscopically-analyzed samples, or other mineral grains from the same hand specimen were determined with the JEOL 733 electron microprobe at Caltech. These compositions are reported in Table 1 and are mostly averages of three or more grains or grain fragments. In a few instances, electron microprobe-determined compositions supplied by sample donors are also reported in Table 1. Caltech analyses were performed at 15 kV accelerating voltage, but at a variety of beam currents from 40 to 100 nA. Counting times were varied according to estimated element abundance and beam current. Because the garnets were analyzed as part of an experimental program aimed at increasing the quality of garnet microprobe analyses, the procedure was not standardized and different analytical procedures were employed at different times. Averaged analyses reported in Table 1 have been weighted according to precision derived from counting statistics (calculated by the analytical program for each elemental analysis). Mg, Al and Si counting times were sufficient so as to attain 0.2% precision in raw count rate. Fe and Ca analyses attained similar, but often slightly less precise counting statistics, depending on abundance. Minor elements were analyzed with extended counting times. Typical peak counting times

at 40-60 nA were : Na 120s, Ti 60s, Cr 60s, Mn 60s, P 180s. Most concentrations were calculated relative to the following standards: Na - natural (Amelia) albite, Mg, Si, Al - synthetic pyrope, Ca - natural wollastonite, Ti - synthetic rutile, Cr - synthetic eskolaite, Mn - natural spessartine, Fe - synthetic almandine, P - natural (Durango) apatite. The K-ratios relative to the above standards were then converted to concentrations by a full ZAF correction procedure (Armstrong 1984).

Results

Contamination by other phases

Petrographic observations. During microscopic examination of doubly polished garnet samples for positioning of the infrared beam, several types of imperfections were encountered. The more obvious features are primary mineral inclusions and large cracks. Primary mineral inclusions may take the form of rounded or rod-like grains and are generally uncommon. They are usually easy to avoid during IR analysis, but where rod-like inclusions were sufficiently densely packed as to effect occasional intersection with the IR beam (e.g., eclogite 390/4), they had no visible effect on the IR spectrum of the garnet. Large cracks are brilliantly highlighted under crossed polarized large-area illumination from below, and are present in almost all garnets. They are commonly lined with other phases, which we have made little effort to identify. Much of the crack-filling is probably related to emplacement and subsequent near-surface processes, and probably comprises kimberlite matrix minerals and their alteration and reaction products with the host garnet. Late-stage deposits from deuteric and groundwater fluids are also probably a significant component of

the crack-lining assemblage. These coarse cracks were rigorously screened from interaction with the IR beam by the placement of a metal aperture.

More troublesome were two varieties of microscopic imperfections. The first variety takes the form of micrometer to submicrometer sized inclusions, often arranged in linear trains oriented parallel to certain crystallographic directions in the host garnet. Individual inclusions occasionally measure up to 20 μm in length, but are typically only on the order of one micrometer in width. Their exact constitution is unknown, but these features are common in both Ti-poor peridotitic garnets as well as eclogitic garnets. Many megacrysts from the Lace kimberlite also contain these inclusions, which are heterogeneously distributed, and were avoided during analysis. In one case they were seen to be concentrated closer to cracks, with their number density decreasing towards a clear central volume of garnet. Their pervasive nature and often regular alignment suggests that these inclusions may not be a near-surface, alteration-related feature and therefore justify closer attention in future studies. Commonly associated with the linear inclusions are fine features having the appearance of cracks, which may surround individual inclusions, or run from one inclusion to another. The presence of these inclusions and crack-like structures is often correlated with absorptions in the 3400 - 3700 cm^{-1} region of the infrared spectrum and their presence in intrinsically OH-poor garnets is a significant obstacle to accurate determination of the true structural OH component. The presence of these micro-inclusions has been denoted in Table 1.

A second imperfection occurs as diffuse clouds of extremely fine wisp-like structures that are only visible under crossed polarizers using the dark-field illumination. These clouds are particularly common in many eclogitic garnets and often appear to have their origins at crack terminations in the garnet, from which they spread out to cover large portions of the grain volume. It is possible that this second variety may be stress-induced microfractures

which formed at some stage during the entrainment and eruption process. These features, in contrast to those described above, do not appear to influence the infrared spectrum in the region of interest, except in occasional cases where they are unusually coarse or dense and a hydrous component appears to be introduced.

IR Spectral characteristics of contaminants. The above section has described several types of visible impurities encountered in the mantle garnets of this study. The extent to which these visible (and perhaps invisible) inclusions contaminate the spectra needs to be addressed. The garnets from the Kimberley peridotites which contain minute oriented inclusions have an OH spectrum characterized by a relatively broad, but sometimes sharply peaked absorption near 3650 cm^{-1} combined with very broad bands centered at lower wavenumbers (Fig. 2j). These features appear to be associated in some way with the inclusions, although they do not necessarily arise directly from them. For example, the broad 3450 cm^{-1} band may be caused by molecules of water in the inclusions, or in microcracks associated with them. Similar spectral features are seen in several of the peridotitic concentrate garnets from Lace; however only some of these contain visible inclusions, the others possibly being submicroscopic. In garnet megacrysts from Lace, the intensity of absorption of the 3570 cm^{-1} band (OH in the garnet structure) was seen to decrease in the presence of these inclusions, which also gave rise to broad absorptions at lower energies.

The fine, wispy crack-like features common in most eclogitic and a number of peridotitic garnets appear to have little effect on the recorded OH spectrum. Where these features are especially dense, a high wavenumber (3650 cm^{-1}) absorption may sometimes appear, which is perhaps related to associated alteration.

Some of the spectra in Fig. 2 (e.g., Figs. 2f and 2l) display a very weak pair of bands at 3610 and 3710 cm^{-1}. It is believed that these are not due to absorptions in the sample

spectrum, but are created by subtraction of a background spectrum slightly contaminated by the presence of water-vapour. Other contamination of the sample spectrum is caused by ice in the detector system, and is illustrated by the broad, low-intensity absorption at 3250 cm^{-1} in Fig. 2j.

The present discussion has served to draw attention to the problem of contaminant phases during OH analysis by IR spectroscopy. The unambiguous identification of these phases and their precise spectral characterization in the O-H stretching region remain subjects for future investigations. We wish to emphasize however, that we have attempted to keep the influence of such phases to a minimum in this investigation. Their contribution to the overall spectrum becomes an important issue only in the evaluation of the relative abundances (and spectral patterns) of OH in garnets of lowest intrinsic OH contents (such as the Roberts Victor eclogites, and common coarse peridotites), or in the occasional circumstances where the only garnet available from a sample contains an unusually high inclusion density (e.g., alkremite JAG-38). They have essentially no influence on the OH spectra of hydrous samples such as megacrysts, or on most of the Colorado Plateau samples described previously by Aines and Rossman (1984b).

Infrared spectral characteristics of the structural OH component of garnet.

Absorption spectra due to O-H stretching vibration in the garnets examined here are broadly similar to spectra of the magnesian garnets described by Aines and Rossman (1984a), but several additional features have been brought to light by this study. For the purposes of discussion we divide the observed OH stretching bands into three groups on the basis of vibration frequency. These groups are referred to here as high-, medium-, and low-

wavenumber groups and occur in specific combinations for garnets of different paragenesis, giving rise to a limited number of characteristic spectral patterns.

The medium wavenumber group. This study confirms that in most pyrope garnet spectra, the dominant feature in the O-H stretching frequency region between 3400 and 3700 cm^{-1} is a band centered near 3570 cm^{-1}. Preliminary indications are that the position of this band maximum shifts in a regular fashion to lower wavenumber as a function of decreasing Mg/(Mg+Fe) ratio in megacrysts. This results in a variation of the peak position from 3580 to 3565 cm^{-1} in the compositional range of our garnets. Although this feature has the appearance of a single band in many samples (Figs. 2a,p), there are indications from some spectra (e.g., Figs. 2b,c) that it may be an unresolved combination of bands, dominated by the strongest component at ~3570 cm^{-1}.

The high wavenumber group. Aines and Rossman (1984a) noted that the above principal band is commonly accompanied by a less intense, often less well-defined and broader band at higher wavenumber, from about 3600 to 3700 cm^{-1}. Although this band complex is often a broad, rather featureless hump (e.g., Fig. 2l), several garnets examined in the present study allow a more precise characterization of this group. It appears that the most commonly occurring well-resolved bands in this region are located at ~3650 and ~3680 cm^{-1} respectively. Both bands occur in the spectra of many megacrysts (e.g., Fig. 2b). More commonly, however, the 3650 cm^{-1} band dominates the spectrum in the high-wavenumber region (Figs. 2a,f,g,h,m and n) and is a ubiquitous component of the spectra of eclogite and peridotite garnets. In the kyanite eclogite samples from Rietfontein (e.g., RFT-1, Fig. 2h) this band accounts for the quite considerable total absorption intensity and is also the dominant feature of the OH spectra of alkremite garnets (Fig. 2n), peridotitic garnets from Kimberley (Fig. 2j), a few lherzolite garnets from Louwrensia (LRA-17, 18) and some

Roberts Victor eclogites (Fig. 2g). It is a prominent feature of the Bobbejaan Cr-rich "megacrysts" (Fig. 2m). This 3650 cm^{-1} band sometimes appears sharper than other garnet OH absorption features and we note that it occurs in a frequency region common to the OH absorptions of many hydrous phases. The ubiquity of this band and its apparent disregard of host composition or paragenesis raises the suspicion that, in many cases, it may represent submicroscopic inclusions of another phase. Microscopic inclusions of the type described above are observed in many of the garnets where these absorptions are prominent. However, these absorptions do occur in garnets where such inclusions are not seen, and it may be that two or more OH-bearing phases, including the host garnet, coincidentally absorb in the 3650 cm^{-1} region.

Low wavenumber group. In this study, we commonly observe a shoulder or distinct band on the low-frequency side of the principal band, typically centered at about 3512 cm^{-1}. This low frequency absorption, which occurs only in megacrysts and some peridotite garnets (the Ti-rich ones) may, on rare occasions (e.g., Fig. 2e), be the most intense band present. It is commonly observed in megacrysts, which yield the highest quality spectra, that the intensity of the 3512 cm^{-1} band appears to be inversely correlated with that of the high wavenumber group. This is illustrated in the array of spectra shown in Fig. 2 a-e. If real, this apparent correlation may arise from the interconversion of H between two distinct OH sites. In the light of our aforegoing comments on the source of the high wavenumber absorptions, it is conceivable that the structural OH responsible for the low wavenumber (3512 cm^{-1}) absorption is removed from the garnet structure to form minute inclusions of a hydrous phase, which are responsible for the high-wavenumber absorptions. However, the apparent inverse correlation may also be generated by the mixing of two types of spectra, where one type has both high wavenumber bands and a strong 3570 cm^{-1} band, which tends to overlap and obliterate the 3512 cm^{-1} band. In addition to the intrinsic

garnet band at 3512 cm^{-1}, the low wavenumber region may also exhibit a very broad absorption from 3500 to 3100 cm^{-1} (see Fig. 2j) if a crack or inclusion (probably containing molecular water) is intersected.

The spectral patterns illustrated in Fig. 2a-p are a representative selection of the various types of spectra resulting from combinations of the above features.

Abundance of OH in mantle garnets

The OH contents of the garnets are reported in Table 1 as ppm H_2O by weight and a comparison of the distribution of OH in different mantle rock-types is shown in histogram form in Fig. 3.

Garnet megacrysts. The most hydrous garnets encountered in this study are those of the Cr-poor megacryst suite, representative spectra of which are illustrated in Figs. 2a-e. The OH contents of the megacrysts from kimberlites are highly variable, from 8 ppm H_2O to 135 ppm in the most iron-rich kimberlitic megacryst garnets. Several interesting systematic trends are evident, suggesting that the OH content of these megacrysts is in some way a reflection of their conditions of formation.

In all suites of megacrysts from individual kimberlites, there is a strong positive correlation between the structural OH content and degree of iron enrichment, as reflected in decreasing Mg number (Mg number = 100Mg/Mg+Fe) of the garnet. This is illustrated in Fig. 4 by a suite of garnet megacrysts from the Monastery Mine. Rim-to-rim traverses of selected samples reveal a general lack of zoning in OH for the megacrysts, in accord with the homogeneous distribution of major and minor elements typical of megacrysts from the localities studied. There are also no variations in OH concentration in the proximity of the ubiquitous cracks which riddle virtually all mantle-derived xenoliths.

Megacryst suites from different kimberlites define somewhat different trends on a plot of OH content versus Mg number (Fig. 5). Of particular interest is the displacement of the Lace kimberlite garnet trend to higher OH contents than the majority of other suites.

In order to compare the kimberlite megacrysts with similar garnets from related, but possibly less volatile-rich environments, we have analyzed megacrysts from an alkali basalt (Kerem Maharal, Mt. Carmel, Israel) and reanalyzed garnet megacrysts from the Malaita alnoite (previously reported by Aines & Rossman 1984b) and the basalt at Chanthaburi, Thailand. Sample PHN-3986A from the alnoite contains 3 ppm and the basaltic megacrysts less than 1 ppm H_2O. Thus all three are, in comparison with the kimberlite-hosted megacrysts, extremely poor in OH.

Peridotites. The abundances of OH in garnets extracted from lherzolites and harzburgites are shown in Figs. 3b and c. Concentrations in typical peridotites range from undetectable amounts (< 1 ppm) to about 30 ppm. In the Premier and Jagersfontein peridotite suites, strong correlations between textural type, bulk- and mineral-chemistry and pressure and temperature of origin of the peridotites have been demonstrated (Danchin 1979, Winterburn et al. 1990, Hops et al. 1989). The OH contents of the peridotitic garnets reflect these petrological differences. At Premier, variable, but typically high OH contents are found in orange-red or brownish-red, Ti-rich (0.3-1.5 wt. % TiO_2) garnets from the high-temperature, deformed lherzolites. Purple coloured, Ti-poor (<0.2 wt. % TiO_2) garnets, whether from coarse-granular or deformed peridotites are poor in OH. At Jagersfontein, the garnets from high-temperature, often Ti-rich peridotites are also generally more hydrous than their Ti-poor counterparts. Spectral characteristics of the two types of garnets are also somewhat different. The OH-rich samples show two well developed bands (Fig. 2k); the usual principal band near 3570 cm^{-1} and the lower frequency band near 3512 cm^{-1}, which in two of the garnets is the more intense. OH-poor garnets are different in lacking the 3512

cm^{-1} band, but having instead a poorly defined absorption near 3620 to 3650 cm^{-1}. With reference to the discussion on contamination above, some of this high wavenumber component may not be intrinsic to the garnet. The presence of this absorption contributes somewhat to the overlap of the Ti-rich and Ti-poor peridotite garnet OH concentrations in Fig. 3.

The peridotites from the off-craton Louwrensia kimberlite in Namibia contain garnets that are similar in overall OH content to those from the Premier and Jagersfontein lherzolites. Once again, there is a distinct association of higher OH content with high Ti in the garnets. Many of these Ti and OH-rich garnets are chemically zoned. The data of Mitchell (1984) reveal that high-Ti garnets typically come from peridotites that record high temperatures, lying on an inflected (high thermal gradient) limb of the geotherm. However, the Louwrensia peridotite garnets are different from their on-craton counterparts in that both high- and low-OH garnets exhibit the same spectral characteristics (Fig. 2l is typical), with none showing an absorption band at 3512 cm^{-1}.

Fig. 6. shows that the OH and Ti contents of peridotite garnets from both on- and off-craton peridotites are positively correlated. This plot excludes all garnets in which inclusions were visible under the microscope (see Table 1), or whose IR spectra indicated possible contamination from inclusions. The sum of the absorbances at 3570 cm^{-1} and 3512 cm^{-1}, rather than the integrated absorbances have been used to indicate relative OH content, because of the greater sensitivity of the integrated absorbance to contamination effects. Because of the positive correlation between Na and Ti in these garnets, the OH contents also exhibit a positive correlation with Na.

Garnets from a small suite of lherzolites and harzburgites from the Boshof Road and other mine dumps (Kimberley) have large integrated absorbances related to a somewhat sharp absorption at 3650 cm^{-1}, accompanied by a very broad component extending from 3600 to 3300 cm^{-1}. All the garnets, however, contain oriented inclusions of the type

described above. In estimating the OH contents of these samples, we have excluded the broad, low wavenumber absorptions, which we believe are due to liquid water. We believe that the true structural OH content of these garnets may be even less than the 6 to 21 ppm H_2O reported in Table 1, and that much of the absorbance may be due to microscopic imperfections. Similar features are evident in some of the peridotitic xenocryst grains from Lace.

Relatively high OH contents are recorded in two "Cr-rich megacrysts" from the Bobbejaan Fissure, and the highest OH content (86 ppm H_2O) measured in garnets of broadly peridotitic paragenesis occurs in a green garnet xenocryst, WTV-1, from the Weltevreden Mine. This garnet measures approximately 8 by 10 mm and is intergrown with Cr-spinel, Cr-diopside and some phlogopite of uncertain paragenesis. It is similar in composition and appearance to those described by Schulze (1989).

Eclogites. Eclogite garnets are highly variable in OH content (Fig. 3d). Those from "on-craton" sources, including the diamond-bearing samples, are generally very poor in OH. In the Roberts Victor suite there is no apparent correlation of OH content with garnet composition (Fig. 7). It is interesting to note that in this suite the Ca-rich eclogitic garnets are not noticeably richer in OH, despite of speculation that OH is associated with the grossular component (Lager et al. 1989). Eclogite garnet spectra do not exhibit the low-frequency absorption band near 3512 cm^{-1}. While it is common for a high-frequency band complex near 3650 cm^{-1} to contribute a significant proportion of the total absorption, it is not clear whether this component is truly a structural element of the garnet.

The OH contents of many eclogite garnets from those pipes situated adjacent to the inferred craton boundary (Markt, Lovedale and Roodekraal kimberlites) are similar to those of the on-craton samples, with the somewhat elevated OH contents of garnets from the Roodekraal kimberlite possibly due to visible microscopic inclusions. Eclogite garnets

from the Rietfontein kimberlite, situated some two hundred kilometers to the West of the craton (Fig. 1), do not contain visible micro-inclusions and their OH contents (46 to 86 ppm H_2O) are unambiguously higher than the Roberts Victor garnets. There are also distinct spectral differences between two relatively calcic (13.7 wt % CaO) garnets from Rietfontein kyanite-bearing eclogites, in which a strong band appears at 3660 cm^{-1}, and the other 8 samples from this locality, which have spectra like those of the off-craton peridotites.

Diamond Association. Diamond-inclusions are difficult to analyze on account of their small size and thus commonly yield somewhat poorer quality spectral data than other garnets. Two inclusions, a lilac Cr-rich garnet of peridotitic paragenesis and an orange eclogitic garnet were analyzed in this study. The eclogitic garnet inclusion (P-108 from the Premier Mine) has a very low OH content (3 ppm H_2O), whereas the peridotitic garnet (F99-B from the Finsch Mine) yielded a poor quality spectrum from which we are only able to infer an upper limit to the possible OH content of about 15 ppm H_2O. Three lilac-coloured xenocryst garnets from the Lace mine, which have compositions equivalent to peridotitic paragenesis diamond inclusion garnets, contain low OH contents (1-7 ppm H_2O). Four diamond bearing eclogite samples, from geographically well separated localities on the Kaapvaal Craton, have garnets with OH contents ranging from 2 to 17 ppm H_2O.

Discussion

The systematic distributions of OH in mantle garnets, demonstrated above, are a strong indication that H in these garnets follows a consistent geochemical behavior, and that the observed variations are not of a random nature. This implies the potential to provide useful

information on some aspects of the geological history of the samples. Exactly which aspects of their geochemical environment are being recorded by these hydrous (or anhydrous) garnets is an important question. The regular geochemical trends and consistent petrological correlations reported in this study argue for preservation of source information, although we have demonstrated in reconnaissance laboratory studies that hydrogen can be removed from megacryst garnets by heating in air and replaced by hydrothermal treatment. In the following section we discuss some petrological implications of the observed systematics, with the assumption that the OH content of the garnets is a feature retained from the source region. The extent to which this assumption is valid will hopefully be revealed by ongoing studies into the stability of the hydrous component and garnet crystal chemistry.

Hydroxyl in garnet megacrysts : an indicator of OH in mantle melts.

Most studies of Cr-poor megacrysts in kimberlites appear to favour an origin for this suite of minerals as deep-seated fractional crystallization products from a magma near the base of the lithosphere (e.g., Nixon and Boyd 1973b, Harte and Gurney 1981, Harte 1983, Mitchell 1986, Schulze 1987). This crystallization may involve the interaction with some peridotite wall rock (Jones 1987, Neal and Davidson 1989) but the dominant influence on mineral compositions appears to be the evolving magma (e.g., Gurney et al. 1979). The physical setting of the megacrysts prior to their entrainment in the transporting kimberlite is unknown, but Harte and Gurney (1981) proposed a stockwork of vein and mantle pegmatites, in contrast to an earlier proposal by Nixon and Boyd (1973b) of crystals distributed in a partially molten zone.

Garnet megacrysts from the Monastery and Lace kimberlites were chosen specifically for their regularity of minor element variation as a function of Mg number, taken to be a

differentiation index. The results obtained in this study appear to indicate that hydrogen behaves in a similar fashion to other minor and trace magmatic components, with its concentration in the crystallizing solid phase being controlled by a rational solid-liquid equilibrium. The regular increase of OH in the garnet as a function of decreasing Mg number is an expected consequence of the incompatibility of OH in the nominally anhydrous crystallizing minerals. Although the stoichiometrically hydrous phase phlogopite is believed to crystallize from the megacryst magma at Monastery, it does so at an advanced stage of the differentiation process (Moore 1986), possibly after garnet has ceased to crystallize. It is in any event likely that the OH content of the evolved melt will exceed that of the fractionating mineral assemblage, and that the concentration of magmatic water will continue to increase during the final stages of differentiation.

Garnets from the Lace kimberlite exhibit a higher OH content for a given Mg number compared with those of the other kimberlites studied (Fig. 5). It is the only micaceous (group II) kimberlite studied, which suggests that if garnet megacrysts are in fact related to their host kimberlite magmas, as envisioned by Jones (1987) and others, then water may play a more important role in the near-source evolution of micaceous kimberlites than it does for non-micaceous (group I) kimberlites.

There is no obvious difference in OH content between the garnet megacrysts from on- and off-craton kimberlites, suggesting a general similarity in water content between the parent magmas. This is in accord with the other chemical features of their megacrysts (Mitchell 1987). Mitchell (1984) has alluded to the uniformity of the kimberlite-forming process in these two environments in southern Africa.

The field for garnet megacrysts from the Kaalvallei kimberlite is somewhat more scattered than those of the other megacryst suites in Fig. 5 and contains one outlying data point. This is sample 13-53-63, one of four relatively magnesian garnets from this locality. The reason for the anomalous behaviour of this sample is unclear. The overall greater scatter in

the Kaalvallei suite is less surprising, as crystallization from several similar, but not identical parent magmas, or differential degrees of wallrock interaction during the crystallization - differentiation process could produce this more erratic behaviour.

In contrast to the kimberlitic megacrysts, the megacrysts which we have analyzed from rock-types poorer in volatiles than kimberlites (alnoite, alkali basalt) are markedly less hydrous. The data suggest a progression towards lower water contents in the magmas parental to the garnets, supporting the contention (e.g., Chapman 1976) that these parental melts are in some way genetically related to the erupted, xenolith-transporting magma. However, caution must be exercised in the comparison of garnets from volcanic hosts with different eruption styles, as our laboratory studies have shown that OH can be lost from the samples by high temperature treatment in an oxidizing environment.

Water in garnet peridotites.

The results presented in Table 1 show that garnet in mantle peridotites can contain bound hydroxyl in limited amounts. Even in the most hydrous peridotitic garnets, the estimated amounts are only on the order of 80 ppm H_2O. Assuming garnet to comprise about 10% by volume of the upper mantle, the maximum observed amount of garnet-hosted water is therefore about 8 ppm. Considering garnets from Colorado Plateau diatremes studied by Aines & Rossman (1984a,b), this figure could be raised to about 15 ppm. It is difficult to estimate how much more water could be bound in the structure of mantle garnet as OH, but it seems unlikely that this could amount to the weight percent levels required if garnet were the major reservoir for the 1000 ppm water estimated by Ringwood (1975) in undepleted mantle.

The higher OH contents of garnets from commonly deformed, high temperature peridotites at Premier and Jagersfontein provide further evidence for their formation in a

different mantle regime from the common coarse lherzolites as shown by Nixon and Boyd (1973a) for the northern Lesotho xenolith suite. Our study indicates that the "fertile" peridotites appear to have formed or equilibrated in a more hydrous environment, and that water is associated geochemically with other incompatible elements like Ti and Na. This is consistent with the suggestion of Gurney and Harte (1980) and recent geochemical evidence from several workers (e.g., Smith and Boyd 1987, Hops et al. 1989, Griffin et al. 1989) that these deformed xenoliths have acquired their "fertile" character by interaction with a silicate melt which was parental to the Cr-poor megacryst suite, and which may be the cause of the higher ferric/ferrous iron ratios reported by Luth et al. (1990) for such xenoliths. The infiltration of such peridotites by a fluid is also indicated on microstructural grounds (Drury and Van Roermund 1989).

Low temperature peridotite garnets contain OH contents varying from below detection limit to about 20 ppm. At these low levels, relative abundances are determined with difficulty and identification of the true structural OH component of garnet is hampered by the common occurrence of microscopic inclusions. Nevertheless, the general impression is gained that the "on-" and "off-craton" peridotitic portions of the continental lithosphere are probably similar in terms of the OH content of the nominally anhydrous mineral reservoir. Isotopic and petrographic studies of peridotite xenoliths reveal a complex history of melt extraction, subsolidus re-equilibration and open-system material exchange. The linking of garnet OH content to a specific petrogenetic event in the history of the host rock is therefore not a simple matter.

Two large dark purple (in hand sample) megacrystic garnets, of the type commonly found in group II kimberlites in the Kimberley - Barkly West area (e.g., Roberts Victor and Bobbejaan kimberlites) contain 30 and 31 ppm H_2O respectively. These garnets have compositions somewhat similar to those of the Cr-rich megacrysts described by Eggler et al. (1979), but are poor in titanium and thus more akin to garnets from depleted peridotites.

Some of the garnets in the suite from which these two samples were selected (including sample BBB-16) contain inclusions of chromite, Cr-diopside, sulphide and phlogopite. These garnets are more hydrous than typical "on-craton" low-Ti peridotite garnets. The high OH content and apparent stable coexistence of phlogopite are consistent with crystallization of these garnets in a water-rich environment which, based on the low Ti and high Cr content of the garnets, is different from that of the Cr-poor megacrysts. There is to our knowledge little published work on the petrogenesis of these Cr-rich garnets.

The high OH content of the green Ca- and Cr-rich garnet WTV-1 sets this sample apart from common peridotite garnets, and does not appear to be due to foreign phase contamination (see Fig. 2o). This garnet has an OH spectrum identical to many garnets from the Colorado Plateau diatremes. The similarity in OH content and spectral features to Colorado Plateau garnets may be significant in light of the proposals by Schulze (1989) and Helmstaedt and Schulze (1988) that both have their origins in subducted lithosphere.

A note on phlogopite-bearing peridotites: Phlogopite occurs commonly as an accessory phase in peridotite and eclogite xenoliths, locally assuming considerable modal importance. The presence of texturally equilibrated "primary" mica (terminology of Carswell 1975 and Delaney et al. 1980) is commonly attributed to the metasomatic action of a hydrous and potassic fluid (e.g., Holmes 1936, Aoki 1975), inferred to have infiltrated at some time prior to the eruptive event. It might be expected that the garnets from such modally metasomatized xenoliths would record higher hydroxyl contents in response to the apparently hydrous environment. Phlogopite-bearing garnet peridotites examined here often do not exhibit intensified absorptions that are readily assigned to structural OH. On the other hand, several of these peridotites, as well as the alkremite JAG-38, contain garnets with high concentrations of microscopic inclusions. In the less-common cases where phlogopite-bearing assemblages contain apparently inclusion-free garnets (BBB-14,

BBB-16, WTV-1), the OH concentrations are relatively high.

In many modally metasomatized peridotites, the lack of Nd isotopic equilibrium between phlogopite and garnet, commonly in a direction that cannot be explained by age differences between the minerals (Richardson et al. 1985, Waters 1987), suggests that garnet has commonly failed to equilibrate with the proposed hydrous metasomatic fluid. Petrographic evidence for garnet consumption during mica-forming reactions in such rocks (Erlank et al. 1987) furthermore suggests that garnet is often not stable in the presence of these fluids. Even if the attainment of equilibrium is strongly indicated on textural or isotopic criteria, it is possible that crystal chemical factors such as those discussed below inhibit the formation of significantly OH-bearing garnets. The resolution of this issue depends on analysis of samples where a strong case for chemical equilibrium between garnet and phlogopite can be made, and where the difference between true structural OH and that due to minute imperfections and cracks, which may be introduced during the passage of fluid through the rock, has been established.

Eclogite garnets.

Eclogitic garnets from the Roberts Victor mine are remarkable in being consistently OH-poor, despite their large compositional variability. At first hand, this appears to indicate relatively anhydrous conditions of formation. Although the samples we have analyzed are not those for which oxygen isotope data are available, it is probable that a similar range in $\partial^{18}O$ to that reported by Garlick et al. (1971) occurs in our samples and that they may represent subducted oceanic crust, as suggested by Jagoutz et al. (1984) and other workers, or a reworked version thereof. If these garnets were formed in a prograde metamorphic event within subducting lithosphere, and their OH contents are well preserved from their time of formation, then it would appear that garnets transport little water back

into the mantle during subduction. In fact, the data of Skogby et al. (1990) and Smyth et al. (1991) suggest that omphacitic pyroxene is more interesting from this point of view. However, the interpretation of OH in eclogitic garnets (and pyroxenes) is further complicated by the complex geological history of some samples as revealed in studies by Lappin and Dawson (1975), Harte and Gurney (1975), Sautter and Harte (1989) and Smyth et al. (1989). Several of these and other studies have argued for an igneous origin for the eclogites, followed by subsolidus cooling and exsolution of garnet from aluminous pyroxene in some samples. The low intrinsic OH contents of the Roberts Victor garnets are consistent with a relatively anhydrous, igneous origin for the eclogite garnets, but with present lack of understanding of the controls on OH in garnets, cannot be used as a reliable discriminant between the two hypotheses.

While a good mineral barometer is not available for most mantle-derived eclogites, the presence of diamond in certain samples from the Roberts Victor Mine does suggest a mantle origin for the suite as a whole. Basu et al. (1986) suggest a pressure range of 30 to 50 kbar for the Roberts Victor eclogites by calculating the pressures at which eclogite mineral thermometer temperatures are commensurate with the peridotite-derived geotherm for the Kaapvaal Craton. Studies of eclogites from the northern Lesotho (Griffin et al., 1979) and Karoo (Robey 1981) kimberlites have indicated a lower crustal origin for these rocks. Pressure estimates on granulite xenoliths, considered by Robey (1981) to be co-facial with the eclogites, are in the range 10 to 20 kbar (Robey 1981, Van Calsteren et al. 1986). Eclogites from the off-craton Rietfontein kimberlite may derive from considerably shallower depths than the Roberts Victor samples, if they are equivalent to other eclogites from off-craton kimberlites in southern Africa. The elevated OH contents of the Rietfontein eclogites and of individual garnet grains from the Colorado Plateau diatremes assumed on the basis of color and composition to derive from eclogites, suggests either that these rocks were originally formed in a more hydrous environment than their on-craton counterparts, or

that the probable lower pressures involved facilitate OH incorporation into garnet as predicted by the arguments of Martin and Donnay (1972).

Diamond inclusions and diamond-associated rocks.

Our limited data set (two samples) suggests that garnets of both peridotitic and eclogitic affinity, isolated as inclusions within diamonds, have low OH contents. At face value, this may be taken to indicate a water-poor environment of formation, but it is possible that crystal-chemistry has a role to play. The OH-poor nature of the eclogitic garnet inclusions and diamondiferous xenoliths suggest (assuming no H loss through the encapsulating diamond with time) that diamonds of this paragenesis did not grow from water-rich fluids, and almost certainly not from incompatible element-rich hydrous melts, such as those believed to be parental to megacrysts. It is interesting that both the peridotitic and eclogitic parageneses of diamond-included garnet are essentially identical in terms of OH content to garnets of allied, but macroscopically non-diamondiferous peridotitic and eclogitic xenoliths respectively. In other words, the OH signature of diamond inclusion garnets records little or nothing of the diamond-forming events. Perhaps these events are coincident with the major petrogenetic processes giving rise to garnet formation in mantle peridotites and eclogites. Although little can be said about the nature of the diamond-forming process from our data, our preliminary conclusion is to regard the precipitation of typical garnet inclusion-bearing diamonds from the type of material identified as inclusions in coated diamonds by Navon et al. (1988), or from kimberlite-like melts as unlikely.

Effects of crystal-chemistry

At several points in the previous discussion, it has been speculated that the crystal chemistry of the garnet may exert some influence on the amount of OH it contains. There

are several reasons for this possibility: (a) The hydropyrope structure is predicted to be unstable (Martin and Donnay 1972, Lager et al. 1989) and the presence of anomalous cations or other "defects" in the crystal structure may provide the necessary local distortion to accommodate OH. (b) OH may occur in a form other than the hydrogarnet substitution (Birkett and Trzcienski 1984, Rossman and Aines 1991), implying a deviation from normal charge - site relationships for garnet. OH may therefore be incorporated as a charge balancing ion in fixed proportion to another cation carrying a charge greater than that of ions usually occupying the particular site, for example, Ti^{4+} in the octahedral site. (c) It has been observed that OH is commonly more abundant in garnets of certain compositions. As an example, grossular garnets can sometimes be very OH-rich, whereas pyrope and almandine garnets commonly are not. (d) Crystal defects involving Fe^{3+} are suggested to play a role in the incorporation of small amounts of hydrogen as OH (16 to 80 H/10^6 Si atomic) in natural olivines treated hydrothermally in the laboratory (Mackwell and Kohlstedt 1990). It would be useful to determine whether or not a related mechanism operates in garnets.

It is difficult, when examining a suite of natural samples, to separate the potential structural effects of crystal chemistry from those of geological environment. Nevertheless, we have tried to evaluate whether or not there exists a simple crystal chemical parameter which can account for the variation of OH concentrations in our data set. Although they are not reproduced here, plots for the entire suite studied here of OH content versus any of the analyzed chemical components display either very poor or non-existent correlations and none of the compositional variables appears obviously or solely responsible for the facilitated incorporation of OH. Furthermore, we are unable to seriously test the possibility of a hydrogarnet type substitution (4H = Si) with the low OH contents of this study and present precision of microprobe analysis. In fact, the simple coupled substitution of H

with any of the minor elements analyzed in garnet is unlikely as H is so much less abundant than elements such as Na, Ti and even P.

Although there are indications that high OH concentrations in peridotitic garnets from southern Africa occur preferentially in those of Ti-rich composition (Figs. 3 and 6), this is not borne out by purple garnets (probably peridotite-derived) from Colorado Plateau diatremes (Aines and Rossman 1984b and unpublished data), or when the megacryst garnets are considered. Similarly, many garnets with elevated OH contents contain substantial amounts of calculated ferric iron. However, the amount of Fe^{3+} greatly exceeds the hydrogen content of many of these samples, so that the existence of a simple relationship between the two is unlikely. From a geochemical point of view, it is to be expected that components such as H_2O, Ti and Fe^{3+} will be associated in occurrence, due to their relative geochemical coherence as incompatible components in common igneous systems. We cannot at this point rule out a role for crystal chemical factors in enhancing the ability of mantle garnets to incorporate OH, but identification of specific mechanisms and determination of the importance of this effect relative to that of external factors such as water fugacity will require further careful study. The precise evaluation of these possible crystal-chemical effects will be important for the development of a quantitative garnet hydrobarometer.

Conclusions

Analysis of 166 mantle-derived garnets from southern Africa has revealed a considerable variability in structural OH content, from less than 1 ppm to 135 ppm H_2O by weight. While concentrations are insufficient to constitute a large reservoir of mantle water, such as that of primitive, or even depleted (MORB-source) mantle, the variations in OH content follow strikingly systematic patterns. Some of these, for example the inverse correlation

between OH content and Mg number in megacrysts, suggest that with experimental calibration, garnet will be a useful quantitative hydrobarometer for upper mantle (and crustal) rocks.

Most samples studied, with the notable exception of some eclogitic samples from on-craton kimberlites, and diamond inclusions, contain measurable OH. In general, Cr-poor megacrysts (discrete nodules) and some off-craton eclogites are the most hydrous, followed by high-temperature, Ti-rich peridotitic garnets, and finally depleted, Ti-poor peridotite garnets. It cannot be demonstrated that mica-bearing peridotite and eclogite xenoliths contain garnets with higher structural OH contents than the samples without stoichiometrically hydrous phases, although some phlogopite bearing samples (Cr-rich garnet nodules; one alkremite) are relatively OH-rich.

The spectral patterns of OH absorption in the garnets of this study are more complex than previously recognized in mantle samples. There appear to be systematic differences in the frequency and relative intensity distribution of absorption bands as a function of garnet composition and petrological environment, though these two factors are difficult to separate, requiring carefully designed studies of natural and synthetic garnets. OH concentration is not well correlated with any single crystal chemical parameter measured here. For the southern African samples, high OH concentrations are sometimes associated with elevated levels of titanium and ferric iron. This may be a combination of crystal-chemical effects and the natural geochemical association of these components with water in certain mantle systems.

It has not been established that all garnet xenolithic material in kimberlites preserves OH contents unmodified from the source, yet this is suggested as a reasonable deduction based on available data, and forms the basis for the following qualitative petrological conclusions:

1. Megacryst garnets reflect the buildup of water in their differentiating parent magmas, and attest to the hydrous nature of these melts, which may be protokimberlitic. Garnet

megacrysts from the micaceous, group II Lace kimberlite are more hydrous than compositionally equivalent megacrysts from group I kimberlites, which are in turn richer in OH than garnet megacrysts from an alnoite and an alkali basalt, reflecting probable water contents of their parent magmas.

2. High-temperature, "fertile" peridotite garnets from the Premier and Jagersfontein kimberlites are OH-rich, possibly reflecting an association with "megacryst magmas," brought about by infiltration and diffusive exchange.

3. Water contents of garnets from Ti-poor peridotites representing lithospheric upper mantle from different geographic areas, tectonic settings and of different ages from southern Africa, are similar, suggesting relative uniformity in water content for (unmetasomatized) peridotitic subcontinental mantle.

4. Garnets of eclogitic paragenesis, including a diamond-inclusion, from on-craton kimberlites are extremely poor in OH and probably reflect anhydrous conditions of formation.

5. The typical OH concentrations of peridotite and eclogite garnets from southern African mantle samples are significantly lower than those previously observed for garnets from the mantle of the Colorado Plateau, reinforcing earlier suggestions (Aines and Rossman 1984b) of significant large-scale regional heterogeneity in mantle water content.

Acknowledgments. We would like to thank all the sample donors listed in Table 1 for their willingness to contribute samples to this study. In particular, J. J. Gurney and De Beers Consolidated Mines Ltd. are gratefully thanked for access to their impressive xenolith collections. G. H. Read and R. O. Moore were also especially helpful with sample provision and assistance in the field. J. T. Armstrong provided instruction and general wisdom in electron microprobe analysis and P. Carpenter gave analytical assistance. The manuscript benefitted from thoughtful reviews by D. Smith and S. E. Haggerty. DRB gratefully acknowledges financial support from the Harry Crossley Foundation and the American Federation of Mineralogical Societies. This work was funded in part by NSF grants EAR-86-18200 and EAR-88-16006.

References

Ackermann L, Cemic L, Langer K (1983) Hydrogarnet substitution in pyrope: A possible location for "water" in the mantle. Earth planet Sci Lett 62: 208-214

Aines RD, Rossman GR (1984a) The hydrous component in garnets: Pyralspites. Amer Mineral 69: 1116-1126

Aines RD, Rossman GR (1984b) Water content of mantle garnets. Geology 12: 720-723

Aoki K (1975) Origin of phlogopite and potassic richterite bearing peridotite xenoliths from South Africa. Contrib Mineral Petrol 53: 145-156

Armstrong J T (1984) Quantitative analysis of silicate and oxide minerals: A re-evaluation of ZAF corrections and proposal for new Bence-Albee coefficients. In: Romig AD Jr, Goldstein JI (eds) Microbeam Analysis - 1984, San Francisco Press, pp. 208-212

Basu AR, Ongley JS, MacGregor ID (1986) Eclogites, pyroxene geotherm and layered mantle convection. Science 233: 1303-1305

Bell DR, Ihinger PD, Rossman GR, Epstein S (1992) Calibration of an infrared spectroscopic technique for quantitative analysis of hydroxyl in garnet and pyroxene. To be submitted to Amer Mineral.

Birkett TC, Trzcienski WE Jr (1984) Hydrogarnet: multi-site hydrogen occupancy in the garnet structure. Canad Mineral 22: 675-680

Carswell DA (1975) Primary and secondary phlogopites in garnet lherzolite xenoliths. Phys Chem Earth 9: 417-430

Chapman NA (1976) Inclusions and megacrysts from undersaturated tuffs and basanites, East Fife, Scotland. J Petrol 17: 472-498

Danchin RV (1979) Mineral and bulk chemistry of garnet lherzolite and garnet harzburgite xenoliths from the Premier Mine, South Africa. In: Boyd FR, Meyer HOA (eds.) The

Mantle Sample: Inclusions in Kimberlites and Other Volcanics. AGU, Washington, pp 104-126

Delaney JS, Smith JV, Carswell DA, Dawson JB (1980) Chemistry of micas from kimberlites and xenoliths-II. Primary- and secondary- textured micas from peridotite xenoliths. Geochim Cosmochim Acta 44: 857-872

Drury MR, Van Roermund HLM (1989) Fluid assisted recrystallization in upper mantle peridotites from kimberlites. J Petrol 30: 133-152

Eggler DH, McCallum ME, Smith CB (1979) Megacryst assemblages in kimberlite from northern Colorado and southern Wyoming: Petrology, geothermometry-barometry and areal distribution. In: Boyd FR, Meyer HOA (eds.) The Mantle Sample: Inclusions in Kimberlites and Other Volcanics. AGU, Washington, pp. 213-226

Erlank AJ, Waters FG, Hawkesworth CJ, Haggerty SE, Allsopp HL, Rickard RS, Menzies MA (1987) Evidence for mantle metasomatism in peridotite nodules from the Kimberley pipes, South Africa. In: Menzies MA (ed) Mantle Metasomatism. Academic Press, pp. 221-311

Finger LW, Prewitt CT (1989) Predicted compositions for high-density hydrous magnesium silicates. Geophys Res Lett 16: 1395-1397

Fyfe WS (1970) Lattice energies, phase transformations and volatiles in the mantle. Phys Earth planet Int 3: 196-200

Garlick GD, MacGregor ID, Vogel DE (1971) Oxygen isotope ratios in eclogites from kimberlites. Science 172: 1025-1027

Griffin WL, Carswell DA, Nixon PH (1979) Lower crustal granulites and eclogites from Lesotho, southern Africa. In: Boyd FR, Meyer HOA (eds.) The Mantle Sample: Inclusions in Kimberlites and Other Volcanics. AGU, Washington, pp 59-86

Griffin WL Smith D, Boyd FR, Cousens DR, Ryan CG, Sie SH, Suter GF (1989) Trace element zoning in garnets from sheared mantle xenoliths. Geochim Cosmochim Acta 53: 561-567

Gurney JJ (1984) A correlation between garnets and diamonds in kimberlites. In: Glover JE and Harris PG (eds) Kimberlite occurrence and origin: a basis for conceptual models in exploration. Geology Department and University Extension, University of Western Australia. Spec Publ 8: 143-16

Gurney JJ, Harte B (1980) Chemical variations in upper mantle nodules from southern African kimberlites. Phil Trans Royal Soc London A297: 273-293

Gurney, J.J., W.R.O. Jakob and J.B. Dawson (1979) Megacrysts from the Monastery kimberlite pipe, South Africa. In: Boyd FR, Meyer HOA (eds.) The Mantle Sample: Inclusions in Kimberlites and Other Volcanics. AGU, Washington, pp. 227-243

Gurney JJ, Mathias M, Siebert C, Moseley G (1971) Kyanite eclogites from the Rietfontein kimberlite pipe, Mier Coloured Reserve, Gordonia, Cape Province, South Africa. Contrib Mineral Petrol 30: 46-52

Harte B (1983) Mantle peridotites and processes - the kimberlite sample. In : Hawkesworth CJ, Norry MJ (eds) Continental basalts and mantle xenoliths. Shiva, Cheshire, pp. 46-91

Harte B, Gurney JJ (1975) Evolution of clinopyroxene and garnet in an eclogite nodule from the Roberts Victor kimberlite pipe, South Africa. Phys Chem Earth 9 : 367-388

Harte B, Gurney JJ (1981) The mode of formation of chromium-poor megacryst suites from kimberlites. J Geol 89: 749-753

Hartnady CJ, Joubert P, Stowe CW (1985) Proterozoic crustal evolution in southwestern Africa. Episodes 8: 236-244

Hatton CJ (1978) The geochemistry and origin of xenoliths from the Roberts Victor Mine. Unpubl. Ph. D. thesis, University of Cape Town

Helmstaedt HH, Schulze DJ (1988) Eclogite facies ultramafic xenoliths from Colorado Plateau diatreme breccias: comparison with eclogites in crustal environments, evaluation of the subduction hypothesis, and implications for eclogite xenoliths from diamondiferous kimberlites. In: Smith DC (ed) Eclogites and eclogite-facies rocks. Elsevier, Amsterdam pp 387-450

Holmes A (1936) A contribution to the petrology of kimberlite and its inclusions. Trans geol Soc S Afr 39: 379-427

Hops JJ, Gurney JJ, Harte B, Winterburn P (1989) Megacrysts and high temperature nodules from the Jagersfontein kimberlite pipe. In : Kimberlites and Related rocks. Volume 2. Their mantle / crust setting, diamonds and diamond exploration. Geol Soc. Australia spec Publ 14: 759-770

Jagoutz E, Dawson JB, Hoernes S, Spettel B, Wanke H (1984) Anorthositic oceanic crust in the Archean Earth (abstr) Lunar and Planetary Science Conference XV abstracts : 395-396

Jones RA (1987) Strontium and neodymium isotopic and rare-earth element evidence for the genesis of megacrysts in kimberlites of southern Africa. In: Nixon PH (ed) Mantle xenoliths. John Wiley and Sons, Chichester, pp. 711-724

Lager G, Armbruster T, Rotella FJ, Rossman GR (1989) OH substitution in garnets : X-ray and neutron-diffraction, infrared, and geometric-modeling studies. Amer Mineral 74: 840- 851

Lappin MA, Dawson JB (1975) Two Roberts Victor cumulate eclogites and their re-equilibration. Phys. Chem Earth 9: 351-366

Liu, L. (1987) Effects of H_2O on the phase behavior of the forsterite-enstatite system at high pressures and temperatures and implications for the earth. Phys Earth planet Int 49: 142-167

Luth RW, Virgo D, Boyd FR, Wood BJ (1990) Ferric iron in mantle-derived garnets; implications for thermobarometry and for the oxidation state of the mantle. Contrib Mineral Petrol 104: 56-72

MacGregor ID (1975) Petrologic and thermal structure of the upper mantle beneath South Africa in the Cretaceous. Phys Chem Earth 9: 455-466

Mackwell SJ, Kohlstedt DL (1990) Diffusion of hydrogen in olivine: implications for water in the mantle. J geophys Res 95: 5079-5088

Martin RF, Donnay G (1972) Hydroxyl in the mantle. Amer Mineral 57: 554-570

Mitchell RH (1984) Garnet lherzolites from the Hanaus-I and Louwrensia kimberlites of Namibia. Contrib Mineral Petrol 86: 178-188

Mitchell RH (1986) Kimberlites : mineralogy, geochemistry and petrology. Plenum, New York, 442 pp

Mitchell RH (1987) Megacrysts in kimberlites from the Gibeon field, Namibia. Neues Jahrb Mineralogie Abh 157: 267-283

Moore RO (1986) A study of the kimberlites, diamonds and associated rocks and minerals from the Monastery Mine, South Africa. Unpubl. Ph.D. thesis, University of Cape Town

Navon O, Hutcheon ID, Rossman GR, Wasserburg GJ (1988) Mantle-derived fluids in diamond micro-inclusions. Nature 335: 784-789

Neal CR, Davidson JP (1989) An unmetasomatized source for the Malaitan alnoite (Solomon Islands) : petrogenesis involving zone refining, megacryst fractionation, and assimilation of oceanic lithosphere. Geochim Cosmochim Acta 53: 1975-1990

Nixon PH, Boyd FR (1973a) Petrogenesis of the granular and sheared ultrabasic nodule suite in kimberlite. In: Nixon PH (ed.) Lesotho Kimberlites. Lesotho National Development Corporation, Maseru, pp. 48-56

Nixon PH, Boyd FR (1973b) The discrete nodule (megacryst) association in kimberlites from northern Lesotho. In: Nixon PH (ed.) Lesotho Kimberlites. Lesotho National Development Corporation, Maseru, pp. 67-75

Paterson MS (1982) The determination of hydroxyl by infrared absorption in quartz, silicate glasses and similar materials. Bull Mineral 105: 20-29

Richardson SH, Erlank AJ, Hart SR (1985) Kimberlite-borne garnet peridotite xenoliths from old enriched subcontinental lithosphere. Earth planet Sci Lett 75: 116-128

Ringwood AE (1975) The composition and petrology of the earth's mantle. McGraw-Hill, New York, 668 pp

Robey JV (1981) Kimberlites of the Central Cape Province, South Africa. Unpubl. Ph.D. Thesis, University of Cape Town

Rossman GR, Aines RD (1991) The hydrous components in garnets : grossular-hydrogrossular. Amer Mineral 76: 1153-1164

Rossman GR, Rauch F, Livi R, Tombrello TA, Shi CR, Zhou ZY (1988) Nuclear reaction analysis of hydrogen in almandine, pyrope and spessartite garnets. Neues Jahrb Mineral Monatshefte 1988 (4): 172-178

Sautter V, Harte B (1988) Diffusion gradients in an eclogite xenolith from the Roberts Victor kimberlite pipe: I. Mechanism and evolution of garnet exsolution in Al_2O_3-rich clinopyroxene. J Petrol 29: 1325-1352

Schulze DJ (1984) Cr-poor megacrysts from the Hamilton Branch kimberlite, Elliott County, Kentucky. In : Kornprobst J (ed.) Developments in Petrology, Vol 11B, Kimberlites II. The Mantle and Crust-Mantle Relationships. Elsevier, Amsterdam, pp 97-108

Schulze DJ (1987) Megacrysts from alkalic volcanic rocks. In: Nixon PH (ed) Mantle xenoliths. John Wiley and Sons, Chichester, pp 433-451

Schulze DJ (1989) Green garnets from South African kimberlites and their relationship to wehrlites and crustal uvarovites. In Kimberlites and Related rocks. Volume 2. Their mantle / crust setting, diamonds and diamond exploration. Geol Soc Australia spec Publ 14: 820-826

Skogby HS, Rossman GR (1991) The intensity of amphibole OH bands in the infrared absorption spectrum. Phys Chem Minerals 18: 64-68

Skogby H, Bell DR, Rossman GR (1990) Hydroxide in pyroxenes; variations in the natural environment. Amer Mineral 75: 764-774

Smith D, Boyd FR (1987) Compositional heterogeneities in a high temperature lherzolite nodule and implications for mantle processes. In: Nixon PH (ed) Mantle xenoliths. John Wiley & Sons, Chichester, pp. 551-561

Smyth JR, Bell DR, Rossman GR (1991) Hydroxyl in upper mantle clinopyroxenes. Nature 35: 732-735

Smyth JR, Caporuscio FA, McCormick TC (1989) Mantle eclogite: evidence of igneous fractionation in the mantle. Earth planet Sci Lett 93: 133-141

Van Calsteren PWC, Harris NBW, Hawkesworth CJ, Menzies MA, Rogers NW (1986) Xenoliths from southern Africa : perspectives on the lower crust. In: Dawson JB, Carswell DA, Hall J, Wedepohl KH (eds) The nature of the lower continental crust. Geol Soc spec Publ 24: 351-362

Waters FG 1987 A geochemical study of metasomatized peridotite and MARID nodules from the Kimberley pipes, South Africa. Unpubl. Ph.D. thesis, University of Cape Town

Wilkins RWT, Sabine W (1973) Water content of some nominally anhydrous silicates. Amer Mineral 58: 508-516

Winterburn PA, Harte B, Gurney JJ (1990) Peridotite xenoliths from the Jagersfontein kimberlite pipe: I. Primary and primary-metasomatic mineralogy. Geochim Cosmochim Acta 54: 329-341

Table 1. Garnet sample locations, paragenesis, compositions and OH contents.

Sample Number	Locality	Assemblage	Na_2O	MgO	Al_2O_3	SiO_2	CaO	TiO_2	Cr_2O_3	MnO	FeO[a]	P_2O_5	Total	$\int A$[b]	H_2O[c]	Source
Cr-poor megacrysts																
ROM263-GT02	Monastery, S.A.	gt	0.10	19.28	21.27	41.45	4.50	1.13	0.55	0.26	10.70	0.04	99.3	63.4	46	1
ROM263-GT03	Monastery, S.A.	gt	0.11	19.35	20.88	42.31	4.48	1.13	0.48	0.27	11.03	0.05	100.1	56.0	40	1
ROM263-GT04	Monastery, S.A.	gt	0.11	19.20	20.53	41.90	4.58	1.25	0.52	0.27	11.20	0.05	99.6	72.6	52	1
ROM263-GT06	Monastery, S.A.	gt	0.11	19.74	20.90	42.34	4.57	1.23	0.62	0.26	10.49	0.07	100.3	46.3	33	1
ROM263-GT09	Monastery, S.A.	gt	0.10	19.21	21.18	41.50	4.54	1.17	0.57	0.27	10.85	0.04	99.4	55.1	40	1
ROM263-GT10	Monastery, S.A.	gt	0.12	19.01	20.87	41.98	4.61	1.27	0.48	0.28	11.49	0.03	100.2	79.3	57	1
ROM263-GT25	Monastery, S.A.	gt	0.10	19.83	21.15	41.68	4.60	1.14	0.79	0.25	9.90	0.04	99.5	44.3	32	1
ROM263-GT31	Monastery, S.A.	gt	0.10	19.22	20.47	41.81	4.61	1.22	0.57	0.28	11.03	0.06	99.4	73.3	53	1
ROM263-GT34	Monastery, S.A.	gt	0.09	17.69	21.27	41.53	4.40	0.76	0.01	0.39	13.35	0.05	99.6	79.6	57	1
ROM263-GT36	Monastery, S.A.	gt	0.08	17.37	21.74	40.95	4.48	0.78	0.01	0.39	13.62	0.05	99.5	102.6	74	1
ROM263-GT44	Monastery, S.A.	gt	0.09	20.34	20.57	41.96	4.53	1.10	0.87	0.22	9.49	0.08	99.3	26.8	19	1
ROM263-GT49	Monastery, S.A.	gt	0.10	18.66	21.49	41.40	4.54	1.12	0.20	0.32	11.64	0.04	99.5	83.0	60	1
ROM263-GT52	Monastery, S.A.	gt	0.09	20.52	21.25	41.87	4.42	0.98	1.03	0.24	8.95	0.04	99.4	20.9	15	1
ROM263-GT68	Monastery, S.A.	gt	0.10	19.47	20.71	41.91	4.50	1.15	0.56	0.28	10.57	0.06	99.3	59.5	43	1
ROM263-GT71	Monastery, S.A.	gt	0.08	17.35	21.84	41.05	4.45	0.70	0.01	0.38	13.43	0.04	99.3	82.0	59	1
ROM263-GT75	Monastery, S.A.	gt	0.11	19.38	20.64	41.85	4.51	1.16	0.55	0.27	10.77	0.06	99.3	65.9	47	1
MON-9	Monastery, S.A.	gt	0.11	19.52	20.39	42.20	4.62	1.25	0.62	0.28	10.89	0.05	99.9	78.2	56	11
LAC-17	Lace, S.A.	gt	0.05	21.44	20.53	42.00	4.80	0.55	2.58	0.24	7.03	0.03	99.3	41.5	30	11
LAC-40	Lace, S.A.	gt	0.09	18.03	20.63	41.05	5.61	1.25	0.36	0.36	11.60	0.04	99.0	130.8	94	11
LAC-49	Lace, S.A.	gt	0.06	20.86	20.97	41.98	4.72	0.63	1.71	0.25	7.86	0.03	99.1	47.6	34	11
LAC-55	Lace, S.A.	gt	0.07	19.18	21.46	41.44	4.53	0.75	0.50	0.33	10.70	0.03	99.0	114.8	83	11

Table 1 - cont.

Sample Number	Locality	Assemblage	Na_2O	MgO	Al_2O_3	SiO_2	CaO	TiO_2	Cr_2O_3	MnO	FeO[a]	P_2O_5	Total	$\int A$[b]	H_2O[c]	Source
LAC-65	Lace, S.A.	gt	0.06	19.98	21.40	41.80	4.63	0.72	0.82	0.29	9.51	0.03	99.3	77.4	56	11
LAC-85	Lace, S.A.	gt	0.06	20.83	21.08	42.00	4.77	0.70	1.50	0.24	8.11	0.03	99.3	65.2	47	11
KLV-1	Kaalvallei, S.A.	gt	0.07	18.24	22.62	42.13	4.51	0.48	0.24	0.43	11.79	0.04	100.6	96.5	69	11
KLV-2	Kaalvallei, S.A.	gt	0.07	18.20	22.38	41.74	4.73	0.57	0.32	0.45	12.14	0.05	100.7	129.2	93	11
KLV-3	Kaalvallei, S.A.	gt	0.09	17.27	21.98	41.94	4.60	0.65	0.15	0.51	13.90	0.04	101.2	102.8	74	11
KLV-4	Kaalvallei, S.A.	gt	0.08	15.93	21.91	41.39	5.37	0.56	0.05	0.54	15.04	0.05	100.9	148.5	107	11
KLV-5	Kaalvallei, S.A.	gt	0.11	18.53	21.63	42.03	4.63	1.04	0.10	0.40	12.53	0.05	101.1	138.0	99	11
KLV-6	Kaalvallei, S.A.	gt	0.09	17.52	22.31	41.80	4.31	0.58	0.14	0.49	13.77	0.04	101.1	106.4	77	11
KLV-7	Kaalvallei, S.A.	gt	0.11	20.64	22.21	42.61	4.28	0.70	1.39	0.36	8.80	0.03	101.1	59.0	42	11
KLV-8	Kaalvallei, S.A.	gt	0.08	15.86	21.84	41.30	5.48	0.57	0.06	0.55	14.83	0.06	100.7	160.3	115	11
KLV-9	Kaalvallei, S.A.	gt	0.08	18.00	22.51	42.22	4.45	0.55	0.22	0.41	12.41	0.05	100.9	88.5	64	11
KLV-10	Kaalvallei, S.A.	gt	0.07	18.11	22.25	41.57	4.38	0.54	0.22	0.38	12.54	0.04	100.1	99.7	72	11
KLV-11	Kaalvallei, S.A.	gt	0.08	17.47	21.98	41.41	4.55	0.54	0.12	0.47	13.75	0.04	100.4	75.3	54	11
KLV-12	Kaalvallei, S.A.	gt	0.07	16.51	21.98	41.61	5.79	0.53	0.15	0.48	13.78	0.05	101.0	171.0	123	11
KLV-13	Kaalvallei, S.A.	gt	0.07	16.43	21.78	41.35	5.53	0.57	0.16	0.48	13.80	0.06	100.3	188.1	135	11
KLV-17	Kaalvallei, S.A.	gt	0.12	20.36	21.65	41.97	4.73	0.73	0.84	0.24	8.52	0.03	99.2	11.6	8	11
KLV-18	Kaalvallei, S.A.	gt	0.08	18.91	22.41	41.40	4.35	0.59	0.20	0.34	10.98	0.05	99.3	105.4	76	11
KLV-19	Kaalvallei, S.A.	gt												98.2	71	11
KLV-20	Kaalvallei, S.A.	gt												77.1	55	11
KLV-21	Kaalvallei, S.A.	gt	0.08	17.92	22.02	41.14	4.29	0.65	0.05	0.40	12.75	0.03	99.4	76.7	55	11
13-52-49	Kaalvallei, S.A.	gt	0.13	20.48	22.01	42.14	4.86	0.79	0.71	0.30	9.27	n.a.	100.7	3.9	3	2[e]
13-52-57	Kaalvallei, S.A.	gt	0.14	20.19	22.19	42.40	4.87	0.96	0.45	0.24	10.59	n.a.	102.0	38.1	27	2[e]
13-53-60	Kaalvallei, S.A.	gt	0.14	19.91	21.48	42.16	5.05	1.04	0.50	0.28	10.20	n.a.	100.8	48.5	35	2[e]
13-53-63	Kaalvallei, S.A.	gt	0.06	20.54	22.03	42.10	4.49	0.49	1.29	0.35	9.14	n.a.	100.5	138.0	99	2[e]

Table 1 - cont.

Sample Number	Locality	Assemblage	Na_2O	MgO	Al_2O_3	SiO_2	CaO	TiO_2	Cr_2O_3	MnO	FeO[a]	P_2O_5	Total	$\int A$[b]	H_2O[c]	Source
JJH-B15	Jagersfontein, S.A.	gt	0.11	20.29	21.38	41.59	4.41	0.98	1.05	0.26	8.98	n.a.	99.1	16.8	12	3[e]
JJH-B34	Jagersfontein, S.A.	gt	0.12	19.16	20.90	41.02	4.54	1.22	0.73	0.31	11.13	n.a.	99.1	70.2	51	3[e]
JJH-B72	Jagersfontein, S.A.	gt	0.11	19.81	21.52	41.22	4.46	1.10	0.68	0.28	10.78	n.a.	100.0	35.1	25	3[e]
KOH-1	Koherab, Namibia	gt	0.06	19.16	21.26	41.70	5.51	0.90	1.55	0.31	9.29	0.03	99.8	48.7	35	11
KOH-2	Koherab, Namibia	gt	0.07	18.44	21.69	41.34	5.62	1.10	0.44	0.32	10.05	0.02	99.1	101.9	73	11
KOH-3	Koherab, Namibia	gt	0.06	19.64	21.72	41.37	5.26	0.91	1.03	0.29	8.84	0.03	99.2	44.0	32	11
KOH-4	Koherab, Namibia	gt	0.07	19.29	21.89	41.54	5.42	1.06	0.59	0.33	9.27	0.03	99.5	51.8	37	11
KOH-5	Koherab, Namibia	gt	0.06	19.91	21.52	41.86	5.15	0.79	1.65	0.31	8.70	0.02	100.0	30.5	22	11
KOH-6	Koherab, Namibia	gt	0.05	20.12	21.56	41.88	5.21	0.66	1.87	0.28	8.06	0.03	99.7	18.1	13	11
KOH-24	Koherab, Namibia	gt	0.06	19.80	22.25	42.18	5.57	0.92	0.81	0.28	8.56	0.02	100.5	42.8	31	4
PHN-3986A	Malaita, Solomon Isl.	gt (alnoite host)	0.07	19.53	23.11	40.94	4.78	0.58	0.26	0.30	9.61	0.02	99.2	4.3	3	5
1493	Kerem Maharal, Israel	gt (basalt host)	0.03	16.34	22.87	40.99	5.55	0.62	0.00	0.39	13.54	0.03	100.4	0.4	<1	6
1495	Kerem Maharal, Israel	gt (basalt host)	0.03	16.35	22.89	40.84	5.56	0.67	0.02	0.38	13.60	0.03	100.4	0.0	0	6
GRR-1046	Chanthaburi, Thailand	gt (basalt host)												0.0	0	10
Eclogites																
390/4	Roberts Victor, S.A.	gt+cpx	0.06	9.78	21.43	40.28	9.55	0.19	0.05	0.34	18.38	0.01	100.1	0.0	0	4
CSRV-3	Roberts Victor, S.A.	gt+cpx	0.05	8.25	21.52	39.95	11.25	0.16	0.00	0.50	18.19	0.00	99.9	0.6	0	4
SRV-1	Roberts Victor, S.A.	gt+cpx+coes+san	0.07	7.41	21.98	40.31	18.45	0.17	0.04	0.29	11.12	0.06	99.9	9.8	7	8
KRV-2	Roberts Victor, S.A.	gt^i+cpx	0.10	14.19	22.24	40.85	4.30	0.31	0.13	0.58	17.60	0.03	100.3	27.5	20	4
KRV-7	Roberts Victor, S.A.	gt^i+cpx	0.15	10.14	21.68	40.48	12.34	0.32	0.79	0.28	13.99	0.08	100.3	46.1	33	4
HRV-272	Roberts Victor, S.A.	gt^i+cpx	0.13	10.39	21.60	40.42	12.90	0.31	0.94	0.22	12.89	0.09	99.9	24.6	18	4
JJG-14	Roberts Victor, S.A.	gt^i+cpx+ky	0.09	15.21	23.27	41.62	10.66	0.23	0.06	0.17	8.69	0.03	100.0	17.1	12	4
HRV-309	Roberts Victor, S.A.	gt^i+cpx+graph	0.09	18.54	23.11	41.98	3.14	0.30	0.04	0.36	12.08	0.03	99.7	13.8	10	4
HRV-67	Roberts Victor, S.A.	gt+cpx	0.04	13.88	22.75	41.25	8.95	0.10	0.21	0.32	12.30	0.00	99.8	0.0	0	4

Table 1 - cont.

Sample Number	Locality	Assemblage	Na_2O	MgO	Al_2O_3	SiO_2	CaO	TiO_2	Cr_2O_3	MnO	FeO[a]	P_2O_5	Total	$\int A$[b]	H_2O[c]	Source
HRV-147	Roberts Victor, S.A.	gt+cpx+ky	0.10	12.93	22.73	41.00	11.00	0.28	0.08	0.24	11.38	0.01	99.8	5.2	4	4
JJG-316	Roberts Victor, S.A.	gt[i]+cpx	0.12	14.32	22.82	41.25	6.71	0.31	0.08	0.44	13.82	0.05	99.9	23.6	17	4
HRV-173	Roberts Victor, S.A.	gt[i]+cpx	0.05	20.40	22.64	42.57	4.30	0.21	0.60	0.29	8.54	0.02	99.6	12.0	9	4
HRV-161A	Roberts Victor, S.A.	gt+cpx	0.06	18.78	23.19	41.94	3.81	0.12	0.20	0.22	11.51	0.06	99.9	0.0	0	4
XRV-5	Roberts Victor, S.A.	gt[i]+cpx	0.13	10.14	22.07	39.76	6.32	0.41	0.07	0.43	21.07	0.06	100.5	9.0	6	4
JJG-5	Roberts Victor, S.A.	gt[i]+cpx	0.04	15.46	22.60	40.87	5.78	0.16	0.26	0.35	14.51	0.00	100.0	3.7	3	4
RVC-22	Roberts Victor, S.A.	gt[i]+cpx	0.03	12.28	23.20	41.23	14.87	0.07	0.04	0.18	8.17	0.02	100.1	13.5	10	4
RVC-28	Roberts Victor, S.A.	gt+cpx	0.06	21.59	22.44	42.48	4.26	0.25	2.08	0.34	6.40	0.02	99.9	20.8	15	4
GRR-657	Roberts Victor, S.A.	gt+cpx+ky	0.12	10.28	22.67	40.29	13.40	0.33	0.03	0.23	12.52	0.04	99.9	0.0	0	9
FSM-15	Frank Smith Mine, S.A.	gt+cpx+ky+cor	0.12	9.83	22.62	40.40	15.42	0.31	0.05	0.17	10.97	0.04	99.9	0.0	0	4
KLV-25	Kaalvallei, S. A.	gt+cpx+dia	0.13	13.70	22.59	40.78	6.71	0.45	0.11	0.32	15.49	0.05	100.3	3.3	2	11
OPA-11	Orapa, Botswana	gt[i]+cpx+dia	0.10	13.31	22.40	40.62	7.72	0.48	0.06	0.60	15.00	0.09	100.4	7.3	5	4
LAC-86	Lace, S.A.	gt[i]+cpx+dia	0.10	11.25	23.54	40.92	16.29	0.16	0.02	0.13	7.86	0.13	100.4	22.9	16	11
STR-1	Star, S.A.	gt[i]+dia	0.08	10.98	23.00	40.04	14.80	0.13	0.02	0.15	8.86	0.06	98.1	24.2	17	11
P108-A	Premier, S. A.	inclusion in diamond	n.a.	17.30	22.70	40.80	3.24	0.51	0.13	0.32	14.50	n.a.	99.5	3.5	3	4[e]
RFT-1	Rietfontein, S.A.	gt+cpx+ky	0.03	9.23	22.72	40.28	13.73	0.10	0.02	0.25	13.85	0.02	100.2	74.8	54	4
RFT-2	Rietfontein, S.A.	gt+cpx+ky	0.03	9.15	22.76	40.54	13.71	0.11	0.02	0.26	14.00	0.02	100.6	70.8	51	4
RFT-3	Rietfontein, S.A.	gt+cpx	0.02	21.16	23.69	42.59	4.86	0.08	0.68	0.34	7.00	0.01	100.4	65.2	47	4
RFT-4	Rietfontein, S.A.	gt+cpx	0.03	20.56	23.59	42.49	4.42	0.11	0.60	0.37	8.31	0.02	100.5	120.0	86	4
RFT-5	Rietfontein, S.A.	gt+cpx+opx	0.04	19.15	23.27	42.10	3.94	0.14	0.70	0.36	10.91	0.02	100.6	96.3	69	4
RFT-6	Rietfontein, S.A.	gt+cpx	0.03	17.69	23.30	41.72	4.22	0.13	0.28	0.35	12.97	0.02	100.7	90.2	65	4
RFT-7	Rietfontein, S.A.	gt+cpx+opx	0.03	17.56	23.22	41.73	4.33	0.16	0.33	0.33	12.90	0.02	100.6	111.7	80	4
RFT-8	Rietfontein, S.A.	gt+cpx	0.03	20.33	23.77	42.51	4.08	0.13	0.12	0.41	9.15	0.02	100.6	63.6	46	4
RFT-9	Rietfontein, S.A.	gt+cpx	0.03	19.22	23.52	42.10	4.32	0.12	0.33	0.39	10.74	0.03	100.8	75.8	55	4

Table 1 - cont.

Sample Number	Locality	Assemblage	Na_2O	MgO	Al_2O_3	SiO_2	CaO	TiO_2	Cr_2O_3	MnO	FeO[a]	P_2O_5	Total	$\int A$[b]	H_2O[c]	Source
RFT-10	Rietfontein, S.A.	gt+cpx	0.03	18.93	23.52	42.18	3.95	0.10	0.18	0.27	11.52	0.03	100.7	73.5	53	4
RKL-1	Roodekraal, S.A.	gt[i]+cpx	0.02	9.86	22.55	39.84	12.52	0.07	0.06	0.35	14.38	0.01	99.7	61.5	44	4
RKL-2	Roodekraal, S.A.	gt[i]+cpx	0.02	9.90	22.60	40.20	12.61	0.07	0.07	0.31	14.40	0.02	100.2	32.0	23	4
JAR-02053	Lovedale, S.A.	gt[i]+cpx	0.05	11.39	22.49	40.38	8.70	0.14	0.12	0.40	16.36	0.05	100.1	12.6	9	4
LOV-1	Lovedale, S.A.	gt[i]+cpx+ky												23.1	17	4
JJG-2279	Markt, S.A.	gt[i]+cpx												18.2	13	4
Alkremites																
JAG-38	Jagersfontein, S.A.	gt[i]+sp+phl	0.04	18.10	23.26	41.94	7.71	0.15	0.34	0.39	8.08	0.06	100.1	69.2	50	4
KLV-24	Kaalvallei, S.A.	gti+sp+cor	0.03	15.99	23.38	41.82	10.90	0.06	0.10	0.23	7.51	0.05	100.0	120.0	86	11
Peridotites																
PMR-2	Premier Mine, S.A.	gt+ol+opx+cpx	0.02	22.09	20.00	42.29	4.73	0.27	4.79	0.23	5.63	0.01	100.1	1.4	1	11
PMR-5	Premier Mine, S.A.	gt+ol+opx+cpx[d]	0.11	21.14	20.12	41.99	4.66	1.36	2.59	0.25	7.65	0.03	99.9	20.3	15	11
PMR-6	Premier Mine, S.A.	gt+ol+opx+cpx[d]	0.10	21.03	20.66	41.85	4.60	1.22	2.05	0.24	7.81	0.04	99.6	26.0	19	11
PMR-9	Premier Mine, S.A.	gt+ol+opx+cpx[d]	0.13	20.82	17.59	41.46	5.28	1.66	5.60	0.27	7.06	0.04	99.9	27.6	20	11
PMR-11	Premier Mine, S.A.	gt+ol+opx+cpx[d]	0.11	21.29	18.35	41.75	5.20	1.32	5.27	0.27	6.49	0.04	100.1	33.0	24	11
PMR-20	Premier Mine, S.A.	gt+ol+opx+cpx[d]	0.12	20.77	17.55	41.45	5.30	1.55	5.90	0.24	7.00	0.04	99.9	37.3	27	11
PMR-27	Premier Mine, S.A.	gt+ol+opx+cpx[d]	0.06	21.51	20.58	42.19	4.68	0.68	3.22	0.24	6.87	0.03	100.1	20.3	15	11
PMR-45	Premier Mine, S.A.	gt+ol+opx+cpx[d]	0.04	21.58	20.79	42.26	4.70	0.25	3.39	0.23	6.47	0.02	99.7	7.4	5	11
PMR-46	Premier Mine, S.A.	gt+ol+opx+cpx	0.05	21.90	20.55	42.45	4.80	0.47	3.35	0.24	6.23	0.02	100.1	4.7	3	11
PMR-47	Premier Mine, S.A.	gt+ol+opx+cpx[d]	0.04	21.24	20.27	42.12	5.24	0.16	4.10	0.24	6.50	0.03	99.9	3.3	2	11
PMR-48	Premier Mine, S.A.	gt+ol+opx+cpx[d]	0.06	21.50	20.16	42.13	4.76	0.61	4.08	0.25	6.51	0.02	100.1	8.2	6	11
PMR-49	Premier Mine, S.A.	gt+ol+opx+cpx[d]	0.12	20.43	19.47	41.72	4.76	1.49	2.97	0.27	8.69	0.03	100.0	18.0	13	11
PMR-50	Premier Mine, S.A.	gt+ol+opx+cpx[d]	0.08	21.23	19.81	42.09	4.96	1.01	3.71	0.28	6.89	0.02	100.1	20.9	15	11
PMR-51	Premier Mine, S.A.	gt+ol+opx+cpx[d]	0.13	21.56	19.81	42.06	4.70	1.49	3.00	0.25	7.04	0.03	100.1	22.2	16	11

Table 1 - cont.

Sample Number	Locality	Assemblage	Na_2O	MgO	Al_2O_3	SiO_2	CaO	TiO_2	Cr_2O_3	MnO	FeO[a]	P_2O_5	Total	$\int A$[b]	H_2O[c]	Source
JJH-2	Jagersfontein, S.A.	gt[i]+ol+opx+cpx[d]	0.04	21.50	20.26	41.30	5.10	0.27	4.27	0.26	6.34	n.a.	99.3	13.5	10	3[e]
JJH-35	Jagersfontein, S.A.	gt+ol+opx+cpx[d]	0.01	19.46	19.22	40.93	6.10	0.10	6.27	0.30	6.94	n.a.	99.3	3.8	3	3[e]
JJG-1706	Jagersfontein, S.A.	gt[i]+ol+opx+cpx	0.04	21.54	20.12	42.16	4.96	0.21	4.07	0.26	6.22	0.06	99.6	6.2	4	4
JJG-1713	Jagersfontein, S.A.	gt[i]+ol+opx+cpx[d]	0.05	20.11	20.84	42.62	4.73	0.34	3.89	0.27	6.58	n.a.	99.4	15.9	11	3[e]
JJG-1728	Jagersfontein, S.A.	gt[i]+ol+opx+cpx	0.04	21.52	20.65	41.17	4.56	0.02	5.12	0.33	6.00	0.08	99.5	24.8	18	4
JJG-1738	Jagersfontein, S.A.	gt[i]+ol+opx+cpx	0.01	20.37	22.27	41.74	4.44	0.01	2.12	0.41	8.16	0.02	99.6	9.2	7	4
JJG-1751	Jagersfontein, S.A.	gt+ol+opx	0.01	23.69	18.41	41.86	2.29	0.10	7.74	0.27	5.32	0.03	99.7	4.1	3	4
JJG-1753	Jagersfontein, S.A.	gt+ol+opx+cpx[d]	0.09	20.93	22.04	42.17	4.44	0.66	1.86	0.24	8.14	n.a.	100.6	41.7	30	3[e]
BFT-6	Bultfontein, S.A.	gt[i]+ol+opx+chr+phl	0.04	20.95	20.33	42.18	5.26	0.08	4.81	0.33	6.38	0.06	100.4	13.4	10	11
BFT-17	Bultfontein, S.A.	gt[i]+ol+opx[d]	0.02	20.61	20.96	42.18	5.60	0.01	4.61	0.34	6.52	0.08	100.9	12.6	9	11
BFT-19	Bultfontein, S.A.	gt[i]+ol+opx+cpx	0.02	20.09	22.47	42.07	4.82	0.07	2.37	0.45	8.26	0.01	100.6	16.5	12	11
BFT-20	Bultfontein, S.A.	gt[i]+ol+opxd	0.02	23.77	22.33	43.03	2.63	0.01	3.24	0.26	5.37	0.02	100.7	8.4	6	11
BFT-21	Bultfontein, S.A.	gt[i]+ol+opx	0.03	22.73	21.97	42.35	3.84	0.04	3.44	0.27	5.68	0.03	100.4	11.0	8	11
BFT-66	Bultfontein, S.A.	gt[i]+ol+opx+cpx+phl	0.01	19.97	22.20	41.69	4.77	0.05	2.14	0.46	8.43	0.02	99.7	29.4	21	11
LAC-A	Lace, S.A."	gt xenocryst	0.03	18.99	17.17	41.57	7.36	0.08	9.60	0.45	6.23	0.04	101.5	2.1	2	7
LAC-B	Lace, S.A.	gt xenocryst	0.02	18.66	17.13	41.65	7.30	0.07	9.63	0.44	6.14	0.03	101.1	4.1	3	7
LAC-C	Lace, S.A.	gt xenocryst	0.03	19.00	17.55	41.75	6.99	0.07	9.08	0.45	6.26	0.03	101.2	<1.0	<1	7
LAC-D	Lace, S.A.	gt xenocryst	0.03	19.40	17.68	41.68	6.83	0.07	8.74	0.45	6.28	0.02	101.2	4.8	3	7
LAC-E	Lace, S.A.	gt xenocryst	0.01	25.23	20.49	43.22	1.18	0.01	5.80	0.23	4.89	0.02	101.1	1.9	1	7
LAC-F	Lace, S.A.	gt xenocryst	0.01	25.24	20.43	43.37	1.20	0.00	5.75	0.24	4.60	0.00	100.9	10.4	7	7
LAC-G	Lace, S.A.	gt xenocryst	0.01	25.21	20.43	43.25	1.19	0.01	5.80	0.25	4.78	0.01	100.9	2.8	2	7
LAC-H	Lace, S.A.	gt[i] xenocryst	0.01	20.39	20.23	42.39	5.58	0.00	5.52	0.38	6.91	0.00	101.4	5.7	4	7
LAC-I	Lace, S.A.	gt[i] xenocryst	0.02	20.63	20.10	42.26	5.22	0.01	5.87	0.37	6.82	0.02	101.3	10.9	8	7
F99B	Finsch, S.A.	inclusion in diamond	n.a.	24.10	19.10	42.00	1.37	0.00	7.31	0.35	5.77	n.a.	100.0		<15	4[e]

Table 1 - cont.

Sample Number	Locality	Assemblage	Na_2O	MgO	Al_2O_3	SiO_2	CaO	TiO_2	Cr_2O_3	MnO	FeO[a]	P_2O_5	Total	$\int A^b$	H_2O^c	Source
BBB-16	Bobbejaan, S. A.	gt+cpx+chr+phl	0.03	19.81	18.66	41.95	5.25	0.06	6.39	0.44	7.64	0.07	100.3	43.5	31	4
BBB-14	Bobbejaan, S. A.	gt+cpx+chr+phl	0.03	19.70	18.80	42.13	5.48	0.06	6.32	0.38	7.46	0.08	100.5	41.2	30	4
WTV-1	Weltevreden, S.A	gt+cpx+chr+phl	0.02	14.26	15.37	40.09	13.86	0.28	9.79	0.37	5.71	0.04	99.8	113.8	82	11
LRA-1	Louwrensia, Namibia	gt+ol+opx+cpx+chr[d]	0.01	20.30	20.64	41.99	4.94	0.34	2.68	0.35	9.14	n.a.	100.4	16.4	12	11
LRA-2	Louwrensia, Namibia	gt+ol+opx+cpx	0.02	20.88	22.29	42.52	4.78	0.09	2.59	0.35	7.68	0.00	101.2	3.5	3	11
LRA-3	Louwrensia, Namibia	gt[i]+ol+opx+cpx	0.03	20.55	21.44	42.32	5.09	0.28	3.45	0.38	7.73	0.03	101.3	28.2	20	11
LRA-4	Louwrensia, Namibia	gt+ol+opx+cpx[d]	0.03	20.98	20.91	42.25	5.02	0.49	4.12	0.31	7.17	0.06	101.3	16.7	12	11
LRA-5	Louwrensia, Namibia	gt+ol+opx+cpx	0.01	20.24	21.71	42.59	5.29	0.04	3.28	0.40	7.95	0.00	101.5	9.7	7	11
LRA-6	Louwrensia, Namibia	gt+ol+opx+cpx	0.03	20.90	21.89	42.68	4.80	0.24	2.90	0.37	7.67	0.02	101.5	19.2	14	11
LRA-7	Louwrensia, Namibia	gt+ol+opx+cpx	0.02	20.00	20.70	42.37	5.60	0.07	4.59	0.41	7.69	0.01	101.5	3.5	3	11
LRA-8	Louwrensia, Namibia	gt[i]+ol+opx+cpx	0.02	20.19	21.73	42.50	5.25	0.04	3.17	0.39	8.04	0.05	101.4	14.7	11	11
LRA-9	Louwrensia, Namibia	gt+ol+opx+cpx[d]	0.04	20.45	21.09	42.38	5.19	0.30	3.81	0.38	7.80	0.03	101.5	26.0	19	11
LRA-10	Louwrensia, Namibia	gt+ol+opx+cpx	0.07	21.11	20.11	42.39	5.56	0.81	4.55	0.29	6.50	0.02	101.4	14.5	10	11
LRA-11	Louwrensia, Namibia	gt+ol+opx+cpx	0.05	21.09	21.99	42.80	4.73	0.29	2.62	0.36	7.50	0.01	101.4	15.2	11	11
LRA-12	Louwrensia, Namibia	gt+ol+opx+cpx	0.03	20.62	22.17	42.55	4.81	0.13	2.52	0.35	8.09	0.02	101.3	16.4	12	11
LRA-13	Louwrensia, Namibia	gt+ol+opx+cpx+chr	0.01	19.76	18.99	42.07	6.60	0.07	6.80	0.39	6.78	0.07	101.6	16.0	12	11
LRA-14	Louwrensia, Namibia	gt+ol+opx+cpx	0.03	20.62	21.28	42.40	5.24	0.30	3.63	0.35	7.46	0.04	101.4	30.3	22	11
LRA-15	Louwrensia, Namibia	gt[i]+ol+opx+cpx	0.01	20.21	21.77	42.56	5.27	0.07	3.18	0.40	8.00	0.01	101.5	8.0	6	11
LRA-16	Louwrensia, Namibia	gt[i]+ol+opx+cpx	0.01	20.10	21.25	42.57	5.57	0.02	3.97	0.41	7.65	0.02	101.6	18.3	13	11
LRA-17	Louwrensia, Namibia	gt[i]+ol+opx+cpx	0.01	20.16	21.53	42.52	5.48	0.03	3.51	0.38	7.72	0.00	101.3	8.4	6	11
LRA-18	Louwrensia, Namibia	gt[i]+ol+opx+cpx	0.01	20.30	21.53	42.49	5.35	0.06	3.43	0.38	7.70	0.01	101.3	11.4	8	11
LRA-20	Louwrensia, Namibia	gt+ol+opx+cpx	0.01	20.44	21.79	42.53	5.20	0.04	3.20	0.39	7.73	0.00	101.3	20.4	15	11
LRA-21	Louwrensia, Namibia	gt+ol+opx+cpx[d]	0.04	20.53	20.71	42.40	5.23	0.29	4.28	0.38	7.44	0.03	101.3	19.6	14	11
LRA-23	Louwrensia, Namibia	gt+ol+opx+cpx+chr[d]	0.03	20.94	20.33	42.25	5.38	0.42	4.86	0.33	6.48	0.04	101.1	20.9	15	11

Table 1 - cont.

Sample Number	Locality	Assemblage	Na_2O	MgO	Al_2O_3	SiO_2	CaO	TiO_2	Cr_2O_3	MnO	FeO[a]	P_2O_5	Total	$\int A$[b]	H_2O[c]	Source
LRA-24	Louwrensia, Namibia	gt+ol+opx+cpx	0.02	21.09	22.26	42.76	4.78	0.06	2.62	0.35	7.38	0.01	101.3	5.6	4	11
KOH-7	Koherab, Namibia	gt[i]+ol+opx	0.01	19.68	20.94	42.31	6.05	0.02	4.38	0.40	7.34	0.00	101.1	0.1	<1	11
KOH-8a	Koherab, Namibia	Cr-rich gt nodule	0.02	19.31	20.00	41.93	6.32	0.10	5.30	0.39	7.15	0.01	100.5	3.1	2	11
KOH-8d	Koherab, Namibia	Cr-rich gt nodule	0.02	18.73	19.09	41.80	6.66	0.10	6.63	0.46	7.53	0.01	101.0	3.1	2	11

[a] All Fe expressed as FeO; [b] Integrated absorbance in cm^{-1} of the OH bands between 3300 cm^{-1} and 3700 cm^{-1} per cm sample thickness; [c] OH content expressed as ppm H_2O by weight; [d] deformed texture; [e] : analysis provided by sample donor; [i] garnet contains microscopic inclusions (described in text). Sample sources: 1. R. O. Moore (Univ. Cape Town) 2. D. J. Schulze (Univ. Toronto) 3. J. J. Hops (Univ. Cape Town) 4. J. J. Gurney (Univ. Cape Town) 5. P. H. Nixon (Leeds Univ.) 6. M. Stein (Hebrew Univ., Jerusalem) 7. G. H. Read (Anglo American Corporation) 8. J. R. Smyth (Univ. Colorado) 9. P. Grew (Univ. Minnesota) 10. L. T. Silver (Caltech) 11. Collected by DRB.

Abbreviations: chr - chromite; coes - coesite; cor - corundum; cpx - clinopyroxene; dia - diamond; graph - graphite; gt - garnet; ky - kyanite; ol - olivine; opx - orthopyroxene; phl - phlogopite; san - sanidine; sp - Al-spinel.

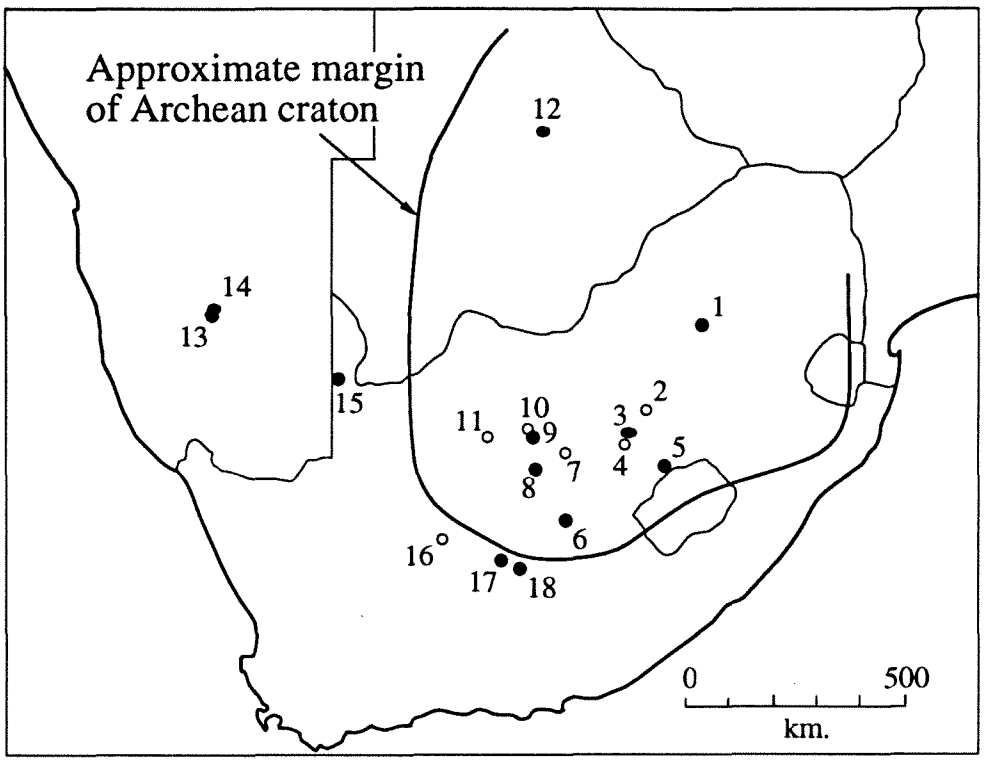

Figure 1. Map of southern Africa showing location of kimberlites yielding xenoliths for this study and their relationship to the Archean Kaapvaal Craton. Filled circles represent type I ("basaltic") kimberlites and open circles type II (micaceous) kimberlites. 1. Premier; 2. Lace; 3. Kaalvallei; 4. Star; 5. Monastery; 6. Jagersfontein; 7. Roberts Victor; 8. Bultfontein; 9. Frank Smith / Weltevreden; 10. Bobbejaan (Bellsbank group); 11. Finsch; 12. Orapa; 13. Koherab; 14. Louwrensia; 15. Rietfontein; 16. Markt; 17. Lovedale; 18. Roodekraal.

Figure 2. Representative infrared absorption spectra of southern African mantle-derived garnets in the region 3000 - 4000 wavenumbers. All spectra are normalized to a sample thickness of one millimeter and are offset vertically for clarity. The broad absorption rising towards higher wavenumbers is due to an electronic transition in Fe^{2+}. Details of the spectral features are discussed in the text. Megacrysts : (a) KLV-13, Kaalvallei (b) ROM263-GT36, Monastery (c) ROM263-GT04, Monastery (d) LAC-40, Lace (e) ROM263-GT-09, Monastery. Eclogite garnets : (f) RFT-2 kyanite eclogite, Rietfontein (g) KRV-7 eclogite, Roberts Victor (h) RFT-4 eclogite, Rietfontein (i) CSRV-3 eclogite, Roberts Victor. Peridotite garnets : (j) BFT-6 coarse garnet harzburgite, Kimberley (k) PMR-11 deformed garnet lherzolite, Premier (l) LRA-9 deformed garnet lherzolite, Louwrensia. Other garnets : (m) BBB-14 large Cr-rich garnet, Bobbejaan (n) JAG-38 phlogopite-bearing alkremite, Jagersfontein (o) WTV-1 green garnet xenocryst, Weltevreden (p) GRR1134-C3 purple garnet xenocryst, Garnet Ridge, Arizona.

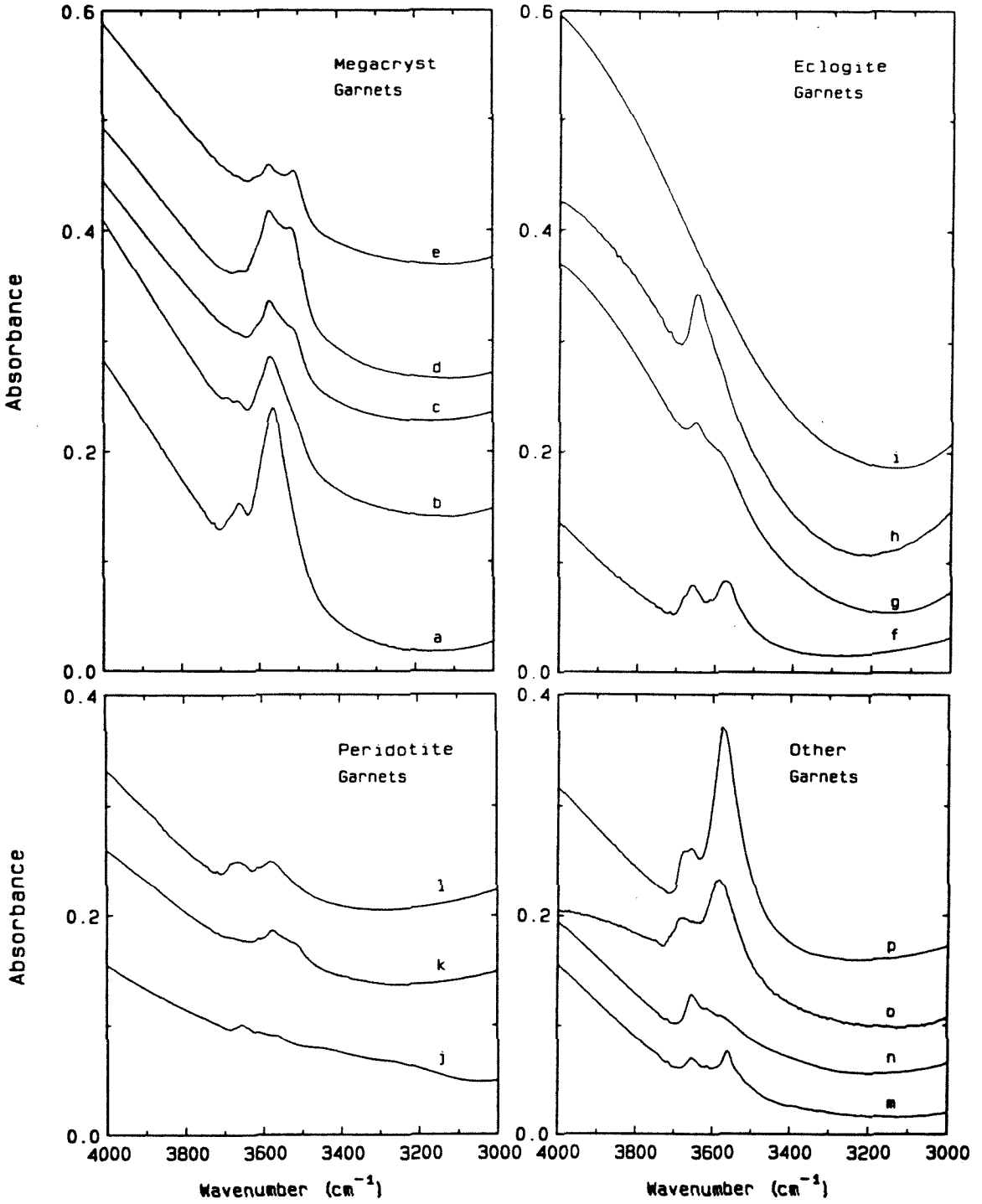
Megacryst
Garnets
Eclogite
Garnets
Peridotite
Garnets
Other
Garnets
Absorbance
Absorbance
Wavenumber (cm⁻¹)
Wavenumber (cm⁻¹)
a
b
c
d
e
f
g
h
i
j
k
l
m
n
o
p
0.0
0.2
0.4
0.6
4000
3800
3600
3400
3200
3000

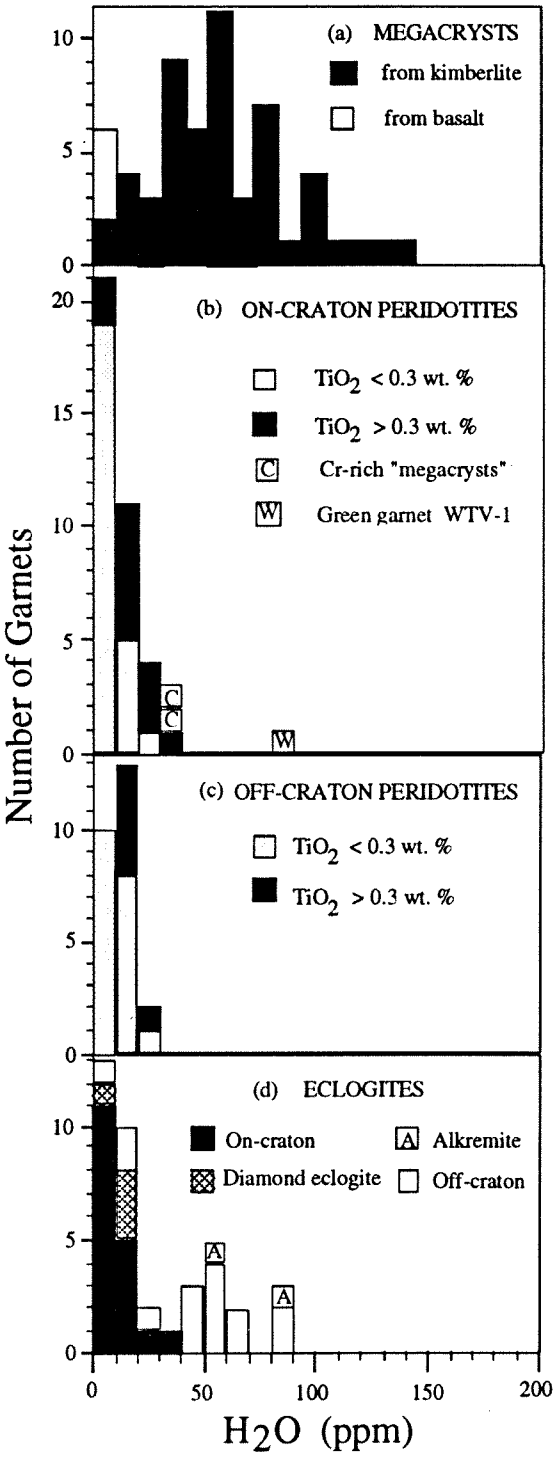

Figure 3. Histograms illustrating the distribution of abundances of OH, expressed as ppm H_2O, in different mantle xenolith types from southern African kimberlites.

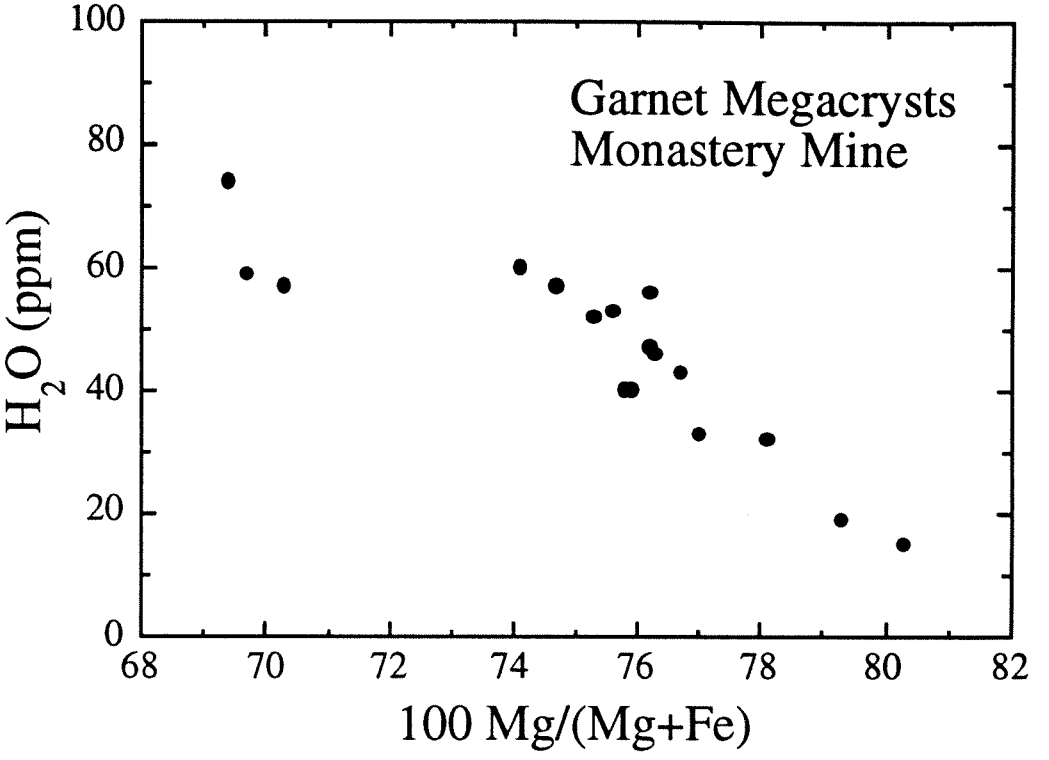

Figure 4. The variation of OH (expressed as ppm H_2O) in Cr-poor megacryst garnets of the Monastery Mine as a function of Mg number of garnet. Water content increases to the left of the diagram as the Mg number decreases during progressive fractionation of the parental megacryst magma.

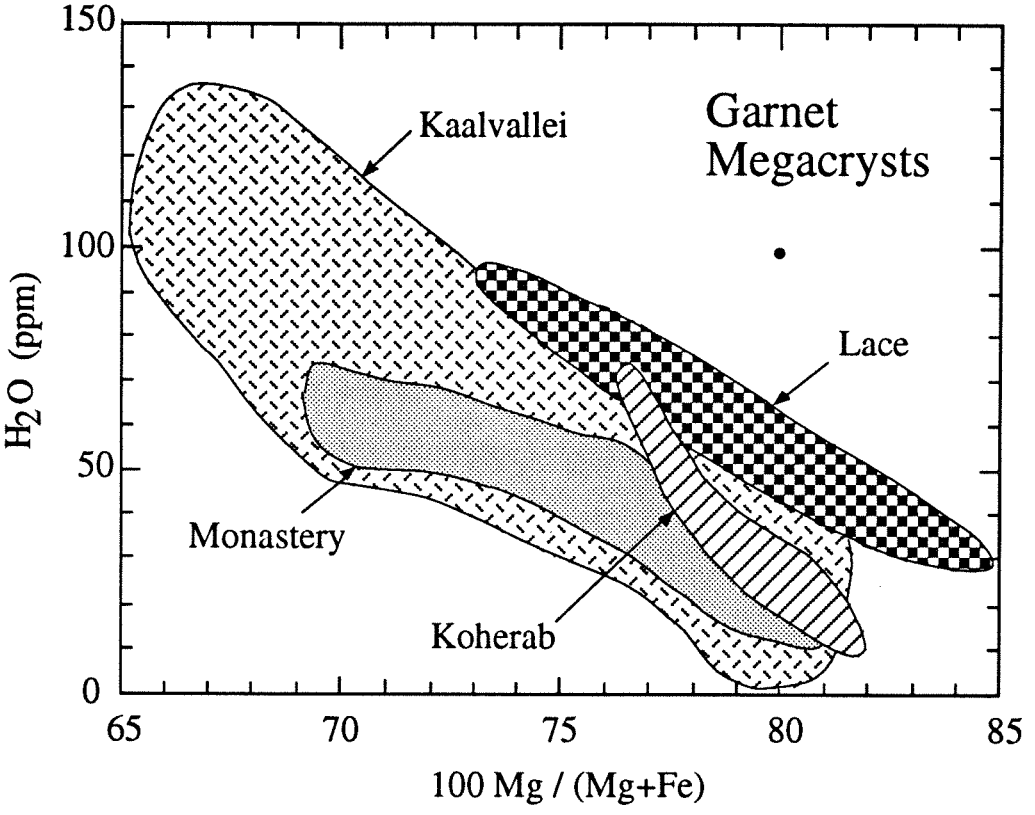

Figure 5. OH concentration (expressed as ppm H_2O) as a function of Mg number for several southern African garnet megacryst suites. Notable features are the consistency of the inverse correlations and the relatively high OH contents of the group II Lace kimberlite megacrysts. The outlying data point at high H_2O and Mg number is sample 13-53-63 from the Kaalvallei kimberlite.

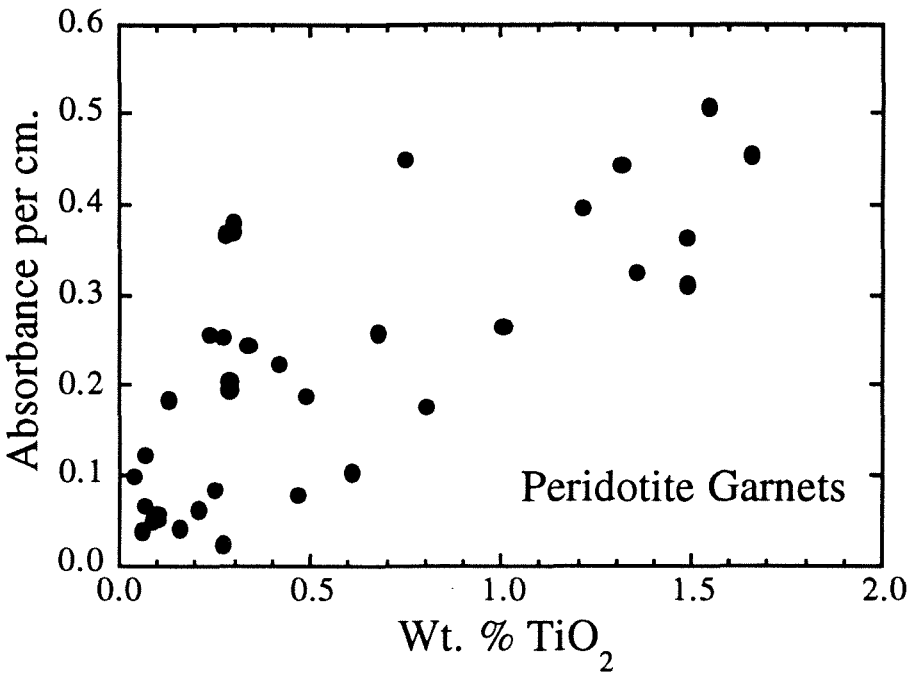

Figure 6. Summed absorption intensity of the main OH band near 3570 cm^{-1} and the 3512 cm^{-1} OH band plotted vs. TiO_2 content of the garnet for peridotite garnets from the Louwrensia, Jagersfontein and Premier kimberlites. The summed absorption intensity is proportional to OH content and demonstrates the positive correlation between H and Ti contents in these garnets. Only data for garnets free of microscopic inclusions, and the spectra of which indicate no contamination by possible non-structural OH, have been plotted.

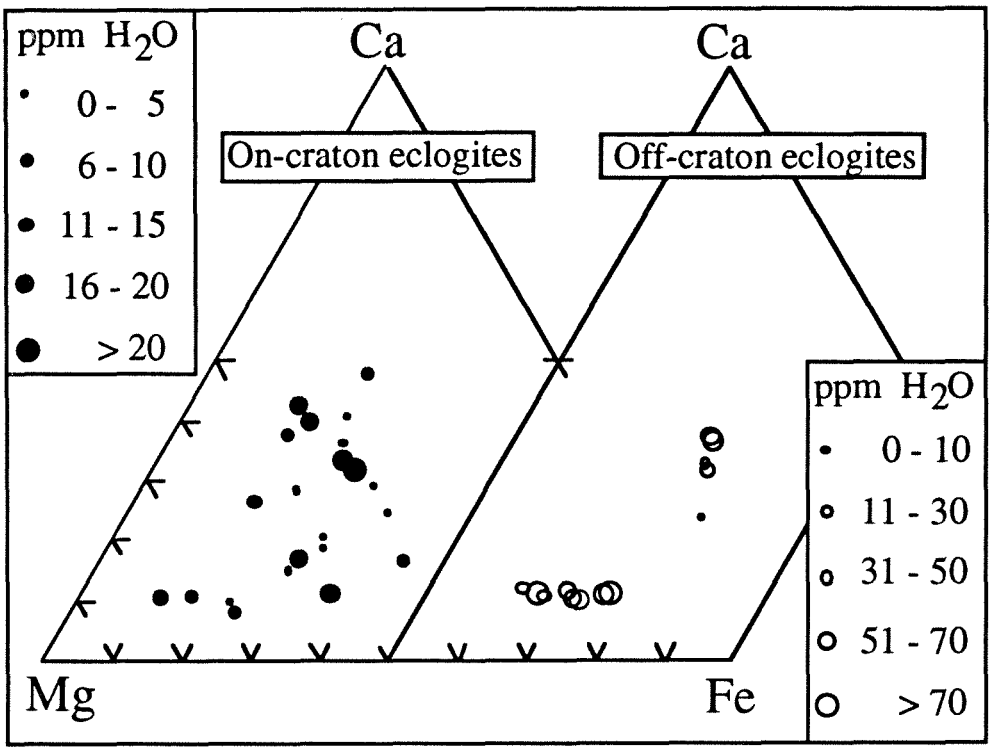

Figure 7. Compositions of eclogite garnets analyzed in this study expressed as atomic proportions of Ca, Mg and Fe, with OH contents illustrated by relative size of plotted symbols.

Chapter 2. Water in Earth's mantle: the role of nominally anhydrous minerals.

Abstract

Most minerals of the Earth's upper mantle contain small amounts of hydrogen, structurally bound as hydroxyl (OH). The OH concentration in each mineral species is variable, in some cases reflecting the geological environment of mineral formation. Of the major mantle minerals, pyroxenes are the most hydrous, typically containing ~200 to 500 ppm H_2O by weight, and probably dominate the water budget and H geochemistry of mantle rocks that do not contain a hydrous phase. Garnets and olivines commonly contain ~1 to 50 ppm. Nominally anhydrous minerals constitute a significant reservoir for mantle H, possibly accommodating all water in the depleted mantle, and providing a possible mechanism to recycle water from the Earth's surface into the deep mantle.

Geologists recognize that water (1) has an important influence on the behaviour of molten rock systems. The variability in style and vigor of volcanic eruptions is just one manifestation of this effect. Small amounts of water or hydroxyl (OH) may also enter the structure of many minerals, the chemical formulae of which indicate that they are anhydrous. These hydrous components can have a disproportionately large influence on the physical and chemical properties of silicate minerals. They may modify the mechanical strength of the host phase, increase its internal rate of ionic diffusion (2), modify its dielectric properties (3), influence its rate of weathering (4), change its response to radiation damage (5), influence its optical properties, and modify its stoichiometry.

Interest in the hydrous components in nominally anhydrous minerals was stimulated by early studies of the influence of water on the mechanical strength of quartz (6), one of the commonest nominally water-free minerals of the Earth's crust. Spectroscopic studies showed that quartz can contain both water molecules and hydroxyl groups, and that the hydroxyl groups were crystallographically oriented, as evidenced by their anisotropic absorption of infrared radiation (7). Subsequently, infrared spectroscopic studies of a variety of minerals demonstrated that a trace amount of OH is a common constituent of most rock-forming minerals of the Earth's crust and upper mantle (8, 9) (Table 1).

Although the concentrations of OH (typically tens to hundreds of parts per million H_2O by mass) in nominally anhydrous minerals are often too low to allow the acquisition of precise structural information, the OH is easily detected by infrared spectroscopy and can be quantified (10). Systematic studies of the variability of OH content of nominally anhydrous minerals of natural origin have consistently revealed that for any given mineral species, those samples of high-pressure or mantle origin are commonly among the most hydrous examples. While the list of anhydrous minerals containing structurally-bound OH continues to grow, greater emphasis on quantitative analysis is needed in constraining

water in the mantle (10). In this article, we report measurements of concentrations of this form of hydrogen in minerals and rocks from the Earth's mantle and discuss the implications for the geochemistry of water in the Earth's interior.

The problem of water in the mantle

Determination of the Earth's water budget and identification of suitable repositories for H (colloquially "water") in the mantle are long-standing problems in geology with important implications for evolution of the planet as a whole. An early conclusion that the oceans and atmosphere have accumulated throughout Earth's history by progressive degassing of the interior (11) drew attention to the need for suitable storage sites for water in the mantle. More recent studies have implicated early catastrophic degassing (12), possibly contemporaneous with accretion (13), in the formation of the atmosphere and oceans, and the importance of recycling (14) in the geochemical cycles of the Earth's volatile constituents. Because of the important role of the mantle in degassing and recycling processes, an appreciation of the concentrations and chemical speciation of these volatile components in the mantle is imperative if we are to understand the evolutionary history of the atmospheres and oceans, and their links to reservoirs of volatiles in the Earth's interior.

The variable, but ubiquitous occurrence of water in mantle-derived magmas, and the occurrence of hydrous minerals such as mica and amphibole in samples of the mantle brought up as xenoliths in volcanic eruptions, testify to the presence of water in the upper mantle. This water can be present as OH in minerals, or as a free vapor phase, or be dissolved in a silicate or carbonate melt (15). Among the candidate mineral phases for water storage in the mantle are a number of dense, OH-bearing magnesium silicates, that have either been synthesized in high-pressure experiments (16) or been predicted to occur

on the basis of cystal-structure systematics (17). However, it remains to be demonstrated that these phases would be stable under the temperature and bulk compositions prevailing in the upper mantle. In addition to these stoichiometrically hydrous minerals, the ß-spinel polymorph of Mg_2SiO_4 has also been proposed as a possible repository for mantle water (18).

Importance of structural OH in the mantle The water contained in minerals with hydroxyl as an essential structural component, such as micas and clay minerals, dominates the water content of most crustal rocks, because the concentrations of OH in these minerals are typically orders of magnitude greater than those in the nominally anhydrous minerals. However, because of the volatility of water, these stoichiometrically hydrous minerals break down to anhydrous minerals plus a free vapor phase at the high temperatures of most of the mantle. Although the stability ranges of some hydrous minerals, such sodium- or potassium-bearing amphiboles and micas persist into the mantle, their abundance, and hence their water-storing capacity, is limited by the low alkali content of average mantle rocks. In contrast, nominally anhydrous, OH-bearing minerals such as pyroxenes, olivine, and garnet, which probably make up most of the upper mantle, have a wide pressure-temperature stability range and no special compositional requirements. Their relative importance as repositories of mantle H may therefore be considerable.

Besides the global geochemical consequences, OH in minerals of major abundance, such as olivine, appears to have important implications for the physical properties of planetary mantles, and several recent studies have addressed the effects of water and OH on the rheology of olivine (19). The presence of hydrogen in olivine has also been proposed to account for the electrical conductivity of the Earth's upper mantle (20).

Initial indications of the potential importance of OH substitution in anhydrous mantle minerals were provided by both experimental (21) and theoretical (22, 23) investigations. The known replacement of SiO_4 by $(OH)_4$ in garnets of the hydrogrossular series provided

an attractive substitutional mechanism (the "hydrogarnet substitution") for OH incorporation in all the anhydrous silicates, and was suggested by several workers (22, 24) to play an important role in the mantle. The importance of this substitution for mantle water was questioned by others (23, 25), however, and multiple substitutional mechanisms for H are indicated for many natural garnets on infrared spectroscopic and other grounds (26, 27). These probably include substitution of single OH groups for oxygen anions, the mechanism suggested by Martin and Donnay (23) to be important for water storage in the mantle.

Despite the numerous conjectures, few studies of the water contents of actual mantle rocks have been attempted, and our best current measurements of mantle water abundances (a few hundred parts per million) come from studies of mantle melting products in the form of quenched submarine basaltic glasses (28, 29, 30). However, these studies are rarely, if ever, able to identify the host phase for water in the mantle.

Concentrations of structural OH in mantle minerals

A number of studies have reported infrared data on OH (or lack thereof) in individual minerals of mantle origin. These include garnet (31, 32, 33), olivine (34, 35), pyroxenes (36, 37), kyanite (38, 39, 40), rutile (39, 40, 41), zircon (42), corundum, sanidine, and coesite (39), and H in diamond (43). We determined OH concentrations in 216 mineral samples of mantle origin by infrared spectroscopy (Figure 1). The sample preparation and IR spectroscopic procedures follow methods outlined previously (31, 35, 36). Almost all samples are from xenoliths of mantle xenoliths in kimberlites and alkali basalts. To supplement these data, we have compiled 115 (53 mantle-derived and 62 crustal samples) determinations of OH concentration from the literature, some of which we have revised using the preferred set of calibrations [see (10)]. The concentration data (Figure 2) show

that OH abundances in nominally anhydrous mantle minerals from different petrological environments (rock types) range from less than 1 ppm to on the order of 1000 ppm H_2O.

The large number of garnets (185) reveal a wide range of OH concentrations (<1 to 200 ppm H_2O), with most containing less than 60 ppm H_2O. The OH contents display a number of interesting petrological correlations, which are discussed elsewhere (33). Of particular interest is our confirmation of the observation (32) that garnets from the mantle beneath the Colorado Plateau of the southwestern United States have OH contents that are invariably more hydrous (by about a factor of 2) than garnets from the mantle regions below southern Africa. All orthopyroxenes analyzed contain significant amounts of OH, with most falling in the range of 100 to 450 ppm. The highest OH concentrations are recorded in orthopyroxenes from coarse-grained garnet peridotites, which may have reacted with hydrous fluids in the mantle (metasomatism). In addition to OH in the pyroxene structure reported in Table 2, the IR spectra of these orthopyroxenes indicate the presence of OH in amphibole lamellae.

Clinopyroxenes of varying composition, including diopsides, omphacites and augites, are all significantly OH-bearing, and omphacites, particularly those with cation vacancies (37), display the greatest OH absorption intensities (44). The greatest OH concentration in a mantle diopside (about 580 ppm H_2O) was observed in a Cr-rich megacryst from Kimberley, South Africa. Clinopyroxene is typically the most OH-rich mineral of major volumetric importance in the mantle rocks studied. Olivines show a considerable range in OH concentration (<1 to >100 ppm H_2O). Olivines from garnet peridotites typically contain more OH than those from spinel lherzolites (45). The highest OH content found to date in a mantle olivine is from an Fe-rich olivine megacryst from the Monastery kimberlite, South Africa (Fig. 2c)(46).

Some phases apparently incorporate very little OH. We have detected no OH in spinels from spinel peridotites and two alkremites (garnet + spinel ± corundum rocks), but

detection limits are high because of interference from absorptions due to tetrahedral Fe^{2+} in the OH region. An earlier study (39) detected no OH in coesite or corundum, and we have confirmed this result on corundum from eclogites and an alkremite.

Among the other accessory phases, rutile exhibits extremely strong OH absorptions, particularly in those samples from highly metasomatized environments (41) which are rich in hydrous minerals. Our and other (39) data on rutile in eclogite suggest that this phase can accommodate considerable amounts of OH, although its modal abundance is usually less than 1%. Although the presence of considerable OH is indicated, a suitable quantitative calibration for OH in this mineral remains to be determined. The apparently high OH contents of rutile suggest that its structural analogue, stishovite, may be similarly hydrous and act as a possible H reservoir, if it occurs in the mantle. Zircon, which is believed to belong to the megacryst suite (48), an assemblage of coarsely crystalline minerals probably formed by crystallization of a magma at high pressure, is routinely hydrous at the 50 to 100 ppm level, but its rarity in the mantle renders it of little consequence for storing significant amounts of OH. Kyanite exhibits a range of OH contents, from 50 to 200 ppm, which is correlated with host rock type (40).

Stability of OH in minerals during transport from mantle to the surface. An unresolved issue is the degree to which the OH contents of nominally anhydrous minerals are perturbed during their transport to the surface in volcanic eruptions. It is possible that some hydrogen has been lost by oxidation reactions (49), such as have been recognized to occur in amphiboles (50), particularly in the samples that were contained in basalt flows. At the present stage, we can not rule out the possibility that the OH contents of some mineral samples have been perturbed to some degree by post-mantle processes. On the other hand, the numerous correlations of mineral water content with petrological environment (xenolith type) for samples with similar transport and eruption histories suggest that source information is preserved. The stability of the hydrous component in

synthetic pyrope has been demonstrated up to 50 kbar and 1100 °C (51). More studies on the OH content of synthetic and natural minerals equilibrated under known conditions are required to evaluate the stability of the hydrous components and their kinetic response to changes in external conditions.

The water content of the mantle

Mantle peridotites. We have calculated the OH concentrations in the anhydrous mineral fractions of seven peridotites and four eclogites by analysis of their constituent phases and modal proportions. Details of the mineral concentrations and assumptions made, together with the calculated concentrations, are reported in Table 2. In peridotites, these range from 28 ppm H_2O in a spinel lherzolite from West Kettle River, British Columbia, to 175 ppm in a coarse-grained garnet lherzolite from Jagersfontein, South Africa. Many of the samples are derived from the lithospheric mantle beneath continents, which has had a complex geological history, and it is thus not clear how representative these samples are of the upper mantle. Nevertheless, the data indicate that the nominally anhydrous minerals in this region of the mantle can hold at least 175 ppm H_2O.

In many kimberlite-derived, coarse-grained garnet lherzolites the OH in anhydrous minerals may be subordinate to water bound in phlogopite and amphiboles, which are relatively common hydrous phases. However, these hydrous minerals are unevenly distributed, and where they are absent the water concentrations reported here may represent something close to the total water content of the peridotitic continental upper mantle. The much higher OH concentrations in peridotitic garnets from the Colorado Plateau suggest that water concentrations may be particularly high in some regions of the subcontinental mantle. Hydrous minerals are common in mantle samples from this region (52), and the inferred high water content of this region of the mantle is quite possibly related to the

subduction of wet oceanic lithosphere at a shallow angle beneath western North America during the late Cretaceous and early Tertiary (53).

High-temperature deformed garnet peridotites from kimberlites typically do not contain primary hydrous minerals, and most of their water budget is probably held in anhydrous minerals, although fluid and melt inclusions may play a role (54). These peridotites appear to be related to the megacrysts in kimberlites (55), possibly having equilibrated to variable degrees with the hydrous, incompatible element-rich megacryst magmas. Thus these peridotites and the kimberlite-hosted megacrysts may represent local areas of increased water activity.

Water in the depleted upper mantle (MORB source region). Recent estimates of mantle water contents from basalt glasses (29, 30) are in the range of 100 to 200 ppm H_2O for a normal mid-ocean ridge basalt (N-MORB) source. This amounts to approximately 10% of the present ocean mass, if this source region is assigned to the upper 670 km of the mantle. The data in Table 2 show that the minerals olivine, orthopyroxene, clinopyroxene and garnet, which probably constitute 99% or more of this source region, can accommodate much or all of this water. If we reconstitute a spinel or garnet lherzolite using estimates of the modal abundances in primitive upper mantle (56) and assign to each mineral the greatest OH abundance measured in this study (an indication of the minimum possible saturation level for OH in these phases), then the resulting concentrations of 245 ppm H_2O (garnet lherzolite) or 290 ppm H_2O (spinel lherzolite) suggest that it is possible to contain all the water in the N-MORB source in the nominally anhydrous minerals.

If N-MORB is produced by somewhere between 5 and 25% melting of peridotite, and we assume a bulk distribution coefficient for water between basalt and solid residue of 0.01 (57) then the residual peridotite after basalt extraction is predicted to contain in the vicinity of 5 to 35 ppm H_2O. The higher concentrations measured in most of our samples suggest

that these rocks are either residues of more hydrous partial melting events, such as might be expected above subduction zones, or have seen later introduction of H. The lowest peridotite OH contents (28 ppm H_2O) were observed in a spinel lherzolite xenolith from the West Kettle River, British Columbia. Xenoliths from this locality are believed to have originated in the oceanic mantle (58), and our sample WKR may represent a region of the mantle that has been little influenced by later hydrous processes.

Water in undepleted or enriched mantle. The water contents of relatively undifferentiated basaltic magmas of ocean islands such as Hawaii and enriched (E-type) MORB are typically higher than those of N-MORB and have been estimated to be in the region of 0.35% (29, 59). For a distribution coefficient of ~0.01 for water and 5 to 15% partial melting, the water content of this source region is calculated to be in the range of 200 to 550 ppm, and is rather insensitive to the precise value of the assigned distribution coefficient for water, so long as it is $<<1$. This range agrees with a previous estimate of 250 to 450 ppm for E-MORB source mantle (30). The accommodation of this much water in upper mantle anhydrous minerals would depend on OH solubilities higher than have been demonstrated in this study. It has been argued that hydrous minerals (60) or fluids (61) are present in the source regions of Hawaii, which suggests that the anhydrous minerals may become saturated in OH at bulk water concentrations in this range.

With the maximum measured OH contents in the anhydrous minerals, an amount of water equivalent to 85% of the current ocean mass can be accommodated in the whole mantle. Alternatively, if the oceans were in fact derived from the mantle (which is not established) and originated from that portion modeled to have degassed to yield the Earth's atmosphere [about 46% (12)], then these maximum observed OH concentrations suggest that up to 40% of the present ocean could originally have been stored in this form. However, it should be stressed that these measured OH concentrations do not provide

strong constraints on the upper bounds for water storage in minerals, because of the unknown effects of pressure on H solubilities.

Implications for mantle processes

Melting and degassing. The comparatively high OH concentrations recorded in pyroxenes is in accord with observations (27, 28) that a small amount of water is retained in the solid mantle after partial melting and extraction of ocean-ridge basalts. The strong preference of OH for both orthopyroxene (opx) and clinopyroxene (cpx) over olivine (ol) measured in most xenoliths implies that the behaviour of water during mantle melting will be governed by the [opx+cpx]/ol ratio. In contrast, most other incompatible trace elements, such as K, Rb, Ba, U, and the rare-earth elements reside in clinopyroxene or garnet, and their fractionation during melting is determined by the [cpx+gt]/[opx+ol] ratio. Because garnet and clinopyroxene preferentially enter the liquid phase during partial melting, H should be retained in the solid residue to a greater extent than many other incompatible trace elements. This effect is enhanced at high degrees of partial melting, where the only solid phases remaining are orthopyroxene and olivine. The OH concentrations observed in pyroxenes provide an explanation for the relative compatibility of H_2O [more compatible than K, Rb, Nb, Cl and La, but less compatible than Zr, Ti, Y, and Nd (30)] during MORB genesis. These relations suggest that the depletion rate of water from the mantle by melting, eruption, and degassing of basalt, is slightly slower relative to that of other elements with high incompatibility.

Distribution of hydrous phases in the mantle. Fig. 3 depicts the predicted principal host phases for water in a peridotitic upper mantle, assuming that the OH concentrations measured in the most OH-rich minerals are close to saturation levels for these phases under

general upper mantle conditions. The uncertainty in this assumption may result in some shift in the magnitude of the nominally anhydrous mineral field in Fig.3, as the variation of OH solubility in these minerals under mantle conditions becomes established.

Because only the upper 150 km or so of the mantle (with rare exceptions) is represented in xenolith suites, the OH contents of minerals of deeper origin cannot be measured directly. Although no firm conclusions can be drawn at this stage, general trends in our data suggest that OH concentration in some anhydrous minerals increases at higher pressures. The far lower OH contents of pyrope garnets than both orthopyroxenes and clinopyroxenes suggests that as increasing amounts of pyroxene become dissolved in the garnet structure with depth in the mantle, the solubility of OH in the anhydrous minerals may be reduced. However, the proposed transformation of olivine to ß-Mg_2SiO_4 near 400 km depth (62) may increase the water carrying capacity of nominally anhydrous minerals in the transition zone. The estimates of OH solubility in nominally anhydrous minerals suggest that stoichiometrically hydrous high-pressure phases (the so-called dense hydrous magnesium silicates) are not required to be present in the depleted upper mantle. There may be exceptions where the mantle has been hydrated by, for example, proximity to a dehydrating lithospheric plate in a subduction zone, or contamination in the neighborhood of a plume.

The local distribution of hydrous phases is further complicated by the capability of water-rich fluids to transport alkali metals such as Na and K. Thus, hydrous minerals with appreciable high temperature and pressure stability, such as F-bearing potassic richterite (63), and possibly phlogopite, may be locally concentrated where alkali and halogen concentrations are elevated along with water.

Water recycling. Lithospheric plates returned to the mantle at subduction zones are water-rich in their upper regions because of their interaction with the hydrosphere.

However, most water held in the subducting slab will be released on compression of pore-space and when hydrous minerals such as opal, zeolites, clays, chlorite, serpentine and amphibole undergo dehydration reactions (64). It has been predicted that almost all water originally present in the oceanic crust will be prevented from entering the deep mantle because of these dehydration reactions. However, the oceanic crust transforms to eclogite, a roughly 50-50 mix of garnet and omphacitic clinopyroxene, in response to increasing pressure during subduction. Our studies of mantle eclogites reveal that although most high-pressure eclogitic garnets are OH-poor, the omphacitic pyroxenes in these rocks contain comparatively large amounts of OH. Thus deep subduction of omphacitic pyroxene, perhaps supplemented by the accessory minerals rutile and kyanite, may allow the transport of water (up to about 500 ppm) into deep regions of the mantle. Pods of eclogite situated in peridotitic mantle may form local areas of comparatively high water concentration, at least as far as the nominally anhydrous minerals are concerned, and such material may contribute to the source region of ocean island basalts (65).

It is a commonly held view that some water derived from dehydration of the subducting slab infiltrates the overlying mantle wedge, where it has been implicated in partial melting processes that give rise to arc magmas (66). The comparatively water-rich nature of primary arc basalts [1 to 2% by weight (67)], suggests that their solid mantle residues may contain up to 200 ppm or so of water, bound in nominally anhydrous minerals, and there may be regions of the mantle wedge where nominally anhydrous minerals are saturated in OH. The fate of this hydrated peridotite is not known, but it may end up in the continental lithosphere, remain in the shallow mantle, or be dragged into the deep mantle by the descending slab. Although the response of the hydrous component of the nominally anhydrous minerals to increases in temperature and pressure is poorly known at present, there is the possibility that H bound in this form can survive transport to considerable depths. Because peridotite is believed to flow continuously through the

mantle wedge above a subduction zone (66, 68), this material can be continually hydrated and either recycled into deeper regions of the mantle or contribute to a hydrated uppermost mantle. The water content predicted for the nominally anhydrous minerals in the hydrated mantle wedge appears to be sufficient to account for that of the MORB source region. The continuous conveyor belt of OH-saturated, but nominally anhydrous peridotite above subduction zones may contribute to steady-state recycling of water through the upper regions of the Earth, a process inferred on the basis of uniformity of primary hydrogen isotope compositions of igneous rocks to be important in the Earth's water cycle (69).

References and Notes.

1. Geological literature is generally not precise in its designation of the element hydrogen in the mantle. The term "water" is commonly used to encompass all chemical forms of hydrogen, perhaps with the implied assumption of the oxidized form of the element. In this paper we follow this loose usage in referring to hydroxyl (OH) bound in minerals as one form of mantle "water." Although the H occurs as OH in the minerals of this study, and is detected as such by infrared spectroscopy, we follow the convention for other elements in reporting analyses of H in terms of the charge-balanced oxide, H_2O (by weight).
2. J. R. Goldsmith, *Contrib. Mineral. Petrol.* **95**, 311 (1987).
3. A. K. Ganguli, A. J. Vega, R. D. Shannon, G. R. Rossman, *in preparation.*
4. G. R. Rossman and G. C. Solomon *in preparation.*
5. A. M. Hofmeister and G. R. Rossman, *Am. Mineral.* **70**, 794 (1985).
6. D. T. Griggs and J. D. Blacic, *Science* **147**, 292 (1965).
7. A. Kats, *Phillips Res. Rep.* **17**, 133 (1962), R. D. Aines, S. H. Kirby, G. R. Rossman, *Phys. Chem. Minerals* **11**, 204 (1984).
8. R. W. T. Wilkins and W. Sabine, *Am. Mineral.* **58**, 508 (1973).
9. R. D. Aines and G. R. Rossman, *J. Geophys. Res.* **89**, 4059 (1984); G. R. Rossman, *Rev. Mineral.* **18**, 193 (1988).
10. The difficulty of reliable and accurate quantitative calibration compared with the relative ease and intriguing variability of the infrared measurements has caused the determination of absolute concentrations to lag somewhat behind the descriptive studies. Many studies have used the generic calibration developed by M. S. Paterson [*Bull. Mineral.* **105**, 20 (1982)], but it has become apparent that this is not (and was not intended to be) suitable for rigorously quantitative analysis of OH in minerals.

Progress towards accurate mineral-specific calibrations has been evolutionary, with consecutive calibration studies often generating progressively lower estimates of H concentration as the analytical technology improves. The convergence of results from recent manometric measurements [D. R. Bell, P. D. Ihinger, G. R. Rossman, S. Epstein, *in preparation*] and those from nuclear reaction analysis [D. Kuhn, F. Rauch, H. Baumann, *Nucl. Instrum.* **B 45**, 252 (1990) and unpublished data] provides the basis for most calibrations used here. The calibrations for Ca- and Mg-rich garnets agree within uncertainty, but pyroxene calibrations are based on precise analysis of single samples, and have not been tested on a variety of mineral compositions. We estimate that the uncertainty in accuracy of the measured OH contents of most minerals is on the order of a few tens of percent relative.

11. W. W. Rubey, *Geol. Soc. Am. Bull.* **62**, 1111 (1951).

12. C. J. Allegre, T. Staudacher, P. Sarda, *Earth Planet. Sci. Lett.* **81**, 127 (1987).

13 Y. Abe and T. Matsui, *Proc. Lunar Planet. Sci. Conf.* **17**, E291 (1986).

14. H. D. Holland, *The Chemical Evolution of the Atmosphere and Oceans.* (Princeton Univ. Press, Princeton, 1984); G. Schubert, D. L. Turcotte, S. C. Solomon, N. H. Sleep, in *Origin and Evolution of Planetary and Satellite Atmospheres*, S. K. Atreya, J. B. Pollack, M. S. Matthews, Eds. (Univ. Arizona Press, Tucson, 1989), pp.450-483.

15. P. J. Wyllie, *Min. Soc. Am. Spec. Pap.* **3**, 3 (1970).

16. A. E. Ringwood and A. Major, *Earth Planet. Sci. Lett.* **22**, 130 (1967); C. B. Sclar, L. C. Carrison, C. M. Schwartz, *Trans. Am. Geophys. Union* **46**, 184 (1965).

17. L. W. Finger and C. T. Prewitt, *Geophys. Res. Lett.* **16**, 1395 (1989).

18. J. R. Smyth, *Am. Mineral.* **72**, 1051 (1987); J. W. Downs, *Am. Mineral.* **74**, 1124 (1989); T. E. Young, H. W. Green II, A. M. Hofmeister, *Eos* **72**, 144 (1991).

19. M. G. Justice, E. K. Graham, R. E. Tressler, I. S. T. Tsong, *Geophys. Res. Lett.* **9**, 1005 (1982); S. J. Mackwell, D. L. Kohlstedt , M. S. Paterson, *J. Geophys. Res.* **90**, 11319 (1985); S. Karato, M. S. Paterson, J. D. FitzGerald, *J. Geophys. Res.* **91**, 8151 (1986); M. R. Drury, *Phys. Chem. Minerals* **18**, 106 (1991).

20. S. Karato, *Nature* **347**, 272 (1990).

21. C. B. Sclar, L. C. Carrison, O. M. Stewart, *Trans. Am. Geophys. Union* **48**, 226 (1967).

22. W. S. Fyfe, *Phys. Earth Planet. Inter.* **3**, 196 (1970).

23. R. F. Martin and G. Donnay *Am. Mineral.* **57**, 554 (1972).

24. L. Ackermann, L. Cemic, K. Langer, *Earth Planet. Sci. Lett.* **62**, 208 (1983).

25. G. A. Lager, T. Armbruster, F. J. Rotella, G. R. Rossman, *Am. Mineral.* **74**, 840 (1989).

26. G. R. Rossman and R. D. Aines, *Am. Mineral.* **76**, 1153 (1991).

27. T. C. Birkett and W. E. Trzcienski, *Can. Mineral.* **22**, 675 (1984).

28. J. G. Moore, *Contrib. Mineral. Petrol.* **28**, 272 (1970).

29. J. E. Dixon, E. M. Stolper, J. R. Delaney, *Earth Planet. Sci. Lett.* **90**, 87 (1988).

30. P. J. Michael, *Geochim. Cosmochim. Acta* **52**, 555 (1988).

31. R.D. Aines and G.R. Rossman, *Am. Mineral.* **69**, 1116 (1984).

32. R.D.Aines and G.R. Rossman, *Geology* **12**, 720 (1984).

33. D. R. Bell and G. R. Rossman, *Contrib. Mineral. Petrol. in preparation.*

34. M. Kitamura *et al., Nature* **328**, 143 (1987).

35. G. H. Miller, G. R. Rossman, G. E. Harlow, *Phys. Chem. Minerals* **14**, 461 (1987).

36. H. S. Skogby, D. R. Bell, G. R. Rossman, *Am. Mineral.* **75**, 764 (1990).

37. J. R. Smyth, D. R. Bell, G. R. Rossman, *Nature* **351**, 732 (1991).

38. A. Beran and M. A. Götzinger, *Mineral. Petrol.* **36**, 41 (1987).

39. G. R. Rossman and J. R. Smyth, *Am. Mineral.* **75**, 775 (1990).

40. D. R. Bell and G. R. Rossman, *Eos* **71**, 523 (1990).

41. D. Vlassopoulos, G. R. Rossman, S. E. Haggerty, *Eos* **71**, 626 (1990).

42. J. A. Woodhead, G. R. Rossman, A. P. Thomas, *Am. Mineral.* **76**, 1533 (1991).

43. E. Fritsch, K. Scarratt, A. Collins, in *New Diamond Science and Technology, Materials Res. Soc. Internat. Conf. Proc. 1990,* R. Messier, J. T. Glass, J. E. Butler, R. Roy, Eds, pp 671-676 (1991); O. Navon, I. D. Hutcheon, G. R. Rossman, G. J. Wasserburg, *Nature* **335**, 784 (1989).

44. While the large infrared absorptions observed in omphacite pyroxenes (solid solutions of primarily the diopside and jadeite endmembers) suggest that they commonly have the greatest OH concentrations among mantle-derived pyroxenes, the OH infrared spectra of jadeite-rich omphacites differ from diopside and augite pyroxenes in the number and frequency of the OH absorptions [see (36)]. This difference prompts caution in application of the present calibration of the OH spectrum of clinopyroxene (based on augitic diopside), and indicates some uncertainty in the analysis of OH in omphacitic pyroxenes. Based on systematics in the relationship between absorption coefficient and band energy of amphiboles [H. S. Skogby and G. R. Rossman, *Phys. Chem. Minerals* **18,** 64 (1991)] it is suggested [D. R. Bell, P. D. Ihinger, G. R. Rossman, S. Epstein, *in preparation*] that this calibration may overestimate the OH contents of jadeite-rich omphacites by about 30%.

45. Because garnet lherzolites derive from greater depths than spinel lherzolites (see Fig. 3), the higher OH contents observed in olivines from garnet lherzolites may indicate a pressure effect on OH solubility in olivine. However, the garnet peridotites were transported to the surface in volatile-rich kimberlites, whereas all spinel lherzolites studied here derive from basalts, and may have suffered some dehydration.

46. Olivine is currently the least well-calibrated mineral in terms of quantitative OH analysis. Earlier workers (35, 47) have used the calibration of Paterson [see (10)] and

we have applied a similar method here. It is worth noting that this calibration tends to give lower OH contents when applied to pyroxenes and garnet than the mineral-specific calibrations. In spite of the uncertainties in calibration, the OH absorption intensity difference between pyroxenes and most olivines is very marked (up to three orders of magnitude in integrated absorbance), and we feel confident in concluding that pyroxenes are significantly more hydrous.

47. S. J. Mackwell and D. L. Kohlstedt, *J. Geophys. Res.* **95**, 5079 (1990).

48. P. Kresten, P. Fels, G. Berggren, *Mineral. Dep.* **10**, 47 (1975); R. O. Moore, thesis, Unversity of Cape Town (1986).

49. It has been argued (47) that the OH content of mantle derived olivines will decrease as the ambient H_2 fugacity drops with decreasing total pressure during eruption. This is possible because of the very rapid diffusion of H in olivine and the reversible redox reaction involving a Fe^{2+}/Fe^{3+} couple. A similar reaction has been proposed for dehydroxylation of pyroxenes in air [H. S. Skogby and G. R. Rossman, *Am. Mineral.* **74**, 1059 (1989)]. This rapid diffusion of H is contrasted with the much slower diffusivity of possible OH defect sites in olivine and implies that the ultimate solubility of H, that is, the "OH carrying capacity" of the mineral, is relatively unaffected during transport. If OH is lost upon eruption as suggested by Mackwell and Kohlstedt (47), then the measured OH concentrations are most likely underestimates of concentrations in the mantle.

50. V. E. Barnes, *Am. Mineral.* **15**, 393 (1930); M. W. Phillips, J. E. Draheim, R. K. Popp, C. A. Clowe, A. A. Pinkerton, *Am. Mineral.* **74**, 764 (1989).

51. C. A. Geiger, K. Langer, D. R. Bell, G. R. Rossman, B. Winkler, *Am. Mineral.* **76**, 49 (1990).

52. T. R. McGetchin and L. T. Silver, *J. Geophys. Res.* **77**, 7022 (1972); D. Smith, in *The Mantle Sample: Inclusions in Kimberlites and Other Volcanics,* F. R. Boyd and

H. O. A. Meyer, Eds. (American Geophysical Union, Washington, DC, 1979), pp. 345-356.

53. H. H. Helmstaedt and R. Doig, *Phys. Chem. Earth* **9**, 95 (1975); P. Bird, *Tectonics* **3**, 741 (1984).

54. M. R. Drury and H. L. M. van Roermund, *Geology* **16**, 1035 (1988).

55. P. H. Nixon and F. R. Boyd, in *Lesotho Kimberlites*, P. H. Nixon, Ed. (Lesotho National Development Corporation, Maseru, 1973) pp. 67-75; J. J. Gurney and B. Harte, *Phil. Trans. Roy. Soc. London* **297A**, 273 (1980).

56. W. F. McDonough, *Earth Planet. Sci. Lett.* **101**, 1 (1990).

57. The choice of partition coefficient is based on a study of the geochemistry of MORB glasses demonstrating similarity of partitioning behaviour of water to that of La during partial melting (29). Some uncertainty is associated with the choice of the actual value of the partition coefficient for La [done in (29) on the basis of estimates from the literature], which may cause the upper estimate of 35 ppm to double. However, our calculations were done assuming batch melting, which may be unrealistic, particularly at high melt fractions, where a fractional melting model may be more appropriate. The fractional melting model would predict water concentrations in the solid residue closer to the lower end of the given range.

58. X. Xue, H. Baadsgaard, A. J. Irving, C. M. Scarfe, *J. Geophys Res.* **95**, 15879 (1990).

59. D. A. Clague, W. S. Weber, J. E. Dixon, *Nature*, in press (1991).

60. D. A. Clague and F. A. Frey, *J. Petrol.* **23**, 447 (1982).

61. D. A. Clague and J. E. Dixon, *Eos* **72**, 563 (1991), J. E. Dixon, D. A. Clague, E. M. Stolper, in preparation.

62. A. E. Ringwood, *Phys. Earth Planet. Inter.* **3**, 109 (1970), C. R. Bina and B. J. Wood, *J. Geophys. Res.* **92**, 4853 (1987).

63. S. F. Foley, *Geochim. Cosmochim. Acta* **55**, 2689 (1991).

64. S. M. Peacock, *Science* **248**, 329 (1990).

65. A. W. Hoffman and W. M. White, *Earth Planet. Sci. Lett.* **57**, 421 (1982).

66. I. Kushiro, *J. Geophys. Res.* **95**, 15929 (1990).

67. M. O. Garcia, N. W. K. Liu, D. W. Muenow, *Geochim. Cosmochim. Acta* **43**, 305 (1979).

68. J. H. Davies and D. J. Stevenson *J. Geophys. Res. in press.*

69. H. P. Taylor, *J. Geol. Soc. London* **133**, 509 (1977).

70. J. Ingrin, K. Latrous, J. C. Doukhan, N. Doukhan, *Eur. J. Mineral.* **1**, 327 (1989).

71. E. Jagoutz *et al, Proc. Lunar Planet. Sci. Conf.***10**, 2031 (1979).

72. L. G. Liu, *Phys. Earth Planet. Inter.* **49**, 142 (1987).

73. L. Finger *et al., Nature* **341**, 140 (1989).

74. T. Gasparik, *J. Geophys. Res.* **95**, 15751 (1990).

75. This research was supported by National Science Foundation grants EAR 88-16006 and EAR 91-04059. D.R.B. acknowledges financial support from the Harry Crossley Foundation and the American Federation of Mineralogical Societies. We thank our numerous sample donors, in particular J. J. Gurney, for their generosity, De Beers Consolidated Mines Ltd. for access to xenolith localities and collections, and G. S. Mattioli for help in the field. We are grateful to D. Endisch and F. Rauch at the University of Frankfurt for willingness to share unpublished nuclear reaction analysis data relevant to the calibrations used here. We have benefitted from discussions with P. D. Ihinger, G. S. Mattioli, and E. M. Stolper, and thank T. J. Ahrens, D. L. Anderson, J. E. Dixon, R.B. Hanson, P. J. Wyllie and two anonymous reviewers for their comments on drafts of this paper.

76. This is Division of Geological and Planetary Sciences contribution no. 5071.

Table 1. Nominally anhydrous, rock-forming minerals in which occurrence of OH or H_2O has been demonstrated.

andalusite	olivine
cordierite	Clinopyroxenes
Feldspars	aegirine
sanidine	augite
orthoclase	diopside
microcline	hedenbergite
plagioclase	omphacite
Garnets	Orthopyroxene
almandine	enstatite
andradite	quartz
grossular	rutile
pyrope	scapolite
spessartine	sillimanite
kyanite	titanite
nepheline	zircon

Table 2. Water concentrations in anhydrous minerals in mantle xenoliths. Abbreviations: Cpx - clinopyroxene, Gt - garnet, Ky - kyanite, Ol - olivine, Opx - orthopyroxene, Sp - spinel.

			OH concentration (ppm H_2O)				
Sample	Rock type	Locality	Ol.	Opx.	Cpx.	Gt	Whole Rock
KBH-1	Sp. lherzolite	Kilbourne Hole, NM	3	186	530	-	105
KBH-9	Sp. lherzolite	Kilbourne Hole, NM	3	180	490	-	100
WKR	Sp. lherzolite	West Kettle River, BC	<1	50	150	-	28
KOH-29	Gt. lherzolite	Koherab, Namibia	10	180	370	<5	70
JJG1738	Gt. lherzolite	Jagersfontein, SA	55	400	[600][1]	7	175
PMR-50	Gt. lherzolite	Premier, SA	17	210	[500][2]	15	80
BFT-20	Gt. harzburgite	Kimberley, SA	79	460	-	6	125
JAG-18	Gt .websterite	Jagersfontein, SA	-	200	500	5	260
HRV-147	Eclogite	RobertsVictor, SA	-	-	470	4	235
RFT-2	Ky. eclogite	Rietfontein, SA	-	-	1080	51	565
Prim. Mantle[3]	Sp. lherzolite		140	460	590	-	290
Prim. Mantle[3]	Gt. lherzolite		140	460	590	200	245

1. OH in clinopyroxene detected by IR but difficult to quantify because of spectral interference from other features believed due to amphibole lamellae. The concentration assigned is equivalent to the maximum observed in mantle Cr-diopside, and is a probable minimum for the sample, given the OH partitioning observed between orthopyroxene and clinopyroxene in other rocks.
2. OH in clinopyroxene not measured, but assigned on the basis of orthopyroxene - clinopyroxene partitioning.
3. Mineral proportions from McDonough (53), OH concentrations are the maximum observed in each mineral (see text for discussion).

Fig. 1.

Representative infrared spectra of mantle minerals in the OH stretching region. All spectra normalized to 1mm sample thickness. The positive features between 3000 and 3800 cm^{-1} correspond to stretching vibrations of OH in the mineral structures and their intensities are approximately proportional to the OH concentration. Broad absorptions between 3800 and 4200 cm^{-1} are due to electronic transitions in Fe^{2+}, and features at frequencies less than 2600 cm^{-1} arise from overtones of fundamental Si-O vibrations. (A) Garnet MON-9, Monastery, South Africa, unpolarized. (B) Kyanite GRR-343, Rietfontein, South Africa, (100) section, unpolarized. (C) Olivine ROM250-OL26, Monastery, South Africa, unpolarized. (D) Enstatite PMR-54, Premier, South Africa, (100) section, polarized parallel to [001]. (E) Zircon KLV-33.R, Kaalvallei, South Africa, polarized parallel to [001]. (F) Omphacite HRV147, Roberts Victor Mine, South Africa, polarized parallel to gamma.

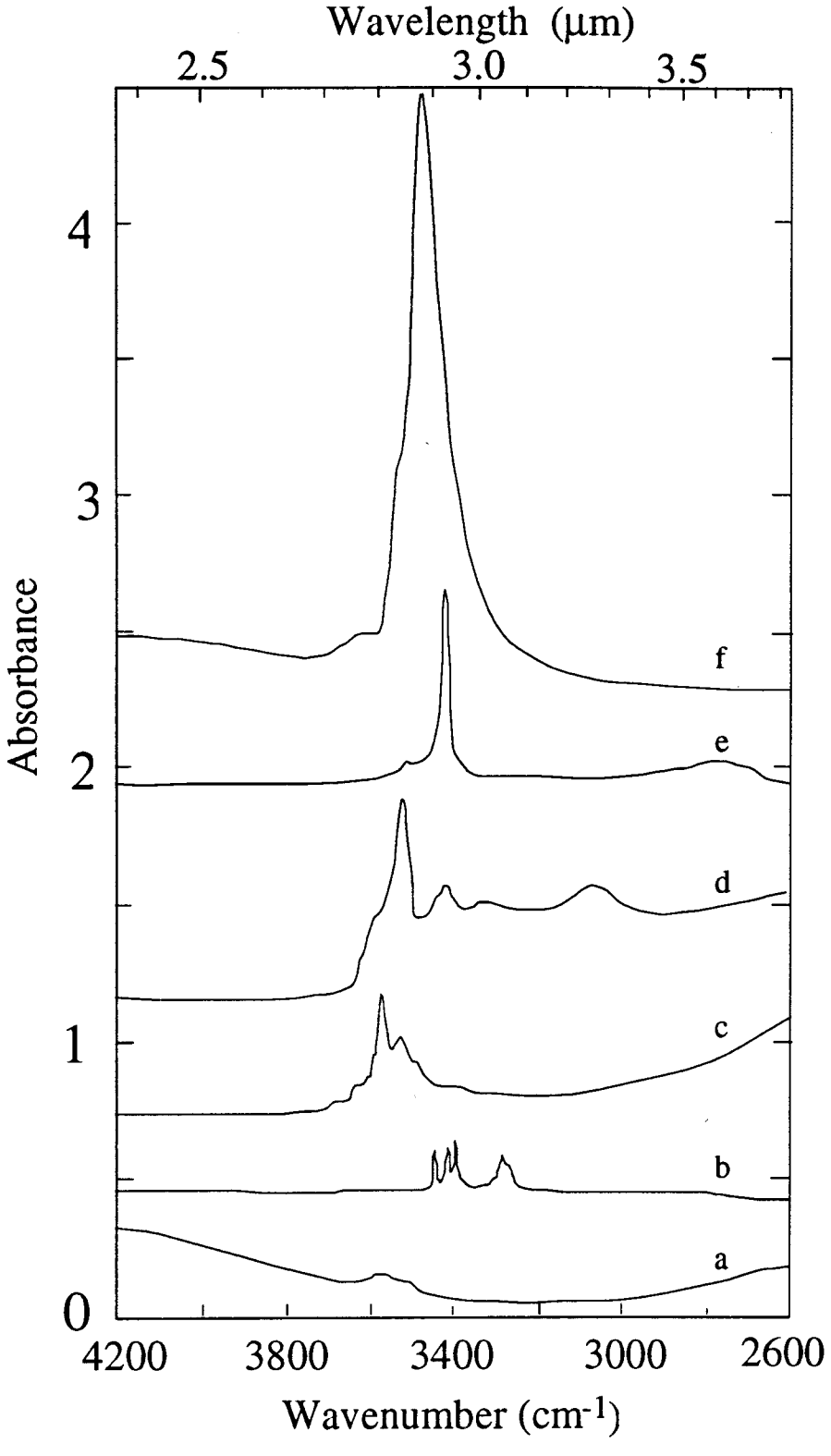
Wavelength (μm)
2.5
3.0
3.5
Absorbance
0
1
2
3
4
f
e
d
c
b
a
4200
3800
3400
3000
2600
Wavenumber (cm-1)

Fig. 2.

Range of OH contents of mantle minerals, expressed as ppm H_2O. Note change in concentration scale at 100 and 500 ppm. For each mineral, the corresponding range of OH contents in crustally-derived samples is displayed for comparison. The letters C and M refer to crustal- and mantle-derived samples respectively and n is the number of mantle mineral analyses reported. Data from this work (216 analyses) and from the literature (115 analyses). Sources of data: Garnets (31, 32), Clinopyroxenes (8, 36, 37, 70), Orthopyroxenes (36) Olivines (35), Kyanite (38, 39), Zircon (42).

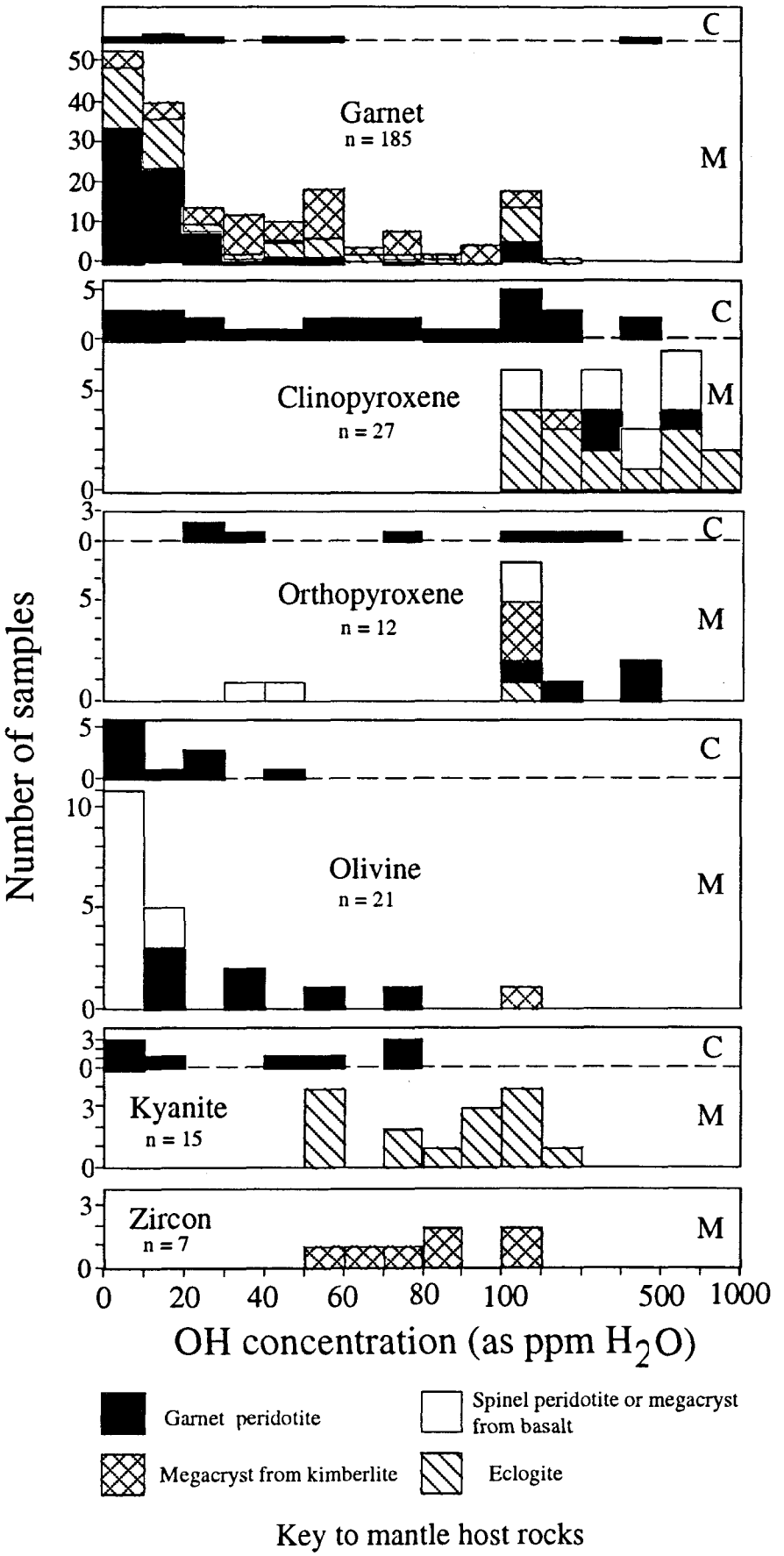
C
M
Garnet
n = 185
Clinopyroxene
n = 27
Orthopyroxene
n = 12
Olivine
n = 21
Kyanite
n = 15
Zircon
n = 7
Number of samples
0 20 40 60 80 100 500 1000
OH concentration (as ppm H_2O)
Garnet peridotite
Spinel peridotite or megacryst from basalt
Megacryst from kimberlite
Eclogite
Key to mantle host rocks

Figure 3. Diagram showing the major repositories of H in peridotitic upper mantle with increasing degree of hydration, as a function of pressure. The temperature-depth profile assumed here corresponds approximately to an oceanic geotherm. The range of estimated upper mantle water contents is shown by the hatched bar on top. Nominally anhydrous minerals are estimated to accommodate up to about 300 ppm H_2O in the bulk rock before saturation with hydrous minerals (at lower pressures) or a liquid phase (at high pressures). The maximum amounts of water that can be stored in amphiboles and micas is limited by the alkali content of the bulk rock, which here corresponds to the values of Jagoutz *et al.* (71) for primitive mantle. The fields of melt and fluid are defined by the intersection of the solidus for peridotite-H_2O with the temperature-depth profile (geotherm) chosen. In addition to the phases illustrated here, it has been suggested (72) that the synthetic hydrous minerals such as Phase A ($Mg_7Si_2O_{14}H_6$) and Phase B ($Mg_{12}Si_4O_{21}H_2$) play a role in water-bearing mantle. However, their thermal stability at normal mantle temperatures and in appropriate bulk compositions has been questioned (73). In regions of the mantle colder than the average, such as encountered in a downgoing slab, the phase boundaries for the stoichiometrically hydrous minerals, as well as the onset of melting, are displaced to higher pressures, and hydrous phases, such as brucite, the humite group minerals, phase A and phase B may be stable at a range of pressures, particularly in the olivine-rich bulk compositions that are expected to be generated by melting and extraction of ocean-ridge basalt. Abbreviations: ol, olivine; opx, orthopyroxene; cpx, clinopyroxene; gt, garnet; sp, spinel; en, enstatite (magnesian orthopyroxene); c-en, magnesian monoclinic pyroxene; ß-sp, beta-spinel polymorph of olivine (Mg_2SiO_4). Labelled tics on the right hand ordinate indicate pressure-induced phase changes in the solid mantle mineral assemblage. High pressure solid phase relations are from Gasparik (74).

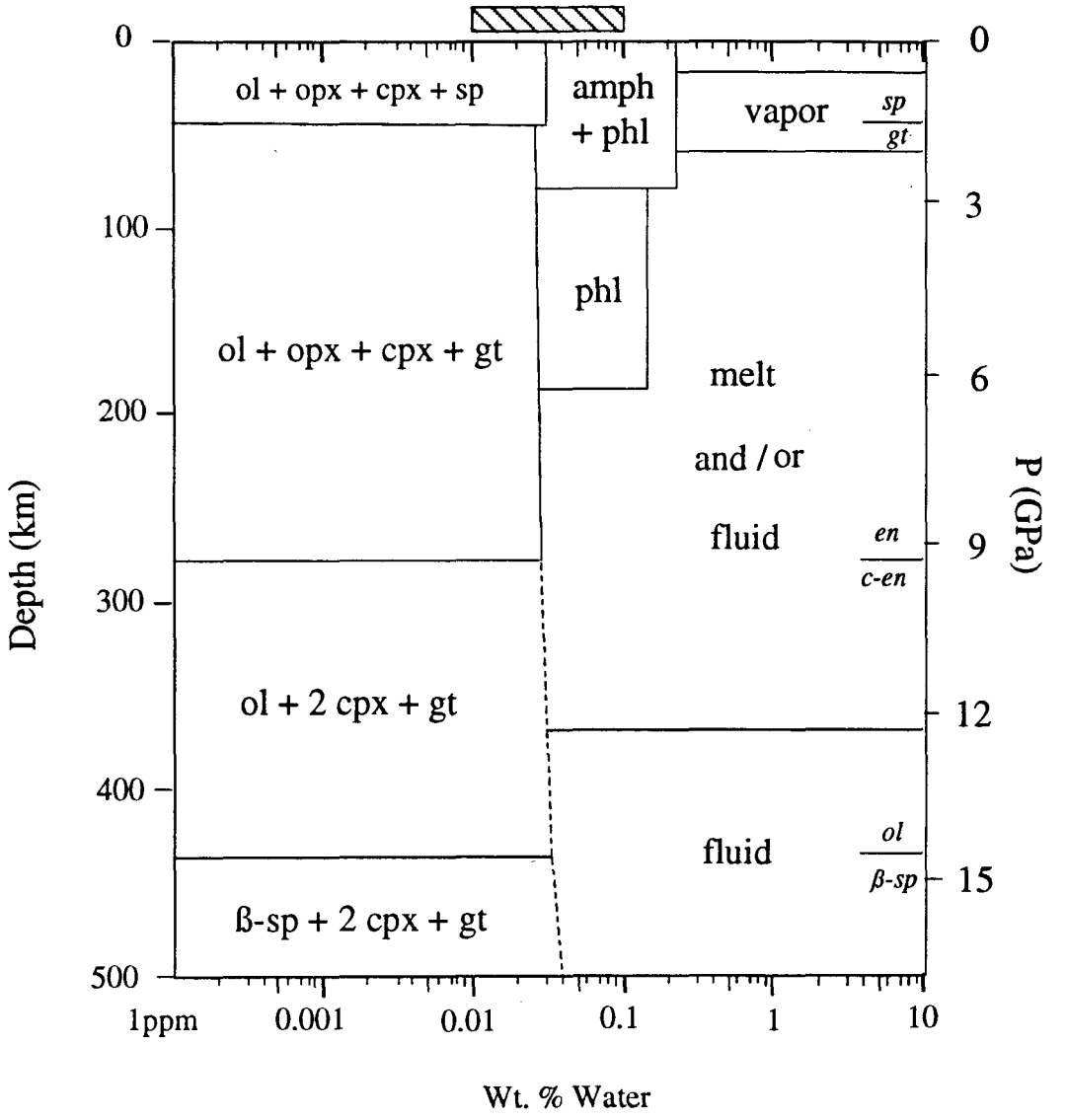
0
100
200
300
400
500
Depth (km)
ol + opx + cpx + sp
amph
+ phl
vapor
sp
gt
phl
ol + opx + cpx + gt
melt
and / or
fluid
en
c-en
ol + 2 cpx + gt
fluid
ol
β-sp
ß-sp + 2 cpx + gt
0
3
6
9
12
15
P (GPa)
1ppm
0.001
0.01
0.1
1
10
Wt. % Water

Chapter 3. Abundance and partitioning of hydroxyl in a high-pressure igneous system: megacrysts from the Monastery kimberlite, South Africa.

ABSTRACT

OH, major and trace element concentrations have been determined in a suite of co-genetic mantle-derived megacrysts from the Monastery kimberlite, South Africa. These megacrysts (olivine, orthopyroxene, garnet, clinopyroxene and zircon) display regular variations in OH content that are correlated with variations in major and other trace elements and reflect igneous differentiation of a high-pressure magma. The trends in OH contents of the megacryst minerals as a function of differentiation display features which are not readily explicable by constant partitioning of H between mineral and melt, and indicate the influence of mineral, and possibly melt composition on partitioning behavior of H. In particular, Ti substitution appears to affect H incorporation on garnet, clinopyroxene, and has been linked with a specific OH absorption band at 3512 cm^{-1} in the infrared spectrum of garnet. K in clinopyroxene exhibits similar variations to OH, thus establishing an independent precedent for this geochemical behavior, and reducing the likelihood that the observed variations in OH are caused by late-stage H mobility in a crustal environment. Inter-mineral distribution coefficients (D's) for water have been calculated based on a parameterization of published coexisting major element compositions of megacrysts and of the trends of OH in the minerals as a function of composition established in this study, and have been confirmed by measurement in coexisting megacryst mineral pairs. These D's are highly composition dependent for partitioning involving garnet, varying by approximately a factor of six over the range of compositions represented, but are relatively constant among the other phases. Water fugacities calculated from the OH content of olivine (up to 37 kbar) are compatible with a mantle origin for the OH, but the OH contents could have been produced in the crust under special circumstances, nevertheless plausible in the kimberlite emplacement environment. OH contents of some annealed olivine tablets are lower than those of strained porphyroclasts from the same sample, suggesting re-equilibration of

olivine to lower water fugacity conditions during transport. The water content of a megacryst magma, proposed to have precipitated sample MON-24, a garnet -olivine pair, at 1340 °C and 52.5 kbar has been calculated at 1.3 wt.% using the thermodynamic model of Silver & Stolper (1985) for water in silicate melts. Mineral-melt D's for water calculated from this estimate are similar to those calculated from petrogenetic studies on MORB using the inter-mineral D's established here. These results confirm the hydrous nature of mantle minerals in the appropriate environment and present a quantitatively consistent picture for the partitioning of H between mantle phases under apparent ambient conditions, with appropriate regard for compositional effects. At present, all observations on these natural minerals are consistent with, but do not yet prove, the hypothesis that the concentrations of OH measured are those established in the mantle.

(1) INTRODUCTION

There is now a substantial body of information indicating that OH is incorporated in trace, but measurable amounts in the structure of most common minerals, whose chemical formulae suggest that they are anhydrous. Several studies have dealt with the infrared spectroscopic characteristics of OH in these minerals, the issue of quantitative analysis thereof, and the stability of this component under various conditions. Most of these studies have concentrated on single phases and not examined coexisting assemblages of anhydrous minerals, or coexisting anhydrous and hydrous minerals. Although the suggestion that nominally anhydrous minerals may be useful indicators of water activity was made two decades ago (Martin and Donnay 1972), there have been few attempts to use nominally anhydrous minerals in tracing the behavior of hydrous volatiles in igneous or metamorphic systems. Bell and Rossman (1992a) noted that the OH concentration in garnet megacrysts from kimberlites was positively correlated with indices of magmatic differentiation, which

we suggested was due to equilibrium partitioning of OH between garnet and differentiating silicate melt of progressively increasing water content. The relationship between OH in nominally anhydrous minerals and the fugacity of hydrous species with which the minerals have equilibrated has recently been the subject of experimental investigation. Geiger *et al.* (1991) synthesized OH-bearing pyrope garnets under water-saturation in a variety of pressure and temperature conditions, but did not explore the quantitative relationships between OH content and partial pressure of water because of evidence for lack of chemical equilibrium in the experiments. Most recently, Bai and Kohlstedt (1992a) have determined the OH content of a natural Mg-rich olivine, hydrothermally annealed under controlled fugacities of H_2 and O_2. These studies have begun to lay the basis for an understanding of how and in what quantities OH is incorporated in nominally anhydrous minerals under given conditions. However, the complexities of natural geological systems require that these fundamental experimental investigations in simple chemical systems or under a limited range of conditions be complemented by studies on natural assemblages in order to be more useful in geology.

In this study, we examine in detail the relationship between OH content and other compositional and textural features in a suite of co-magmatic megacryst minerals (garnet, olivine, orthopyroxene, clinopyroxene and zircon) from the Monastery kimberlite, South Africa. The compositional dependence of partitioning behavior of OH among high pressure minerals is described and the relationship of the OH concentrations to water fugacity and concentration in the source is evaluated quantitatively with reference to the problems of hydrogen mobility under igneous conditions.

(2) THE MONASTERY MEGACRYST SUITE

(2.1) Overview

The Monastery kimberlite in the south-eastern Orange Free State, South Africa contains a spectacular suite of coarsely crystalline, commonly monomineralic mineral inclusions of a distinctive Fe- and Ti-rich, and Cr-poor character, relative to the compositions of minerals in common coarse-granular textured garnet lherzolite xenoliths in kimberlites. This class of mineral inclusion, referred to variably as "discrete nodules" (Nixon & Boyd 1973) or "Cr-poor megacrysts" (Eggler *et al.*, 1979) is a striking feature of many kimberlite xenolith suites and has been well studied and described in the literature. The large size, mineral diversity and great abundance of the megacryst suite at the Monastery mine has led to a number of studies on these samples, with the result that they represent one of the best documented and best understood kimberlite-hosted megacryst assemblages.

(2.2) Setting for megacryst formation

Essentially all studies on such megacrysts agree on an origin by association with some type of magma in the mantle. Nixon *et al.* (1963) suggested that this magma might have been the host kimberlite, whereas Boyd & Nixon (1973) envisioned a magma dispersed over some tens of kilometers depth at the base of the continental lithosphere, corresponding with a seismic low-velocity layer. The regular variation in mineral chemistry correlated with temperature at approximately constant pressure computed from mineral thermometers and barometers led Gurney *et al.* (1979) to propose that the Monastery megacrysts were the cumulate products of a magma undergoing fractional crystallization at about 140 km depth in the mantle. A number of studies of other megacryst suites (e.g., Eggler *et al.*, 1979, Garrison & Taylor 1980, Schulze 1984, Hops *et al.*, 1992) support the fractional crystallization model. Although the data in general support of this conclusion for the

Monastery suite have recently been extended to trace elements (Moore *et al.*, 1992), the fractional crystallization hypothesis has yet to be tested by quantitative modeling for any megacryst suite. Harte & Gurney (1981) viewed the physical setting for the magmatic fractionation as a stockwork of veins (mantle pegmatites) emplaced into the thermal aureole of a magma body of limited vertical extent. In this view, the disruption of these pegmatitic veins produces the megacrysts recovered in the kimberlite at the surface. Although the composition of the parental "megacryst magma" is still disputed (Harte 1983, Mitchell 1986), models have been proposed suggesting a link with some precursor to the erupted magma hosting the megacrysts (Jones 1987, Neal & Davidson 1989).

(2.3) Chemical evolution of the Monastery megacryst suite

The Monastery megacryst suite comprises olivine, garnet, clinopyroxene, orthopyroxene, ilmenite, phlogopite and zircon (Gurney *et al.*, 1979). Because these megacrysts commonly occur as isolated crystals, dispersed within the host kimberlite matrix, the petrologic relationships of the minerals to one another are not immediately obvious and must be established by examination of samples where one or more minerals are intergrown. Indications from such studies are that the crystallization sequence begins with multiple saturation at the liquidus with magnesian olivine (~Fo 88), orthopyroxene, garnet and highly subcalcic clinopyroxene (Ca/Ca+Mg ~0.3), joined at lower temperature by ilmenite (commonly in the form of lamellar pyroxene-ilmenite intergrowths)(Jakob 1977, Gurney *et al.*, 1979, Moore 1986). The compositional relationships of the major silicates are shown in Fig. 1. The relationship of the other megacrysts, namely Fe-rich olivine, zircon and phlogopite to those mentioned above (the so-called "main trend") has been poorly understood.

Recent detailed chemical analysis of coexisting megacryst assemblages (intergrowths of one or more megacryst minerals) at Monastery (Moore *et al.*, 1992) has revealed that, in addition to the two populations of olivine recognized by Gurney *et al.* (1979), more than one population of ilmenite and clinopyroxene occur. The data presented by Moore *et al.* (1992) also allow some aspects of the relationship of phlogopite to the other megacryst minerals to be determined (discussed further below). Moore *et al.* (1992) have made a case for continued differentiation of the magmatic parent of the main silicate trend (cpx + opx + gt ± ol ± ilm) to produce the Fe-rich olivines, zircon and their intergrowths with phlogopite and ilmenite, but this is still considered a tenuous link and other explanations for the origin of these megacrysts are viable. The most recent view of the interrelationships of the Monastery megacryst minerals is definable only by a combination of major and trace element data and observation of physical coexistence of minerals. Fig. 2, modified from Moore *et al.*, 1992 illustrates the complexities of the various megacryst associations revealed by trace element studies. The points of importance to this study are:

(1) The "main silicate trend" of garnet + subcalcic clinopyroxene + calcic orthopyroxene ± Fe-poor olivine ± Cr-poor ilmenite represents a cohesive and "well-behaved" suite.

(2) Phlogopite is never observed to coexist in hand sample with "main trend" silicates or ilmenite, but may occasionally be associated with Fe-rich olivine, zircon, Nb- and Cr-rich ilmenite and perhaps calcic clinopyroxene.

(3) In the simple assumption of closed system crystal fractionation, calcic clinopyroxenes are apparently not an extension of the "main silicate trend," thus affecting the interpretation of their trace element contents in relation to other clinopyroxenes.

(4) The relationship of the association Fe-rich olivine - Nb-, Cr-rich ilmenite - zircon ± phlogopite to the main trend silicates is uncertain. This is of interest to the present study when OH concentrations in the two olivine populations are compared.

Because of these complexities, most of the discussion in this paper is focused on the main trend silicates and ilmenite, although data on the other minerals are presented.

(2.4) Chemical equilibrium and the suitability of megacrysts for OH studies

Megacrysts offer several advantages over other minerals of high-pressure origin for studies of the behavior of OH under mantle conditions. Their large size and chemical homogeneity on a cm-scale greatly facilitates the preparation of samples for infrared spectroscopic analysis, the preferred analytical method (see below). Ideally, the study of inter-mineral partitioning should proceed by analysis of spatially adjacent pairs, a procedure which is difficult in megacryst suites because coexisting intergrown megacrysts are relatively uncommon. However, the systematic relationships between composition (both major and trace elements) and degree of chemical differentiation for each mineral species are such that equilibrium partitioning relationships between mineral species are readily established by interpolation between analyses of occasional coexisting pairs (e.g., Gurney *et al.*, 1979). Later in this paper we make extensive use of this principle to calculate inter-mineral partition coefficients for OH and in extending the hydrobarometer calibration for olivine of Bai & Kohlstedt (1992) to garnet, pyroxenes and zircon.

Megacryst minerals record high temperatures of equilibration (1100-1400 °C) (Nixon & Boyd 1973, Hops *et al* ., 1989), from which they appear to have quenched rapidly (McCallister *et al*.., 1979). These conditions are ideal for establishing and measuring equilibrium chemical compositions. Sr and Nd isotopic studies of megacrysts (and the chemically similar sheared lherzolites) support the probability of general chemical and isotopic equilibrium at the time of extraction from the mantle, i.e., kimberlite eruption (e.g., Richardson *et al.*, 1985, Jones 1987, Hops *et al.*, 1989). These systematics contrast

with those often seen in mantle xenoliths of lower temperature origin, in which metasomatic events of unknown nature and age conspire to perturb chemical and isotopic equilibrium (e.g., Richardson *et al.*, 1985, Erlank *et al.*, 1987). Intra-mineral chemical zonation (Smith & Boyd 1992) and apparently unexpected inter-mineral partitioning relationships (Köhler & Brey 1990, Brey 1991) provide further evidence for lack of chemical equilibrium in these xenoliths, suggested previously by Fraser & Lawless (1978). Although the significance of these effects in petrological studies is contentious (e.g., Carswell, 1978, Boyd *et al.*, 1992), the issue is of particular concern in the case of hydrogen, where rapid diffusion has been demonstrated in olivine (Mackwell & Kohlstedt 1990) and probably occurs in other minerals.

On the other hand, Bai & Kohlstedt (1992) showed the importance of complete recrystallization (their "dynamic annealing") of olivine in producing equilibrium OH concentrations. In the absence of this annealing, the final OH content of a mineral subjected to an influx of H may be predetermined by the previous set of conditions under which the mineral equilibrated. For this reason, it is questionable as to how much of the observed partitioning of OH among minerals in peridotite or eclogite xenoliths (e.g., Rossman & Smyth 1990, Bell & Rossman 1992b) represents the equilibrium state. In particular, it is difficult to understand the very high concentrations of OH in clinopyroxenes from eclogites and coarse peridotites compared with the usually extremely low OH concentrations in garnet from these rocks in the context of equilibrium partitioning.

(3) SAMPLES

Samples selected for this study were a subset of large collections previously studied by Jakob (1977), Gurney *et al.* (1979) and Moore (1986). The minerals for study were

chosen on the basis of previously determined electron microprobe analyses (Moore, 1986 and unpublished data) to span the complete compositional range of each mineral observed for the large sample suites. For olivine, orthopyroxene and garnet the selection criterion was 100Mg/(Mg+Fe) [Mg#], whereas clinopyroxene samples were chosen on the basis of 100Ca/(Ca+Mg) [Ca#]. Zircon samples were all from bi- or polymineralic intergrowths and were chosen on the basis of the Mg# of the coexisting olivine or ilmenite. OH contents of coexisting minerals were determined on pairs of garnet-clinopyroxene (1), garnet-olivine (1) and olivine-zircon (3). In addition, the OH contents of three clinopyroxene samples coexisting with ilmenite in the form of lamellar intergrowths were determined. The mineral associations of the samples are given in Table 1. and their relationship to the overall range of compositions recorded for each mineral is shown in Fig.1.

(3.1) Petrography of olivine "megacrysts"

Although the olivines associated with the Monastery and other megacryst suites are often referred to as megacrysts, they are commonly polycrystalline aggregates showing many textures indicating a history of deformation and are more accurately termed porphyroclastic dunites. Because of this textural difference from other megacrysts and other factors relating to their degree of preservation and dull appearance, their association with, and prevalence in Cr-poor megacryst suites has been somewhat under-appreciated. The olivine "megacrysts" are made up of variable proportions of large, often strained porphyroclasts, small (sub-millimeter) neoblasts and euhedral recrystallized tablets. While other megacrysts examined in this study are pure, petrographically homogeneous minerals on the scale of a few mm down to the diameter of the IR beam (200 - 500 μm), the olivine megacrysts are internally heterogeneous from one grain of the polycrystalline aggregate to another, as well as within individual grains, where a variety of dislocations, tilt walls,

microfaults, healed fractures and inclusions may be present in individual aggregates. Many of the features, both in terms of mineral habit and fabric, and internal mineral microstructure are identical to those seen in olivines from high-temperature deformed lherzolites (Boullier & Nicolas 1973, 1975, Gueguen 1977, 1979, Drury & Van Roermund 1988, 1989 and in Fe-rich dunites and peridotites from the Kimberley pipes (Dawson *et al.*, 1981). Noting that any of these structures might be accompanied by OH groups or H_2O molecules, the petrographic features visible with the optical microscope to a magnification of 400X of each sample analyzed have been recorded (Table 2).

Despite these textural heterogeneities, the olivine "megacrysts" define two coherent geochemical groups (low-Fe, high-Ni and high-Fe, low-Ni respectively), each displaying good positive correlations of Ni content with Mg number and consistency in their mineral associations, the low-Fe group with orthopyroxene, clinopyroxene and garnet, and the high-Fe group with zircon, phlogopite and a group of ilmenites distinctive from those which commonly coexist with the other silicates (Moore 1986, Moore *et al.*, 1992).

Degree of homogeneity in OH content of the Monastery olivines has been investigated by the analysis of multiple spots within individual grains as well as by analysis of multiple and petrographically different grains from individual "megacrysts."

(4) METHODS

(4.1) Sample preparation

Megacryst minerals, while coarsely crystalline, are commonly riddled by a network of fractures that have developed during and after emplacement of the host kimberlite. This

necessitated the coarse crushing of the samples so that grains relatively free of fractures or included foreign phases could be identified by hand-picking under a binocular microscope. Garnet grains were ground and polished to produce two parallel surfaces, i.e., a plate. The anisotropic minerals were oriented by optical methods before preparation of the parallel surfaces perpendicular to the principal axes of the optical indicatrices. This orientation involved manipulating the grains until centered interference figures were obtained with conoscopic observation on an optical microscope. The procedure introduces some uncertainty into the measurement of the OH content of minerals with strongly pleochroic OH absorptions. Where possible, all three polarization directions were measured on a single grain of the mineral so as to compensate for any misorientation. However, for small olivine grains only the two most intense absorption directions were commonly measured. Unfortunately, this mineral is highly pleochroic and misorientation of occasional grains may lead to uncertainties on the order of ± 10%.

(4.2) Infrared spectroscopy

Our procedure for quantitative IR spectroscopic analysis of minerals has been described by Bell and Rossman (1992a) and Bell *et al.* (1992.). All OH concentrations were derived from integrated intensities of the OH absorptions from 4000 to 2800 cm^{-1}, using the molar absorption coefficients given in Table 1. We estimate that the uncertainty (95% confidence level) in the integrated absorbances and, therefore, in the relative OH concentrations, are approximately 10% for garnet, pyroxenes and zircon and 15% for olivine. Absolute accuracy of the OH concentrations varies according to precision and accuracy of the calibration method and the precise features of the OH absorption spectra and is discussed in Bell *et al.* (1992) and Endisch *et al.* (in prep). The analyses are roughly accurate to a few tens of percent.

The issue of the change in molar absorption coefficient with composition for any given mineral becomes of some importance when we try to establish trends for OH abundance in these minerals as a function of composition. This subject cannot be addressed adequately with the present level of calibration studies. In this study we assume a constant integrated molar absorption coefficient for each mineral. Because this parameter is related to the frequency of light absorbed (e.g., Paterson 1982, Skogby & Rossman 1991) some idea of the relative importance of this effect can be gleaned from the nature of the spectra themselves. Here it is assumed that the more similar the OH spectra of compositional variants of the same mineral are to one another, particularly in terms of the relative contribution to the total absorbance from different frequencies (expressed in cm^{-1}), the more valid is the application of a single absorption coefficient to the whole range of samples and the more confidence we place in the trends. Given the general trend of the variation in OH molar absorption coefficient as a function of frequency (more absorbance per mole at lower wavenumbers) it is possible to make some predictions about the probable sense of deviation from uniformity where spectra are different. OH contents derived from the preferred set of calibrations (Table 1) for the Monastery megacryst minerals are presented along with the compositional data in Table 2.

(4.3) Electron microprobe

Initial wavelength-dispersive electron microprobe analyses for sample selection were performed on a Cameca Camebax instrument (15° take-off angle) at the University of Cape Town, operating at 15 kV. Data processing followed the PAP method (Pouchou & Pichoir 1991) used by Cameca. Garnets and pyroxenes were re-analyzed at Caltech on a JEOL 733 instrument with five moveable spectrometers and 40° take-off angle, operated at 15 and 20

kV accelerating voltage and beam currents from 30 to 500 nA depending on element abundances. Data reduction was by the ZAF method (Armstrong 1988, 1991). Both laboratories used a variety of natural and synthetic mineral standards. An interlaboratory comparison of the Mg# in garnet megacrysts is shown in the appendix. The good agreement between these analyses is a confirmation of both analytical accuracy, to the extent it is required for establishing the compositional trends, as well as mineral homogeneity, because the analyses were done on different grains. Operating conditions, standards and typical counting statistics errors and detection limits for analysis of the different elements in garnet and pyroxenes are given in Table 3. Standard errors of the mean composition for samples derived from replicate analyses are shown on the appropriate figures ($\pm 2\sigma$). Fe^{3+} contents of garnets were calculated from stoichiometry and agree to within 20% relative with Mössbauer spectroscopic analyses (Bell and Mattioli, unpublished data).

(5) CHARACTERISTICS OF OH SPECTRA

(5.1) Garnet

The garnet spectra (Figs. 3.1a-c) are identical to those illustrated in Fig. 2a-e of Bell and Rossman (1992a) and are typical of OH in kimberlite megacrysts. The spectra show a regular change in shape with changing Mg# of the garnet. Fig 4 shows the shift in frequency of the principal (~3570 cm^{-1}) band towards lower wavenumber at higher Fe contents. In addition, relative proportions of the two principal bands change with composition. This is discussed further in a later section with refernce to compositional dependence of OH partitioning involving garnet. The variation in the OH infrared spetrum

may induce small changes in the overall integrated molar absorption coefficient for OH, but is not expected to account for the large variation seen in OH concentration.

(5.2) Clinopyroxene

Clinopyroxene spectra (Fig. 3.2) are generally similar to those described by Skogby *et al.* (1989), but show some composition-dependent variability. Fig. 5 shows the relative changes in intensity of the four main OH infrared bands across the compositional spectrum of these samples. A notable change occurs in the relative proportions of the 3600 cm^{-1} and 3540 cm^{-1} bands, which increase and decrease respectively with increasing Ca#. This effect is not necessarily related directly to the Ca substitution on the clinopyroxene M2 site, as the increase in Ca# is inferred to be accompanied by a decrease in Al^{IV} (Gasparik 1985, Yamada & Takahashi 1984) but not total Al (Fig. 11f). Ca^{M2} and Al^{IV} substitutions are strongly temperature dependent and therefore not easily resolved with the megacryst sample suite, which has a specific ("univariant") temperature - mineral composition variation. Evidence for the effect of the substitution of tetrahedral M^{3+} is shown in Fig 4c, in which the relative proportion of the 3360 cm^{-1} band increases at the expense of the 3540 cm^{-1} band with increasing Si content, while the intensity of the 3600 cm^{-1} band remains relatively constant. The behavior of these three bands suggests that the 3600 cm^{-1} band may be associated with the substitution of M2 cations, whereas the lower wavenumber bands could be associated with trivalent cation substitutions. These observations are at variance with previous conclusions of Skogby *et al.* (1990) on OH band - cation associations in clinopyroxenes, but do not contradict conclusions of Smyth *et al.* (1991). These multiple substitutional mechanisms in pyroxenes will need to be unravelled in order to formulate meaningful thermodynamic descriptions of the behavior of hydrogen in these systems.

The variation in proportional contribution of the various bands to the total integrated absorbance in pyroxenes may lead to a small degree of compositional dependence of the total integrated molar absorption coefficient for OH in clinopyroxene. If the relationship of Paterson (1982) between ε and absorbance is appropriate for the pyroxene OH system, it is calculated that the molar absorption coefficient for OH may decrease by some 8% between Ca# =32 and Ca#=45. However the calculated ε for the most calcic sample (Ca# = 49) is slightly higher (6%) than that of the least calcic one. Unpublished data of Stolper on silicate glasses predict a less sensitive correlation between vibration frequency and ε than that of Paterson (1982). These effects have yet to be substantiated for the pyroxene system and are probably small enough for their potential effect on the determination of relative OH content to be ignored in this study.

(5.3) Orthopyroxene

The three orthopyroxene spectra (example in Fig.3.3) also show the same general features as those exhibited by the orthopyroxene megacryst from the Premier kimberlite, illustrated in Fig. 6 of Skogby *et al.* (1990). As shown in Fig. 6 (this study), there are slight variations in the proportions of bands which comprise the OH spectrum, but these are relatively minor and not expected to cause significant changes in the integrated absorbtion coefficient.

(5.4) Olivine

Olivine infrared OH spectra are similar to those previously reported by Miller *et al.* (1987), but whereas that study described a large number of different types of spectra, the spectra of

samples studied here display a limited variability, which is correlated with mineral composition and association. As noted by Miller *et al.* (1987) for most olivines, these samples exhibit by far the strongest absorption for IR radiation polarized with **E** || [100] (i.e., γ), with absorption intensity for most bands decreasing in the order [100] (γ) > [001] (β) > [010] (α). This emphasizes the need for consistent orientation of olivine samples for comparative studies. Representative olivine spectra are shown in Fig. 3.4a-c. and the OH concentrations derived therefrom are plotted as a function of olivine composition in Fig. 7a.

The relationship of characteristic OH IR spectrum to olivine composition is illustrated by reference to Figs. 3.4a-c and 7a, in which three groups are outlined for convenience of description. We discuss mainly the features observed in [100] polarization. Group 1 olivines are the more magnesian olivines and correspond to the low-Fe, high Ni group of Moore (1986) and Gurney *et al.* (1979). A typical spectrum of olivine from this compositional group is shown in Fig. 3.4a. This spectrum is dominated by a band at 3572 $\pm$ 2 cm^{-1}, which has a shoulder on the low-frequency side. A subordinate pair of bands occurs at 3540 and 3526 cm^{-1}, with the latter commonly the more intense band. Additional bands occur at 3487 cm^{-1} on the low-frequency side and at 3596 cm^{-1}, 3610 cm^{-1}, 3623 cm^{-1} and 3638 cm^{-1} on the high-frequency side of the main peak, the last three bands being very weak. An additional band, which has been assigned to serpentine by Miller *et al.* (1987) occurs near 3710 cm^{-1}. This is a common, but not ubiquitous feature of these megacrysts and the integrated absorbance from this band is always less than 5% of the total. It is not included in the determination of OH content. The frequency of the 3572 cm^{-1} band is independent of composition, as appears to be the case for most bands from the data at hand. Group 2 olivines correspond to the high-Fe, low-Ni population of Moore (1986) and Gurney *et al.* (1979). In addition to their compositional differences, these olivines differ in one aspect of their microstructure from group 1 olivines in lacking the

very fine "granularity" which is apparent in optical microscope examination at high magnification (400X). In the Group 2a olivines (Fig.3.4b), which have relatively low OH contents, the intensity of the 3572 cm^{-1} and 3526 cm^{-1} bands is reduced and the 3592 cm^{-1} band is commonly the most intense in the spectrum. These spectra have more intense bands at high wavenumbers (3610 cm^{-1}, 3623 cm^{-1}, 3638 cm^{-1} and 3670 cm^{-1}) than the spectra of Group 1 olivines. Because of the reduced intensity of the 3572 cm^{-1} band in the Group 2a olivines, the [001] (b) spectrum consists of one, rather than two bands as in the case of Group 1 olivines. All three olivine samples which are intergrown with zircon fall into group 2a. Group 2b olivines (only two samples) have the highest OH contents of all samples and IR spectra (Fig. 3.4c) that are intermediate in character between groups 1 and 2a (they contain features of both groups). In none of the samples where significant variation in OH abundance was recorded did we see variations in the appearance of the OH spectrum, i.e., all bands increased or decreased in intensity in constant proportion to one another. Group 1 and to a lesser extent Group 2 spectra indicate the possibility of some molecular water in the samples (manifested by a broad band centered near 3420 cm^{-1}), but this is difficult to quantify unambiguously because of overlap with the mineral OH bands. In calculation of the integrated absorbances in Table 4, we have included this component because its elimination can only be done with poor precision and may lead to an obscuring of the observed trends. Furthermore it is possible that this water has an internal origin, having been precipitated in response to changing conditions, as proposed for fluid inclusions (thought to be mostly CO_2) in similar mantle-derived olivine by Green & Gueguen (1983). This possible molecular water may occupy the microcracks that pervade many of the samples, or may be associated with the minute inclusions described above.

Heating an olivine megacryst at progressively higher temperature from 100 °C to 600 °C in air for one hour intervals did not produce any change in the appearance of these broader

features or in the sharper bands. At 800 °C, the bands began to decrease in intensity and after 14 hours the sample suffered considerable oxidation, forming a red surface layer (see Chapter 5). Unlike garnet, OH only appeared to be lost from olivine with noticeable destruction of the mineral outer surfaces, although development of this oxidation at the site of OH incorporation in the grain interiors was not necessary for H loss.

(5.5 Zircon

The zircon spectra are very similar to that of sample 1229 from Kimberley (Woodhead *et al.*, 1991, Fig. 2), consisting of two sharp pleochroic bands superimposed on a small amount of broad, featureless absorption. Upon heating to 400 °C, much of this broader component is incorporated into the sharper bands (see chapter 5), suggesting that it may have originally been bound in the zircon structure. A similar behavior has previously been reported by Woodhead *et al.* (1991).

(6) OH CONCENTRATIONS AND CORRELATIONS WITH MINERAL COMPOSITION

Tables 2 and 4 list the OH concentrations, expressed as ppm H_2O by weight (the usage throughout this paper) for the Monastery megacryst minerals. The relative abundances of OH are similar to those observed in these minerals from other mantle environments and concentrations fall within the ranges previously defined for these minerals from the mantle (Bell & Rossman 1992b), decreasing in the order clinopyroxene (291 to 620 ppm) > orthopyroxene (215 to 263 ppm) > olivine (43 to 245 ppm) ≥ garnet (15 to 74 ppm) ≥ zircon (28 to 34 ppm) . In the following section we discuss the relative variations in OH concentration as a function of composition for the five megacryst minerals.

(6.1) Garnet

It was in garnets that the correlation of OH content with degree of differentiation (expressed in the form of the Mg#) was first reported (Bell & Rossman 1992a). Figure 4 from that work is reproduced here in modified form as Fig. 8a. One aspect of this plot that was not discussed in the earlier work was the apparent change in slope in the trend of increasing OH with decreasing Mg number, occurring around $Mg^{\#} = 74$. Given the rather limited data at more Fe-rich garnet compositions, the change in slope is rather loosely constrained, but it appears to occur at or shortly after the entry of ilmenite into the crystallization sequence. The point of onset of ilmenite crystallization is well-defined by the analysis of a large number of coexisting garnet-ilmenite pairs (Gurney *et al.*, 1979), and is further illustrated by the break in slope of the V vs. Mg# plot (Fig. 8d), caused by the relative compatibility of V in the ilmenite structure. Figs. 8c and 8e illustrate, respectively, the behavior of Ti and Zr in the garnets with progressive differentiation. All these plots show breaks in slope of the data trends at Mg# ~74, which are not apparent in the trends of the silicate-compatible elements Cr and Ni (Figs. 8j, k).

In Figs. 9a-c, the positive correlations of the garnet OH content with the incompatible elements Ti, V and Zr are examined further. It is estimated that for a likely fractionating assemblage of unknown proportions of garnet, clinopyroxene, olivine and orthopyroxene before the point of ilmenite entry, these three elements all possess bulk crystal-liquid distribution coefficients (D's) ≤ 0.2 and probably smaller. They therefore are expected to behave roughly as perfectly incompatible elements during fractional crystallization. Water probably has an even lower bulk D, and should be comparably enriched in the residual magma. However, up to Mg# = 74, H in garnets is enriched by a factor of three over the

other three incompatible elements. This suggests that the relative garnet-liquid distribution coefficients for these elements are changing with differentiation. The fact that the enrichment of H_2O over each of the other three elements occurs by the same factor (3.3 ± 0.2) strongly suggests that it is D_{H_2O} which is changing (increasing). Nevertheless, we cannot exclude entirely the possibility that D's decreasing similarly for Ti, V and Zr contribute to the relative enrichment in OH over these elements in the garnets. A similar conclusion is reached from the rare-earth element abundances (bulk D also « 1), determined by ion-microprobe in samples MON-9, ROM263 GT-36 and ROM263 GT-52 and the Monastery garnet standard (Bell and Kennedy, unpubl. data). Like Ti, V and Zr, the REE suggest on the order of 20% crystallization from Mg# of 80 to Mg# of 74 (Fig. 10). The REE, like Zr, but unlike Ti, V and OH, show little or no effect of ilmenite fractionation on the general upward trend in their concentrations in the most Fe-rich garnets. This contrasting behavior between OH and similarly bulk-incompatible REE and Zr indicates either crystal chemical control on OH incorporation in garnet, or some change in the activity of water at the point of ilmenite entry. Evidence in support of increasing garnet-liquid D_{H_2O} with differentiation is presented in a later section.

(6.2) Clinopyroxene

In clinopyroxene the Ca/Ca+Mg ratio ($Ca^{\#}$) is a convenient measure of the degree of differentiation in the main silicate association of the Monastery megacryst suite. In Fig. 11a, OH contents are plotted as a function of $Ca^{\#}$. If we exclude for the present time the clinopyroxene from MON-26, the clinopyroxene-garnet intergrowth (reasons given below), the OH in clinopyroxene shows a trend of gently increasing OH content, followed by a sharp decrease as differentiation proceeds ($Ca^{\#}$ increases) beyond the appearance of ilmenite at Ca# ~38. As in garnet, the change in slope occurs around the point of ilmenite

entry into the crystallization sequence, and the decrease in H content is mirrored by a decrease in Ti (Fig 11b). However, K in clinopyroxene follows a very similar behavior (Fig 11d), resulting in a regular positive correlation between K and H in clinopyroxene (Fig. 12).

Fig 11d demonstrates that sample MON-26 is also somewhat anomalous in terms of K_2O, and it is marginally richer in Mg, Cr and Ni contents than would be predicted for its Ca# from the trends followed by the other clinopyroxenes (Figs. 11g-i). One possible explanation for the slightly irregular composition of this sample is that it resulted from a greater degree of magma wallrock interaction than the other megacrysts. A modest degree of such interaction is suggested by occasional Sr or Nd isotopic heterogeneity in megacryst samples from any one suite (Jones 1987, Hops *et al.,* 1989). Judging by the xenolith population, most of the lithospheric mantle under Monastery appears to consist of phlogopite peridotite, and local contamination of the megacryst magma and its products with the characteristic elements of this material (Mg, Cr, Ni, K, H) is to be expected. Elements which would be dominated by the magma in such an interaction, such as Na, V and Ti, are unaffected by this process and for MON-26 lie very precisely on the trends defined by the other samples (Figs. 11b,c,e). We note that the intergrowth exhibits smaller grain size than the other samples in this study, and this, together with the fact that it is an intergrowth and thereby anomalous to begin with, indicates that this sample is not an ideal representative of the Monastery megacryst suite. Nevertheless, it remains the only coexisting garnet-clinopyroxene pair we have analyzed and is important in the evaluation of calculated inter-mineral OH distribution coefficients presented later in this paper.

The H-K correlation is examined in greater detail in Fig 13, which shows that the H/K ratio for all subcalcic clinopyroxenes (including MON-26) is constant at 11.06 ± 1.94 (2σ). This

ratio differs significantly from the H/K ratio of 22.5 ± 2.6 for the calcic clinopyroxene ROM270-DI10 and further confirms the different petrological history of the calcic clinopyroxene population at Monastery. Although the precise relationship of the two pyroxene populations to one another has not been established, there is some trace element evidence that they are petrologically related, and furthermore that, in contrast to the subcalcic clinopyroxenes, at least some of the calcic population has crystallized together with phlogopite. Removal of phlogopite from a magma parental to the most evolved subcalcic clinopyroxenes would produce the required decrease in H/K to account for the composition of sample ROM270-DI10 (see Fig. 12).

One explanation for the correlated K and H contents is that the decreasing concentrations of these elements reflect the removal from the system of a phase enriched in these components at about the point of first ilmenite crystallization. Phlogopite and hydrous vapor are potential candidates, and phlogopite is a common megacryst phase at Monastery. Although it is tempting to ascribe the depletion to phlogopite removal, we emphasized in an earlier section that there is no evidence for the co-crystallization of phlogopite with these "main silicate trend" minerals. Indeed, the Cr content of phlogopite and the Cr and Nb content of ilmenite in phlogopite-ilmenite pairs are incompatible with the coexistence of phlogopite with the "main silicate trend" minerals (Fig. 2). As in garnet, we must consider whether the changing distribution coefficients for H and K are the cause of the sudden change in the trends for these elements.

The most Ca-rich clinopyroxene (ROM270 DI10) is not part of the "main silicate trend" and belongs to the separate population of calcic clinopyroxenes that may coexist with relatively Mg-, Cr-rich ilmenite and phlogopite. Nevertheless, this sample, continues the trend of decreasing OH content with Ca#. This sample is the most OH and K-poor clinopyroxene,

despite the coexistence of other samples like it with phlogopite. Although this suggests that crystal chemistry might exert a strong control on the incorporation of these components in clinopyroxene, the presence of phlogopite does not necessarily indicate a more H- and K-rich environment because the parental liquid might be quite different structurally (e.g., carbonatitic).

Whatever, their cause, the constant H/K ratio in clinopyroxenes (except for a sample which is petrologically less related *in the mantle*) would seem to argue that the OH contents of clinopyroxenes have not been changed during their ascent and eruption in the kimberlite, because it is unimaginable that the K contents of these large crystals could have been altered sympathetically. However, as with other similar arguments that have been made on the basis of composition (Bell & Rossman 1992a), there is always the possibility that OH and K coincidentally share the same response to Ti incorporation in clinopyroxene; K in the mantle during growth of the crystal and H in the crust during eruption.

(6.3) Orthopyroxene

Although only three orthopyroxene samples were analyzed, they span the entire range of $Mg^{\#}$ of Monastery orthopyroxenes, one of the least common on the megacryst minerals. In contrast to garnet and clinopyroxene, the three orthopyroxenes display a trend of regularly decreasing OH content with decreasing Mg number (Fig. 15a). Although the trend appears regular, the paucity of data prevents the unequivocal dismissal of kinks or breaks in slope. The orthopyroxene H contents are not correlated with elements affected by ilmenite crystallization, such as Ti (Fig. 15b), but are well correlated with Na, Ca and Al (Figs. 15c-e). Although only the two more magnesian orthopyroxene samples are believed to crystallize in the regime where OH contents of garnets, clinopyroxenes and olivines

increase, the observed decrease in OH content for orthopyroxenes with decreasing Mg# suggests control of crystal-liquid distribution coefficients for OH by compositional parameters. These distribution coefficients are probably strongly affected by the changing crystal chemistry of the orthopyroxene.

(6.4) Olivine

Analysis of different grains from the same "megacryst" reveals that substantial heterogeneity in OH content can occur, but it is perhaps less dramatic than expected from the variation in internal structural heterogeneities observed (Table 4). Four spots in a single grain (13.1) from sample ROM250-OL13 are identical in OH content within uncertainty of measurement and are also indistinguishable from a second grain (13.2) with different internal structure (see Table 2) from the same "megacryst." Although these samples are petrographically different, all contain features indicating deformation. In contrast, petrographically different grains from ROM250-OL42 have significantly different OH contents. A highly strained porphyroclast traversed by shear fractures (OL42.1) has OH content similar to other megacrysts while two tablets (OL42.2, OL42.3) which appear to have recrystallized and annealed, though still showing some traces of relic deformation features, have much lower OH contents. Annealed grains in other samples do not show this dramatic reduction in OH content, and it appears that, in general, there is little relationship of the OH content to grain microstructure or inclusion content. For this reason we suggest that the lower OH content of the OL42 tablets may be due to their annealing during ascent or emplacement of the kimberlite (Mercier 1979) when water pressures are likely to be reduced from those in their mantle source. On the other hand, Dawson *et al.* (1981) have recorded chemical differences between porphyroclasts and neoblasts of olivine

from Fe-rich deformed dunite xenoliths from Kimberley, raising the possibility that variations in OH content could be linked to trace element compositional differences.

Several samples have variations in OH content which agree approximately within experimental uncertainty, yet there are some for which true intergranular variability appears to exist. In general these variations serve to scatter, but not destroy, the general trend displayed in Fig. 7a. If we proceed on the assumption that the most OH-rich sample from each megacryst represents the closest approach to the original H concentration, with lower concentrations produced by post-incorporation annealing (see above), then it appears from Fig. 7a that the OH content of the Fe-poor olivines increase slightly with decreasing Mg number. This trend is nevertheless weakly defined in comparison with that seen in garnets, for example. The Fe-rich olivines cluster into two groups in terms of their OH contents. One group (2a) has OH concentrations similar to the Fe-poor olivines, apparently continuing from the end of the Fe-poor olivine trend, but with the suggestion of a decrease in OH content with decreasing Mg number. The other group (2b - samples OL13 and OL26) has much higher OH concentrations.

It has been previously stressed that the Fe-poor and Fe-rich olivine groups are distinct in their mineral association and Ni contents. Fe-poor olivines are associated with other silicates (garnet, olivine and pyroxenes), but are never found in association with ilmenite, in contrast to the Fe-rich olivines, which in addition to ilmenite, also may coexist with phlogopite and zircon. The mineral association observations and equilibrium relationships established in the next section strongly suggest that Fe-poor olivines cease to crystallize at some point in the magmatic evolution near, and possibly coincident with, the point of ilmenite entry. The appearance of a continuous increase in OH content of these samples with decreasing Fo content is thus similar to the trends seen in clinopyroxene and garnet.

The relationship of the Fe-rich olivines to this group is not clear, although it would appear that they have precipitated from a more geochemically evolved system, i.e., with higher Fe and incompatible element contents in themselves and in their associated minerals. The pattern of decreasing OH content at higher Fo contents is strikingly similar to that seen in the clinopyroxenes that coexist with ilmenite, and indeed the Fo contents of these olivines are consistent with the Mg numbers of garnets and clinopyroxenes that are associated with ilmenite. Although the high Fe-olivines as a group are observed to coexist with ilmenite, this ilmenite is not compositionally equivalent in terms of its trace element contents with the ilmenite associated with the common silicates (the *main trend silcates*). These Fe-rich olivines therefore cannot represent the same environment as the garnets and clinopyroxenes that coexist with ilmenite, even though they appear to display similar geochemical features in terms of H. We have no explanation at present for the apparent existence of two groups of Fe-rich olivine in terms of OH content. However, it should perhaps be emphasized that, once again, the coexistence, or lack thereof, with ilmenite appears to play a role in the H content of these minerals.

We have not determined trace element contents of these olivines to evaluate the connection with, for example, Ti in a charge-coupled substitution. This would seem a worthwhile pursuit, given the correlations observed between H and Ti in the other minerals. We note that Drury and Van Roermund (1988, 1990) have drawn attention to densely distributed submicroscopic inclusions that contain various elemental impurities in olivine such as that examined here . While some of the OH we detect may reside in such inclusions, this may have precipitated from the olivine itself (Hervig 1990).

The preferential incorporation of H into olivine in association with some other trace component, such as Fe^{3+} or Ti is particularly important for application of the

hydrobarometer of Bai & Kohlstedt (1992), as varying concentrations of these trace components would restrict accurate application of the experimental calibration.

(6.5) Zircon

Zircon concentrations are relatively uniform in the three samples analyzed, all of which are intergrown with Fe-rich olivine. The range in concentration determined on two grains from the same sample is greater than that observed between all three samples and is approximately at the limit of analytical precision, i.e., the total variation observed could be caused by analytical uncertainties. This situation arises because the broad absorption contributes a substantial portion to the total integrated intensity and such features have greater uncertainty in their baseline.

(7) EQUILIBRIUM RELATIONSHIPS BETWEEN MEGACRYST MINERALS

While the trends in Figs. 7a, 8a, 11a and 15a show the evolution of OH content of each mineral with degree of differentiation, we have not analyzed sufficient coexisting mineral pairs to establish how these trends are related to one another. This is not necessarily a straightforward matter, as the minerals we have analyzed do not cover the same degrees of differentiation of the parent magma and in some cases may not be related in a simple way to the same parent. At Monastery, the coherency of major and trace element trends makes a strong case for a comagmatic origin of minerals of the "main silicate trend" (see Figs. 1, 2 and Moore *et al.*, 1992).

(7.1) Parameterization of coexisting compositional relationships

In order to establish the relationship of the "main silicate trend" minerals to one another, we have described the documented coexisting relationships by a series of linear or second-order polynomial equations. These equations are then used to derive the major element compositions (either Mg# or Ca#) of the other minerals that are predicted to be in equilibrium with the sample in question. Once the major element composition of the predicted coexisting phases has been estimated, the OH contents of these minerals can be calculated using regression equations derived from the data in Figs 7, 8a, 11a and 15a. The inter-mineral distribution coefficients are then calculated from the measured OH content of one mineral and the calculated OH content of the phases with which it is predicted to be in equilibrium. The form of the equations is arbitrary and is not based on any assumed physical model; those giving the best fit to the data arrays and providing a certain degree of internal consistency were chosen by trial and error. Further details can be found in the appendix to this paper.

The "documented coexisting relationships" referred to above are published or unpublished analyses of spatially coexisting (intergrown) megacrysts or, in some cases, minerals in peridotite xenoliths. Megacrysts used in the parameterization derive from the kimberlites of Lesotho, and Monastery, Lekkerfontein, Jagersfontein and Kaalvallei in South Africa. All these suites have similar compositional variations with decreasing temperature for the major elements, but may vary in their spread of compositions (degree of differentiation) or in details of minor element chemistry. Because megacrysts have a very specific temperature-composition relationship (such as the progressive increase in Fe/Mg as temperature drops), partitioning data from coexisting peridotite minerals are generally inappropriate unless the temperature and mineral compositions can be matched to megacrysts. In general, the level of precision and accuracy of mineral thermometers does not allow this. However, where

megacryst data are scarce certain compositional inter-relationships derived from peridotite xenoliths (typically those relatively independent of temperature) can be applied with caution.

The principal indices of differentiation used in this study are Mg# in garnet and Ca# in clinopyroxene. Clinopyroxene is actually present over much (but not all) of the differentiation sequence, and Ca/Ca+Mg can be related to an estimate of temperature in a simple way (e.g., Finnerty & Boyd 1987). In Fig. 16 we use the parameterization discussed above to relate the degree of differentiation of all minerals to Mg# in garnet, with calculated Ca# in clinopyroxene plotted for reference. This plot confirms that the OH content of garnet, clinopyroxene and Fe-poor olivine increase from their most magnesian compositions to the point of ilmenite entry, at which OH in garnet and clinopyroxene decreases, while magnesian olivine disappears from the crystallization sequence.

(7.2) Partitioning relationships involving garnet

(7.2.1) Garnet - clinopyroxene partitioning

The calculated distribution of OH between garnet and clinopyroxene, together with the single measurement of OH in coexisting garnet and clinopyroxene (MON26) are shown in Fig. 17a as a function of Mg# of garnet. The agreement between the D's calculated from the garnet data with those from the clinopyroxene data are a reflection of the well defined trends that H_2O follows with Mg# and Ca# in these minerals respectively. The first crystallized clinopyroxene incorporates about 40X more OH than its coexisting garnet, diminishing to a factor of about 6X for the clinopyroxenes coexisting with the most Fe-rich garnets. Despite the fact that the pattern of OH incorporation into both garnet and

clinopyroxene changes at the point of ilmenite entry, the distribution of OH between these phases displays a regular variation, with no change in the trend of inter-mineral partitioning. The very large change in partitioning of OH between garnet and clinopyroxene over the range of temperature-composition of the main silicate trend megacrysts demonstrates the danger of assuming a constant crystal-liquid D_{H_2O} for nominally anhydrous minerals.

What properties of H are responsible for this striking change in partitioning behavior? We have applied a similar analysis in calculating clinopyroxene-garnet D's for Na, Ti, V, Cr and Ni, none of which exhibit anything like the dramatic variations seen for H. Other trace elements, the concentrations of which in clinopyroxene depend strongly on the Ca content thereof, such as the LREE or Sr (McKay *et al.* 1986), may show increasing $D^{cpx\text{-}gt}$ with increasing $Ca^{\#}$. The temperature range over which this change occurs is believed to lie between about 1350 °C and 1100°C (Nixon & Boyd 1973, Gurney *et al.*, 1979, Moore 1986). It appears that a detailed understanding of the substitution mechanisms of H in these minerals may be necessary in order to answer this question satisfactorily.

(7.2.2) Garnet-olivine partitioning

The distribution of OH between garnet and olivine, calculated as above and measured in the coexisting sample MON-24 is illustrated in Fig. 17b. Because olivine is substantially more heterogeneous with respect to OH than the other minerals, the trend is not as well constrained. Given the probable recrystallization effects in olivine, the highest value for $D^{ol\text{-}gt}_{H_2O}$ from any given sample is probably the most accurate. Nevertheless, it appears that olivine-garnet OH partitioning follows a similar pattern to clinopyroxene garnet. We have restricted our analysis of olivine-garnet and olivine-clinopyroxene partitioning

relationships to the Fe-poor olivines, because of uncertainty surrounding the relationship of the more Fe-rich olivines to other megacrysts, and because these Fe-rich olivines appear to fall into two groups of different OH content. Olivine and garnet coexist over a more restricted range of the differentiation sequence than garnet and clinopyroxene, but the overall variation in $D^{ol\text{-}gt}_{H_2O}$ is approximately six-fold (from $D^{ol\text{-}gt}_{H_2O}$ ~13 to ~2), similar to the relative change in $D^{cpx\text{-}gt}_{H_2O}$.

(7.2.3) Garnet -orthopyroxene partitioning

Although only three values for $D^{opx\text{-}gt}_{H_2O}$ have been calculated, they show (Fig. 17c) the same basic pattern as seen in the other partitioning relationships involving garnet. Because the trend of the orthopyroxene OH content cannot be established with only three data points, values for $D^{opx\text{-}gt}_{H_2O}$ could not be calculated from the garnet data. Values for $D^{opx\text{-}gt}_{H_2O}$ are similar to $D^{ol\text{-}gt}_{H_2O}$, varying from 14 at high Mg# to ~3 at low Mg# where the minerals coexist with ilmenite.

(7.3) Olivine - orthopyroxene - clinopyroxene partitioning

In contrast to partitioning relationships involving garnet, the distribution of H between olivine, clinopyroxene and orthopyroxene is relatively uniform. This is shown in Fig. 18a-c, where the calculated D_{H_2O} values for cpx/ol, cpx/opx and opx/ol are plotted as a function of Ca#. In all three cases, the D_{H_2O} values are more or less consistent with a single distribution coefficient for each mineral pair, independent of mineral composition and temperature over the range investigated. This is a noteworthy point, considering the variation in the OH abundances of the individual minerals and the changes in slope exhibited by their OH trends. The partitioning of OH between ortho- and clinopyroxene in

megacrysts ($D^{cpx/opx}_{H_2O}$ = 1.85 ± 0.37 (2σ, n=3)) overlaps the range of values derived from the data of Bell & Rossman (1992b) for peridotites and a garnet websterite ($D^{cpx/opx}_{H_2O}$ = 2.6 ± 0.7 (2σ, n=5)). These latter values are, however somewhat less accurately determined because of the analytical method employed in that study (unpolarized spectra in some cases). In contrast, partitioning of OH between olivine and the pyroxenes is grossly different ($D^{px/ol}_{H_2O}$ is far higher in the earlier study) because of the very low OH concentrations in olivines from spinel lherzolite xenoliths. That study also employed a different calibration for the OH content of olivine which resulted in concentration estimates approximately a factor of two lower than those which would be derived from the calibration used here.

The lower OH content of basalt-hosted olivines was noticed by Miller *et al.* (1987), who suggested that these samples may have lost OH in the near-surface eruption environment. Circumstantial support for this notion has come from the determination of extremely rapid diffusivity of hydrous species in olivine (Mackwell & Kohlstedt 1990). Mackwell & Kohlstedt (1990) and Bai & Kohlstedt (1992) contend that hydrogen is less readily removed from pyroxenes, thereby accounting for relatively high OH content of the pyroxenes in the spinel lherzolite xenoliths studied by Bell & Rossman (1992b). Bai & Kohlstedt (1992) cite a personal communication from Mackwell in support of this. In fact, Mackwell's comments relate to experiments on an extremely Fe-poor enstatite (~ En_{98}) which probably has very limited capacity for redox reactions believed to accompany H loss in these minerals, and is therefore not necessarily relevant to the natural situation.

The contention of Bai & Kohlstedt (1992) is contrary to our experimental observations and those of Skogby (pers. comm.) which indicate that H may be more rapidly removed from pyroxenes (particularly clinopyroxene) than olivine by heating in an oxidizing environment. The pressures of origin of spinel lherzolites in basalts do allow for substantial OH contents

in the olivines in sufficiently water-rich environments (fH_2O ~ 100 kbar at 20 kbar pressure and 1200 °C), but is difficult to assess how often conditions approaching water-saturation are attained. Loss of H from olivine may occur in response to crystal annealing as much as from H diffusion.

(7.4) Olivine - zircon partitioning

The three olivine-zircon intergrowths yield a mean $D^{ol/zir}_{H2O}$ = 3.2 ±0.9 (2σ, n=4), assuming that the heterogeneity seen in both olivine and zircon in ROM181 are correlated.

(8) CRYSTAL-CHEMICAL CONTROL ON OH INCORPORATION IN NOMINALLY ANHYDROUS MINERALS

(8.1) Garnet

The above observations on the OH content of Monastery garnet megacrysts indicate that as differentiation of the megacryst suite proceeds, OH is incorporated into this mineral in amounts progressively greater than would be expected from other trace element concentrations in the garnet and than would be expected based on the OH contents of coexisting pyroxenes and olivine. In this section one possible cause for this behavior, namely the influence of Ti in garnet, is investigated.

It is shown in Fig. 19a that the proportion of the total OH absorbance due to the low wavenumber (3512 cm^{-1}) band is proportional to the Ti content of the garnet. This plot does not show an intercept at the origin because there is always some measured absorbance at 3512 cm^{-1} due to the breadth of the 3570 cm^{-1} band. The actual intensity of the 3512

cm^{-1} band is not correlated with Ti content (Fig. 19b) because this intensity also depends on the overall OH content of the system, which is not directly correlated with Ti in garnet. It is suggested here that OH in these garnets is contained in two principal sites; one characterized by absorption at 3570 cm^{-1}, dependent in frequency on the general major element composition of the garnet (Fig 4), and the other (with absorption at 3512 cm^{-1}) associated with the presence of Ti. These two bands have different thermal stabilities in air, the 3512 cm^{-1} band being more resistant to removal by heating. OH is incorporated into both these sites in response to increasing water fugacity, but is enhanced by the concomitant increase in Ti content of the garnet. When ilmenite enters the crystallization sequence and the activity of Ti no longer rises (as rapidly) in the system, the garnet can no longer increase its OH content as rapidly by this mechanism. This produces the break in slope on Fig 8c. at Mg# = 74.

In actual fact, even considering the 3570 cm^{-1} band alone, garnet appears to incorporate OH preferentially to other trace elements during differentiation, that is, the mechanism proposed above may only account for some of the observed effect. It is possible that the additional effect of OH enhancement is provided by dropping temperature. The OH content of hydrogrossular garnets coexisting with a hydrous fluid has been shown to be highly temperature dependent, decreasing continuously to anhydrous grossular as temperature is increased at constant pressure (Yoder 1950, Pistorius & Kennedy 1960). While it cannot be assured that the hydrogarnet substitution mechanism is operating in the megacryst garnets, a similar temperature-dependent behavior in these samples seems plausible.

The precise nature of the Ti-coupled substitution was not established, and may prove to be only linked indirectly to Ti. For example, it has been recognized in this study and previous studies on Ti-rich high-pressure garnets (Akella & Boyd 1974, Hervig *et al.*, 1986) that

there are insufficient monovalent cations (including H) to charge balance tetravalent Ti in these garnets, with Si contents not allowing for any significant tetrahedral substitutions. Thus, either octahedral divalent cations (e.g., Fe^{2+}, Mg) or vacancies are indicated. The former are common stoichiometric components of synthetic garnets (Geller 1967) and have also been observed in Ti-rich low-pressure garnets (Amthauer *et al.*, 1977). Thus H may be bonded to oxygens associated with such cations as well as Ti, or Na, which is also proportional to Ti in these garnets. At this point we cannot distinguish between these possible associations.

(8.2) Other minerals.

Because the minerals other than garnet exhibit constant partitioning relationships to one another, and because we do not have as many trace element data with which to compare OH behavior, it is more difficult to recognize possible effects of crystal chemistry on the partitioning of OH. However, the downward - turning OH trends for both olivine and clinopyroxene that are believed to co-precipitate with ilmenite (with concomitantly decreasing Ti in clinopyroxene) (Figs 7 and 11a,b) suggest that this element might play a role in OH incorporation into these minerals as well. Gasparik (1985) has argued that Ti incorporation into synthetic kosmochlor ($NaCrSi_2O_6$ clinopyroxene) is accompanied by a vacancy). The constant ratio of Ti to H (Fig. 14) in Monastery clinopyroxenes supports the likelihood of some crystal-chemical association between the two. Because the nature of the Monastery megacryst magma and its differentiates is not well understood, it is difficult to predict what changes in liquid composition might produce changing trends in mineral-melt D_{H_2O}. The onset of ilmenite crystallization accompanied by the disappearance of magnesian olivine from the crystallizing assemblage indicates some probable change in the character of the evolving liquid.

(9) CALCULATION OF WATER FUGACITIES

(9.1) Olivine as a hydrobarometer

Bai & Kohlstedt (1992a) have determined experimentally the OH content of Mg-rich natural olivine as a function of fO_2, fH_2 and fH_2O at pressures of 1 to 2 kbar. The resulting power-law relationship between H content and fH_2O predicts substantial OH contents of olivines equilibrated at high water pressures. In this section we extrapolate this relationship over 1-2 orders of magnitude in H concentration to calculate the fH_2O under which the Monastery megacryst olivines equilibrated. The legitimacy of this extrapolation is supported by a comparison of the IR spectrum of a typical Fe-poor Monastery megacryst olivine with that of a hydrothermally annealed hydrous olivine from the study of Bai & Kohlstedt (1992b) (Fig. 3.4d). It can be seen that there is extremely good correspondence between the two OH spectra, virtually every band in the experimental sample being present, in roughly appropriate intensity proportion, in the natural. This implies that H is located in the same sites in the two olivines, and suggests that the same mechanism of incorporation is operating over a very large pressure range, although this can only be thoroughly confirmed by *in situ* spectroscopy at high pressure and temperature. The spectral correspondence of the experimental sample to the Fe-poor olivine megacrysts (but less so to the Fe-rich olivines) gives us some confidence in applying the extrapolation. The experiments of Bai and Kohlstedt were carried out at 1300 °C, which is approximately in the center of the range calculated for the Monastery megacrysts which crystallized before ilmenite (Gurney *et al.*, 1979, Moore 1986). Despite these favorable circumstances, there remains considerable uncertainty in the extrapolation in pressure, temperature and composition from the experiments to the natural system and we regard the derived water

fugacities as no more than approximate. Even greater uncertainty surrounds the calculation of magma water contents in the next section.

Table 4 and Fig 7b show the water fugacities calculated from the relationship:

$$H \text{ per } 10^6 \text{ Si} = 0.279 * fH_2O^{0.8} \text{ (Bai \& Kohlstedt 1992a).} \quad (1)$$

The first order observation is that these fugacities are far greater than that of pure H_2O in the upper crustal emplacement environment of the kimberlite. The lowest fH_2O of 3900 bars (a recrystallized tablet, OL42.3) is appropriate to pure water at 1300°C and ~3100 bars and could have been generated in a water-rich environment at comparatively high levels in the crust. We would expect that P_{H2O} is always less than total pressure in this natural system because of the high solubility of SiO_2 and alkalis in aqueous fluids at high P and T and alternatively because of the CO_2 rich nature of kimberlite volatiles. On the other hand, those olivines that are considered to be the least disturbed in terms of primary OH contents cannot be the products of upper crustal annealing. Despite these indications, there are possible scenarios in which to generate such high OH concentrations in the emplacement environment of kimberlite. These rely on the quenching in of defects set at high fO_2 and fH_2 in the mantle, followed by gain of H from a very H-rich fluid such as might occur in certain regions of a solidified kimberlite body as a result of deuteric serpentinization processes. It therefore appears that a crustal origin for the H in olivine cannot be completely ruled out at present, though it requires a set of rather special circumstances, including an initially hydrous mantle setting. In the following section we show that these water fugacities are consistent with petrological expectations for the mantle source region of the megacrysts.

(9.2) Garnet as a hydrobarometer

The IR spectra of pure pyrope garnets synthesized under a variety of P and T conditions in the presence of "pure" water (Geiger *et al.* 1991 - Appendix 2) have been analyzed to give quantitative estimates of the OH contents and plotted as a function of the fugacity of water at the conditions of synthesis (calculated from the equation of state of Saxena & Fei (1987) and using the method outlined in that paper for the evaluation of fugacity coefficients at P>5 kbar). A power-law fit to the data gives the relationship (see chapter 5):

$$H_2O \text{ (ppm) in pyrope} = 0.0443 \cdot f_{H_2O}^{0.668}. \qquad (2)$$

This relationship has been used to calculate the expected water content of a garnet at f_{H_2O} = 18000 bars, the water fugacity calculated for the MON-24 olivine, giving an answer of 31 ppm H_2O in the garnet. The olivine of sample MON-24 coexists spatially with garnet with 35 ppm H_2O. The agreement between the calculated and the measured OH contents of this garnet is noteworthy, and suggests that a measure of self-consistency has been attained in these experimental studies and their relationship to the natural system. The close similarity of the numbers is probably fortuitous because of known inaccuracies and substantial uncertainties in eqn. (2) (see chapter 5) and the spectroscopic differences between synthetic and natural pyrope, but it is encouraging that OH contents of the correct order of magnitude are predicted by these studies. The self-consistency of these studies is viewed as evidence in support of, but not confirming, the preservation of original mantle OH contents of the natural mineral samples.

(10) WATER CONTENT OF THE MONASTERY "MEGACRYST MAGMA"

If it is assumed that the water fugacities recorded by the olivines are those present in the magma from which they crystallized, then some estimate of the water content of this melt can be made with the use an appropriate thermodynamic model. From equation (18) of Silver & Stolper (1989) for water-saturated melt, and assuming Henry's Law is valid for the solution of water molecules in the melt, the following expression can be written for the concentration of water molecules dissolved in a melt, not necessarily in equilibrium with a vapor:

$$X^{m}_{H_2O,\,mol}(P,T) = X^{m}_{H_2O,\,mol}(P_r,T_r).\frac{f_{H_2O}(P,T)}{f_{H_2O}(P_r,T_r)}.\exp\left[-\int_{P_r}^{P}\frac{V^{0,m}_{H_2O}(P',T)}{RT}dP' + \int_{T_r}^{T}\frac{\Delta H^{0}_{H_2O}(P,T')}{RT'^{2}}\right] \quad (3)$$

where $X^{m}_{H_2O,\,mol}$ represents the mole fraction of water molecules in the melt, f_{H_2O} is the fugacity of water, $V^{0,m}_{H_2O}$ is the molar volume of water molecules in the melt, $\Delta H^{0}_{H_2O}$ is the standard enthalpy of solution of water in silicate melt and P, T, P_r and T_r are pressure and temperature at the conditions of interest and at some reference conditions, respectively. This allows the concentration of water molecules in a silicate melt to be determined under conditions of P and T and fH_2O if their concentration is known under a set of reference conditions.

(10.1) Estimation of P-T conditions

Gurney *et al.* (1979) estimate that the Monastery megacrysts formed essentially isobarically at 45 kbar, based on the assumed equilibrium relations between garnet and orthopyroxene and using the barometer of Wood (1974). More recent estimates on selected multiphase megacryst aggregates by Moore (1986) place the pressure of origin between 50 and 55

kbar, using the barometer of Nickel & Green (1985) in combination with the pyroxene solvus thermometer of Bertrand & Mercier (1986). Application of the O'Neill & Wood (1979) garnet - olivine thermometer to those samples to which the Bertrand & Mercier (1985) pyroxene solves thermometer has been applied produces similar results (to within ~30 °.) This does, however, rely on a reasonably accurate estimate of the Fe^{3+} content of the garnet, which in Monastery garnet megacrysts amounts to about 10% of the total Fe (Bell and Mattioli, unpubl. Mössbauer spectroscopic data). Sample MON-24 consists of coexisting garnet and olivine crystals, the Fe-Mg exchange equilibrium between which can be used to infer the temperature of formation. Using the temperature calibration of O'Neill & Wood (1979) as corrected by O'Neill (1980) for this exchange, MON-24 is calculated to have formed at a temperature of 1337 °C at an assumed pressure of 52.5 kbar.

(10.2) Calculation of water content of melt in equilibrium with MON-24.

From the 500 bar, 1200 °C experiments on the solubility of water in the presence of mixed H_2O - CO_2 fluids of Dixon (1992), the following relationship is established:

$$X^{m}_{H_2O,\,mol}(500b,1473K) = 3.26 \text{ X } 10^{-5}\, f_{H_2O}\,(500b,1473K). \qquad (4)$$

Substituting (4) into (3) and setting $P_r = 500$ bars, $T_r = 1473$K gives:

$$X^{m}_{H_2O,\,mol}(P,T) = 3.26 \text{ X } 10^{-5}.f_{H_2O}(P,T).\exp\left[-\int_{500}^{P}\frac{V^{0,m}_{H_2O}(P',T)}{RT}dP' + \int_{1473}^{T}\frac{\Delta H^{0}_{H_2O}(P,T')}{RT'^{2}}\right].$$

(5)

Because the calculations on the megacrysts involve very large extrapolations in pressure, the choice of $V^{0,m}_{H_2O}$ is fairly important. Here I use a value of 12 cm^3 per mole, which was derived by Dixon (1992) from a fit of equation (1) to the high-pressure water solubility data of Hamilton *et al.* (1964). Incidentally, the pre-exponential constant in equation (5) above is very close to that derived from the fit to the Hamilton *et al.* (1964) data by Dixon (1992) as well. It should be stressed that $V^{0,m}_{H_2O}$ is not well known at present and may be composition - dependent, so that the calculated water contents at high pressures are attended by substantial uncertainty. The extrapolation in temperature only on the order of 150 °, so that the choice of $\Delta H^0_{H_2O}$ is less important. Here I use the value of -3000 cal.mol^{-1} determined by Silver & Stolper (1989) for albite melt. Incorporating these constants and R = 1.987 cal.$mol^{-1}.K^{-1}$ gives the following expression for the concentration of water molecules in a basalt-like liquid as a function of P, T and f_{H_2O}:

$$X^m_{H_2O,\,mol}(P,T) = 3.26 \times 10^{-5}.f_{H_2O}(P,T).\exp\left[\frac{-0.1443[P-500]}{T} + 1.0236 - \frac{1507.76}{T}\right]. \quad (6)$$

Using the estimated P-T conditions of formation of sample MON-24 (discussed above), together with the estimate of f_{H_2O} = 18016 bars derived from the OH content of the olivine by the equation of Bai & Kohlstedt (1992) (Table 4), a molecular water concentration of $X^m_{H_2O,\,mol}$ = 0.006062 is calculated from eqn. (6). It has been established that water is present in silicate melts as OH groups and water molecules (H_2O, mol) (Stolper 1982). Silver & Stolper (1985), present a model for the behavior of water in silicate melt which is based on ideal mixing of OH groups, H_2O molecules and oxygen atoms in the melt. Equation (5.2) of this paper gives the relationship between the concentration of water molecules in the melt and X_B, the total concentration of water in the melt, i.e., the sum of the OH and H_2O contributions. Rewriting this equation gives:

$$\frac{(K_1-4)}{K_1}(X_B) + \left[\frac{1}{4} - \left(\frac{K_1-4}{K_1}\right)(X_B - X_B^2)\right]^{\frac{1}{2}} = X^m_{H_2O,\,mol}\left(\frac{K_1-4}{K_1}\right) + \frac{1}{2} \qquad (7)$$

where K_1 is the equilibrium constant for the reaction describing the homogeneous reaction in the melt:

$$H2O^m + O^m = 2OH^m$$

and is defined in the ideal mixing case by:

$$K_1 = \frac{a^{m\,2}_{OH}}{a^m_{H_2O}.a^m_O} = \frac{X^{m\,2}_{OH}}{X^m_{H_2O}.X^m_O}. \qquad (8)$$

The value of K_1 varies with melt composition; here a value of $K_1 = 0.294$ has been chosen, the mean of 15 determinations calculated from infrared spectroscopic measurements of OH and H_2O concentrations in experimentally quenched hydrous glasses of MORB composition (Dixon 1992). For $K_1 = 0.294$ and $X^m_{H_2O,\,mol} = 0.006062$, eqn (7) gives $X_B = 0.0267$. This is equivalent (Silver and Stolper 1985, eqn. 11) to 1.34 wt.% H_2O. This result is very close to that calculated using the regular solution model of Silver & Stolper (1989). If we assume that $V^{0,m}_{H_2O} = 18$ cm^3.mol^{-1}, the corresponding water content is 0.35 wt.%.

Approximate temperatures of formation (at the assumed pressure of 52.5 kbar) of the other olivine samples, and hence water contents of putative coexisting melts can be calculated from the equilibrium relationships established in the following section between Fo in olivine and the Ca/Ca+Mg ratio in clinopyroxene, or from garnet - olivine Fe-Mg partitioning. However, the uncertainties in the T - dependence of the incorporation of OH

in olivine, combined with uncertainty in the P and T corrections to equation (4) suggest that it is not worthwhile to make quantitative comparisons at this level.

The main point to be gained from this exercise is not the determination of the precise water content of the "megacryst magma" at 1340 °C and 52.5 kbar, but the illustration that the OH contents of these megacryst olivines are entirely consistent with their petrogenetic history in the mantle as crystallization products of an incompatible-element-rich and water-bearing magma. The calculated water content of 1.34 wt.% is lower than commonly measured in (hydrothermally altered - Sheppard & Dawson 1975) kimberlite rocks, which are one possible parent to the megacrysts, but is more or less in concert with the fairly low K_2O contents of Group I kimberlites. The H_2O / K_2O ratios implied by this calculation and the K_2O data of Smith *et al.* (1985) and Shee (1985) are on the order of 1-2 and overlap the range of 0.8 to 4 observed in oceanic basalts (Jambon & Zimmermann 1991). We note that these ratios are also similar to those of the clinopyroxene megacrysts analyzed in this study.

(11) MINERAL-MELT DISTRIBUTION COEFFICIENTS FOR H_2O

The inter-mineral partition coefficients calculated and measured in this study can be combined with the estimates of bulk D_{H_2O} for peridotite - silicate liquid melting to calculate individual mineral-melt distribution coefficients if we assume a particular modal mineralogy for the basalt source. Estimates of bulk D_{H_2O} have been made for melting giving rise to specific examples of mid-ocean ridge basalt from the correlation of H_2O with other trace elements whose bulk distribution coefficients are thought to be known better (Dixon *et al.* (1988); Michael (1988); Jambon & Zimmermann (1991)). Using estimates of D_{H_2O} of 0.01 to 0.02 from these studies, the mineral melt D's in Table 6 columns (1) and (2) have been calculated. These calculations use the primitive mantle modal proportions of

McDonough (1990) and are likely to be slightly in error due to the assumption of modal melting, i.e., that the mineral proportions in the residue are those of the source before melting. For comparison, the D's for minerals in equilibrium with MON-24 olivine and garnet and the megacryst magma with 1.3 wt.% H_2O are shown in column (3) of Table 6. These values are in surprisingly good agreement considering the assumptions of the thermodynamic model and all the uncertainties involved.

We can calculate the expected OH content of olivine in equilibrium with primitive MORB at 15 kb and 1350 °C (approximate mean melting conditions) using the thermodynamic model of Silver & Stolper (1985) in combination with equation (1). For K_1 of 0.298 (the mean of 15 determinations of K_1 on experimentally hydrated MORB by Dixon (1992), and with 0.1-0.2 wt% H_2O in the melt, the olivine is predicted to contain 0.07 - 0.19 ppm H_2O giving $D^{ol\text{-}l}_{H2O}$ = 0.00007 to 0.0001 under these conditions. These are extremely low concentrations, but are approached by some mantle-derived olivines from basalts (Miller *et al.* 1987). Thus the extremely low OH contents of olivines seen in basalt-hosted xenoliths are not necessarily a consequence of late dehydration, and are consistent with certain petrogenetic scenarios. In fact, the OH contents of most basalt-hosted olivines are higher than would be predicted from pure partial melting processes, and may attest to the migration of water-bearing fluids in the continental lithosphere from which these xenoliths derive.

(12) SUMMARY AND CONCLUSIONS

OH contents of a suite of co-genetic megacryst minerals from the Monastery kimberlite display regular variation in their structural OH contents that are correlated with both major and minor element composition. A change in OH content of garnet and clinopyroxene

occurs with the appearance of ilmenite in the megacryst crystallization sequence. Because there is no independent evidence for changes in activity of water in the melt at this point, the OH contents of the minerals appear to be most readily explicable in terms of composition-dependent mineral-melt partitioning for H_2O. The variations in OH can be interpreted to result from the incorporation of OH into the minerals precipitating from a fractionating melt at high pressure, in response to (i) change in water content in the melt as a result of fractional crystallization and (ii) change in minor element (e.g., Ti), and perhaps major element concentrations in the minerals resulting from their varying activities in the melt. The link between OH content and Ti in these minerals is substantiated by correlation of a specific absorption band in the infrared spectrum with Ti content. Calculated and measured partitioning of OH between coexisting minerals is either invariant (ol, opx, cpx) or a smooth function of composition (partitioning involving garnet).

A similar response of partitioning to composition to that of OH is seen for K in clinopyroxene. Because H contents of these minerals may be susceptible to post-mantle disturbance and K is not, this observation is important in establishing an independent precedent for such partitioning behavior.

The OH contents of megacryst garnets and olivines are consistent with their petrogenetic history in the mantle as crystallization products of a water bearing melt at ~50 kbar pressure, although some olivines appear to have equilibrated with lower water fugacities as they annealed during or after transport from the mantle. The calculated distribution coefficients for water between these minerals and their parent magma are also consistent with bulk partitioning relationships established for water from petrogenetic studies on MORB. Together, these observations present a consistent picture for the behavior of H in the principal minerals of the upper mantle. Although the known mobility of H in high-

temperature processes is of concern in terms of preservation of mantle source information in these minerals, all observations so far on the natural minerals are consistent with, but do not prove, the hypothesis that the concentrations of OH measured are those established in the mantle.

(13) ACKNOWLEDGMENTS

This research was supported by NSF grants EAR 88-16006 and EAR 91-04059 We thank Mr. Sidney Gasson for permission to visit and sample the Monastery kimberlite and Q. Bai and D. L. Kohlstedt for access to unpublished material and permission to reproduce Figure 3.4 (d) here. This paper has benefited from discussions with J. E. Dixon, P.D. Ihinger and E. M. Stolper.

(14) REFERENCES

Akella, J. & Boyd, F. R. 1972 Partitioning of Ti and Al between pyroxenes, garnets, and oxides. *Carnegie Inst. Washington Yearb.* **71**, 378-384.

Amthauer, G., Annersten, H. & Hafner, S. S. 1977. The Mössbauer spectrum of ^{57}Fe in titanium-bearing andradites. *Phys. Chem. Minerals* **1**, 399-413.

Armstrong, J. T. 1988. Quantitative analysis of silicate and oxide materials: comparison of Monte Carlo, ZAF and $\phi(\rho z)$ procedures. In: Newbury, D. E. (ed) *Microbeam Analysis 1988,* San Francisco Press, pp. 239-246.

Armstrong, J. T. 1991. Quantitative elemental analysis of individual microparticles with electron beam instruments. In: Heinrich, K. F. J. & Newbury, D. E. (eds.) *Electron probe quantitation.* Plenum, New York. pp. 261-316.

Bai, Q & Kohlstedt, D. L. 1992. Substantial hydrogen solubility in olivine and implications for water storage in the mantle. *Nature* **357**, 672-674.

Bell, D. R., Ihinger, P. D., Rossman, G. R., Epstein, S. 1992. Calibration of an infrared spectroscopic technique for quantitative analysis of hydroxyl in garnet and pyroxene. To be submitted to *Amer Mineral.*

Bell, D. R. & Rossman, G. R. 1992a. The distribution of hydroxyl in garnets from the sub-continental mantle of southern Africa. *Contrib. Mineral. Petrol.* **111**, 161-178.

Bell, D. R. & Rossman, G. R. 1992b. Water in Earth's mantle; the role of nominally anhydrous minerals. *Science* **255**, 1391-1397.

Bertrand, P. & Mercier, J.-C. C. 1985. The mutual solubility of coexisting ortho- and clinopyroxene: toward an absolute geothermometer for the natural system? *Earth planet. Sci. Lett.* **76**, 109-122.

Boullier, A.-M. & Nicolas, A. 1973. Texture and fabric of peridotite nodules fom kimberlite. In: Nixon PH (ed.) *Lesotho Kimberlites.* Lesotho National Development Corporation, Maseru, pp. 57-66.

Boullier, A.-M. & Nicolas, A. 1975. Classification of textures and fabrics of peridotite xenoliths from South African kimberlites. *Phys. Chem. Earth* **9,** 467-476.

Boyd, F. R. & Nixon, P. H. 1973.Origin of the ilmenite-silicate nodules in kimberlites from Lesotho and South Africa. In: Nixon PH (ed.) *Lesotho Kimberlites.* Lesotho National Development Corporation, Maseru, pp. 254-268 .

Boyd, F. R. & Nixon, P. H. 1978. Ultramafic nodules from the Kimberley pipes, South Africa. *Geochim. Cosmochim. Acta* **42,** 1367-1382.

Boyd, F. R., Nixon, P. H., Pearson, D. G. & Mertzman, S. A. 1992. Low-calcium garnet harzburgites from southern Africa: their relations to craton structure and diamond crystallization. *Contrib. Mineral. Petrol.* in the press.

Brey, G. P., 1991. Fictive conductive geotherms beneath the Kaapvaal Craton. *Extd. Abstrs. 5th Internat. Kimberlite Conf.*, Araxa, Brazil. pp. 23-25.

Carswell, D. A. 1978 Matters arising: Palaeogeotherms: implications of disequilibrium in mantle xenoliths. *Nature* **276,** 737.

Dawson, J. B., Hervig, R. L. & Smith, J. V. 1981. Fertile iron-rich dunite xenoliths from the Bultfontein kimberlite, South Africa. *Fortschr. Mineral.* **59,** 303-324.

Dixon, J. E. (1992) *Water and carbon dioxide in basaltic magmas.* Unpubl. Ph.D. thesis, California Institute of Technology.

Dixon, J. E., Stolper, E. M. & Delaney, J. R. 1988. Infrared spectroscopic ,measurements of CO_2 and H_2O in Juan de Fuca Ridge basaltic glasses. *Earth planet. Sci. Lett.* **90,** 87-104.

Drury, M. R. & Van Roermund, H. L. M. 1988. Metasomatic origin for Fe-Ti-rich multiphase inclusions in olivine from kimberlite xenoliths. *Geology* **16,** 1035-1038.

Drury, M. R. & Van Roermund, H. L. M. 1989. Fluid assisted recrystallization in upper mantle peridotites from kimberlites. *J. Petrol.* **30,** 133-152.

Eggler, D. H., McCallum, M.E. & Smith, C.B. 1979. Megacryst assemblages in kimberlite from northern Colorado and southern Wyoming: Petrology, geothermometry-barometry and areal distribution. In: Boyd, F.R. & Meyer, H.O.A. (eds.) *The Mantle Sample: Inclusions in Kimberlites and Other Volcanics.* AGU, Washington, pp. 213-226.

Fraser, D. G. & Lawless, P. J. 1978. Palaeogeotherms: implications of disequilibrium in garnet lherzolite xenoliths. *Nature* **273,** 220-221.

Garrison, J. R., Jr. & Taylor, L. A. 1980. Megacrysts and xenoliths in kimberlite, Elliott County, Kentucky: a mantle sample from beneath the Permian Appalachian Plateau. *Contrib. Mineral. Petrol.* **75,** 27-42.

Gasparik, T. 1985. Titanium in ureyite: a substitution with vacancy. *Geochem. Cosmochim. Acta* **49,** 1277-1279.

Gasparik, T. 1985. Two-pyroxene thermobarometry with new experimental data in the system CaO-MgO-Al_2O_3-SiO_2. *Contrib. Mineral. Petrol.* **87,** 87-97.

Geiger, C. A., Langer, K., Bell, D. R., Rossman, G. R. & Winkler, B. 1991. The hydroxide component in synthetic pyrope. *Amer. Mineral.* **76,** 49-59.

Geller, S. 1967. Crystal chemistry of the garnets. *Z. Krist.* **125,** 1-47.

Green, H. W. II & Gueguen, Y. 1983. Deformation of peridotite in the mantle and extraction by kimberlite: a case history documented by fluid and solid precipitates in olivine.*Tectonophysics* **92,** 71-92.

Gueguen, Y. 1977. Dislocations in mantle peridotite nodules.*Tectonophysics* **39,** 231-254

Gueguen, Y. 1979. Dislocations in naturally deformed terrestrial olivine: classification, interpretation, applications. *Bull. Mineral.* **102,** 178-183.

Gurney, J.J., Jakob, W. R. O. & Dawson, J. B. 1979. Megacrysts from the Monastery kimberlite pipe, South Africa. In: Boyd, F. R. & Meyer, H. O. A. (eds.) *The Mantle Sample: Inclusions in Kimberlites and Other Volcanics.* AGU, Washington, pp. 227-243.

Hamilton, D. L., Burnham, C. W. and Osborn, E. F. (1964) The solubility of water and effects of oxygen fugacity and water content on the crystallization of mafic magmas. *J. Petrol* **5**, 21-39.

Harte, B. 1983. Mantle peridotites and processes - the kimberlite sample. In : Hawkesworth, C. J. & Norry, M.J. (eds) *Continental basalts and mantle xenoliths.* Shiva, Cheshire, pp. 46-91.

Harte, B. & Gurney, J. J. 1981. The mode of formation of chromium-poor megacryst suites from kimberlites. *J. Geol* **89,** 749-753.

Hervig, R. L. 1990. Comment on "Metasomatic origin for Fe-Ti multiphase inclusions in olivine from kimberlite xenoliths. *Geology* **xx,** 675-676.

Hervig, R. L., Smith, J. V. and Dawson, J. B. 1986. Lherzolite xenoliths in kimberlites and basalts: petrogenetic and crystallochemical significance of some minor and trace elements in olivines, pyroxenes, garnets and spinel. *Roy. Soc Edinburgh Trans., Earth Sci.* **77,** 181-201.

Hops, J. J., Gurney, J. J., Harte, B. 1992. The Jagersfontein Cr-poor megacryst suite: towards a model for megacryst petrogenesis. *J. volcanol. geotherm. Res.* **50,** 143-160.

Hops, J. J., Gurney, J. J., Harte, B., & Winterburn, P. 1989. Megacrysts and high temperature nodules from the Jagersfontein kimberlite pipe. In: *Kimberlites and Related rocks. Volume 2. Their mantle / crust setting, diamonds and diamond exploration. Geol. Soc. Australia spec. Publ.* **14,** 759-770.

Jakob, W. R. O. 1977. *Geochemical aspects of the megacryst suite from the Monastery kimberlite pipe.* Unpubl. M.Sc. thesis, University of Cape Town. 81pp.

Jambon, A. & Zimmermann, J. L. 1991. Water in oceanic basalts: evidence for dehydration of recycled crust. *Earth planet. Sci. Lett.* **101,** 323-331.

Jones, R. A. 1987. Strontium and neodymium isotopic and rare-earth element evidence for the genesis of megacrysts in kimberlites of southern Africa. In: Nixon, P. H. (ed) *Mantle xenoliths.* John Wiley and Sons, Chichester, pp. 711-724.

Köhler, T.P. & Brey, G. P. 1990 Calcium exchange between olivine and clinopyroxene calibrated as a geothermobarometer for natural peridotites from 2 to 60 kb with applications.*Geochim. Cosmochim. Acta* **54,** 2375-2388.

Mackwell, S. J. & Kohlstedt, D.L. 1990. Diffusion of hydrogen in olivine: implications for water in the mantle. *J. geophys. Res.* **95,** 5079-5088.

Martin R.F. & Donnay, G. 1972. Hydroxyl in the mantle. *Amer Mineral* **57,** 554-570.

McCallister, R. H., Meyer, H. O. A & Aragon, R. 1979. Partial thermal history of two exsolved clinopyroxenes from the Thaba Putsoa kimberlite pipe, Lesotho. In: Boyd, F. R. & Meyer, H. O. A. (eds.) *The Mantle Sample: Inclusions in Kimberlites and Other Volcanics.* AGU, Washington, pp. 244-248.

McDonough, W. F. 1990. Constraints on the composition of the continental lithospheric mantle *Earth planet. Sci. Lett.* **101,** 1-18.

McKay, G., Wagstaff, J & Yang, S.-R. 1986. Clinopyroxene REE distribution coefficients for shergottites: The REE content of the Shergotty melt. *Geochim. Cosmochim. Acta* **50,** 927-937.

Mercier, J.-C. C. 1979. Peridotite xenoliths and the dynamics of kimberlite intrusion. In: Boyd, F. R. & Meyer, H. O. A. (eds.) *The Mantle Sample: Inclusions in Kimberlites and Other Volcanics.* AGU, Washington, pp. 197-212.

Michael, P. J. 1988. The concentration, behavior and storage of water in the suboceanic upper mantle: implications for mantle metasomatism. *Geochim. Cosmochim. Acta* **52,** 555-566.

Miller, G. H., Rossman, G. R. & Harlow, G. E. 1987. The natural occurrence of hydroxide in olivine. *Phys. Chem. Minerals* **14,** 461-472.

Mitchell, R. H. 1986. *Kimberlites : mineralogy, geochemistry and petrology.* Plenum, New York, 442 pp.

Moore RO (1986) *A study of the kimberlites, diamonds and associated rocks and minerals from the Monastery Mine, South Africa.* Unpubl. Ph.D. thesis, University of Cape Town.

Moore, R. O., Griffin, W. L., Gurney, J. J., Ryan, C. G., Cousens, D. R., Sie, S. H., Suter, G. F. 1992. Trace element geochemistry of ilmenite megacrysts from the Monastery kimberlite, South Africa. *Lithos*, in the press.

Neal, C. R. & Davidson, J.P. 1989. An unmetasomatized source for the Malaitan alnoite (Solomon Islands) : petrogenesis involving zone refining, megacryst fractionation, and assimilation of oceanic lithosphere. *Geochim.Cosmochim .Acta* **53,** 1975-1990.

Nickel, K.G. and Green, D. H. 1985 Empirical geothermobarometry for garnet peridotites and implications for the nature of the lithosphere, kimberlites and diamonds. *Earth planet. Sci. Lett.* **73,** 158-170.

Nixon P.H. & Boyd, F.R. 1973. The discrete nodule (megacryst) association in kimberlites from northern Lesotho. In: Nixon PH (ed.) *Lesotho Kimberlites.* Lesotho National Development Corporation, Maseru, pp. 67-75.

O'Neill, H. St.C. & Wood, B. J. 1979. An experimental study of Fe-Mg partitioning between garnet and olivine and its calibration as a geothermometer. *Contrib. Mineral. Petrol.* **70,** 59-70.

O'Neill, H. St.C. 1980. An experimental study of Fe-Mg partitioning between garnet and olivine and its calibration as a geothermometer: corrections. *Contrib. Mineral. Petrol.* **72,** 337.

Paterson, M. S. 1982. The determination of hydroxyl by infrared absorption in quartz, silicate glasses and similar materials. *Bull. Mineral.* **105,** 20-29.

Pistorius, C. W. F. T. & Kennedy, G. C. 1960. Stability relations of grossularite and hydrogrossularite at high temperatures and pressures. *Amer. J. Sci.* **258,** 247-257.

Pouchou, J.-L. & Pichoir, R. 1991 Quantitative analysis of homogeneous or stratified microvolumes applying the model "PAP". In: Heinrich, K. F. J. & Newbury, D. E. (eds.) *Electron probe quantitation.* Plenum, New York. pp.31-76.

Richardson, S. H., Erlank, A. J. & Hart, S. R. 1985. Kimberlite-borne garnet peridotite xenoliths from old enriched subcontinental lithosphere. *Earth planet. Sci. Lett.* **75,** 116-128.

Rossman, G. R. & Smyth, J. R. 1990. Hydroxyl contents of accessory minerals in mantle eclogites and related rocks.*Amer. Mineral.* 75, 775-780.

Saxena, S. K. & Fei, Y. 1987. High pressure and high temperature fluid fugacities. *Geochim. Cosmochim. Acta.* **51,** 783-791.

Schulze, D.J. 1984. Cr-poor megacrysts from the Hamilton Branch kimberlite, Elliott County, Kentucky. In : Kornprobst, J. (ed.) Developments in Petrology, Vol 11B, *Kimberlites II. The Mantle and Crust-Mantle Relationships.* Elsevier, Amsterdam, pp 97-108.

Schulze DJ (1987) Megacrysts from alkalic volcanic rocks. In: Nixon PH (ed) Mantle xenoliths. John Wiley and Sons, Chichester, pp 433-451.

Shee, S. R. 1985. *The petrogenesis of the Wesselton Mine kimberlites, Kimberley, Cape Province, R. S. A.* Unpubl. Ph.D. thesis, University of Cape Town.

Sheppard, S. M. F. & Dawson, J. B. 1975. Hydrogen, carbon and oxygen isotope studies of megacryst and matrix minerals from Lesothan and South African kimberlites. *Phys. Chem. Earth* **9,** 747-764.

Silver, L. A & Stolper, E. M. 1985. A thermodynamic model for hydrous silicate melts *J. Geol.* **93,** 161-178.

Silver, L. A & Stolper, E. M. 1989. Water in albitic glasses. *J. Petrol.* **30,** 667-709.

Skogby, H., Bell, D. R. & Rossman, G.R. 1990. Hydroxide in pyroxenes; variations in the natural environment. *Amer. Mineral.* **75,** 764-774.

Skogby, H. S. & Rossman, G. R. 1991. The intensity of amphibole OH bands in the infrared absorption spectrum. *Phys. Chem. Minerals* **18,** 64-68.

Stolper, E. M. 1982. Water in silicate glasses: an infrared spectroscopic study. *Contrib. Mineral Petrol.* **81,** 1-17.

Smith, C. B., Gurney, J. J., Skinner, E. M. W., Clement, C. R. & Ebrahim, N. 1985. Geochemical character of southern African kimberlites: a new approach based on isotopic constraints.*Trans. geol. Soc. S. Afr.* **88,** 267-280.

Smith, D. & Boyd, F. R. 1992. Compositional zonation in garnets in peridotite xenoliths. *Contrib. Mineral. Petrol.*, in press.

Smyth, J. R., Bell, D. R. & Rossman, G. R. 1991. Incorporation of hydroxyl in upper-mantle clinopyroxenes. *Nature* **351,** 732-735.

Wood, B. J. 1974. The solubility of alumina in orthopyroxene coexisting with garnet. *Contrib. Mineral. Petrol.* **46,** 1-15.

Woodhead, J. A., Rossman, G. R. & Thomas, A. P. 1991. Hydrous species in zircon. *Amer. Mineral.* **76,** 1533-1546.

Yamada, H & Takahashi, E. 1984. Subsolidus phase relations between coexisting garnet and two pyroxenes at 50 - 100 kbarin the system CaO-MgO-Al_2O_3-SiO_2.In : Kornprobst, J. (ed.) Developments in Petrology, Vol 11B, *Kimberlites II. The Mantle and Crust-Mantle Relationships*. Elsevier, Amsterdam, pp 247-256.

Yoder, H. S. 1950. Stability relations of grossularite *J. Geol.* **58,** 221-253.

Sample	Na_2O	MgO	Al_2O_3	SiO_2	P *ppm*	K *ppm*	CaO	Sc *ppm*	TiO_2	V *ppm*	Cr_2O_3	MnO	FeO*	Ni *ppm*	Zr *ppm*	H_2O *ppm*	Total	Mg#
Garnets																		
ROM263-GT02	0.099	19.34	21.30	41.47	173	n.a.	4.50	87	1.15	234	0.542	0.27	11.09	91	106	46	99.83	75.7
ROM263-GT03	0.110	19.40	20.90	42.32	164	n.a.	4.47	86	1.10	236	0.483	0.27	11.38	84	104	40	100.51	75.2
ROM263-GT04	0.112	19.24	20.55	41.91	169	n.a.	4.57	87	1.22	231	0.524	0.27	11.56	83	120	52	100.05	74.8
ROM263-GT06	0.107	19.79	20.92	42.36	201	n.a.	4.56	88	1.19	222	0.620	0.26	10.82	114	130	33	100.72	76.5
ROM263-GT09	0.102	19.26	21.21	41.53	159	n.a.	4.54	86	1.18	243	0.571	0.27	11.24	84	115	40	99.98	75.3
ROM263-GT10	0.115	19.06	20.89	41.99	185	n.a.	4.60	85	1.22	235	0.479	0.28	11.86	87	114	57	100.56	74.1
ROM263-GT25	0.093	19.94	21.05	41.85	194	n.a.	4.60	90	1.15	218	0.769	0.25	10.28	117	111	32	100.07	77.6
ROM263-GT31	0.105	19.27	20.49	41.82	154	n.a.	4.60	91	1.25	239	0.568	0.28	11.38	84	131	53	99.86	75.1
ROM263-GT34	0.092	17.74	21.29	41.53	167	n.a.	4.39	115	0.72	151	0.006	0.40	13.77	9	219	57	100.02	69.7
ROM263-GT36	0.084	17.49	21.60	41.12	194	n.a.	4.47	125	0.75	169	0.009	0.40	14.09	4	259	74	100.12	68.9
ROM263-GT44	0.094	20.39	20.59	41.97	197	n.a.	4.51	92	1.11	194	0.864	0.22	9.79	129	132	19	99.64	78.8
ROM263-GT49	0.104	18.72	21.52	41.42	195	n.a.	4.54	94	1.13	231	0.207	0.32	12.04	56	148	60	100.1	73.5
ROM263-GT52	0.093	20.61	21.11	41.97	172	n.a.	4.41	85	0.99	191	1.012	0.23	9.30	141	100	15	99.81	79.8
ROM263-GT68	0.100	19.52	20.73	41.91	168	n.a.	4.49	88	1.17	211	0.560	0.28	10.91	104	105	43	99.75	76.1
ROM263-GT71	0.083	17.40	21.88	41.07	178	n.a.	4.44	119	0.71	170	0.014	0.39	13.91	5	226	59	99.99	69.0
ROM263-GT75	0.107	19.43	20.66	41.86	175	n.a.	4.50	92	1.16	219	0.547	0.27	11.11	93	99	47	99.72	75.7
MON-9	0.106	19.09	20.92	41.25	178	n.a.	4.67	90	1.30	250	0.620	0.28	11.17	96	128	56	99.42	75.3
MON-24	0.098	20.24	21.39	42.08	n.a.	n.a.	4.50	n.a.	1.05	n.a.	0.677	0.28	10.71	n.a.	n.a.	35	101.01	77.1
MON-26	0.096	20.86	21.27	42.05	n.a.	n.a.	4.53	86	1.09	171	1.063	0.25	9.58	151	101	16	100.79	79.5
Clinopyroxenes																		Ca#
ROM273-DI10	1.29	16.20	0.55	55.32	n.a.	38	21.35	n.a.	0.143	289	0.296	0.10	5.08	63	n.a.	195	100.37	48.6
ROM273-DI16	1.54	20.78	2.46	55.82	n.a.	195	13.78	n.a.	0.330	120	0.301	0.12	5.51	674	n.a.	439	100.77	32.3
ROM273-DI21	1.78	19.02	2.54	55.09	n.a.	201	14.93	n.a.	0.486	188	0.196	0.13	6.04	457	n.a.	490	100.33	36.1
ROM273-DI24	2.10	15.94	2.45	54.87	n.a.	126	18.30	n.a.	0.255	194	0.242	0.12	5.98	172	n.a.	291	100.32	45.2
ROM387	1.71	19.87	2.60	55.86	n.a.	187	14.10	n.a.	0.403	157	0.210	0.15	5.98	572	n.a.	501	100.98	33.8
ROM270-CI11	1.81	18.16	2.46	55.49	n.a.	194	15.94	n.a.	0.473	208	0.060	0.13	6.29	305	n.a.	554	100.91	38.7
ROM270-CI25	1.88	17.29	2.42	55.38	n.a.	171	16.76	n.a.	0.363	188	0.008	0.14	6.28	124	n.a.	448	100.59	41.0
MON-25	1.94	17.49	2.54	55.50	n.a.	167	16.33	n.a.	0.408	192	0.014	0.14	6.42	151	n.a.	469	100.85	40.2
MON-26	1.60	20.25	2.45	55.85	n.a.	264	14.26	n.a.	0.391	148	0.305	0.13	5.44	662	n.a.	620	100.81	33.6
Orthopyroxenes																		Mg#
ROM273-OG1	0.28	32.30	1.14	57.30	n.a.	n.a.	1.34	n.a.	0.258	n.a.	0.07	0.10	8.29	n.a.	n.a.	251	101.09	87.4
ROM273-OG2	0.31	32.60	1.29	57.37	n.a.	n.a.	1.52	n.a.	0.209	n.a.	0.13	0.13	7.20	n.a.	n.a.	263	100.75	89.0
ROM-167	0.18	31.31	0.72	56.96	n.a.	n.a.	0.80	n.a.	0.156	n.a.	0.00	0.18	###	n.a.	n.a.	215	100.94	84.0

Table 1. Compositions of garnets, clinopyroxenes and orthopyroxenes. n.a. = not analyzed.

Mineral	Polarizations summed	Calibration used	Integrated Molar Absorption Coefficient ($l.mol^{-1}.cm^{-1}$)	Reference
Garnet	$A = A$ (unpol.)	ppm $H_2O = 0.719 \cdot \int A$ per cm.	20100	This work (Chapter 4)
Olivine	$A = A\beta + A\gamma$	ppm $H_2O = 0.218 \cdot \int A$ per cm	24500	Endisch et al, in prep.
Clinopyroxene	$A = A\alpha + A\beta + A\gamma$	ppm $H_2O = 0.141 \cdot \int A$ per cm	38300	This work (Chapter 4)
Orthopyroxene	$A = A\alpha + A\beta + A\gamma$	ppm $H_2O = 0.0674 \cdot \int A$ per cm	80600	This work (Chapter 4)
Zircon	$A = A//c + 2A\ c$	ppm $H_2O = 1.04 \cdot \int A$ per cm	4740	Endisch et al, in prep

Table 2. Polarizations summed and calibrations used in determining OH contents (as ppm H_2O by weight) of minerals in this study.

Element	Standard.	Crystal	Cup current (nA)	Acc voltage (kV)	Peak ct. time (s)	1σ (high conc.) % rel.	1σ (low conc.) % rel.	d.l. (wt.% / ppm)	Overlap corrections
Garnet									
Na	Amelia albite	TAP	30, 40	15	90, 60	5.1	4	0.007	-
Mg	syn. pyrope DB31	TAP	30, 40	15	30, 40	0.3	0.3	0.010	-
Al	syn. pyrope DB31	TAP	30, 40	15	30	0.3	0.3	0.012	-
Si	syn. pyrope DB31	TAP	30, 40	15	30	0.2	0.2	0.014	-
P	Durango apatite	PET	300	15	2 X 240	2.4	3.0	8	-
Ca	Wollastonite, Anorthite	PET	30, 40	15	40, 30	0.6	0.6	0.012	-
Sc	syn. $Sc_2Si_2O_7$	PET	500	15	2 X 240	3.3	5.0	9	Ca (bkg)
Ti	TiO_2	PET	500	20	60-125	0.2	0.2	0.002	-
V	V_2O_5	LiF	500	20	180	2.0	3.7	10	Ti Kβ
Cr	Cr_2O_3	PET	30, 40	15	60	1.8	100	0.025	-
Mn	syn. tephroite, Nuevo gt	LiF	30, 40	15	50, 60	4.1	6.1	0.021	-
Fe	Fayalite	LiF	30, 40	15	60, 30	0.5	0.6	0.02	-
Ni	syn. liebenbergite	LiF	500	20	180	4.5	100	14	-
Zr	zircon	PET	500	15	240	5.9	15	32	Ca (bkg)
Clinopyroxene									
Na	Amelia albite	TAP	40	15	90	0.6	0.8	0.007	-
Mg	Boyd Forsterite	TAP	40	15	30	0.2	0.3	0.009	-
Al	Ky20 Kyanite	TAP	40	15	90	0.4	0.9	0.005	-
Si	Wollastonite	TAP	40	15	30	0.2	0.2	0.014	-
K	Asbestos Microcline	PET	300	20	2 X 240	1.1	8.2	7	-
Ca	Wollastonite	PET	40	15	40	0.3	0.3	0.011	-
Ti	TiO_2	PET	40	15	90	1.6	4.1	0.010	-
V	V_2O_5	LiF	300	20	100	3.8	8	20	Ti Kβ
Cr	Cr_2O_3	LiF	40	15	60	4.3	100	0.017	-
Mn	syn. tephroite	LiF	40	15	30	9	11	0.023	-
Fe	Fayalite	LiF	40	15	30	0.9	1.0	0.023	-
Ni	syn. liebenbergite	LiF	300	20	180	1.8	16.4	22	-

Table 3. Conditions for electron microprobe analysis. Columns 7 and 8 give the errors due to counting statitics alone on analysis of a single point, for the highest and lowest recorded concentrations, respectively. Detectability limit (column 9) is for a representative single point analysis sample and here is approximated as d.l. = B + 3_{σ}B, where B represents the background count rate.

Table 4. Compositional and IR spectroscopic data for Monastery olivines. Fo contents from Moore (1986). Column 5 gives the "best" present estimate of total OH in the samples and is based on the nuclear reaction analysis calibration for the polarizations listed in Column 3 (see Table 1). Column 6 gives the estimate for OH based on the calibration of Paterson (1982)*of only the polarizations listed in column 3* . These only approach the estimate of total OH in the sample for the sum of $\beta + \gamma$ orientations. Columns 8 and 9 are derived similarly from the restricted integration (3650 - 3450 cm^{-1}) and are used to compute the values in column 10 via the Bai & Kohlstedt (1992a) relationship.

1 Sample	2 Fo	3 Pol.. summed	4 ∫A per cm	5 ppm H_2O (NRA)	6 ppm H_2O (P)	7 ∫A per cm	8 ppm H2O (P)	9 $H/10^6Si$ (P)	10 fH_2O (B & K)
	(mol %)		3650 to 3100 cm^{-1}	3650 to 3100 cm^{-1}	3650 to 3100 cm^{-1}	3650 to 3450 cm^{-1}	3650 to 3450 cm^{-1}	3650 to 3450 cm^{-1}	(bars)
Low-Fe, High-Ni olivines									
MON24-OL1.B#	85.6	β + γ	671.5	147	46.4	516.3	40.0	665	18016
MON24-OL2.B#	85.6	β + γ	543.8	119	37.5	416.5	32.3	538	13802
ROM250-OL2.1	84.2	β + γ	783.4	171	52.3	573.2	44.0	737	20457
ROM250-OL2.2	84.2	α + β	389.9	173	24.5	257.2	19.4	324	-
ROM250-OL16.1	83.1	β + γ	728.2	159	49.8	552.6	42.7	718	19820
ROM250-OL16.1	83.1	β	229.7	185	14.5	148.8	11.0	185	-
ROM250-OL24.1	85.3	β + γ	560.0	122	37.5	419.3	32.1	533	13668
ROM250-OL29.1	86.2	β + γ	881.2	192	56.5	579.9	44.3	736	20422
ROM250-OL42.1	87.0	β + γ	686.3	150	46.5	505.6	39.0	645	17314
ROM250-OL42.2	87.0	β + γ	338.3	74	21.9	228.5	17.5	290	6378
ROM250-OL42.3	87.0	β + γ	232.6	51	15.2	152.2	11.9	195	3895
ROM250-OL54.1	87.8	β + γ	651.2	142	42.9	455.7	35.1	578	15121
ROM250-OL54.2	87.8	β + γ	675.5	147	44.5	459.5	35.6	588	15422
ROM250-OL54.3	87.8	β + γ	694.0	152	46.4	512.8	12.5	206	17349
ROM250-OL54.5	87.8	β + γ	608.1	133	41.2	460.1	35.1	579	15130
High-Fe, Low-Ni olivines									
ROM250-OL13.1A	79.1	β + γ	1085.6	237	79.2	878.8	69.7	1192	37333
ROM250-OL13.1B	79.1	β + γ	1016.4	222	74.2	827.3	65.7	1122	34635
ROM250-OL13.1C	79.1	β + γ	1038.2	227	76.5	857.3	68.4	1168	36399
ROM250-OL13.1D	79.1	β + γ	1028.3	224	76.7	862.9	69.3	1184	37020
ROM250-OL13.2	79.1	β + γ	1077.8	235	76.3	826.2	65.6	1120	34550
ROM250-OL21.1	82.3	β	193.1	156	13.3	143.7	11.4	192	-
ROM250-OL26.1	80.2	β + α	318.0	141	19.8	202.9	15.3	261	-
ROM250-OL26.2	80.2	β + γ	1124.3	245	78.7	878	68.5	1165	36282
ROM250-OL40.1	78.4	β + γ	194.7	43	15.7	167.8	14.9	254	5417
ROM250-OL40.3	78.4	β + γ	363	79	28.4	299.7	25.8	443	10846
ROM177.OL1*	80.8	β + γ	535	117	39.4	412.2	34.5	586	15376
ROM181.OL1*	79.3	β + γ	522.3	114	40.9	456.7	37.6	642	17227
ROM181.OL2*	79.3	β + γ	362	79	27.5	287.1	24.7	421	10165
ROM121-Z010.OL1£	80.4	α + γ	347.9	80	28.3	303.3	26.5	450	-

olivine coexists with garnet. * olivine coexists with zircon. £ olivine coexists with zircon and ilmenite

Table 5.

Olivine	fH_2O (bars) = 74(ppm H_2O) + 0.33(ppm $H_2O)^2$	(1)
Clinopyroxene	fH_2O (bars) = 5016+ 28.71(ppm H_2O)	(2)
Garnet	fH_2O (bars) = 16991+ 45.41(ppm H_2O)	(3)
Zircon	fH_2O (bars) = -22230 + 1177(ppm H_2O)	(4)

Table 5. Equations describing the fugacity of water as a function of OH content of nominally anhydrous minerals from this study. Equation is a fit to the fH_2O values for olivine and the OH content using the nuclear reaction analysis calibration (seeTable 4 for data). Equations (2) and (3) are fits to the water contents of clinopyroxene and garnet that are predicted (using the equations of Table A1), and measured in the case of sample MON-24, to coexist with the olivine for which the fH_2O was determined (Table 4). Equation (4) is derived from the measured OH contents of coexisting olivine - zircon pairs. No corresponding equation for orthopyroxene is presented because the three orthopyroxene samples do not show a monotonic relationship between H_2O and calculated fH_2O. These equations should be viewed as approximate descriptions of the data, applicable to the compositional crystal chemistry and geological conditions of these samples. Their use as hydrobarometric predictors should proceed with considerable caution and regard to uncertainties in their construction.

Table 6.

Mineral	(1) D=0.01	(2) D=0.02	(3) from MON-24
olivine	0.0067	0.013	0.011
orthopyroxene	0.011	0.022	0.019
clinopyroxene	0.021	0.041	0.038
garnet	-	-	0.0026

Table 6. Mineral-melt D_{H_2O} calculated for (a) MORB melting for bulk mantle-MORB D_{H_2O} = 0.01 (Column 1) and D_{H_2O} = 0.02 (Column 2) and (b) megacryst magma - minerals for mineral compositions in equilibrium with sample MON-24 and water content of melt = 1.34 wt.% (see text) (Column 3). Mineral proportions in primitive mantle used in columns (1) and (2) from McDonough (1990).

Fig. 1. Compositions of megacryst olivines, orthopyroxenes, garnets and clinopyroxenes from the Monastery kimberlite. Tie lines indicate compositional relationships between the minerals. Highly calcic clinopyroxenes and Fe-rich olivines occupy compositions beyond the range of the "main-trend" silicates and ilmenites (not shown). Solid circles are analyses from Moore (1986) and unpublished data and represent extensive sampling ($n > 300$). Open circles are samples analyzed for OH in this work, selected mostly from those previously analyzed. Open circle compositions determined at Caltech, with the exception of olivine.

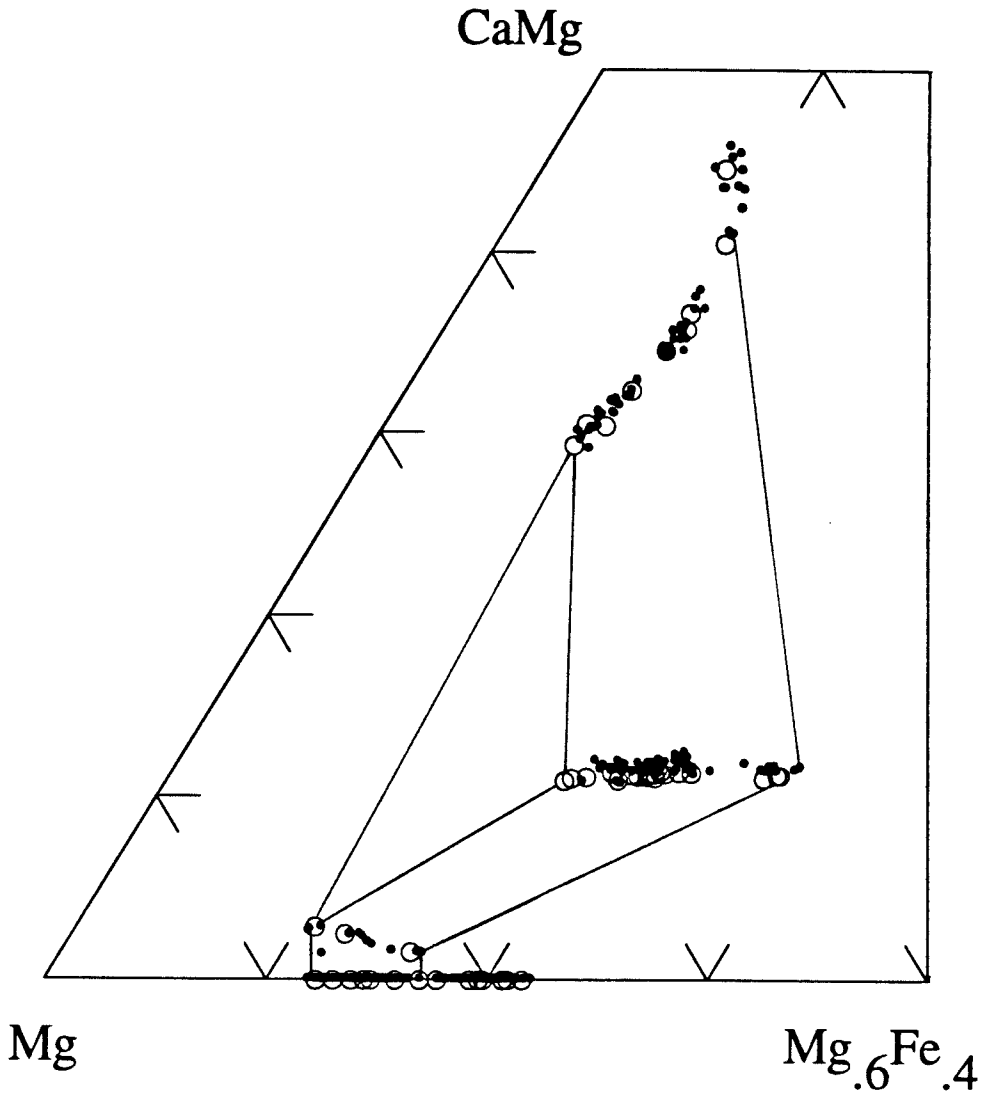
CaMg
Mg
Mg.6Fe.4

Fig. 2. Plot of Nb vs. 100Mg/(Mg+Fe^{2+}) in ilmenite megacrysts from the Monastery kimberlite, illustrating the relationships of phlogopite, Fe-rich olivine, zircon and calcic clinopyroxene to the "main trend" silicates and ilmenite. All samples plotted except the monomineralic ilmenites are spatially intergrown with the phases designated in the figure key. The composition of the ilmenite thus allows the petrological relationships of these other phases to be determined. "Main-trend" silicates coexist with ilmenites that are significantly poorer in Nb (as well as Cr, not shown) than the other megacrysts. Note that the "main trend" (open circles) has undergone substantial crystallization before ilmenite appears (with Mg# ~ 40).

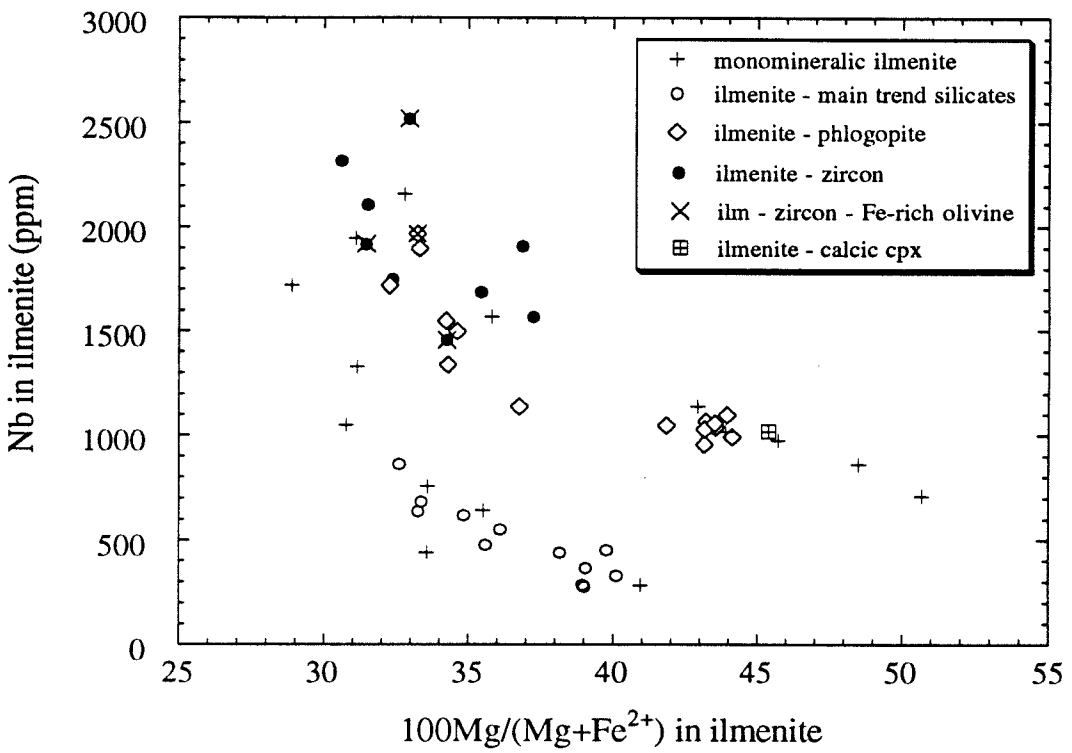
3000
2500
2000
1500
1000
500
0
25
30
35
40
45
50
55
Nb in ilmenite (ppm)
100Mg/(Mg+Fe2+) in ilmenite
monomineralic ilmenite
ilmenite - main trend silicates
ilmenite - phlogopite
ilmenite - zircon
ilm - zircon - Fe-rich olivine
ilmenite - calcic cpx

Fig. 3. Infrared spectra of megacryst minerals normalized to 1mm thickness..

3.1 Garnets - unpolarized, showing change in proportions of bands near 3750 and 3512 cm^{-1}

(a) ROM263-GT09

(b) ROM263-GT25

(c) ROM263-GT36

3.2 Clinopyroxenes - polarized parallel to α, β [010], γ and c [001].

Upper spectrum in each polarization direction: ROM373

Lower spectrum in each polarization direction: ROM271-DI10

3.3 Orthopyroxenes ROM273-OG1 (upper spectra) and ROM-167 (lower spectra) polarized parallel to α [001], β [010] and γ [100].

3.4 Olivine polarized parallel to γ [100] (upper spectra) and β [001] (lower spectra].

(a) Group 1 (ROM250-OL24)

(b) Group 2a (ROM121-Z010.OL1)

(c) Group 2b (ROM250-OL13.1A)

(d) San Carlos olivine, hydrothermallly annealed at fO2 ~ 10-6 MPa. (from Bai & Kohlstedt 1992b). Unpolarized // [100]

3.5 Zircon ROM177.Z1 polarized parallel to the c-axis [001] and perpendicular to c.

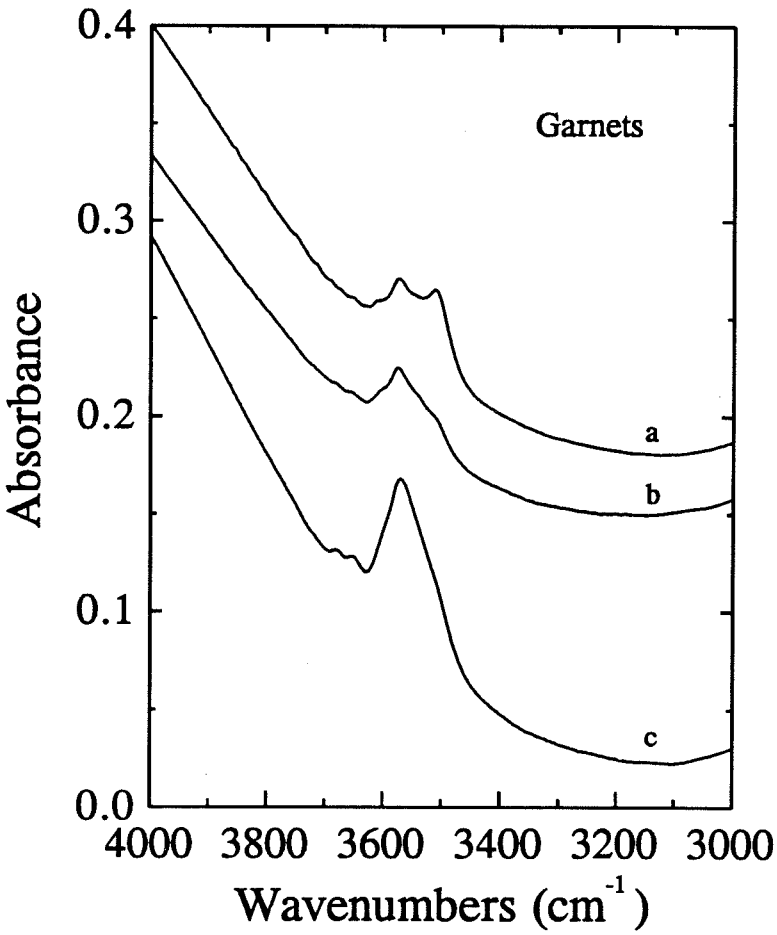
Garnets
a
b
c
Absorbance
0.0
0.1
0.2
0.3
0.4
4000
3800
3600
3400
3200
3000
Wavenumbers (cm-1)

Fig. 3.

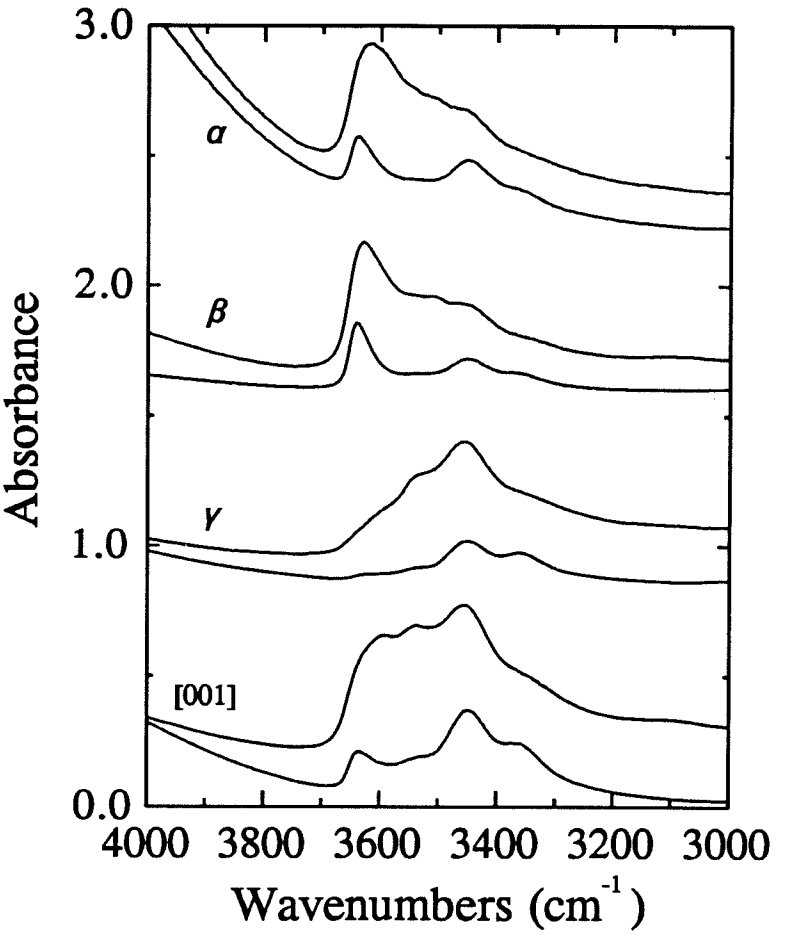
3.0
2.0
1.0
0.0
Absorbance
α
β
γ
[001]
4000 3800 3600 3400 3200 3000
Wavenumbers (cm-1)

Fig 3.2

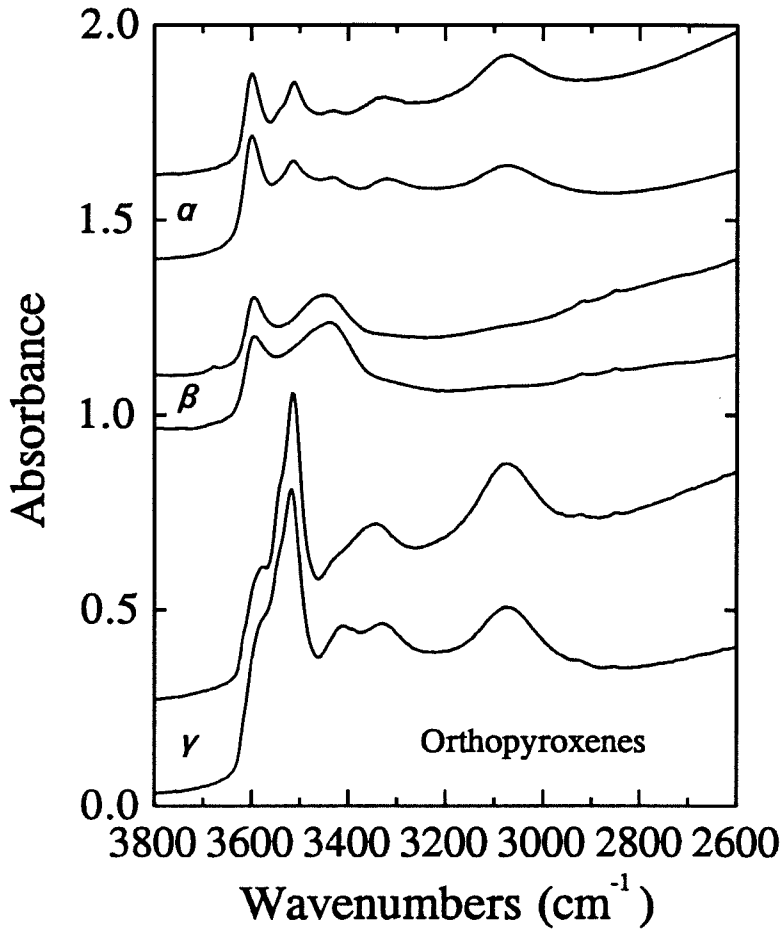
2.0
1.5
1.0
0.5
0.0
Absorbance
α
β
γ
Orthopyroxenes
3800 3600 3400 3200 3000 2800 2600
Wavenumbers (cm-1)

Fig. 3.3

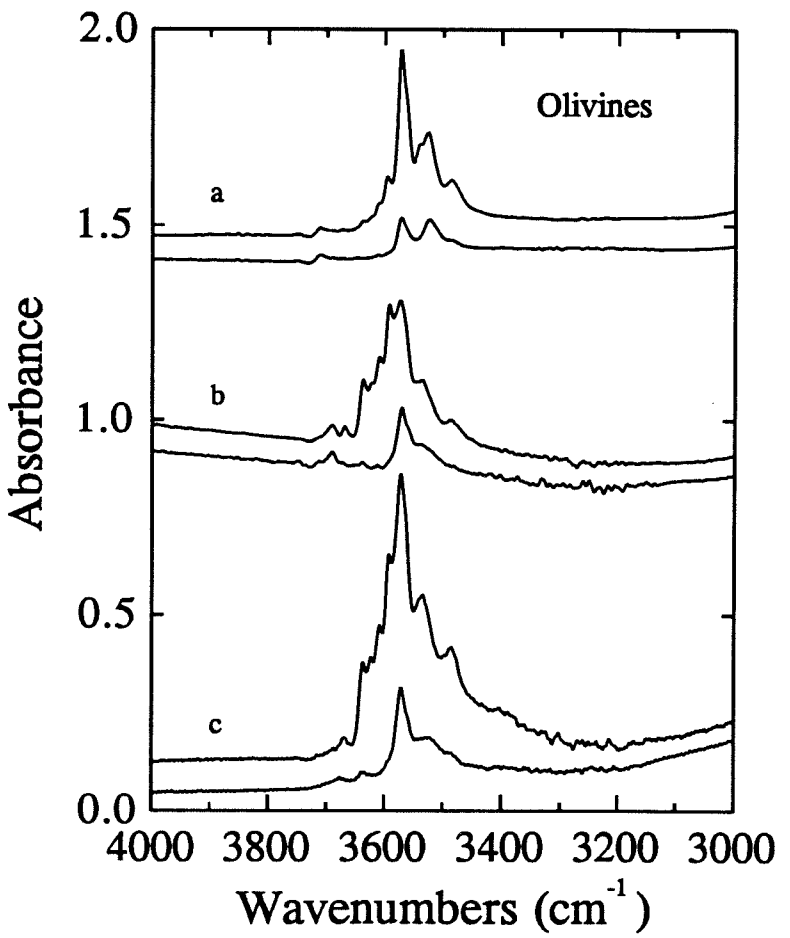
Olivines
a
b
c
Absorbance
2.0
1.5
1.0
0.5
0.0
4000
3800
3600
3400
3200
3000
Wavenumbers (cm-1)

Fig. 3.4

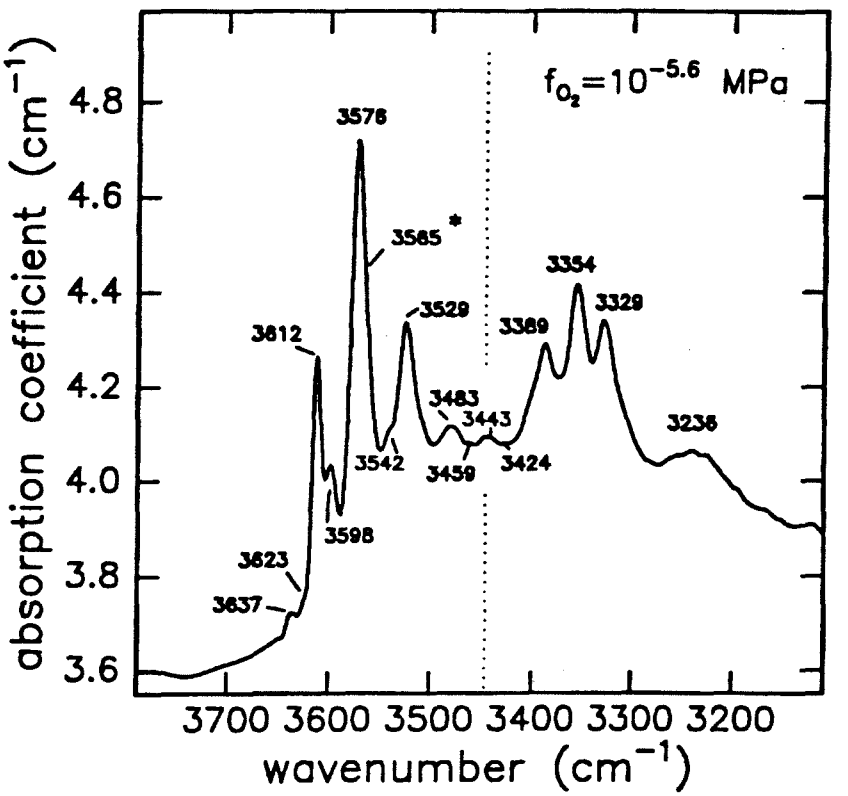
absorption coefficient (cm^{-1})
4.8
4.6
4.4
4.2
4.0
3.8
3.6
$f_{O_2}=10^{-5.6}$ MPa
3576
3585 *
3529
3612
3389
3354
3329
3483
3443
3542
3459
3424
3236
3598
3623
3637
3700 3600 3500 3400 3300 3200
wavenumber (cm^{-1})

Fig. 3.4d

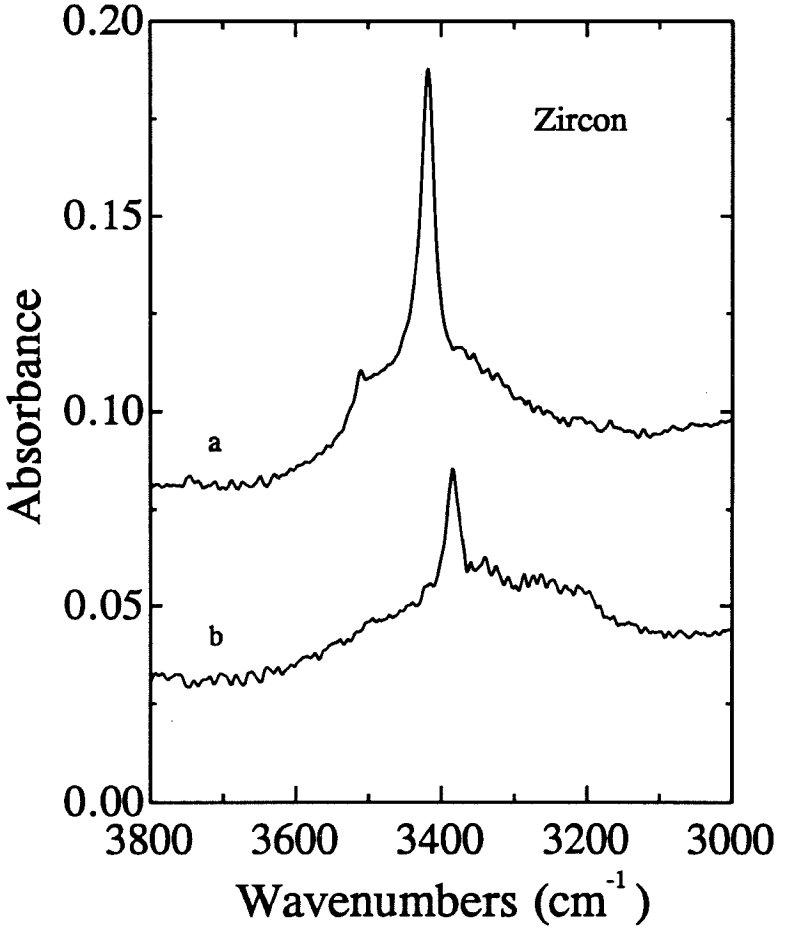
0.20
0.15
0.10
0.05
0.00
Absorbance
Zircon
a
b
3800
3600
3400
3200
3000
Wavenumbers (cm-1)

Fig. 3.5

Fig. 4. Shift in frequency of the principal infrared OH absorption band near 3570 cm^{-1} in megacryst garnets as a function of composition. The shift may result from relative growth of unresolved components in the band, or may be due to shift in frequency of a single main band.

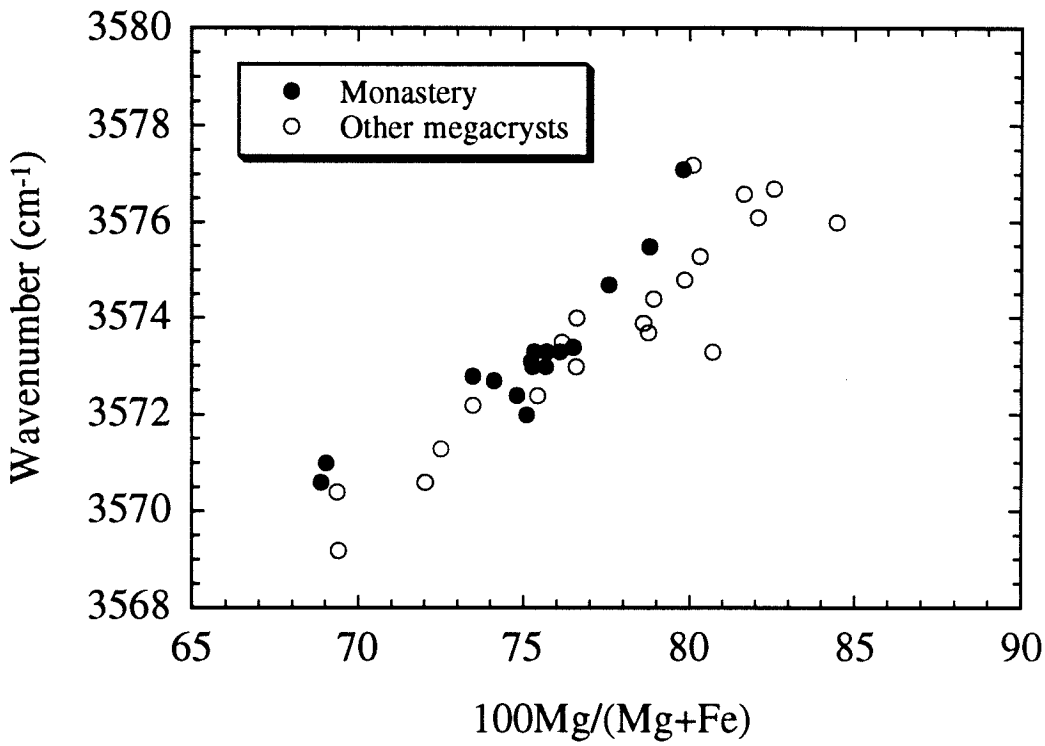
Monastery
Other megacrysts
Wavenumber (cm-1)
3580
3578
3576
3574
3572
3570
3568
65
70
75
80
85
90
100Mg/(Mg+Fe)

Fig. 4

Fig. 5. Changes in the relative contributions of the four main OH absorption bands in the clinopyroxene IR spectrum as a function of mineral composition. The ordinate is the linear absorbance at the peak maximum divided by the sum of the linear absorbances of the four bands.

Fig. 5

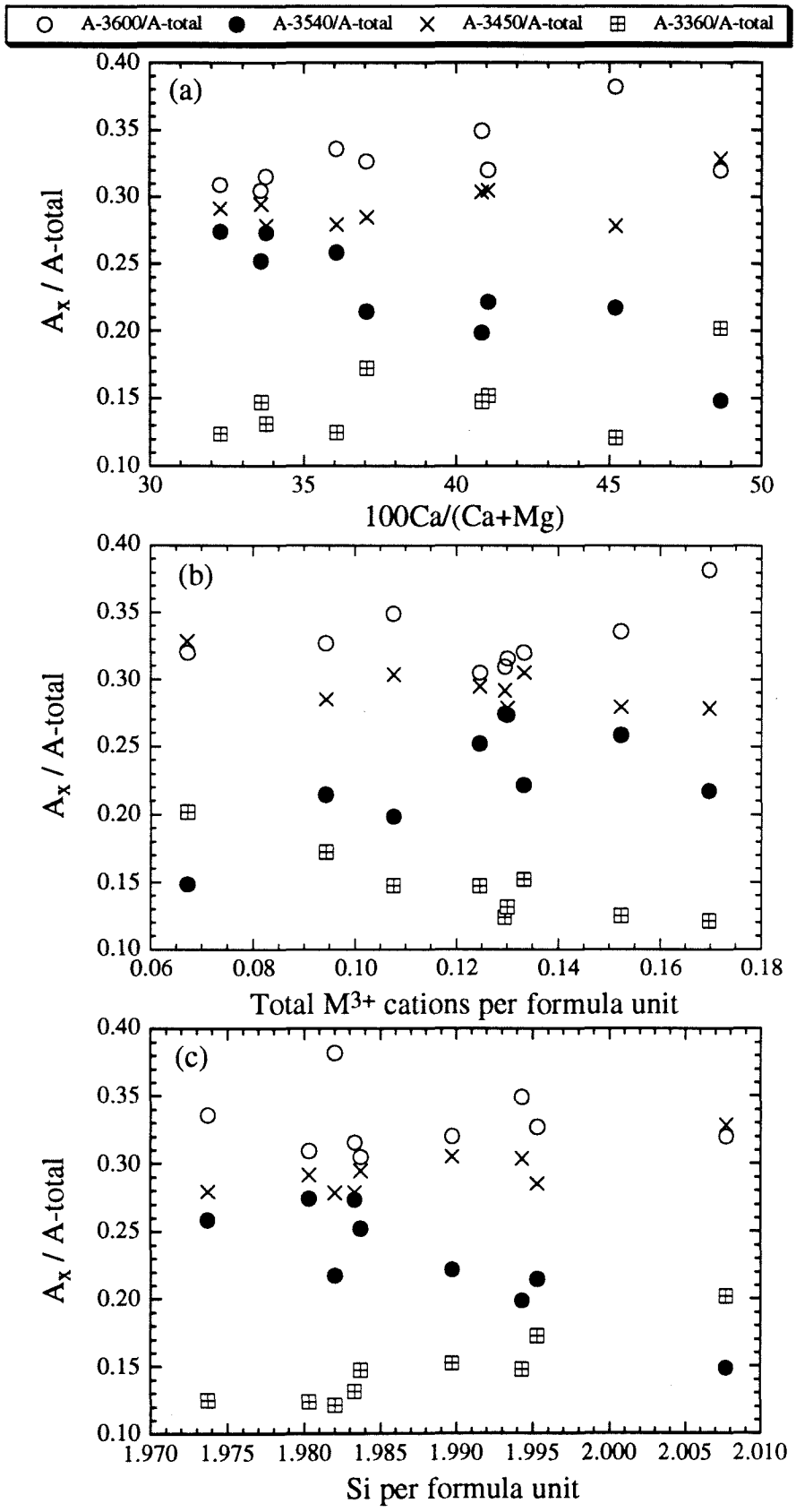
A-3600/A-total
A-3540/A-total
A-3450/A-total
A-3360/A-total
(a)
A_x / A-total
100Ca/(Ca+Mg)
(b)
A_x / A-total
Total M^{3+} cations per formula unit
(c)
A_x / A-total
Si per formula unit

Fig. 6. Changes in the relative contributions of the five main OH absorption bands in the orthopyroxene IR spectrum as a function of mineral composition. The ordinate is the linear absorbance at the peak maximum divided by the sum of the linear absorbances of the four bands.

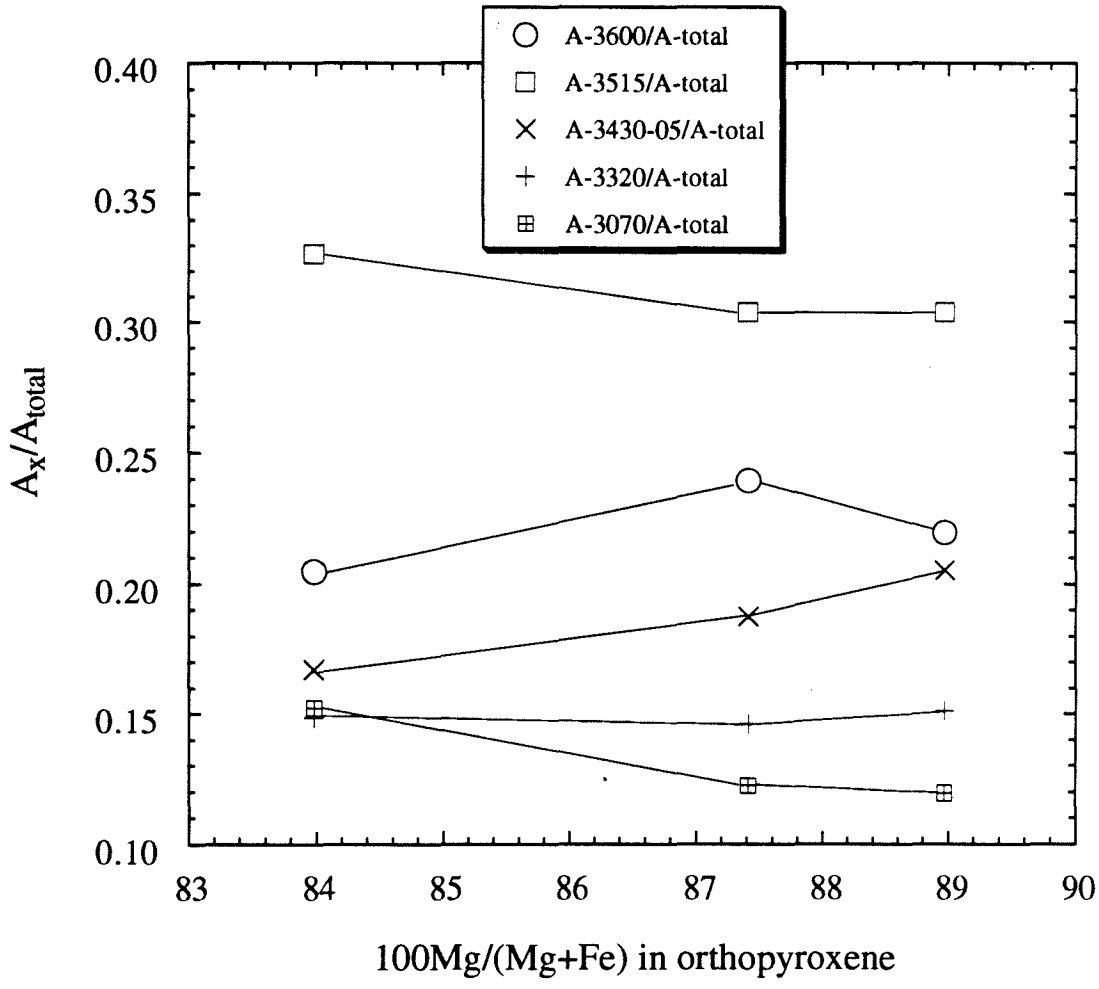
A-3600/A-total
A-3515/A-total
A-3430-05/A-total
A-3320/A-total
A-3070/A-total
0.40
0.35
0.30
0.25
0.20
0.15
0.10
A_X/A_{total}
83
84
85
86
87
88
89
90
100Mg/(Mg+Fe) in orthopyroxene

Fig. 6

Figure 7. OH content (Fig.7a) and corresponding water fugacity (Bai & Kohlstedt, 1992) (Fig.7b) of olivine megacrysts as a function of Fo. content (100Mg/Mg+Fe). Vertical lines connect analyses from the same sample (which may be different grains, or spots in a single grain).

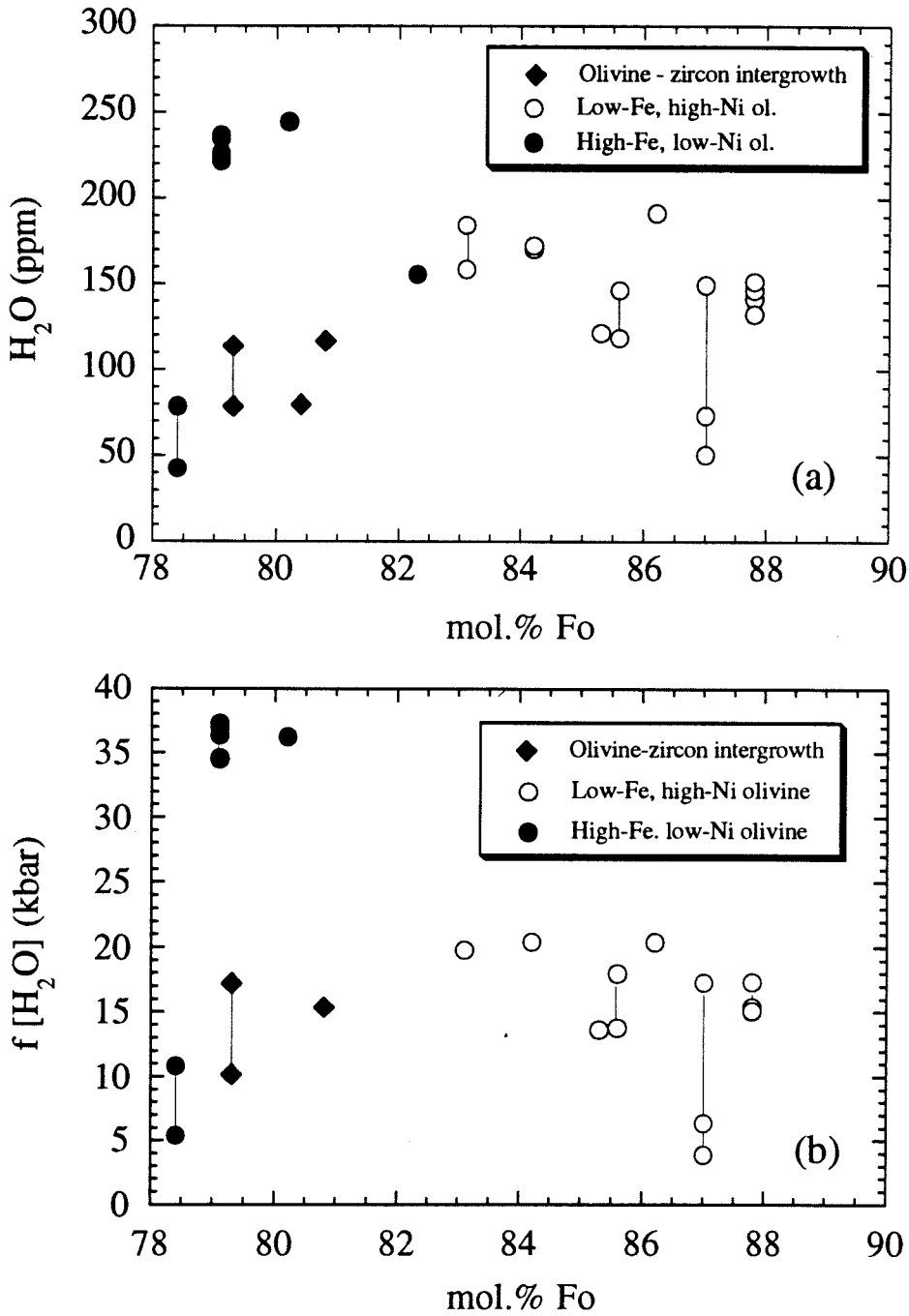
300
250
200
150
100
50
0
H_2O (ppm)
Olivine - zircon intergrowth
Low-Fe, high-Ni ol.
High-Fe, low-Ni ol.
(a)
78
80
82
84
86
88
90
mol.% Fo
40
35
30
25
20
15
10
5
0
f [H_2O] (kbar)
Olivine-zircon intergrowth
Low-Fe, high-Ni olivine
High-Fe. low-Ni olivine
(b)
78
80
82
84
86
88
90
mol.% Fo

Fig. 7

Figure 8. Compositional trends of OH (Fig. 8a) and other elements, determined by electron microprobe, (Figs. 8b-k) in Monastery garnet megacrysts as a function of Mg# in the garnet. Error bars represent 2σ calculated from repeat analyses (except for OH - see text), and reflect sample heterogeneity as well as counting statistics.

Fig. 8

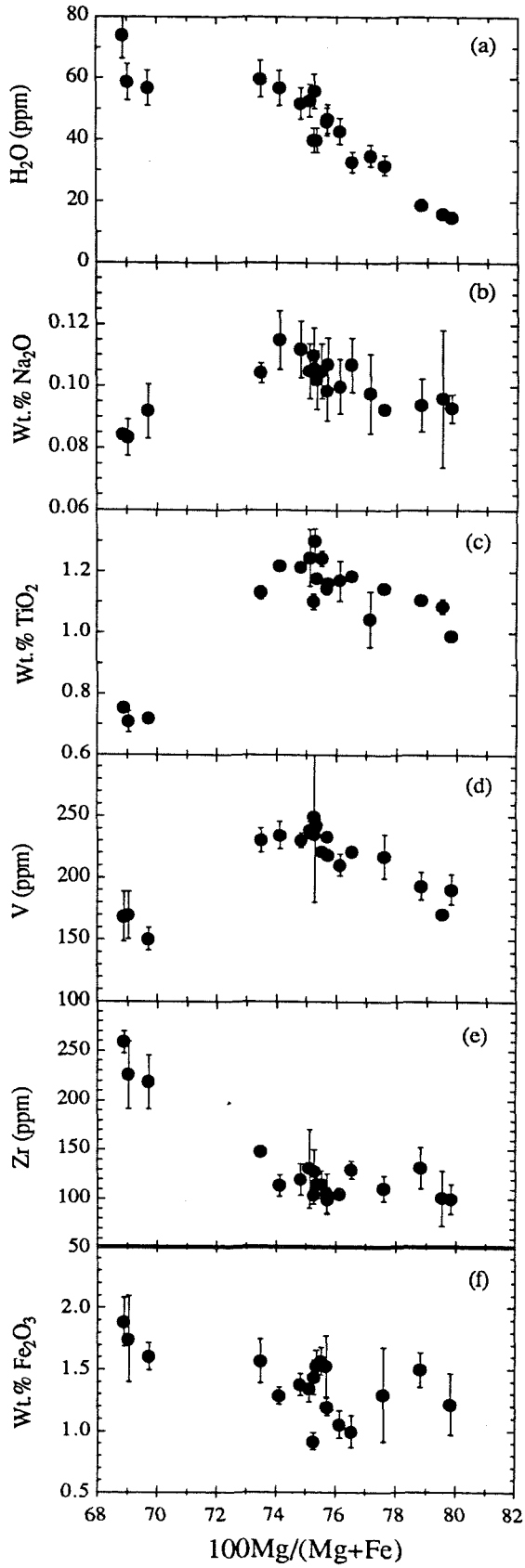
(a)
H_2O (ppm)
80
60
40
20
0
(b)
Wt.% Na_2O
0.12
0.10
0.08
0.06
(c)
Wt.% TiO_2
1.2
1.0
0.8
0.6
(d)
V (ppm)
250
200
150
100
(e)
Zr (ppm)
250
200
150
100
50
(f)
Wt.% Fe_2O_3
2.0
1.5
1.0
0.5
68
70
72
74
76
78
80
82
100Mg/(Mg+Fe)

Fig. 8 - cont.

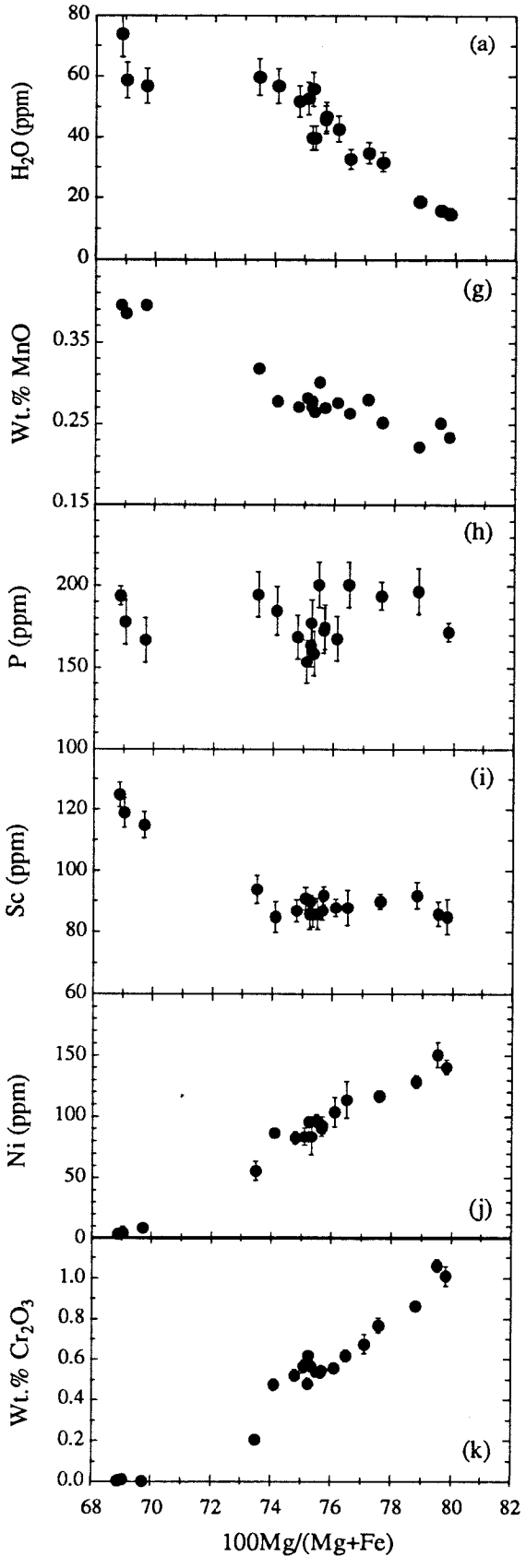
(a)
H_2O (ppm)
80
60
40
20
0
(g)
Wt.% MnO
0.35
0.25
0.15
(h)
P (ppm)
200
150
100
(i)
Sc (ppm)
120
100
80
60
(j)
Ni (ppm)
150
100
50
0
(k)
Wt.% Cr_2O_3
1.0
0.8
0.6
0.4
0.2
0.0
68
70
72
74
76
78
80
82
100Mg/(Mg+Fe)

Figure 9. Plots of incompatible trace element concentrations in garnet vs. OH content. (a) Ti, (b) V, (c) Zr. The relative enrichment in OH over the other three elements from first crystallization to the appearance of ilmenite as a coexisting phase.is constant. Beyond this point, Ti and V decrease relative to OH, whereas Zr increases (off scale in Fig. 9c).

Fig. 9

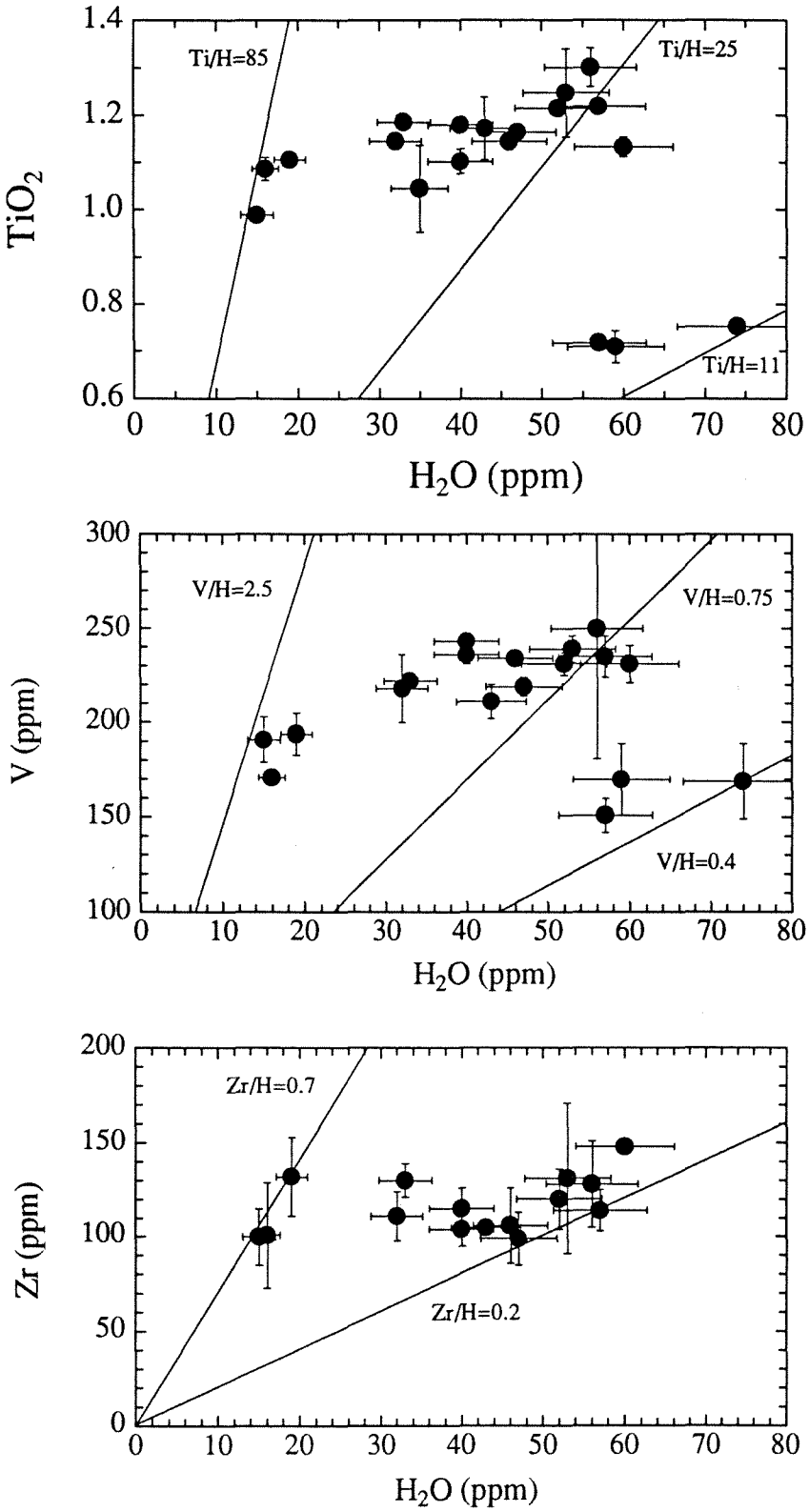
TiO2
Ti/H=85
Ti/H=25
Ti/H=11
H2O (ppm)
V (ppm)
V/H=2.5
V/H=0.75
V/H=0.4
H2O (ppm)
Zr (ppm)
Zr/H=0.7
Zr/H=0.2
H2O (ppm)

Figure 10. Total rare-earth element concentrations in Monastery garnets, determined by ion-microprobe, as a function of Mg#. Error bars represent 2σ due to counting statistics. Point with largest error bars is average and 2σ of three analyses of the Monastery garnet standard during the run. Elements summed: La, Ce, Pr, Nd, Sm, Eu, Gd, Tb, Dy, Ho, Er, Tm, Yb, Lu.

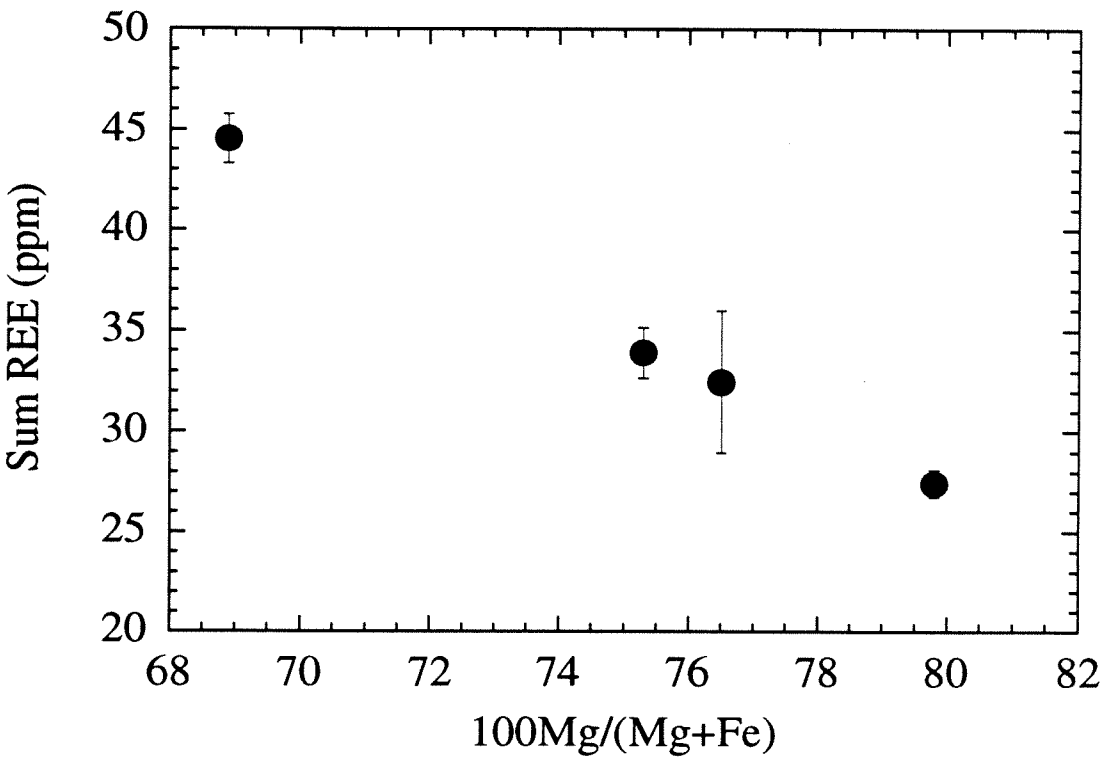

Fig. 10

Figure 11. OH (Fig.11a) and other compositional variation (Figs.11b-i) in clinopyroxene megacrysts from the Monastery kimberlite plotted as a function of Ca#. Differentiation proceeds towards higher Ca#. Error bars as for fig. 8. The diamond symbol is clinopyroxene MON-26, from the garnet-cpx pair and falls slightly off the trend established by the other samples for the elements H, K, Mg, Cr and Ni, but not for other elements (see text for discussion). Changes in slope of trends occur for OH, Ti, V and K at ilmenite entry.

Fig. 11

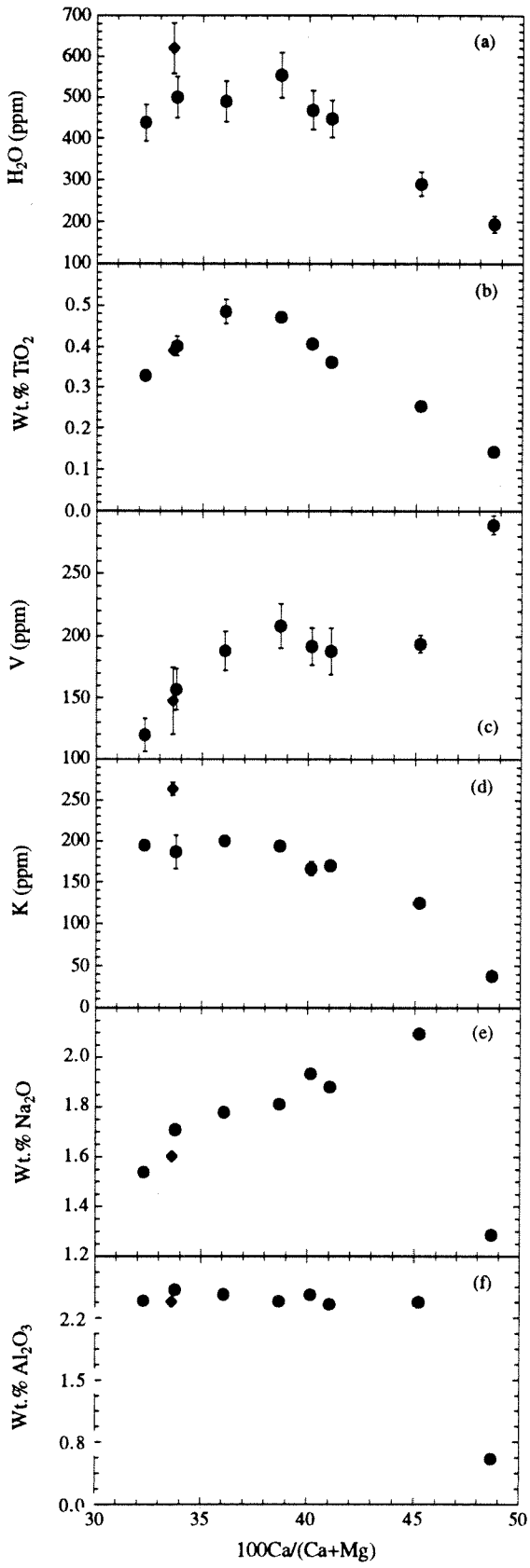
(a)
H_2O (ppm)
700
600
500
400
300
200
100
(b)
Wt.% TiO_2
0.5
0.4
0.3
0.2
0.1
0.0
(c)
V (ppm)
250
200
150
100
(d)
K (ppm)
250
200
150
100
50
0
(e)
Wt.% Na_2O
2.0
1.8
1.6
1.4
1.2
(f)
Wt.% Al_2O_3
2.2
1.5
0.8
0.0
30
35
40
45
50
100Ca/(Ca+Mg)

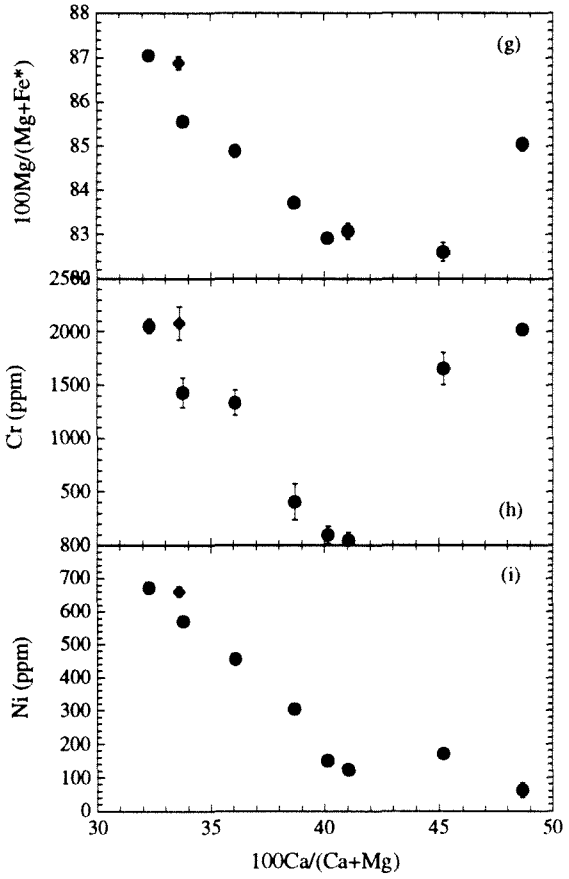
100Mg/(Mg+Fe*)
88
87
86
85
84
83
(g)
Cr (ppm)
2000
1500
1000
500
800
(h)
Ni (ppm)
700
600
500
400
300
200
100
0
(i)
30
35
40
45
50
100Ca/(Ca+Mg)

Fig. 11 - cont.

Figure 12. H_2O vs. K_2O in clinopyroxene megacrysts from Monastery. Diamond sample is sample MON-26..Arrow illustrates the possibility of deriving calcic megacryst ROM273-DI10 from the main trend by phlogopite removal (clinopyroxenes compositionally similar to this sample coexist with phlogopite - see Fig. 2). MON-26 may be related by phlogopite addition to the system (see text).

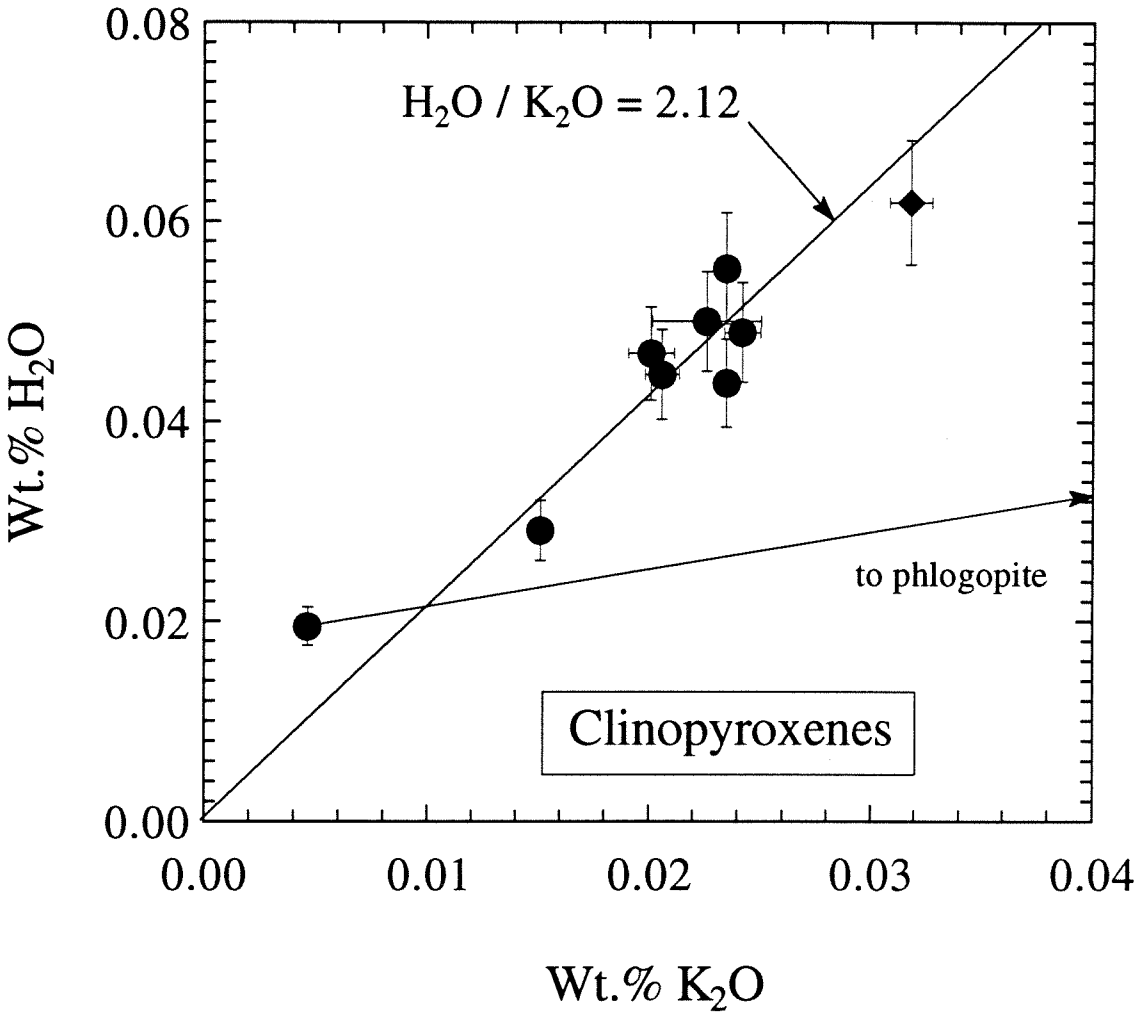
0.08
0.06
0.04
0.02
0.00
0.00
0.01
0.02
0.03
0.04
Wt.% H2O
Wt.% K2O
H2O / K2O = 2.12
to phlogopite
Clinopyroxenes

Fig. 12

Figure 13. Variation in ratio of H to K (atomic) as a function of Ca# in Monastery clinopyroxenes, illustrating the pronounced difference of the calcic clinopyroxene megacryst ROM273-DI10.

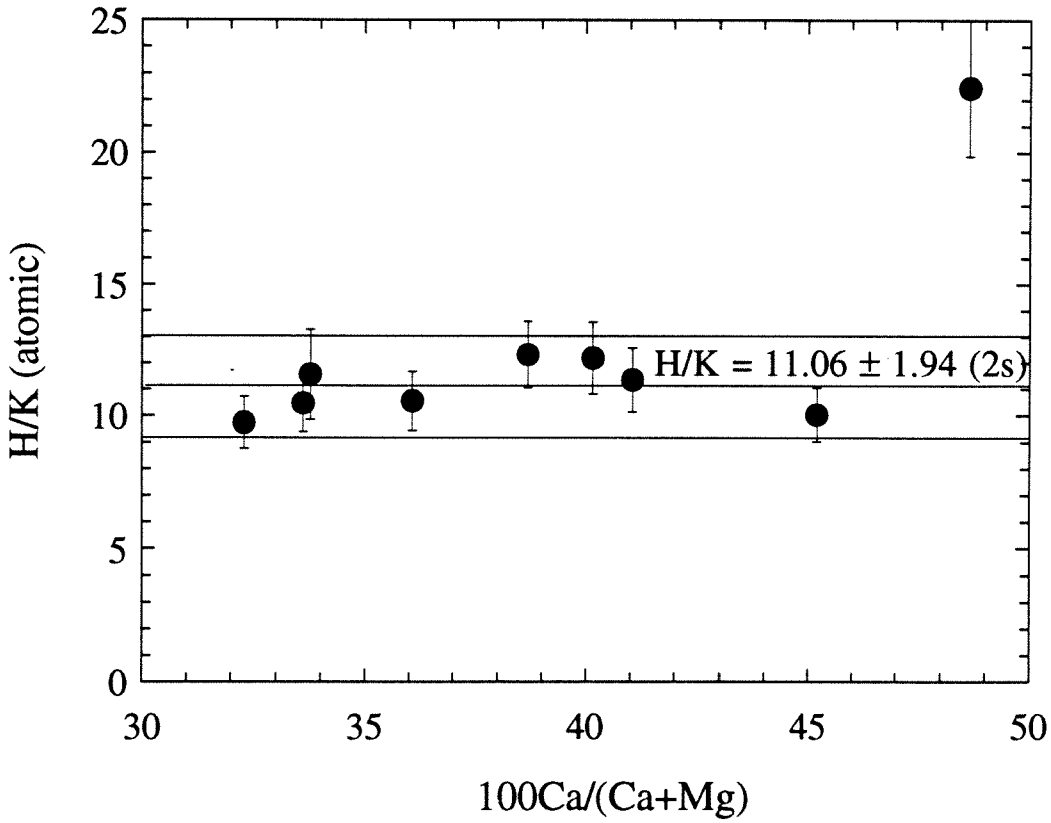

Fig. 13

Figure 14. OH vs. TiO_2 in Monastery clinopyroxene megacrysts. Diamond symbol is garnet - cpx pair MON-26.

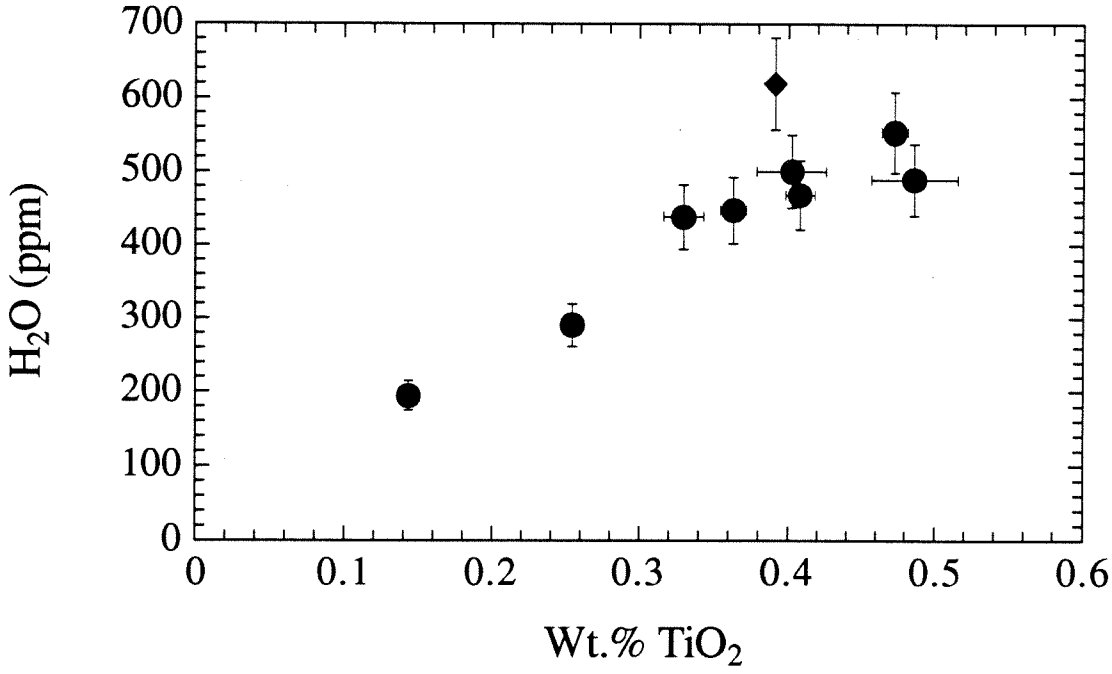

Fig. 14

Figure 15. OH and minor element contents of orthopyroxene as a function of Mg#.

Fig. 15

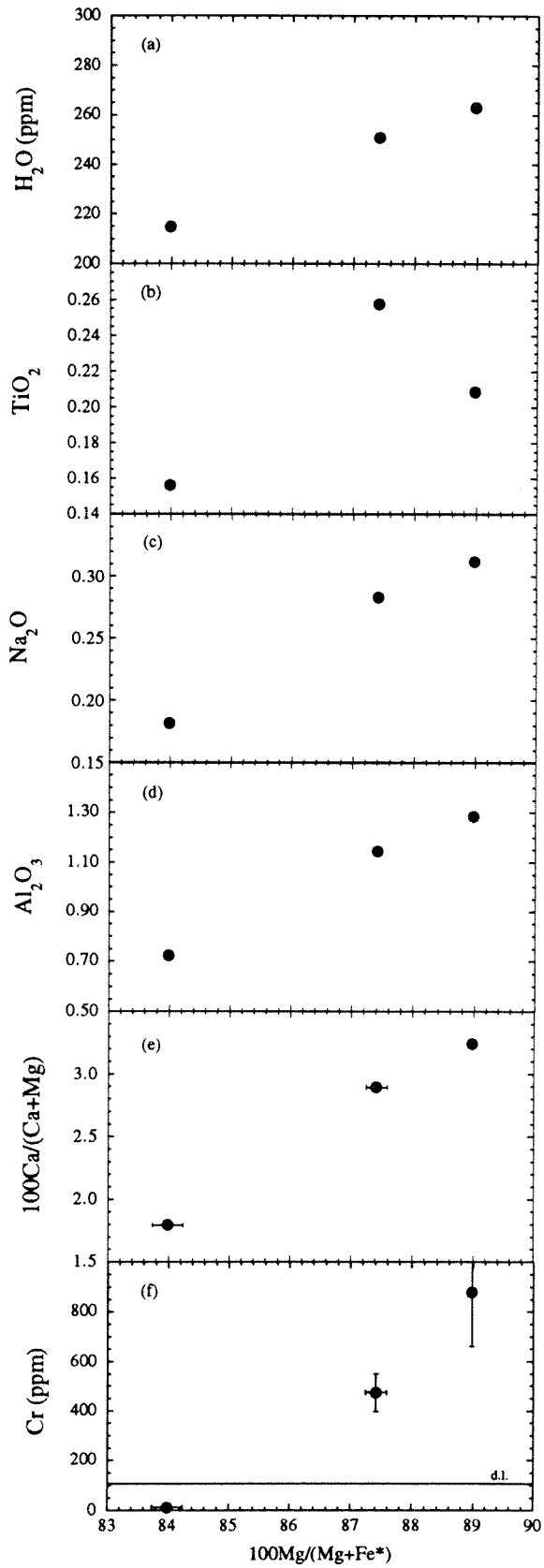
(a)
H_2O (ppm)
300
280
260
240
220
200
(b)
TiO_2
0.26
0.24
0.22
0.20
0.18
0.16
0.14
(c)
Na_2O
0.30
0.25
0.20
0.15
(d)
Al_2O_3
1.30
1.10
0.90
0.70
0.50
(e)
100Ca/(Ca+Mg)
3.0
2.5
2.0
1.5
(f)
Cr (ppm)
800
600
400
200
0
d.l.
83
84
85
86
87
88
89
90
100Mg/(Mg+Fe*)

Figure 16. Composite diagram showing OH contents of all minerals analyzed as a function of differentiation, here expressed as Mg# in garnet (bottom) and Ca# in clinopyroxene (top). Abscissa values calculated for all minerals except garnet (measured) from equations in Table A1. No garnet actually coexists with Fe-rich olivine, zircon and calcic clinopyroxene and the garnet Mg# index in this region is a convenient, but not meaningful, extrapolation. Uncertainties in the equations of Table 1 result in slight shifts of the mineral trends relative to one another, not necessarily by constant amounts along their lengths. Accuracy of the absolute scale is believed to be ± 2-3 Mg# units.

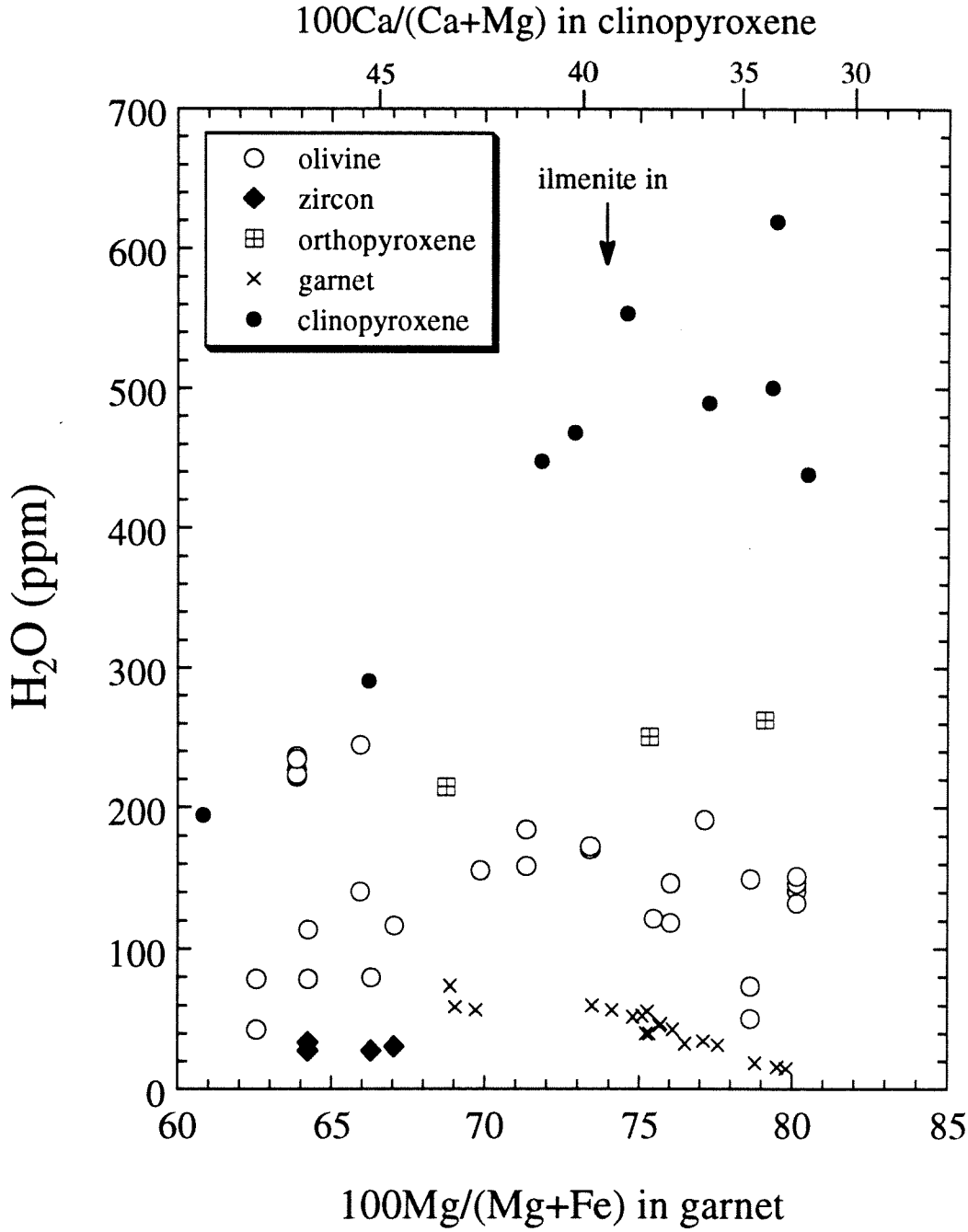
100Ca/(Ca+Mg) in clinopyroxene
45
40
35
30
olivine
zircon
orthopyroxene
garnet
clinopyroxene
ilmenite in
H_2O (ppm)
700
600
500
400
300
200
100
0
60
65
70
75
80
85
100Mg/(Mg+Fe) in garnet

Fig. 16

Figure 17. Partitioning of OH between garnet and (a) clinopyroxene, (b) olivine and (c) orthopyroxene, as a function of Mg# in garnet. Distribution coefficients are calculated as described in the text, and measured in the case of the two coexisting pairs, MON-24 (gt-ol) and MON-26 (gt-cpx).

Fig. 17

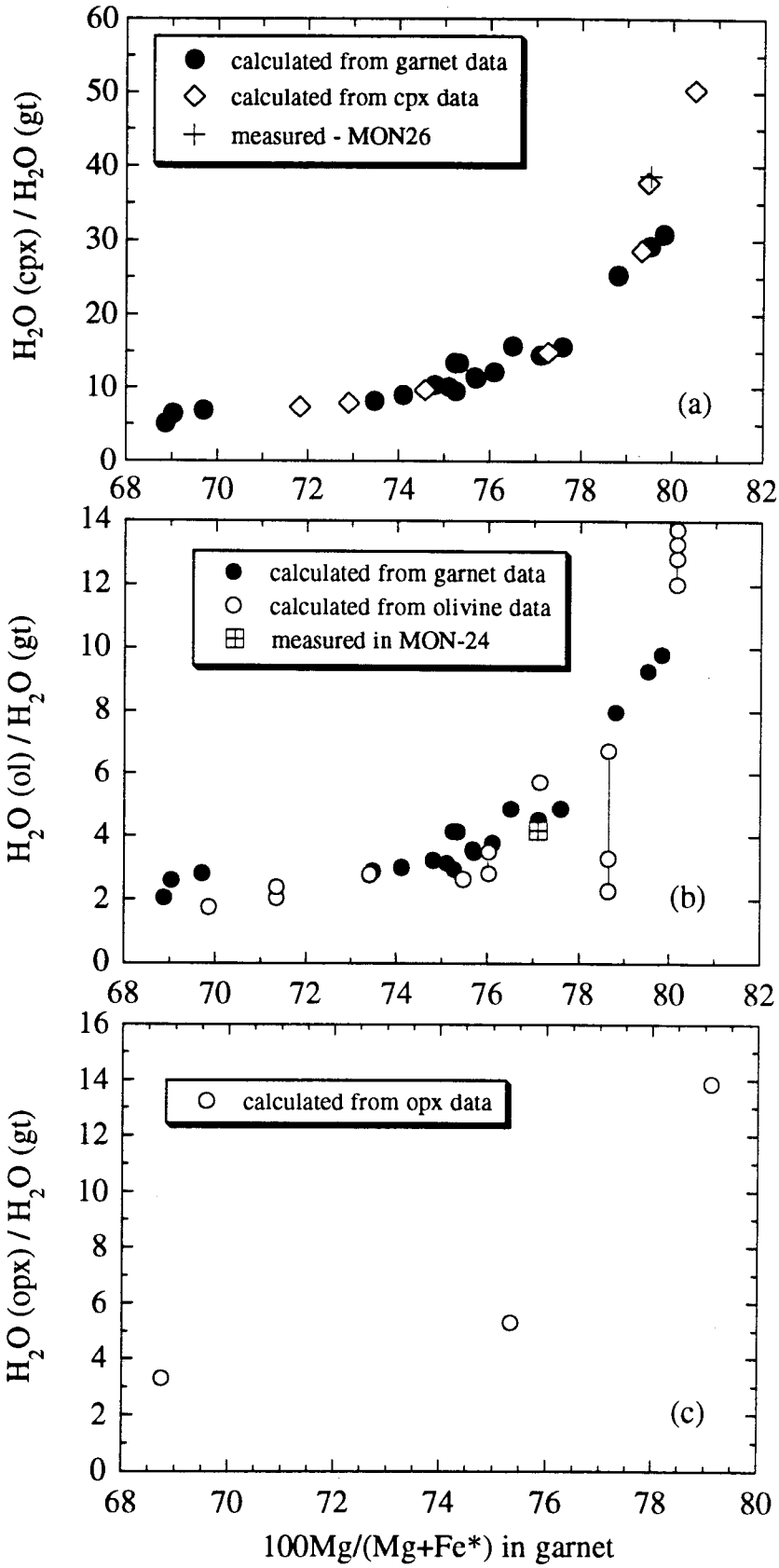
calculated from garnet data
calculated from cpx data
measured - MON26
H2O (cpx) / H2O (gt)
(a)
calculated from garnet data
calculated from olivine data
measured in MON-24
H2O (ol) / H2O (gt)
(b)
calculated from opx data
H2O (opx) / H2O (gt)
(c)
100Mg/(Mg+Fe*) in garnet

Figure 18. Partitioning of OH between (a) clinopyroxene and olivine, (b) clinopyroxene and orthopyroxene and (c) orthopyroxene and olivine as a function of differentiation index (Ca# in cpx, Mg# in opx). Distribution coefficients calculated as described in text.

Fig. 18

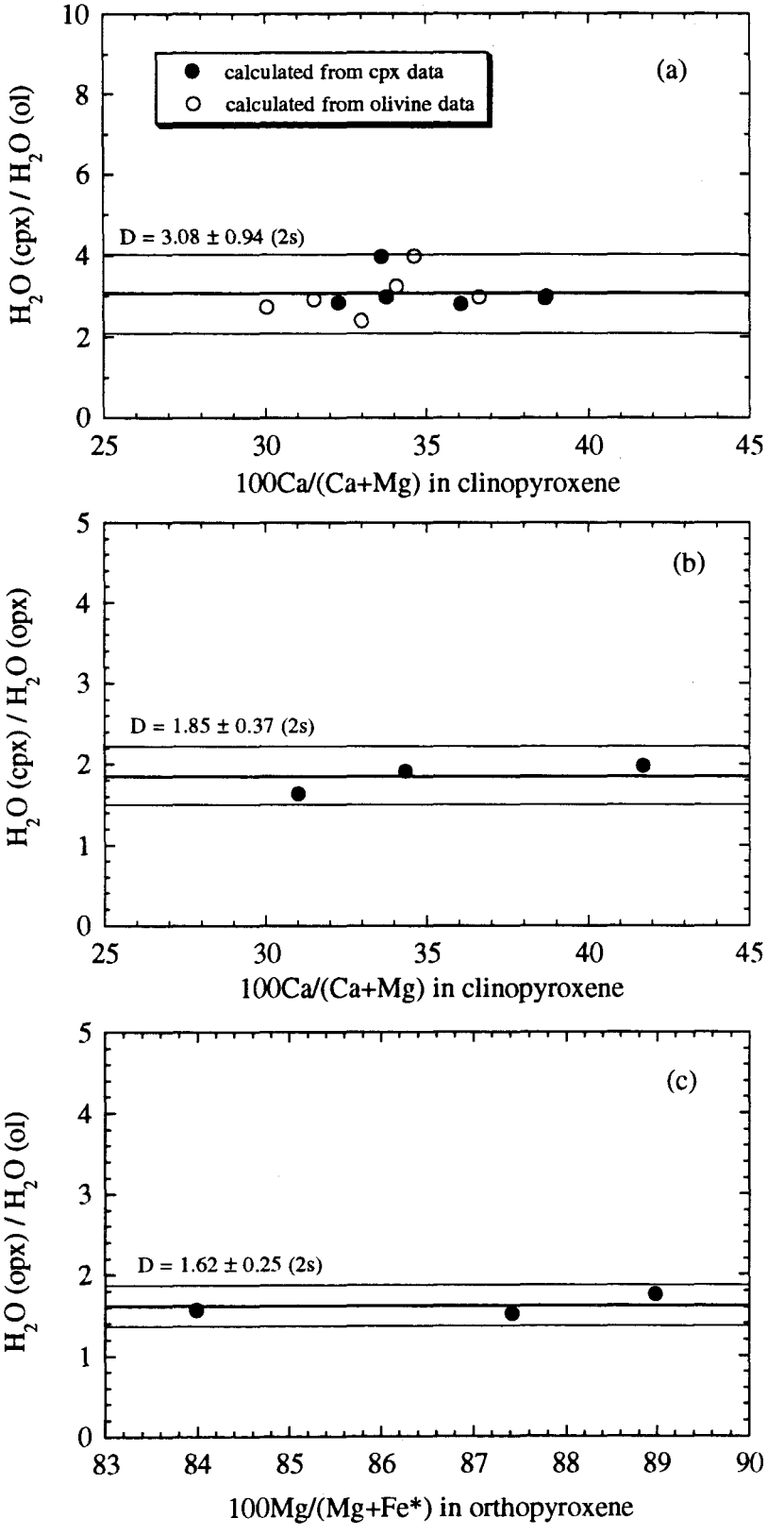
calculated from cpx data
calculated from olivine data
(a)
D = 3.08 ± 0.94 (2s)
H2O (cpx) / H2O (ol)
100Ca/(Ca+Mg) in clinopyroxene
(b)
D = 1.85 ± 0.37 (2s)
H2O (cpx) / H2O (opx)
100Ca/(Ca+Mg) in clinopyroxene
(c)
D = 1.62 ± 0.25 (2s)
H2O (opx) / H2O (ol)
100Mg/(Mg+Fe*) in orthopyroxene

Figure 19. (a) Proportion of total OH absorbance contributed by the 3512 cm^{-1} band vs Ti content in megacryst and micro-inclusion-free peridotite garnets from southern Africa. The plot does not intersect the ordinate at the origin because there is always some absorbance at 3512 cm^{-1} contributed by the 3570 cm^{-1} band. The good correlation observed indicates that OH responsible for the 3512 cm^{-1} absorption is associated with the substitution of Ti into garnet. (b) Absorbance of OH in garnet at 3512 cm^{-1} vs. TiO2 showing no correlation.

Fig. 19

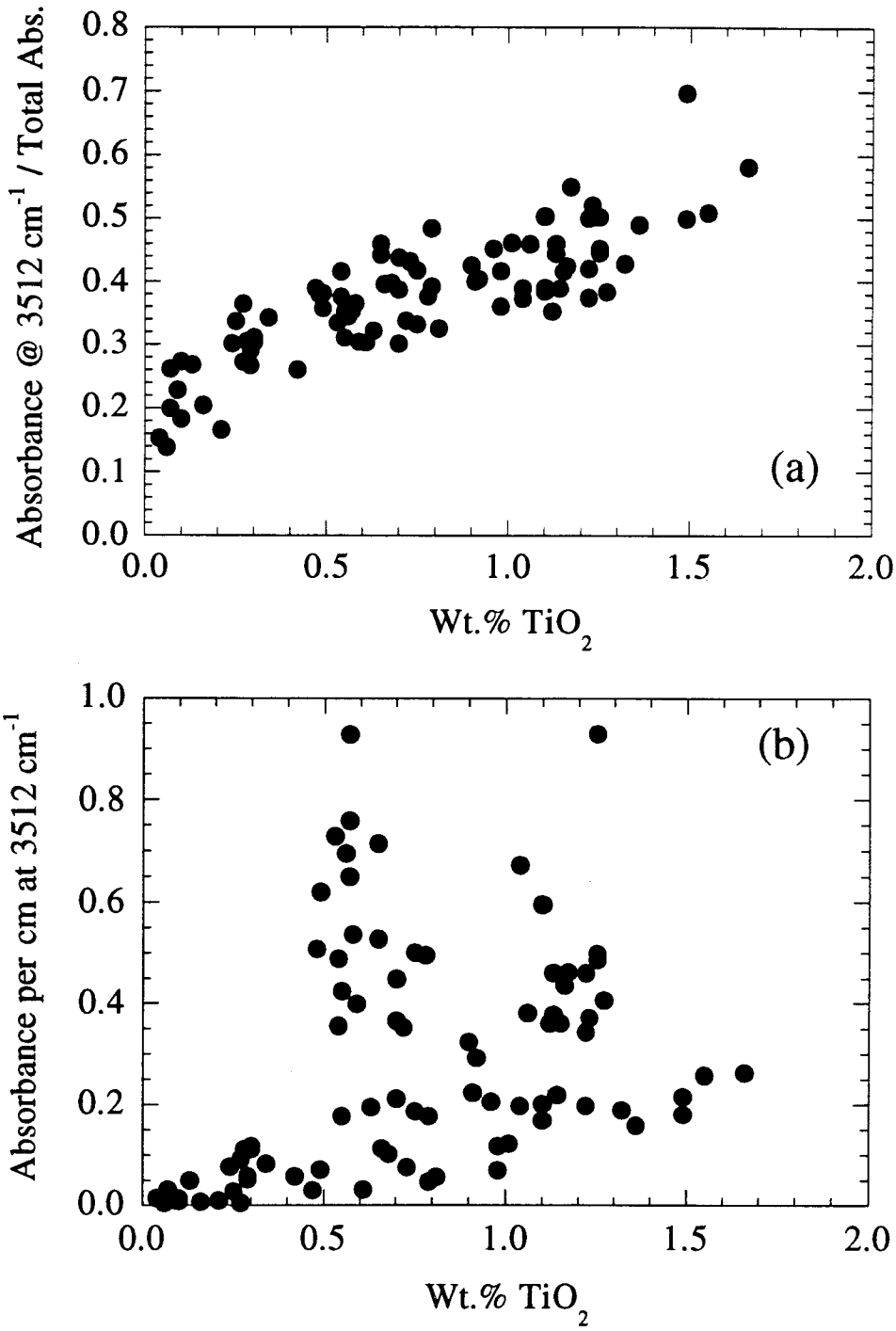
Absorbance @ 3512 cm-1 / Total Abs.
0.0
0.1
0.2
0.3
0.4
0.5
0.6
0.7
0.8
0.0
0.5
1.0
1.5
2.0
Wt.% TiO2
(a)
Absorbance per cm at 3512 cm-1
0.0
0.2
0.4
0.6
0.8
1.0
0.0
0.5
1.0
1.5
2.0
Wt.% TiO2
(b)

Table A1

Sample	Grain	Color Code	Background "granularity"	Paralleli-pipedic cells	Geometrically necessary dislocations	Microfaults or "shear zones"	Inclusions
ROM250_OL2.1	ol	10YR 10 8	1	2	0	0	scattered, 1-4 μm
ROM250_OL2.2	ol	10YR 10 8	1	0	2	0	some 2-10 μm, lilypads
ROM250_OL16.1	ol	7.5YR 10 7	1	0	0	0	0
ROM250_OL16.2	ol	7.5YR 10 7	1	0	0	on one side	1
ROM250_OL24.1	ol	10YR 8 8	1	0	0	0	0
ROM250_OL29.1	ol		1	0	2	0	0
ROM250_OL42.1	ol		?	2	1	2	0
ROM250_OL42.2	ol	2.5Y 4 8.5	1	tr	tr	0	0
ROM250_OL42.3	euhedral tablet	heterogeneous	0	0	0	"healed"	1 μm
ROM250_OL42.3	ol						
ROM250_OL54.1	ol	7.5Y 6 8	1	1	0	1	0
ROM250_OL54.2	ol	2.5Y 8 8.5	1	0	0	0	0
ROM250_OL54.3	ol	heterogeneous	1	0	1	1	1 μm
ROM250_OL54.5	ol	7.5YR 10 7	1	tr, heterog.	1	0	0
ROM250-OL13.1A	ol	7.5-10YR 4 9	0	2	0	1	1 μm (2)
ROM250-OL13.1B	ol	7.5-10YR 4 9	0	2	0	1	1 μm (2)
ROM250-OL13.1C	ol	7.5-10YR 4 9	0	2	0	1	1 μm (2)
ROM250-OL13.1D	ol	7.5-10YR 4 9	0	2	0	1	1 μm (2)
ROM250-OL13.2	ol	7.5-10YR 4 9	0	0	1	0	2
ROM250-OL26.1	ol	10YR 10 8	0	0	0	0	tr
ROM250-OL26.2	ol	10YR 8 8	0	1	0	2	?
ROM250-OL40.1	ol	10YR 6 8	0	0	0	0	?
ROM250-OL40.2	ol	2.5Y 4 9	0	0	0	0	0
ROM250-OL40.3	ol	2.5Y 4 9	0	1(large)	0	2	?
ROM177-OL	ol-zir	2.5Y 4 8.5	0	0	0	1 (large)	1-3μm (2)
ROM181.OL1	ol-zir		0	0	0	2	1-3μm (2)
ROM181.OL2	ol-zir		0	0	0	0	1, but many 2°incls
ROM121-Z010.OL1	ol-zir-ilm		0	0	0	0	tr

Key: 0 = absent; tr = trace present; 1 = present; 2 = abundant

Table A1. Petrographic features of olivine megacrysts. Background granularity refers to fine scale granular features not resolvable at 400X. Parallelipipedic cells and geometrically necessary dislocations defined by Gueguen (1979). Microfaults and "shear zones are disruptions to the crystal in the form of ragged cracks, often running diagonally through the parallelipipedic structure defined by the tilt walls. Commonly discolored to a darker hue. Inclusions refer to apparently primary, often euhedral inclusions, not obviously associated with healed fractures.

Table A1

H_2O

Garnet	H_2O (ppm) = 175.8 - 1.617 $Mg^{\#}$	$Mg^{\#} \leq 74$
	H_2O (ppm) = 609.3 - 7.462 $Mg^{\#}$	$Mg^{\#} > 74$
Clinopyroxene	H_2O (ppm) = 1900.9 - 35.314 $Ca^{\#}$	$Ca^{\#} > 39$
	H_2O (ppm) = -37.92 + 15.168 $Ca^{\#}$	$Ca^{\#} \leq 39$
Olivine	H_2O (ppm) = -1431.4 + 19.377$Mg^{\#}$	$Mg^{\#} \leq 83$
	H_2O (ppm) = 851.7 - 8.0382$Mg^{\#}$	$Mg^{\#} > 83$

Major element differentiation indices:

From garnet	Ca# (cpx)	= -58.54 + 3.535(Mg# in gt) -0.0299(Mg# in gt)^2
	Mg# (opx)	= 52.95 + 0.45502(Mg# in gt)
	Mg# (ol)	= -141.19 + 3.9265(Mg# in opx) - 0.01526(Mg# in opx)^2
From clinopyroxene	Mg# (gt)	= 75.14 + 1.0734(Ca# in cpx) - 0.0281(Ca# in cpx)^2
	Mg# (ol)	= -141.19 + 3.9265(Mg# in opx) - 0.01526(Mg# in opx)^2
	Mg# (opx)	= 5.40 + 0.95502(Mg# in cpx)
From olivine	Mg# (opx)	= 14.67 + 0.85128(Mg# in ol)
	Mg# (gt)	= -116.36 + 2.1977(Mg# in opx)
	Mg# (cpx)	= -5.40 + 1.0471(Mg# in opx)
	Ca# (cpx)	= 211.01 - 2.0512(Mg# in cpx)
From orthopyroxene	Mg# (gt)	= 644.56 - 15.2908(Mg# in opx) - 0.1004(Mg# in opx)^2
	Mg# (ol)	= -141.19 + 3.9265(Mg# in opx) - 0.01526(Mg# in opx)^2
	Mg# (cpx)	= -5.40 + 1.0471(Mg# in opx)
	Ca# (cpx)	= 211.01 - 2.0512(Mg# in cpx)

Table A1. Equations used to parameterize the observed compositional relationships between coexisting megacryst minerals and the trends in OH content for minerals determined in this study.

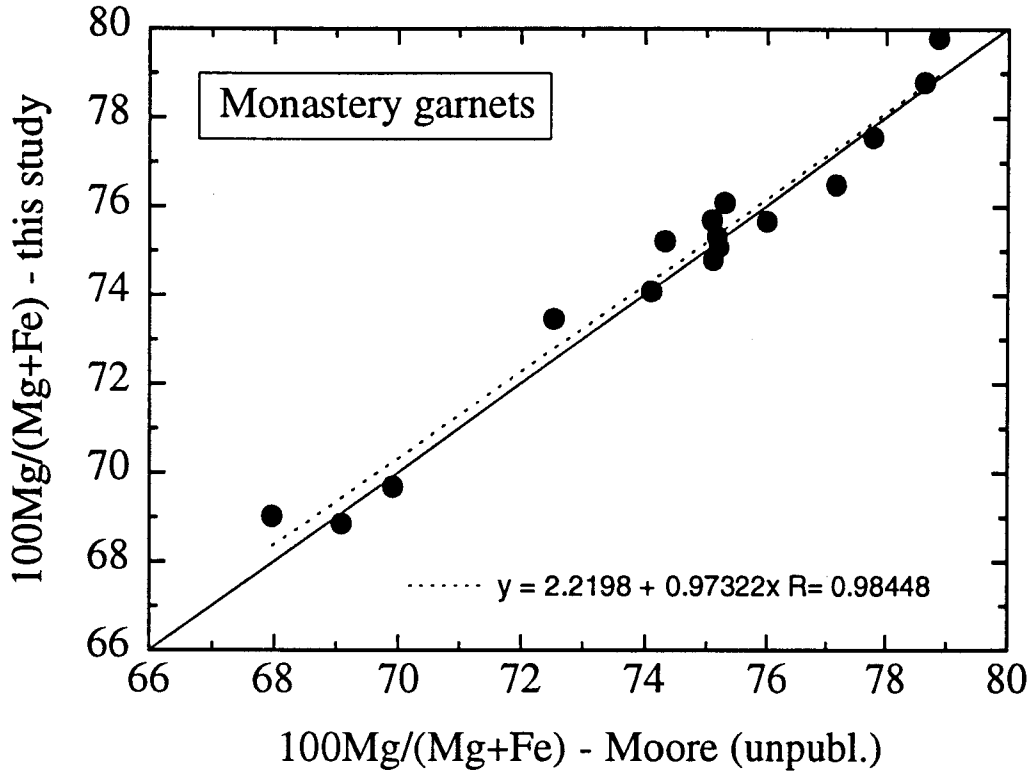

Fig. A1. Comparison of electron microprobe data determined at Caltech (this study) and the University of Cape Town (Moore, unpubl.). Analytical methods described in text and Table 3. Each laboratory prepared and analyzed separate grain mounts from the same megacryst samples, i.e., different fragments from the same parental material are compared here.

Chapter 4. Calibration of an infrared spectroscopic technique for quantitative analysis of hydroxyl in garnet and pyroxene

ABSTRACT

Most common, nominally anhydrous, mantle minerals contain trace amounts of structurally-bound hydroxyl (OH), which has potentially important implications for H geochemistry. Infrared (IR) spectroscopy is the most commonly used method for the detection of trace amounts of OH in minerals. In order to calibrate this technique for quantitative analysis of specific minerals, we have analyzed the concentrations of H in natural, mantle-derived pyrope garnet, augite and aluminous enstatite by manometry, after heating the samples and extraction of H_2 gas under vacuum. Preparation of large (up to 3 gram) quantities of highly pure gem quality sample material allowed detection of H_2 derived from intrinsic OH significantly above vacuum line blank levels, which was well correlated with mass of sample aliquot and apparently unrelated to adsorbed or contaminating hydrous components. IR spectroscopy confirms the presence of intrinsic OH in the samples prior to extraction and indicates between 86% and 100% removal of this component during the extraction procedure. The respective integral specific absorption coefficients of 1.39 ± 0.14 (1σ), 7.09 ± 0.32 and 15.6 ± 0.94 ppm $H_2O^{-1}.cm^{-1}$ for pyrope, subcalcic diopsidic augite and aluminous enstatite allow the determination of the OH content of upper mantle garnets and pyroxenes down to a few ppm with uncertainties in accuracy from about ±10% to ±50%, depending on mineral composition. Relative concentrations of OH in these minerals having similar OH spectra can, however, be determined to within a few percent relative.

INTRODUCTION

Motivation

Hydrogen is present in many nominally anhydrous minerals in minor or trace amounts (see reviews by Rossman 1988 and Bell and Rossman 1992a). In many rock-forming minerals, hydrogen atoms are bound to oxygen anions in the mineral structure, forming hydroxide groups. The incorporation of H into the mineral structure is known to influence various mineral properties, such as rheology, electrical conductivity and ionic diffusivities. A number of recent compilations (Miller *et al.* 1987, Beran and Götzinger 1987, Skogby *et al.* 1990, Bell and Rossman 1992) have demonstrated that high concentrations of hydroxyl commonly occur in mineral samples of high-pressure origin, particularly those from the mantle. This suggests that these nominally anhydrous minerals may be important repositories of mantle water in regions where stoichiometrically hydrous minerals are unstable, and that their OH contents may be useful indicators of the partial pressure of water in those areas where other methods of estimation, such as hydrous mineral equilibria, are inapplicable. Development of these applications and evaluation of the contribution of this form of hydrogen to the global water budget require quantitative analysis of the small amounts of H in such minerals. In this study we have used vacuum extraction and manometry to measure the H contents of spectroscopically charaterized clinopyroxene, orthopyroxene and garnet samples of high purity and use the results to calibrate an infrared spectroscopic technique for quantitative analysis of structurally-bound OH in these minerals. Isotopic composition of the extracted H is discussed in Appendix 1.

Quantitative infrared spectroscopic analysis of OH in minerals

Infrared absorption spectroscopy is commonly used to study the hydrous component in minerals (e.g. Kats 1962, Aines and Rossman 1984a) and is particularly useful due to high sensitivity (to sub-ppm levels) and the ability to distinguish between different types of OH groups and their respective orientations in the mineral structure. The technique is also non-destructive and can be performed with comparatively high spatial resolution (~10μm). In principle, it can become quantitative by application of the Beer-Lambert relationship:

$$c = A / \varepsilon.l, \tag{1}$$

where c is the concentration of the absorbing species (e.g, OH), conventionally expressed as moles of solute per liter of solvent, A is the absorbance and l is the path length of light through the sample. ε is the molar absorption coefficient, a measure of the efficiency of light absorption, and is a function of the compositional and structural properties of the material and the excitation in question. A is measured from the absorption spectrum, either as peak intensity or as integrated peak intensity, and l is commonly approximated as the sample thickness. Where the OH spectrum is composed of multiple peaks of varying halfwidth it is often more appropriate to express quantitative relationships in terms of the integrated absorbance of the family of OH bands.

$$c = \frac{1}{I}\int_{v_1}^{v_2} K(v)dv, \tag{2}$$

where K(v) is the absorption coefficient, that is, the absorbance per unit thickness, as a function of wavenumber (v), and I is the integrated molar absorption coefficient (the equivalent of ε for the integrated absorbance).

An accurate knowledge of ε or I is thus essential for quantitative determination of the absorbing species and requires calibration by an independent method of analysis. OH stretching vibrations in many minerals, including most nominally anhydrous minerals, often produce broad absorptions at a range of frequencies displaced from that of the free OH ion or from bound OH where the O-H bond projects into relatively free space (e.g., the trioctahedral layer silicates). This shift (which is a well-known effect of, but not necessarily caused solely by, H-bonding [Hermansson 1991]) is accompanied by "as is well known, a many fold increase of integrated absorption...and unusual broadening of the same band" (Ikawa and Maeda 1968). Considering this effect and taking into account the orientation of the OH bonds with respect to the vibration direction of light through the crystal gives the following more general expression for the concentration of an absorbing species (Paterson 1982):

$$c = \int_{v_1}^{v_2} \frac{1}{\gamma} \frac{K(v)}{\varepsilon(v)} dv, \qquad (3)$$

where γ is an orientation factor (γ=1 for linearly polarized light with E ~// O-H, γ=0.333 for unpolarized light in an isotropic medium). The consequences of this implied variation in I for analysis of OH in silicates was discussed by Scholze (1960), who drew attention to the need for specific values of ε or I for specific materials. Paterson (1982) presented a general expression for ε(v) for the fundamental OH stretching vibration in the region between 2000 and 4000 cm^{-1}, based on a linear fit to the I - v data on water in various solutions and in glasses. This calibration has been widely applied in later IR studies of OH in minerals. It was not, however, intended for rigorously accurate quantitative infrared

analysis of all forms of OH, but was put forward as a workable general formula for semi-quantitative analysis (Paterson 1982).

The determination of mineral-specific calibrations of the fundamental OH IR absorptions has proved problematic because of the low (0.000x to 0.0x weight percent H_2O)* concentrations typically encountered in nominally anhydrous minerals. Calibrations using nominally anhydrous minerals (Rossman *et al.* 1988, Rossman and Aines 1991, Skogby and Rossman 1991) indicate quite large variations in ε for different compositions, apparently even within the same mineral group. Furthermore, the magnitudes of these molar absorption coefficients can differ significantly (by a factor of at least two or three) from molar absorption coefficients calculated from equation (4) of Paterson (1982) . Until the relationship between ε and v is understood more precisely than described by the best fit equation of Paterson (1982), the quantitative analysis of OH in minerals would seem to require mineral-specific calibrations of molar absorption coefficients.

Previous work on pyroxenes and garnets.

Wilkins and Sabine (1973) analyzed a number of nominally anhydrous minerals, including a pyroxene and several garnets, by a coulometric method involving the use of a P_2O_5 cell. They also provided IR spectra demonstrating the presence of OH in the minerals, but the way in which these data are presented does not allow the calculation of molar absorption coefficients. Aines and Rossman (1984a) used coulometric and manometric techniques to determine the water contents of selected garnets of different composition. The analyzed water contents ranged from 0.06 to 0.36 wt. % with corresponding molar absorption coefficients ranging over nearly two orders of magnitude. The application of nuclear

* In this study, all hydrogen is reported as H_2O, regardless of the chemical speciation

reaction techniques (e.g., Rossman *et al.* 1988) has resulted in further estimates for garnets, but there is still considerable scatter in the data (see review by Rossman 1990). One of the problems may be the vastly different spectroscopic characteristics of OH in the different samples, even in those of similar composition (Aines and Rossman 1984a, Rossman and Aines 1991). Hydroxyl concentrations in pyrope-rich garnets are typically too poor in OH for reliable calibration by initial efforts using this technique (Rossman *et al.* 1988). Calibration of the OH bands in pyroxenes by nuclear reaction analysis has been reported by Skogby *et al.* (1990). Advances in the development of low background detector systems for this technique (Kuhn *et al.* 1990, Rossman *et al.* 1992), and the continuing refinement of ion microprobe techniques hold promise for the future.

In this study, we take advantage of the excellent quality of large, homogeneous pyrope garnet and augitic pyroxene megacrysts and an orthopyroxene separate from a lherzolite xenolith to determine the hydroxyl content by H_2 manometry after extraction under vacuum at high temperature. The abundance is then used to calibrate the linear and integrated absorption intensities for the OH bands in the infrared absorption spectrum of the mineral samples.

SAMPLE DESCRIPTION

One of the greatest obstacles to accurate bulk analysis of low concentrations of H in materials is the presence of trace amounts of contaminant hydrous phases in, or on, the samples themselves. For nominally anhydrous minerals with water concentrations of at most a few hundred ppm, the absence of traces of hydrous phases in the analyzed aliquot is critical for accurate analysis. The samples used in this study were selected for their large size, homogeneity and high degree of purity. The critical factor regarding the latter was the

existence of large volumes (~0.05 to 0.1 cm^3) of flawless material between the inevitable cracks. The clinopyroxene and garnet were large, homogeneous megacrysts, whereas the orthopyroxene was a composite of grains separated from a lherzolite xenolith.

The garnet sample MON-9 was extracted from kimberlite matrix at the Monastery diamond mine, Orange Free State, South Africa. It is a representative of the Cr-poor suite of megacrysts which are abundant at this locality (Gurney *et al.* 1979) and its chemical composition, determined by electron microprobe, is given along with compositions of the other minerals in Table 1. The garnet was a rounded and fractured single crystal, approximately 9 cm in maximum dimension. Deep red gemmy areas up to 1 cm in average dimension were separated by narrow cracks cemented with a blue-green material, possibly a mixture of serpentine and calcite. Apart from these obvious mineral-lined cracks, finer scale fractures also occur within the garnet, the surfaces of which are either free of a lining material or are plated with a very thin calcite veneer. Such fractures were readily visible with the dark field illumination technique described below. Examination of selected gemmy areas under the optical microscope (400X) revealed no evidence of tiny inclusions such as have been described in some mantle olivines by Drury and Van Roermund (1988) and certain mantle garnets (Bell and Rossman, 1992b).

The garnet KM-1493 is a megacryst in alkali basalt from a locality near Kerem Maharal, Mt. Carmel, Israel and was provided by Dr. Mordechai Stein. It is visually similar to the Monastery garnet sample.

The clinopyroxene PMR-53 is also of the so-called Cr-poor megacryst or discrete nodule association found in kimberlites and was collected at the Premier diamond mine, Transvaal, South Africa. The pyroxene is classified as an augite in the scheme of Morimoto *et al.*

(1988), but, in common with many discrete nodule pyroxenes, it is markedly subcalcic, and relatively iron-poor compared with common augites. This sample is dark green in color, measures approximately 3 X 2 X 2 cm and posseses gemmy areas up to 0.5 cm in general dimension that are separated by fractures lined with foreign material. The gemmy areas appear to be free of inclusions, such as are visible under the optical microscope.

The orthopyroxene separate was derived from the spinel lherzolite KBH-1, collected from the tuff ring of the basanite maar at Kilbourne Hole, New Mexico. The grains are a glassy, dark brownish-green color and highly irregular in shape. Typical size is 1 - 3 mm. KBH-1 has the general characteristics of a Group I spinel lherzolite (Frey and Prinz 1978). No primary hydrous minerals were observed during hand picking of mineral separates under the binocular microscope. Orthopyroxene grains are commonly traversed by fractures, the surfaces of which are sometimes lined with another mineral phase, but the grains do not show development of any preferential structural weakness such as cleavage, parting or exsolution lamellae. Grains with fractures were eliminated during the handpicking procedure described below. The surfaces of the orthopyroxene grains that represent original mineral grain boundaries have a clear to lightly frosted appearance, but microscopic examination of the surface revealed a typical absence of other mineral phases. Gemmy interiors of the grains appear inclusion-free under the optical microscope (400X), with the obvious exception of occasional large inclusions of clinopyroxene, olivine and spinel. Grains containing such inclusions were discarded during the preparation of the orthopyroxene separate for analysis.

METHODS

Sample preparation

In order to ensure extremely pure mineral fractions for the hydrogen extraction, two preparation methods were employed. For the orthopyroxene KBH-1, conventional hand picking techniques were applied. The xenolith was unusually friable, so that mineral grains could be separated from one another by hand, or with gentle crushing. This resulted in grains commonly separating along natural grain boundaries. Orthopyroxene grains were then individually handpicked under a binocular microscope in air. This separate was then washed in distilled water, followed by warm dilute HCl in an ultrasonic bath. The clean separate was then re-examined under a binocular microscope, using large area bottom illumination with polarizers in extinction. The mineral grains were immersed in ethanol and each grain was examined for the presence of cracks, foreign inclusions or surface phases, which were well illuminated, especially with the mineral grain oriented in extinction. Grains with internal flaws were discarded. Large grains with minimal contamination that were rejected on the first and second passes were lightly crushed, washed and re-examined. This crushing treatment yielded further clean grains. The final clean separate was washed in ethanol, dried, weighed into three mass fractions and stored in glass vials.

The megacryst samples were treated differently. Each sample (a single crystal) was sliced into a number of wafers using a diamond saw. These measured approximately one millimeter in thickness, depending on the transparency of the sample, and typically two centimeters in diameter. In many cases, especially for the thicker wafers, the wafers were then doubly polished. A wafer from each sample was set aside for core-to-rim homogeneity testing. The wafers were then broken along the pre-existing cracks to yield platelets

(maximum dimension 3 to 12 mm) with gemmy interiors and thin margins consisting of minerals that had lined the fractures. These margins were then ground off with a diamond-impregnated nickel grinding wheel, so that each platelet was bounded by entirely fresh (i.e., artificially generated in the laboratory) surfaces. Each platelet was then examined under the binocular microscope and those entirely free of cracks, inclusions or foreign phases were set aside. Those with minimal contamination were rebroken and reground, or the offending marginal material together with a selvedge of pure mineral chipped off with the aid of forceps under the binocular microscope. The clean material was then crushed to a diameter of $\leq$ 2 mm in the case of the garnet and the fraction less than 100 μm in size discarded. Most sample mass was contributed by grains less than 1mm in diameter. The crushed, sieved and re-washed garnet was then examined in the binocular microscope under ethanol and any visible foreign material removed. In the case of the clinopyroxene samples, only the thickest plates were reduced in size by gentle crushing. In all samples, large grain size was deliberately maintained to minimize the surface to volume ratio. The trade-off with increased diffusion distance resulted in some fraction of the intrinsic OH being retained after extraction, particularly in the coarsest fragments (see below). After a final cleaning in ethanol and isopropanol, the samples were weighed and stored.

Samples for IR spectroscopy were manipulated to orient, in turn, two of the three principle axes of the optical indicatrix vertically by conoscopic observation on an optical microscope, sometimes with the aid of a spindle stage attachment. Two parallel grain surfaces were then ground and polished perpendicular to the respective axis using successively finer grades of alumina-impregnated paper to yield a doubly-polished plate. The final polish was applied with either a 1 μm or 0.3 μm Al_2O_3 grit. The anisotropic materials typically required two orthogonal plates to yield spectra in all three principal vibration directions. In order to establish the homogeneity of the garnet and clinopyroxene samples, spectra were collected

at a number of points on selected large doubly polished wafers. Homogeneity of the orthopyroxene sample was checked by analyzing five separate oriented grains.

Infrared spectroscopy

Polarized infrared spectra in the range 2000 to 10000 wavenumbers (cm^{-1}) were obtained with 2 cm^{-1} resolution on the polished mineral plates using a Nicolet 60SX FTIR spectrometer fitted with an InSb detector. A tungsten lamp and rotatable single crystal $LiIO_3$ polarizer were used to provide an incident beam of linearly polarized infrared radiation. Only sample volumes determined under the binocular microscope to be free of flaws such as inclusions or cracks were intersected during analysis, by screening undesirable parts of the crystal from the infrared beam with a metal aperture. Typical volumes of analysis were thus cylinders with diameters (aperture size) either 300 or 600 μm and lengths (sample thickness) between 200 and 1500 μm.

The sample thickness was measured with an electronic micrometer with a reproducibility of ±0.001 mm. However, it was not always possible to generate perfectly parallel mineral plate surfaces and the errors introduced by slight wedging result in an uncertainty in sample thickness of about ±0.002 mm. Thickness of the samples analyzed in this study ranged from about 0.5 to 2 mm, so that errors introduced by the thickness measurement rarely contribute as much as one percent relative.

The infrared absorption spectra of the fundamental OH stretching vibration in the minerals studied here are composed of a number of partially overlapping bands (Figs. 1-3). These are superimposed on a baseline with contributions from electronic transitions (here due to Fe^{2+}) as well as Si-O vibrations. The precise location of this background (baseline)

absorption is the source of greatest uncertainty in determining the net OH absorbance. In this study, the baselines for orthopyroxene and garnet were obtained from the spectrum of the totally dehydrated minerals, prepared by heating the samples at 1000°C in air (see Figure 2). For the clinopyroxene, some change in character of the 4300 cm^{-1} Fe^{2+} (M2) band occurred after heating, and in this mineral the background was estimated visually with due reference to the dehydrated sample. The OH band intensities and integrated absorbances derived from the IR spectra are given in Table 2.

It is difficult to obtain an accurate assessment of the uncertainty introduced by choice of background for the OH spectrum of clinopyroxene, since the issues of accuracy and precision become somewhat linked. Once determined, the background spectrum is extremely precise, but there is some question as to the accuracy of that position that is difficult to assess. We suggest that errors in the choice of background may result in deviations from the true absorbance and integrated absorbance of up to 10%. We may express this conveniently as ± 5% of some average value for absorbance or integrated absorbance.

In order to test the uncertainties involved in choice of background, the baseline for garnet was determined in three different ways. The results for five different fragments of MON-9 using the three different subtraction methods are shown in Table 3. The method judged most accurate was that which involved computer subtraction of a dehydrated sample of MON-9 and integration of the residual spectrum between 3750 and 3250 cm^{-1} (Method 3 in Table 3). The precise positioning of the background spectrum to be subtracted is subjective, and eight repeated subtractions of the same sample and background spectra produced a standard deviation of 0.3% in the calculated area. The standard deviation for the five separate garnet fragments amounted to 1.7%, making this method the most precise.

A method producing comparable precision (σ=1.8%) but a slightly lower mean value (although within 2σ of the above method), involved fitting the baseline by eye and calculating the integrated absorbance by carefully cutting out the printed spectrum and weighing the area representing the difference between the hydrous and anhydrous garnet spectra. This procedure is the easiest of the three and was used by Bell and Rosssman (1992) in their survey of OH in mantle garnets. It is, however, inherently less precise, and the error in cutting and weighing alone (possibly due to small variations in paper thickness) amounts to 0.73%. The procedure deemed least accurate was a least squares computer fit to the spectrum, modeling the baseline as a third-order polynomial and the OH bands as a combination of six Gaussian peaks. While this method achieved extremely good fits to the sample spectra (Chi squared < 10^{-7}), the resulting sum of Gaussian areas is lower than the first method by about 10%, with s=2.3% and the calculated baseline does not match very well to the spectrum of dehydrated garnet.

In addition to errors introduced during background subtraction, there are uncertainties associated with the procedure of sample orientation for anisotropic minerals, which does not always yield plates that are perfectly perpendicular to a principal vibration direction. We estimate that these deviations from the ideal orientation may be up to 10° and result in discrepancies between measured and true absorptions of up to 5 % in any particular orientation. These differences are reduced when all three vibration directions are summed because of the orthogonality of the vibration directions for any one plate. If all three directions are measured on a single mineral fragment (i.e., with two orthogonal sets of surfaces), then the discrepancy is reduced further because these surfaces are typically very close to within 90 ° of one another (90° ± 5°). The errors reported in Table 2 include all sources of uncertainty for orthopyroxene and garnet because they are derived from the statistics for measurements on multiple samples.

Manometry

The technique of gas extraction follows standard procedures used in sample preparation for measurement of D/H ratios (e.g., Epstein and Taylor 1970, Newman *et al.* 1986). Samples were loaded into a clean, outgassed, platinum crucible in air, covered with a Pt lid, placed into a pyrex heating vessel and attached to the vacuum line. The sample was heated with an induction furnace. Results of temperature calibration attempts to date, using a thermometer, optical pyrometry and melting point determinations for several metals suggest a temperature uncertainty of ~100 °C at high temperatures. The gas collection procedure allows discrimination between oxidized and reduced forms of H. After freezing down of evolved H_2O and CO_2 in a liquid N_2 cold trap, other C- and H- bearing gas evolved during heating was converted to H_2O and CO_2 by passage over hot CuO. H_2O is separated from CO_2 using a cold trap (solid CO_2 [dry ice] - M17 [commercial mixture of chlorinated hydrocarbons] slush) and converted to H_2 by passing the gas over hot U metal. H_2 gas was collected with a mercury Toepler pump and the volume of H_2 measured in a Hg manometer with a reproducibility of $\pm$ 0.05 μmole.

A two stage heating procedure was used in extracting the hydrogen from all samples. Each aliquot was initially held at ~150-200 °C for three hours to remove adsorbed water from the surface of the sample, without releasing structurally bound H. We are confident that no intrinsic OH is lost from the samples at this temperature, because spectroscopically monitored heating experiments in air and vacuum demonstrated onset of intrinsic H loss from the minerals at temperatures of $\geq$ 500 °C (Chapter 5). The H-bearing gas evolved during this low-T step was mostly H_2O. The second heating step involved stepwise elevation of the temperature to that slightly below the sample's melting point. We chose

not to melt the samples because of the greater diffusion distances involved for the coalesced mass, the possibilities of trapping bubbles in the viscous melt and the loss of ability for direct comparison of "before" and "after" IR spectroscopic measurements of OH. It was determined that garnet melted at the lowest temperature (near 1000 °C), so this mineral was heated to ~900 °C, whereas the pyroxenes were heated to higher temperatures (~ 1100 °C). Although the temperature was raised incrementally and the proportions of evolved H_2O to H_2 monitored at intermediate temperatures, all H from temperatures greater than ~150 °C was finally collected together for manometry. In contrast to the low-temperature fraction of evolved gas, the dominant H-bearing species released during the high temperature step was H_2. The length of this step varied from 6 hours for orthopyroxene to 30 hours in total for garnet.

RESULTS

Infrared spectroscopy

Infrared spectra for the three minerals are illustrated in Figs. 1-3. The infrared spectrum of OH in the clinopyroxene (Fig. 1) resembles those of augites described by Skogby *et al.* (1990). Both augites and diopsides display peaks near 3630, 3530 and 3460 cm^{-1} (Wilkins and Sabine 1973, Ingrin *et al.* 1989, Skogby *et al.* 1990), but augite (and our clinopyroxene sample) lacks the band near 3350 cm^{-1} which is typical of diopside. The orthopyroxene OH spectra (Fig. 2) differ somewhat from previously published OH spectra of this mineral, although several bands identified by Beran and Zemann (1986) and Skogby *et al.* (1990) are present. The infrared spectrum of OH in the garnet megacryst (Fig. 3) is similar to those previously described by Aines and Rossman (1984a,b), but displays a peak

at 3512 cm^{-1}, a typical feature of Ti-bearing megacryst and certain other garnets (Bell and Rossman 1992b).

In order to determine the individual band absorbances that contribute to the broad absorption spectra of OH in these minerals, we attempted to model the spectra mathematically using a Gaussian and Lorentzian peak-fitting routine. This procedure was abandoned once the arbitrariness thereof became appparent, that is, good fits to the spectrum were only attained when the number of input bands exceeded the number of peaks in the spectrum. While it is probable that unresolved peaks do occur in these spectra, the positions of the extra "hidden" peaks in the spectrum could not be independently verified or predicted *a priori.* and were thus not considered reliable. In lieu of an appropriate resolution of the component bands in the spectra, the total absorbance in these minerals was determined by summing the absorbances at intensity maxima in the spectra (Table 2). In reality, the molar absorption coefficients appropriate to these frequencies are expected to differ from one another, and should ideally be determined separately as the calibrations are refined.

Infrared spectra of samples taken after H extraction are also shown in Figs 1-3. Figs 2 and 3 show that most, but not all of the intrinsic OH has been removed from the orthopyroxene and garnet samples. No residual OH was detectable in the clinopyroxene (Fig.1). Because garnet was run at the lowest temperature and an initial 15 hour extraction still left significant OH in the thickest grains, the 3000 mg sample was subjected to a second extaction. Typical differences between OH contents of garnets from these extractions are shown in Fig. 3. It has been confirmed by IR analysis of a range of grains of different original thickness that the smallest grains lose a greater proportion of OH than do the larger ones during the extraction, presumably because of the greater diffusion distances involved for

the latter. This residual OH has not been taken into account in calculation of the molar absorption coefficient for garnet because of its small magnitude (Fig 3) and because of the uncertainties in accurately quantifying this amount. The garnet exhibits interesting behavior in that the dominant OH band at 3570 cm^{-1} is quite easily removed during extraction, whereas the smaller 3512 cm^{-1} band is far more stable at high temperatures. This same behaviour has been observed during heating experiments on garnets in air and suggests the presence of at least two distinct OH sites in these garnets. A quantitative assessment of the remaining fraction of OH in the orthopyroxene (14%) is reported in Table 2, and is based on the assumption that the one sample analyzed is representative of the whole batch after extraction. This is an oversimplification because of distribution of grain sizes. In reality, this estimate for residual OH is probably on the high side because the grain chosen for IR analysis was one of the larger fragments in the extracted sample.

Manometry

The amount of extracted H_2 recovered from the high temperature (>150 °C) treatment of each sample aliquot is reported in Table 4 and plotted as a function of aliquot mass in Figure 4. The data display excellent correlations between H yield and sample mass for each mineral studied, which is an indication both of the homogeneity of the sample splits and the reproducibility of the blank added to each extraction (3 μmoles). Furthermore, the consistency of the results indicates that the small amounts of residual OH after extraction (Figs 1-3 and Table 2) do not disrupt the correlation. In other words, if they do influence the measured volumes of H_2, then it is in a coherent and systematic manner in proportion to sample mass. The residual OH is taken into account in the calculation of total OH content of the orthopyroxene, but not garnet. It is apparent that the differential degrees of incomplete degassing that must occur for the range of thicknesses of orthopyroxene and

garnet mineral fragments have not affected the overall yield of each aliquot to substantially different degrees. We are also confident that the positive correlations shown on Fig. 4 are not due to adsorbed material on the fragment surfaces that is stable to temperatures in excess of 150 °C. This is precluded by the manometric analysis 1800 mg of the garnet KM-1493, demonstrated by IR spectroscopy to be extremely poor (<2 ppm) in OH. This sample was analysed with an earlier procedure that produced somewhat higher blanks, but still yielded only 4.9 μmoles of H_2 (including blank of > 3 μmoles). It would be predicted that this mass of sample would yield considerably more H_2 (at least 9 μmoles) if all the high temperature H_2 was derived from adsorbed material that was proportional in quantity to sample mass. The possibility of surface contamination was tested further by subjecting a garnet aliquot that had gone through the extraction procedure to a second acid wash and cleaning in organic solvents (acetone, ethanol, isopropanol). This retreated aliquot was then run through the extraction procedure again and yielded a high-T H_2 concentration comparable to blank level, demonstrating that grain surface residues from the organic solvents are not the cause of the measured H_2.

The estimates for the concentrations of OH (expressed as ppm H_2O) in the minerals were derived by linear regression of the data in Figure 4. and are listed in Table 4 with the associated uncertainties derived from the errors in the slope of the regression lines in Figure 4. These data have been combined with the IR spectroscopic data from Table 2 to calculate a set of molar and specific absorption coefficients (Table 5). The integrated absorbances for the anisotropic minerals have been calculated as the sum of the integrated absobances in the three principal vibration directions per cm of sample thickness. The linear absorbances have been calculated as set out by Skogby *et al.* (1990) and Table 2, but with the exception that our values are for H_2O, rather than OH. The ramifications of these procedures are discussed further below.

The conversion from the measured concentration of μmoles H_2O per gram of mineral to the conventional units of ε of liters per mole requires an estimate for the density of the mineral. We have determined the density of our mineral samples by repeated weighing of pure, gem quality fragments in air and toluene. The densities and their associated uncertainties are reported in Table 1. However, for general application we prefer to express the absorption coefficient as a factor relating absorbance per cm of sample thickness to water concentration in weight percent (see Rossman *et al.* 1988). This circumvents the troublesome density determination and reports concentrations in units more commonly used in geology.

DISCUSSION

The origin of the extracted H_2.

As dicussed earlier, the primary concern of this study has been the elimination of contaminating hydrous materials from our samples. Several arguments can be made to support our claim that the measured H_2 is derived from the breakdown of OH groups within the sample mineral structure, and does not originate from other phases, which may have been present as unseen inclusions or imperfections within mineral grains.

The first argument is that the spectroscopic data show that 86% or more of the intrinsic OH has been removed from the samples. The H_2 yields are of the range of magnitude expected from the intrinsic component, based on recent results on the same samples from nuclear reaction analysis (D. Kuhn, F. Rauch, D. Bell and G. Rossman, unpublished data). In fact, the sample aliquot sizes were selected so that predicted H_2 yields would provide sufficient signal to noise ratio, given the known blank levels of the manometric technique.

Secondly, analysis of the garnet sample with low intrinsic OH content (estimated at <2 ppm H_2O based on IR), the megacryst KM-1493 yielded a predictably low amount of H_2.

The third argument concerns the nature of the alteration phases and the release pattern of hydrous gases. We have not made a study of the hydrous alteration phases occurring along cracks in the minerals, but the assemblage is likely to include serpentines, clays and zeolites as well as possible chlorites and micas. During heating, many of these phases are expected to breakdown by a series of dehydration reactions, releasing water and leaving an anhydrous residue. In contrast, hydrous Fe-bearing minerals that are stable to high temperatures, such as amphiboles and micas lose a considerable amount of their OH as H_2, with the concomitant oxidation of Fe^{2+} to Fe^{3+} before they lose OH as water (Phillips *et al.* 1988). We observe that the gas evolved during the low temperature step is predominantly water, while that evolved at high temperatures is predominantly H_2. Thus although some of the high-T component could be due to H_2 release from Fe-bearing minerals, the lack of water released at these temperatures suggests that several of the more water-rich potential contaminant phases do not appear to contribute substantially to the high temperature component.

Calcite was observed during handpicking as a common and, in some cases, probably the major contaminant phase that lined fine cracks in the samples. Other contaminants were fine grained mineral aggregates probably comprising mixtures of serpentines, clays and possibly other hydrous phases. CO_2 was observed in the gas fraction of both high and low temperature steps (after oxidation of the evolved gases in the CuO furnace), but unfortunately our procedure did not permit us to distinguish between that derived from oxidized or reduced carbon. It is thus possible that some calcite contaminant was introduced with the sample, but this would not influence the amount of H measured. The

presence of traces of hydrocarbons, such as those observed by Tingle *et al.* 1990 and discussed by Mathez (1987) cannot be precluded, other than to emphasize the efforts made to avoid such material during handpicking by excluding cracked grains.

In conclusion, it is believed that most of the blank-corrected hydrogen measured by manometry is derived from the spectroscopically observed, structurally-bound OH within the mineral samples. The argument is weakest in the case of garnet, where sample masses are highest, H concentrations lowest and analytical consistency poorest. We must admit the probability of a small proportion of H contamination from phases that escaped notice, particularly in the case of garnet. In such cases the calibrations determined here place lower limits on the molar and specific absorption coefficients listed in Table 5.

Comparison with previous work.

Table 6 lists a series of calibrations for pyroxenes and garnet from the literature with which our data bear comparison. Our estimate of I = 6700 $l.mol^{-1}cm^{-1}$ for garnet [$\gamma = 1$] differs by about an order of magnitude from the calibrations of Aines and Rossman (1984a) on pyrope-rich garnets. Thus we would estimate water contents of garnets a factor of 20 to 25 lower than estimates using the Aines and Rossman (1984a) calibration. Given the compositional and spectroscopic similarities of their samples to MON-9, it is unlikely that these differences in absorption coefficient are due to intrinsic quantum mechanical effects that govern the interaction of light with the O-H bond. We believe that the discrepancy arises from the presence of foreign phases and possibly adsorbed components in the samples used during the earlier study. The integral molar absorption coefficient for pyrope determined here is within error of the mean molar absorption coefficient of 7070 ± 1030 $l.mol^{-1}.cm^{-1}$ [$\gamma = 1$] calculated from the data presented for seven grossular garnets by

Rossman and Aines (1991). While this agreement is noteworthy, it may be coincidental, as absorption coefficients obtained for almandines and spessartines (Rossman *et al.* 1988) are different, though somewhat scattered. Nuclear reaction analyses for pyrope-almandine garnets reported by Rossman (1990) display a general positive correlation with infrared peak intensity, but with considerable scatter. A best fit line through this dataset, ignoring two aberrant points yields a value for ε per cm of 15.3 $l.mol^{-1}$, assuming density of 3.85 to facilitate comparison. This calibration yields estimates for H_2O about a factor of six higher than that reported here. There are still unsolved problems in nuclear reaction analysis concerned with surface preparation, correction for impurities introduced during surface preparation and possibilities of H migration during analysis and our present bias is thus to favor the calibration from manometry. However, the severe effort involved in preparing large quantities of extremely pure and homogeneous material required by our current experimental procedure render this method impractical for general use and point to high sensitivity, low sample volume techniques as the way of the future.

The OH concentration of the garnet MON-9, calculated from the calibration of Paterson (1982), is 17.16 ± 0.92 (2σ, n=5, not including any errors in the formula) ppm H_2O. The weighted integrated molar absorption coefficient for H_2O is 66440 ± 490 $l.mol^{-1}.cm^{-2}$ [γ = 0.333], very close to the value of 63000 $l.mol^{-1}.cm^{-2}$, predicted from the peak maximum at 3570 cm^{-1}. Thus the OH contents predicted by the Paterson relationship for garnet are a factor of three lower than would be predicted by the present study (note that our value is reported for γ = 1). Unfortunately, water contents a factor of three lower than those measured in garnet MON-9 would not be unambiguously distinguishable from the blank of our extraction procedure, given the present sample sizes. The OH content of the orthopyroxene, calculated from the Paterson (1982) calibration is 214 ± 55 (2σ) ppm H_2O, giving a weighted integral molar absorption coefficient per cm (I) for this sample of 82280

± 22060 (2σ) l.mol^{-1}.cm^{-1}. This is very close to, and well within the uncertainty of, the value of 80580 ± 6400 (2σ) l.mol^{-1}.cm^{-1} determined in this study.

The increase of K in the order garnet, clinopyroxene, orthopyroxene is an expected consequence of the nature of the hydroxyl groups in these minerals, as revealed by their IR spectra. The spread of wavenumbers of the OH absorptions in these spectra show that the degree of hydrogen bonding appears to increase in the above order, that is, that orthopyroxene contains a greater proportion of OH groups that are more significantly H-bonded than does clinopyroxene, which in turn contains more than garnet.

A factor inhibiting the establishment of universal calibrations for mineral species is the difference in the OH spectrum between minerals of similar bulk composition. The fact that the IR spectrum of, say, orthopyroxene can consist of a number of OH bands of different wavenumber (from 3600 to 3050 cm^{-1}) with different relative intensities for different samples implies that there will probably be a variation in the molar absorption coefficient that is virtually sample-specific. It is thus most desirable to determine either the frequency dependence of the molar absorption coefficient for each mineral species, or perhaps more rigorously, to determine the molar absorption coefficient of each component band in the OH spectrum. This latter goal is attainable in principle by determination of OH concentrations in as many samples as there are OH bands in the spectrum and then solving the system of linear equations. In practice, the variation in relative proportions of these bandsmay be insufficient to exceed presently attainable analytical uncertainties.

Comparison of calibrations for anisotropic minerals is more complicated because of the issue of OH vector orientation. Beran (1976), Ingrin *et al.* (1989) and Skogby *et al.* (1990) have shown that both ortho- and clinopyroxene OH spectra consist of multiple

bands with different crystallographic orientations. In general, these bands display a consistent variation in intensity with the orientation of the electromagnetic E-vector (i.e., light polarized parallel to α, β or γ), but the consistency of their orientation has not been tested in detail. Since the contribution of each OH bond to the observed intensity depends on the projection of the OH vector onto the principal vibration directions and total absorption is determined by summing the contribution from all three principle vibration directions, the observed intensity can only be directly compared between samples if the OH vectors are in the same orientation with respect to the principal vibration directions. The maximum apparent discrepancy of a factor of 1.7 arises when the OH vector differs by 45° between samples.

In order to compare our clinopyroxene calibration with that reported by Skogby *et al.* (1990) for augite (Table 6), we have summed the intensities of the bands at 3600, 3520 and 3460 cm^{-1} as shown in Table 2. The ε values agree within error, promoting confidence in the calculation of H contents of augitic pyroxenes. Unfortunately, the calibration for orthopyroxene cannot be compared practically with that of Skogby *et al.* (1990) (see Table 6) because of differences in the spectra and method of determination of total absorbance (not described by Skogby *et al.* 1990).

Applicability of results

Strictly speaking, the calibrations presented here are only applicable to pyrope-rich garnets, augitic and diopsidic clinopyroxenes and aluminous enstatite orthopyroxenes with the same OH absorption bands as the samples analyzed in this study. Spectroscopic analyses of most diopsides and augites of mantle origin show similar features in the OH stretching

region and we suggest that the calibration may be applied to these samples with a reasonable degree of accuracy. However, there is a considerable variability in the OH spectra of crustal diopsides (see Skogby *et al.* 1990, fig. 2) such that the application of the present calibration to such samples must be done with caution. Furthermore, the direct applicability of the diopside calibration to mantle-derived omphacites is not obvious because of consistent spectral differences (see Skogby *et al.* 1990, Smyth *et al.* 1991) . The omphacite OH spectrum is dominated by a single band at about 3450 cm^{-1} whereas the average frequency of absorption in the diopside PMR-53 is closer to 3550 cm^{-1}. We can make an estimate of the possible uncertainty involved in this extrapolation by applying the wavenumber dependence of absorption coefficient of Paterson (1982) of 150 $l.mol\ H^{-1}.cm^{-3}$. This difference in average frequency of absorption produces a predicted difference in K that is 15000 $l.molH^{-1}cm^{-1}$ higher in omphacite than diopside. This would result in estimates of water content of omphacite that were 28 % lower than those derived from the diopside calibration. While the principle of increased absorption coefficient at lower wavenumber is well established, it remains to be demonstrated that the Paterson (1982) parameterization is appropriate for these minerals.

Most pyrope garnets have broadly similar OH infrared spectra and the calibration is probably quantitatively applicable to most such garnets. The observed range in peak maximum for the main garnet OH band in pyropes with less than 50 mole % grossular + almandine is about 3580 to 3560 cm^{-1} (Bell, unpublished data). Sample MON-9 falls approximately in the middle of this range, so following the reasoning outlined above, the expected variation in I for these garnets may be on the order of $\pm$ 5%.

In separate contributions (Bell and Rossman 1992a,b) these quantitative calibrations have been applied to the infrared analysis of a number of samples of mantle derived pyroxenes

and garnets and the results have been used to evaluate the importance of the nominally anhydrous mineral reservoir of water in the upper mantle.

Acknowledgments

This research was funded by NSF grant EAR 88-16006 (G. R. Rossman, P.I.) and DOE grant DE - FG03 - 85ER13445 (S. Epstein and E. Stolper, P.I.'s). DRB thanks Patrick Bartlett, Glen Mattioli, Rory Moore and Moti Stein for help with aquisition of these rare samples and De Beers Consolidated Mines (Ltd) and Mr. Sydney Gasson for access to the Premier and Monastery Mines, respectively . We thank Ed Stolper for encouragement and helpful suggestions.

REFERENCES

Aines, R. D. and Rossman, G. R. 1984a. The hydrous componenent in garnets : pyralspites. *Amer Mineral*. **69** : 1116-1126.

Aines, R. D. and Rossman, G. R. 1984b. Water content of mantle garnets. *Geology* **12**, 720-723.

Aines, R. D. and Rossman, G. R. 1984c. Water in minerals? A peak in the infrared. *J. geophys. Res.* **89**, 4059-4071.

Bell, D. R. and Rossman, G. R. 1992a. Water in Earth's mantle: the role of nomimnally anhydrous minerals. *Science* **255**, 1391-1397.

Bell, D. R. and Rossman, G. R. 1992b The distribution of hydroxyl in garnets from the subcontinental mantle of southern Africa. *Contrib. Mineral. Petrol.* **111**, 161-178.

Beran, A 1976 . Messung des Ultrarot-Pleochroismus von Mineralen. XIV. Der Pleochroismus der OH-Streckfrequenz in Diopsid. *Tsch. Miner. Petr. Mitt.* **23** : 79-85.

Beran, A. and Götzinger, M.A. 1987 The quantitative IR spectroscopic determination of structural OH groups in kyanites. *Mineral. Petrol.* **36** : 41-49.

Beran, A. and Zemann, J. 1986 The pleochroism of a gem quality enstatite in the region of the OH stretching frequency, with a stereochemical interpretation. *Tsch. Miner. Petr. Mitt.* **35** : 19-25

Brunner, G. O., Wondratschek, H and Laves, F. 1960. Zur Ultrarot-Absorption von Quarz und einigen Feldspaten im 3 μ-Gebiet. *Fortschr. Miner.* **38** : 125-126.

Clowe, A. C., Popp, R. C. and Fritz, S. J. (1988) Experimental investigation of the effect of oxygen fugacity on ferric-ferrous ratios and unit cell parameters of four natural clinoamphiboles. *Amer. Mineral.* **73** : 487-499.

Drury, M. R. and Van Roermund, H. L. M. (1988) Metasomatic origin for Fe-Ti-rich multiphase inclusions in olivine from kimberlite xenoliths.*Geology* **16**, 1035-1038.

Epstein, S. and Taylor, H. P. Jr. 1970. The concentration and isotopic composition of hydrogen, carbon and silicon in Apollo 11 lunar rocks and minerals. *Proc. Apollo 11 Lunar Sci. Conf., Geochim. Cosmochim. Acta Suppl.* **1** (2), 1085-1096.

Frey, F. A. and Prinz, M. 1978. Ultramafic inclusions from San Carlos, Arizona: petrologic and geochemical data bearing on their petrogenesis. *Earth planet. Sci. Lett.* **38**, 129-176.

Gurney, J. J., Jakob, W. R. O. and Dawson, J. B. 1979 Megacrysts from the Monastery Mine. In: F. R. Boyd and H. O. A. Meyer (eds) *The mantle sample : inclusions in kimberlites and other volcanics.* AGU, Washington : 227-243.

Hermansson, K. 1991. *Ab Initio* calculations of the fundamental OH frequency of bound OH^- ions. *J. Chem. Phys.* **95**: 3578-3588.

Ikawa, S.-I. and Maeda, S. 1968. Infrared band intensities of the stretching and librational bands of H_2O, D_2O and HDO in solids. *Spectrocim. Acta* **24A**: 655-665.

Ingrin, J., Latrous, K., Doukhan, J. C. and Doukhan, N. 1989. Water in diopside : an electron microscopy and infrared spectroscopy study. *Eur.J. Mineralogy* **1**: 327 - 341.

Kats, A. 1962. Hydrogen in alpha-quartz. *Philips Res. Repts..* **17**, 133-195, 201-279.

Kuhn, D., Rauch, F and Baumann....*Nucl. Instr . Methods B.*

Martin, R. F. and Donnay, G. 1972 Hydroxyl in the mantle. *Amer. Mineral.* **57** : 554-570.

Mathez, E. A. 1987 Carbonaceous matter in mantle xenoliths: composition and relevance to the isotopes. *Geochim. Cosmochim. Acta* **51** : 2339-2347

Miller, G. H., Rossman, G. R. and Harlow, G. E. 1987. The natural occurrence of hydroxide in olivine. *Phys. Chem. Minerals* **14**, 461-472.

Morimoto, N *et al.* 1988. Nomenclature of pyroxenes. *Mineral. Mag.* **52**, 535-550.

Newman, S, Stolper, E. M. and Epstein, S. 1986. Measurement of water in rhyolitic glasses : Calibration of an infrared spectroscopic technique. *Amer. Mineral.* **71** : 1527-1541.

Paterson, M. S. 1982 The determination of hydroxyl by infrared absorption in quartz, silicate glasses and similar materials. *Bull. Mineral.* **105** : 20-29.

Phillips, M. W., Popp, R. K. and Clowe, C. A. 1988 Structural adjustments accompanying oxidation-dehydrogenation in amphiboles. *Amer. Mineral.* **73** : 500-506.

Rossman, G. R. 1990 Hydrogen in "anhydrous" minerals. *Nucl. Instr. Methods Phys. Res.* **B45** : 41-44.

Rossman, G. R. and Aines, R. D. 1991 The hydrous components in garnets : grossular-hydrogrossular. *Amer. Mineral.* **76**, 1156-1164.

Rossman, G. R., Rauch, F., Livi, R., Tombrello, T., Shi, C. R. and Zhou, Z. Y. 1988. Nuclear reaction analysis of hydrogen in almandine, pyrope and spessartite garnets. *Neues Jahrb. Miner. Mh.* **1988** (4) : 172-178

Scholze, H. 1960. Über die quantitative UR-spektroskopische Wasserbestimmung in Silikaten. *Fortschr. Miner.* **38**, 122-123.

Skogby, H. S., Bell, D. R. and Rossman, G. R. 1990 Hydroxide in pyroxenes : variations in the natural environment. *Amer. Mineral.* **75** : 764-774.

Skogby, H. S. and Rossman, G. R. 1989 OH- in pyroxene : An experimental study of incorporation mechanisms and stability. *Amer. Mineral.* **74** : 1059-1069.

Skogby, H. S. and Rossman, G. R. 1991 The intensity of amphibole OH bands in the infrared absorption spectrum. *Phys. Chem. Minerals* **18**, 64-68.

Smyth, J. R., Bell, D. R. and Rossman, G. R. 1991 Incorporation of hydroxyl in upper mantle clinopyroxenes *Nature* **351** : 732-735

Tingle, T. N., Hochella, M. F., Jr., Becker, C. H. and Malhotra, R. 1990 Organic compounds on crack surfaces in olivine from San Carlos, Arizona and Hualalai Volcano, Hawaii. *Geochim Cosmochim Acta* **54**, 477-485.

Vedder, W. and Wilkins, R. W. T. 1969 Dehydroxylation and rehydroxylation, oxidation and reduction of micas. *Amer. Mineral.* **54** : 482-509.

Wilkins, R. W. T. and Sabine, W. 1973 Water content of some nominally anhydrous silicates. *Amer. Mineral.* **58** : 508-516.

Table 1. Compositions and densities of minerals used in this study.

	clinopyroxene (3) PMR-53	orthopyroxene (8) KBH-1.opx	garnet (3) MON-9	garnet (3) KM-1493
SiO_2	54.78	54.68	42.20	40.99
TiO_2	0.35	0.11	1.25	0.62
Al_2O_3	2.83	4.73	20.39	22.87
Cr_2O_3	0.14	0.49	0.62	n.d.
FeO*	6.87	5.88	10.89	13.54
MnO	0.14	0.14	0.28	0.39
MgO	18.30	32.92	19.52	16.34
CaO	13.26	0.86	4.62	5.55
Na_2O	2.13	0.12	0.11	0.03
K_2O	0.05	n.d.	n.a.	n.a.
NiO	0.07	0.10	n.a.	n.a.
P_2O_5	n.a.	n.a.	0.05	0.03
Total	98.92	100.03	99.93	100.36
density	3.339 ± 0.017	3.318 ± 0.017	3.730 ± 0.014	

Numbers in parentheses refer to number of analyses averaged

* All Fe as FeO

Uncertainties in density are ± 2σ.

n.a. not analyzed

n.d. not detected

Table 2. Infrared spectroscopic data.

Mineral	Band energy (cm^{-1})	Band intensity (Abs. per cm) α	β	γ	Σ A†	Integrated absorbance per cm. (before extr.)	Integrated absorbance per cm. (after extr.)	Integrated absorbance per cm. (extracted)
Clinopyroxene	3625	4.09*	6.54*	-	15.72	1903 ± 69	0	1903 ± 69
PMR-53	3540	-	-	1.94*	±			
	3460	1.36	1.43	3.18*	0.43			
Orthopyroxene	3600	4.56*	3.03*	-	30.49	3221 ± 105	461 ± 23	2760 ± 108
KBH-1.opx	3570	-	-	4.23*	±			
	3520	1.44*	-	4.18*	0.69			
	3430	1.48*	2.65*	-				
	3410	-	-	2.31*				
	3300	1.03*	1.32*	1.91*				
	3060	0.60*	0.55*	1.22*				
Garnet	3571	0.621 ± 0.006#			1.119	77.3 ± 1.3	-	~77.3 ± 1.3
MON-9	3512	0.499 ± 0.006#			± 0.007			

† Choice of bands contributing to summed intensity is arbitrary; here bands indicated by asterisks were summed.
* Bands summed to get total intensity
\# Unpolarized
All intensities (absorbances) and integrated absorbances are per cm thickness. Errors represent one standard deviation.

Table 3. Comparison of calculated absorbances and integrated absorbances for garnet using three different methods (see text for discussion).

	Measurement error (%)	Absorbance per cm.	Integrated absorbance per cm.
Method 1*			69.68 ± 1.58
Method 2**	1.07	1.106 ± 0.014	75.32 ± 1.38
Method 3†	0.34	1.119 ± 0.007	77.37 ± 1.30

* Method 1. Polynomial fit to baseline, OH bands fit with combination of Gaussian bands, integrated absorbances calculated from Gaussian band parameters.

** Method 2. Baseline fit by eye, integrated absorbances calculated by cutting and weighing.

† Method 3. Dehydrated MON-9 spectrum used as baseline; subtracted and integrated by Nicolet program.

Errors quoted represent one standard deviation of the mean of five repeat measurements.

Table 4. Sample masses, hydrogen yields measured by manometry and calculated H_2O concentrations.

Mineral Sample	Aliquot mass (mg)	Hydrogen yield (μmoles) low T	high T	H_2O ppm (wt)†
Clinopyroxene				268 ± 7.5
PMR-53	200.0	1.38	5.43	
	497.2	3.10	10.44	
	1024.6	4.02	18.03	
Orthopyroxene				186 ± 1.4
KBH-1.opx	200.1	1.64	5.06	
	645.6	3.00	9.76	
	1299.8	4.12	16.38	
Garnet				55.7 ± 5.5
MON-9	1000.4	4.48	6.95	
	3000.0	4.30	11.16	
	2800.0*	5*	3.96	
KM-1493**	1799.0		4.79	< 1§
Blank	0.0	1.13	2.97	

* The 3000mg fraction of MON-9 was crushed and re-run after IR analysis following the first heating showed residual OH. In the process, 200 mg was lost as fines (< 100 μm).

** Blank levels were higher for this determination due to a different analytical procedure.

† Uncertainty in ppm H_2O calculated from the regression statistics and represents 1σ.

§ Determined by IR spectroscopy.

Table 5. Molar and specific absorption coefficients for OH† in natural pyrope garnet, enstatite and augite, calculated from the data in Tables 1, 2 and 4.

Mineral	Sample number	ε per cm. ($l.mol^{-1}$)	ε* per cm. (ppm^{-1})	I per cm. ($l.mol^{-1}.cm^{-1}$)	I* per cm. ($ppm^{-1}.cm^{-1}$)
Clinopyroxene	PMR-53	316 ± 12	0.0586 ± 0.0023	38300 ± 1700	7.09 ± 0.32
Orthopyroxene	KBH-1	734 ± 21	0.135 ± 0.004	80580 ± 3200	14.84 ± 0.59
Garnet	MON-9	96.9 ± 9.6	0.0201 ± 0.0020	6700 ± 670	1.39 ± 0.14

ε: molar absorption coefficient, ε*: specific absorption coefficient, I: integral molar absorption coefficient, I*: integral specific absorption coefficient

† OH expressed as moles H_2O per liter mineral (ε and I) or as ppm H_2O by weight (ε* and I*).

Uncertainties reported are ± 1σ.

Note that values for ε and ε* correspond specifically to the bands summed as indicated in Table 2.

All absorption coefficients for the pyroxenes are for linearly polarized light, with absorptions in all three orthogonal principal vibration directions summed [$\gamma = 1$]. Those for garnet are based on unpolarized radiation in one direction only, i.e., they have been adjusted for use with $\gamma = 1$ in eqn. (3). In order for the garnet molar and specific absorption coefficients to be compared in a physical sense with the pyroxene values, they should be multiplied by 3.

Table 6. Comparison of this work with published molar absorption coefficients and integral molar absorption coefficients of H_2O in pyroxenes and garnets.

Mineral	Sample	Composition	ε per cm ($l.mol^{-1}$)	I per cm ($l.mol^{-1}.cm^{-1}$)	Ref.
Clinopyroxene	PMR-53	$Ca_{.51}Na_{.15}Mg_{.98}Fe_{.17}Al_{.18}Ti_{.01}Fe_{.03}Si_{1.96}O_6$	316		1
	CIT13123	$Ca_{.95}Na_{.03}Mg_{.95}Fe_{.03}Al_{.11}Cr_{.02}Si_{2.01}O_6$	328		2
	CIT11221	$Ca_{.97}Na_{.02}Mg_{.92}Fe_{.07}Al_{.02}Si_{2.01}O_6$	276		2
	GRR1656	$Ca_{.75}Na_{.09}Mg_{.73}Fe_{.23}Al_{.38}Ti_{.04}Si_{1.78}O_6$	302		2
Orthopyroxene	KBH-1.opx	$Ca_{.03}Na_{.01}Mg_{1.69}Fe_{.17}Al_{.19}Cr_{.01}Si_{1.89}O_6$	734		1
	PMR-54	$Ca_{.03}Na_{.01}Mg_{1.73}Fe_{.19}Al_{.04}Ti_{.01}Si_{1.98}O_6$	140		2
Garnet*	MON-9	$Mg_{.76}Fe_{.24}$	97	6700	1
	CIT15011-rda49	$Mg_{.75}Fe_{.25}$		260	3
	CIT15013-rda113	$Mg_{.75}Fe_{.25}$		340	3
	CIT15013-rda114	$Mg_{.75}Fe_{.25}$		320	3
	Best fit to 13 pyrope - almandine garnets		15.3		4
	Average of seven grossular garnets			7072	5

* Values of I for garnet are for unpolarized radiation, uncorrected for orientational effects [γ=1; Paterson (1982)]

References :
1. This work
2. Skogby et al (1990)
3. Aines and Rossman (1984b)
4. Rossman (1990)
5. Rossman and Aines (1991)

Figure 1. Infrared spectra of OH in clinopyroxene PMR-53 with E polarized // α , β and γ. The upper spectrum in each orientation is the untreated sample, the lower spectrum is after extraction at ~1000 °C for 3 hours and at $200° < T < 900°$ for 2.5 hrs. Spectra normalized to 1 mm thickness.

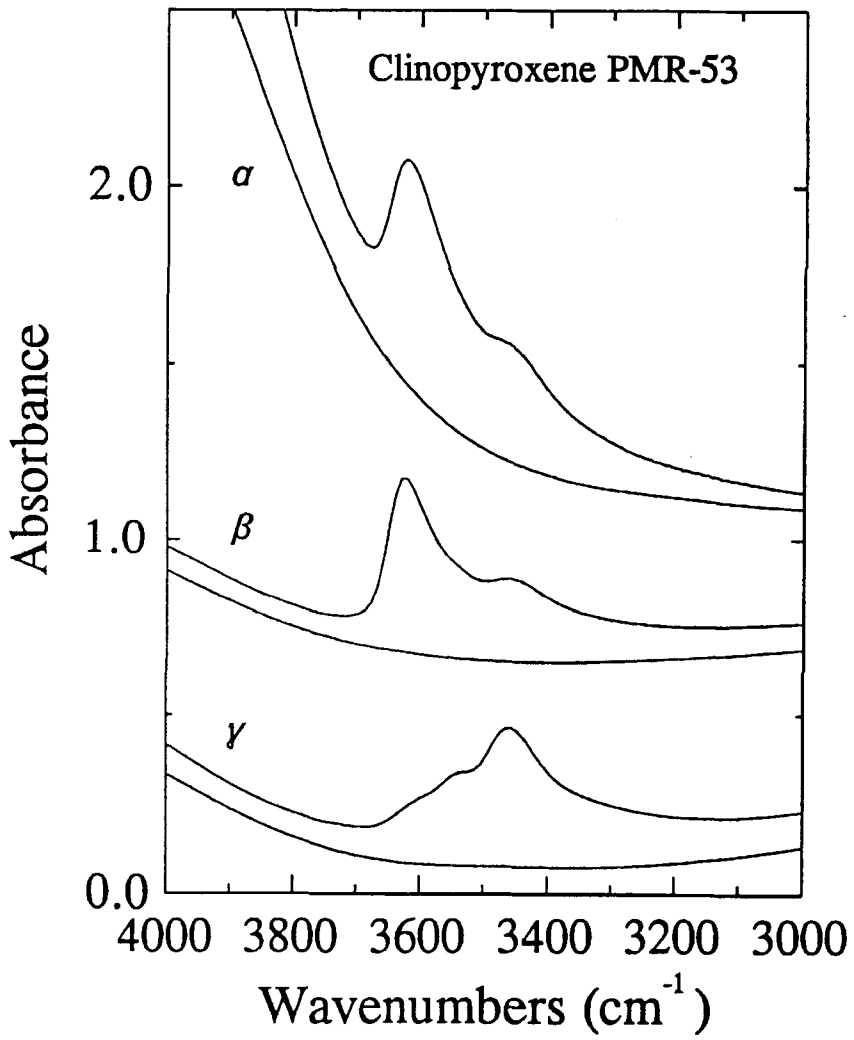
Clinopyroxene PMR-53
α
β
γ
2.0
1.0
0.0
Absorbance
4000 3800 3600 3400 3200 3000
Wavenumbers (cm-1)

Figure 1.

Figure 2. Infrared spectra of OH in orthopyroxene KBH-1.opx with E polarized // a , b and g. The upper spectrum in each orientation is the untreated orthopyroxene sample before extraction, the middle spectrum is after extraction at ~1000 °C for 3.25 hrs and at 200 ° < T < 900 ° for 1.5 hrs. Minimum dimension of sample before polishing > 0.71 mm. b and g spectra taken in direction parallel to thickness (0.71 mm), a spectrum taken parallel to sample length (1.54 mm). The lower spectrum in each orientation is the same fragment heated in air for 24 hrs at 1000°C and is, as far as can be detected, OH-free. Subtraction of this lower spectrum from the upper two was used to determine the OH integrated absorbance in those samples. All spectra normalized to 1mm thickness

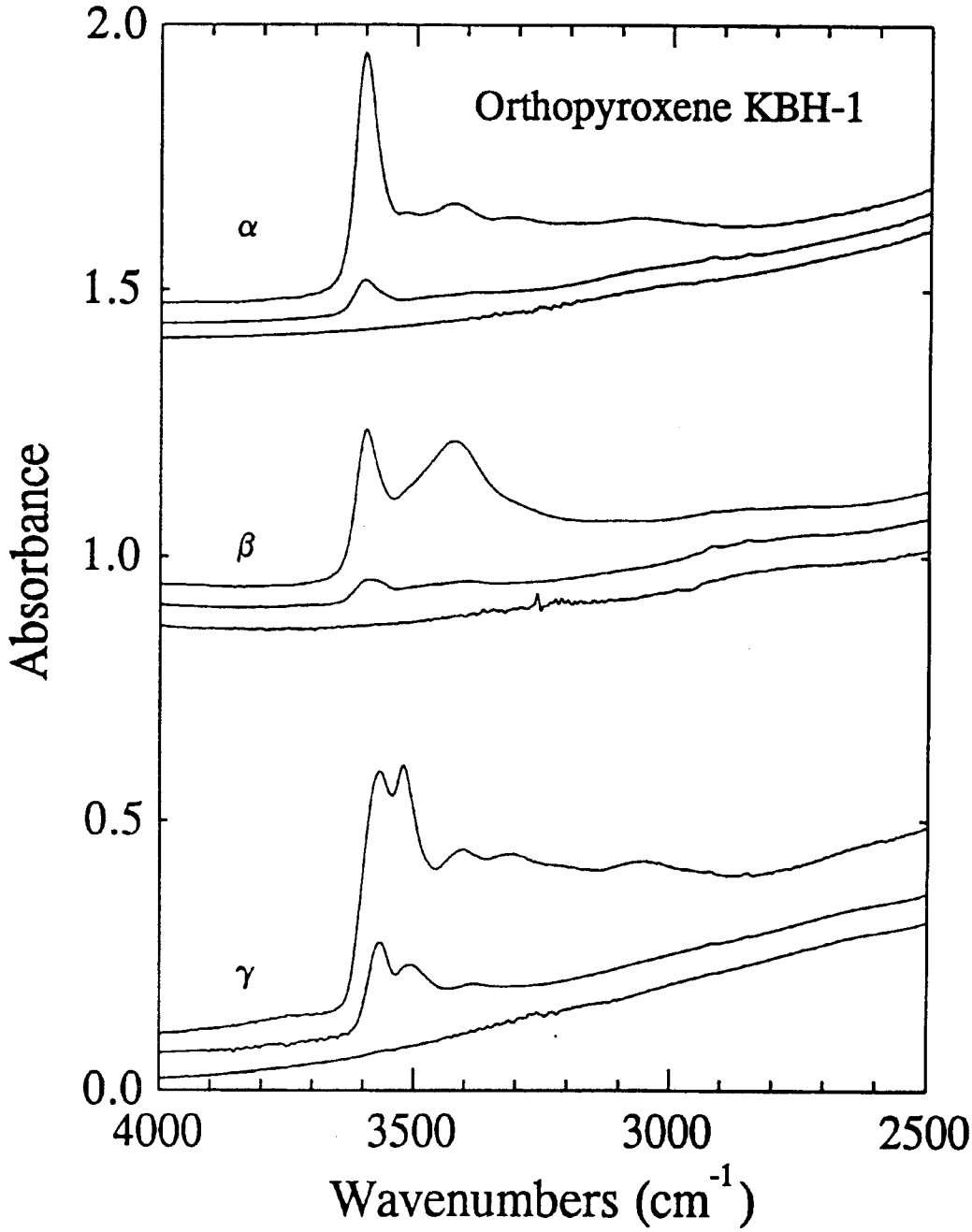
Orthopyroxene KBH-1
α
β
γ
Absorbance
2.0
1.5
1.0
0.5
0.0
4000
3500
3000
2500
Wavenumbers (cm-1)

Figure 2.

Figure 3. Unpolarized IR spectra of garnet MON-9 in the OH stretching region between 3000 and 4000 cm^{-1}. (a) Untreated sample, before extraction. (b) Garnet MON-9 after extraction at ~ 900 °C for 10 hrs. Sample thickness before polishing 0.95 mm. (c) Garnet MON-9 after extraction at ~ 900 °C for 32 hrs. Sample thickness before polishing > 0.43 mm. (d) Garnet MON-9 with all detectable OH removed after heating for 24 hrs in air at 1000 °C. All spectra normalized to 1 mm thickness.

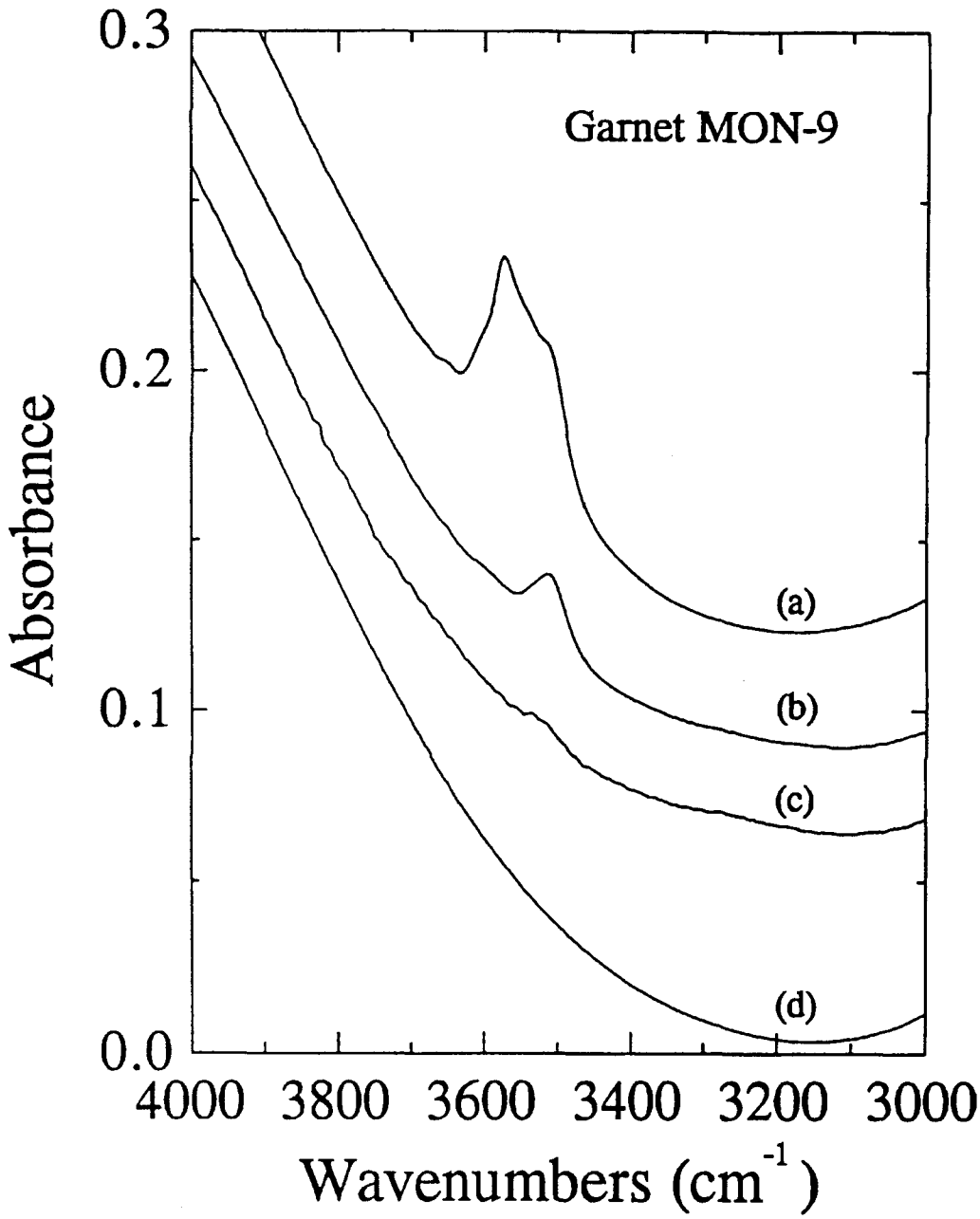
Garnet MON-9
Absorbance
0.3
0.2
0.1
0.0
(a)
(b)
(c)
(d)
4000
3800
3600
3400
3200
3000
Wavenumbers (cm-1)

Figure 3.

Figure 4. Yields of H_2 (determined by manometry) as a function of aliquot mass of sample for the high temperature step (> ~ 150 °C) in the three minerals (a) garnet, (b) enstatite and (c) diopside. The single blank determination (empty Pt crucible) is repeated in each plot and falls on the ordinate. The point corresponding to the greatest mass of garnet (~ 3 g) is the sum of the yields for the two repeated extractions on the same sample minus the blank value of 2.97 μmoles H_2 (The plotted yield therefore includes the contribution from one procedural blank, rather than two.) Linear regression of the data points yields the lines shown, the slopes of which give the concentrations reported in Table 4.

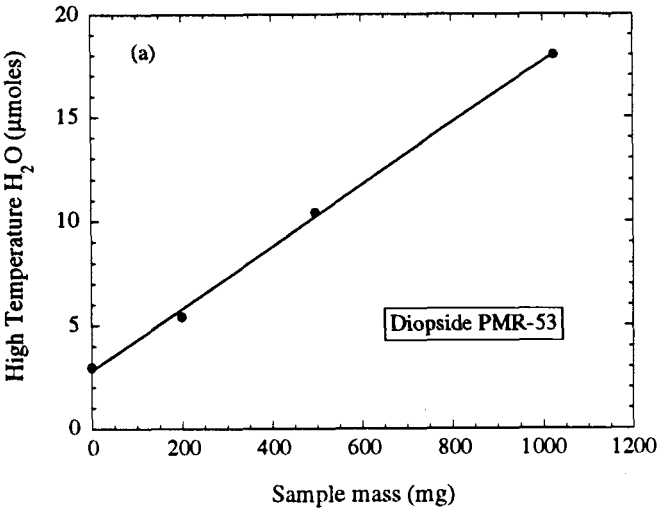
(a)
Diopside PMR-53
High Temperature H_2O (µmoles)
Sample mass (mg)
0
5
10
15
20
0
200
400
600
800
1000
1200

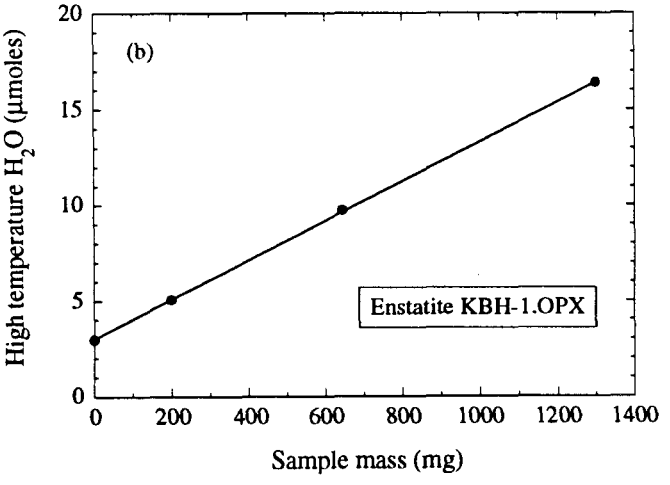
(b)
Enstatite KBH-1.OPX
High temperature H_2O (µmoles)
Sample mass (mg)
0
5
10
15
20
0
200
400
600
800
1000
1200
1400

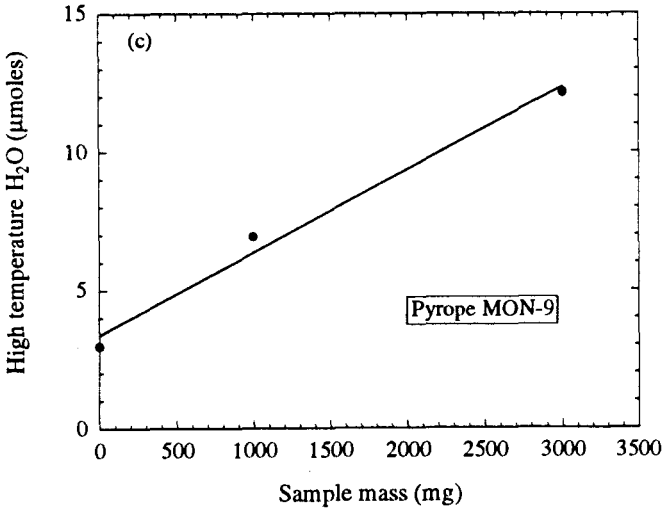
(c)
Pyrope MON-9
High temperature H_2O (µmoles)
Sample mass (mg)
0
5
10
15
0
500
1000
1500
2000
2500
3000
3500

Figure 5. Yields of H_2 (determined by manometry) as a function of aliquot mass of sample for the low temperature (< ~ 150 °C) extraction step.

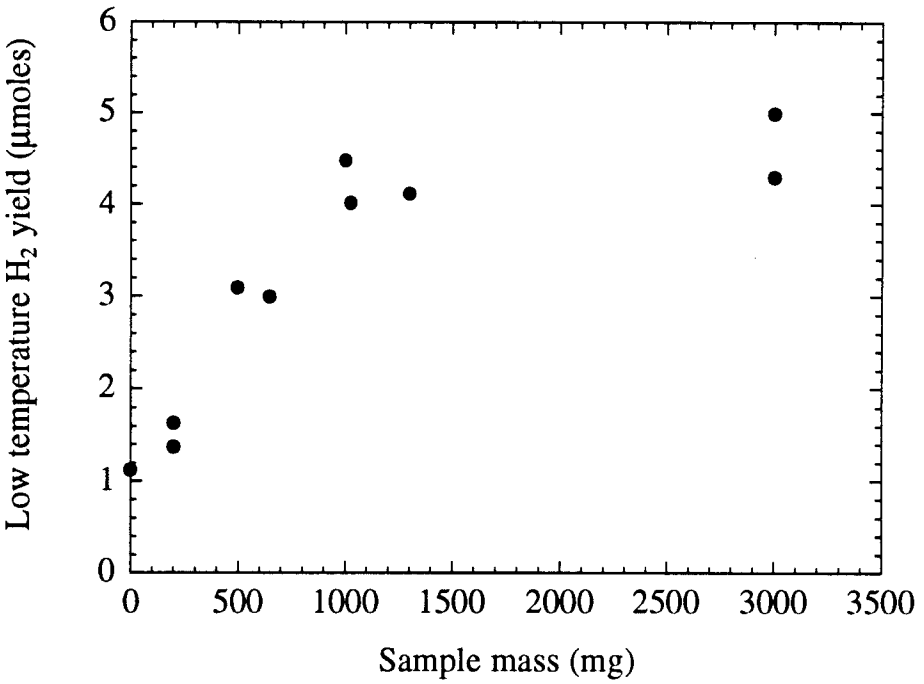
Low temperature H_2 yield (µmoles)
0
1
2
3
4
5
6
0
500
1000
1500
2000
2500
3000
3500
Sample mass (mg)

Chapter 5. Experimental studies of OH in mantle minerals

Abstract

OH in nominally anhydrous minerals can in principle be used to infer concentrations, isotopic compositions and activities of hydrous volatiles in their source regions and are thus potentially powerful probes of geological processes. However, in order for this potential to be realized, H incorporation as a function of volatile fugacities must be calibrated, and the susceptibility of H to changes in concentration or later stage isotopic exhange in response to changing chemical and physical conditions must be evaluated. Here I report results of experiments which investigate aspects of the thermal stability and incorporation mechanisms of OH in nominally anhydrous minerals, with a focus on garnet.

Pyrope garnets synthesized in the presence of excess water in the piston cylinder contain OH which appears to be bound in the mineral structure. This suggests the high temperature stability of OH in garnets. Single crystal infrared (IR) spectroscopy reveals that crystals are commonly zoned with respect to OH content, and that this zoning appears to be preserved during and after garnet growth. This indicates a relatively slow equilibration of hydrous components in synthetic pyrope. There is a general, but scattered positive correlation between garnet rim OH concentrations and approximated fugacity of water in experiments conducted between 20 and 50 kbar.

Natural hydrous Fe-bearing pyrope garnets, as well as pyroxenes, zircon, kyanite and olivine lose H when heated in air, vacuum or impure Ar. In garnets the two principal absorption bands in the OH spectrum have different thermal responses. The main band at 3570 cm^{-1} loses H readily at 800 °C, probably as H_2 accompanied by oxidation of Fe^{2+} to Fe^{3+} in the garnet. Temperatures of ~1000 °C are required to dehydrate the 3512 cm^{-1} band on the hour to day timescales of these experiments.

Hydrothermal treatment of garnets did not increase or decrease the OH content of initially naturally dry or hydrous pyrope. However, naturally hydrous pyrope that was dehydrated prior to hydrothermal treatment was able to retrieve several times the original OH concentration, but only of the 3570 cm^{-1} OH component. A tentative model for H incorporation in natural pyrope is presented.

These results indicate that the OH contents of garnets are susceptible to certain changes as a result of external fluctuations. Rapid homogenization of OH in Fe-bearing natural pyropes during heating or hydrothermal treatment contrasts with slow equilibration of hydrous components in Fe-free synthetic pyrope at even higher temperatures. Hydrothermal deuteration of pyroxenes and other minerals indicates the potential for post-crystallization isotopic exchange in nature. Despite the demonstrated mobility of H under specific circumstances, there are several reasons to suspect that the OH contents of these minerals cannot be arbitrarily set by changes in external conditions, without some degree of internal structural re-adjustment (ionic diffusion other than of H).

It is concluded, based on these and other experiments, combined with observations of natural mineral OH systematics, that these minerals are often likely to preserve original OH contents, but that in attempting to extract petrologic or geochemical information from measurements of such OH, consideration should be given to the individual geological circumstances. Quantitative experimental investigation of incorporation mechanisms and kinetics is probably the highest priority for future research on nominally anhydrous minerals.

Introduction

Trace H that is structurally bound in nominally anhydrous minerals can potentially be used in estimates of the water content and water activity in regions of the Earth from which these minerals derive. In many cases these minerals may be the only H-bearing phases present and therefore provide unique information on the role of water, or other H-bearing chemical species in certain petrologic environments. In order for these minerals to be useful in this way, it must be established how the concentration and speciation of H in the minerals is controlled by variations in pressure, temperature and composition of the system. Aspects of this behavior can be gleaned from study of a well described natural system (Chapter 3), but a deeper understanding more typically requires experimental study in which most physical and chemical variables can be specified. In addition to determination of the chemical mechanisms by which H is incorporated into these minerals, it is desirable to obtain some idea of the kinetics of these processes, so that the effects of various geological processes on the original (possibly equilibrium) state of the minerals can be evaluated.

This chapter describes several sets of experiments that were designed to provide information bearing on the above. By and large, these experiments were not major efforts aimed at a full understanding of H incorporation in any phase, but were designed to answer some questions about the stability and mobility of H in minerals, that were relevant to the interpretation of the natural assemblages studied in Chapters 1, 2 and 3. Initially, it was intended to investigate experimentally the stability and concentration of the hydrous component of pyrope garnet. However, after a few experimental runs had been completed it was discovered that C. A. Geiger and coworkers at the Technische Universität, Berlin were pursuing the same study in much the same way and it was decided to combine the efforts of the two groups, with the German group doing the syntheses and much of the IR

spectroscopic analysis of the run products being done at Caltech. Another reason for suspending the experimental work at Caltech was that it became apparent from the results of the initial piston-cylinder runs that performing the critical experiments in a demonstrably satisfactory manner would be a major undertaking. Although this was seen as a desirable goal, the priority on other activities was higher. Results from the joint study were published in the *American Mineralogist* in 1991 (Appendix 5). Further background to this study, together with details of the work done at Caltech and some discussion beyond that presented in Appendix 5 is presented below. Other experimental studies performed at Caltech and described below constituted less of a focused effort and involved attempted ion-exchange of a number of minerals, investigation of the effects of heating OH-bearing samples in air at 1 atm. pressure and investigation of the incorporation of OH in natural minerals by hydrothermal treatment in cold-seal pressure vessels and the piston-cylinder.

1. Hydroxyl in synthetic pyrope.

1.1 Introduction

The hydrous component in garnet has received considerable attention since the identification of hydrogarnets and the recognition of a solid solution series between anhydrous grossular and hydrogrossular (now known to extend to the Si-free, hydrous end-member katoite $Ca_3Al_2H_{12}O_{12}$). A fine review of the history of hydrogarnet discovery and characterization is given by Passaglia and Rinaldi (1984). OH has been identified in garnet of a wide range of compositions and X-ray studies confirming the garnet structure of the more markedly hydrous variants of many garnet compositions (mostly grandites) have been performed (e.g., Pabst 1937, Foreman 1968, Basso *et al.* 1981, 1983, 1984a,b, Basso 1985, Sacerdoti and Passaglia 1985, Lager *et al* . 1987,

1989). In many hydrogarnets, including hydrogrossular, substitution mechanisms other than the hydrogarnet substitution ($SiO_4 = H_4O_4$) alone appear to play a role (Basso *et al.* 1984a,b, Birkett and Trzcienski 1984, Basso and Cabella 1990, Rossman and Aines 1991, Cho and Rossman, in prep.).

The phase relations of hydrous garnets have been the subject of numerous experimental studies. The stability of the hydrous component in grossular garnet was investigated by Yoder 1950, Carlson 1956, Roy and Roy 1957, Pistorius and Kennedy 1960, Shoji 1974, Huckenholz *et al.* 1975, Hsu 1980 and Huckenholz and Fehr 1982, the latter authors providing a comprehensive review of previous studies. All of these studies show a strong tendency for the OH content of hydrogrossular, as revealed by refractive index or unit sell dimension, to decrease with increasing temperature. However, the low temperatures involved in these experiments create severe problems in achieving equilibrium and hydrous garnets are reported to persist metastably in hydrothermal runs of longer than a year at a temperature of 420 °C (Hsu 1980). Hsu (1980) concluded that at 2 kbar water pressure the thermal stability of hydrogrossular, i.e., grossular garnet with an OH content measurable by a change in unit cell edge from anhydrous garnet, is limited to a maximum of 420 °C. This low thermal stability for hydrogrossular was disputed by Huckenholz and Fehr (1982) who concluded that grossular garnets contained measurable OH contents up to ~ 700 °C, although hydroandradites were restricted to lower temperatures.

The hydrous component in other garnet compositions, such as andradite and spessartine have also been investigated in experimental studies (e.g., Flint *et al.* 1941, Matthes 1961, Gustafson 1974, Shoji 1975, Hsu 1968, 1980, Schiffman and Liou 1978, Huckenholz and Fehr 1982, Kobayashi and Shoji 1987) and a variety of synthetic hydrogarnets were prepared by Ito and Frondel (1967). Gustafson (1974) noted an increase in andradite cell-

dimension below 550 °C (implying hydroandradite formation), but also reported differences in this parameter that were dependent on starting materials used, indicating lack of equilibrium. Similar observations were made by Huckenholz and Fehr (1982), who were able to rank various starting materials in order of their likelihood to produce metastable hydrogarnets. In spite of the kinetic problems, the general conclusion drawn from these studies is that the OH content of hydrogarnets is a strong function of temperature (inversely correlated) under conditions of water and quartz saturation. The above studies are likely to be relevant specifically to the hydrogarnet substitution, which is manifested by an increase in cell dimension over anhydrous garnet, but do not necessarily convey any information on the OH content of the garnets that is present in other crystallographic sites, which may not lead to measurable changes in unit-cell parameters. None of the above studies were aimed at investigation of the small contents of OH such as is typically contained in common pyralspite series garnets (Aines and Rossman 1984).

The suggestion that synthetic pyrope might contain a hydrous component was made by Seifert and Schreyer (1969), who noticed that the refractive index of pyropes synthesized in the presence of water were slightly lower than expected for the pure anhydrous end-member. The existence of this component was confirmed by Ackermann *et al*. (1983), who used single-crystal IR spectroscopy to identify small amounts of OH (~0.05 wt.% H_2O) in pyropes synthesized, by themselves and others, at 25 kbar and 1000 °C. The IR spectra also indicate the presence of water molecules in the garnets, and it is not clear that the OH band near 3600 cm^{-1}, assigned to the stretching vibrations of a "hydropyrope" component, is due to OH incorporated structurally within the garnet. Certainly there appears to be little substantiation for the claim made that the spectroscopic observations prove the existence of hydropyrope, i.e., a pyrope with OH specifically in the hydrogarnet substitution. Synthesis of OH-bearing pyrope was also reported by Begley and Sclar

(1984). Despite the uncertainties in interpretation, the probability of existence of an OH component in pyrope at temperatures and pressures of the upper mantle was sufficient motivation for further study, particularly in view of the advances in IR spectroscopic technology since the earlier studies. In order to investigate variations in the abundance of this component in response to changing P_{H_2O} and T, a series of synthesis experiments in the piston cylinder were planned.

1.2 Experimental methods.

Pyrope was synthesized from a gel of $Mg_3Al_2Si_3O_{12}$ composition, prepared by D. R. Baker and provided by P. J. Wyllie. Known masses of gel and water were loaded into gold capsules, along with two small seeds of natural pyrope in one of the runs. Capsules were welded shut, with water loss during the weld monitored by weighing. Typical water contents of experimental charges were on the order of 20 wt.%. Capsules were pressed into NaCl and run in a 0.5 inch NaCl furnace assembly and run in the four-post piston cylinder apparatus in the laboratory of P. J. Wyllie. Temperature was monitored at 1000 °C by a W-WRe thermocouple which provided temperature control for the automatic power supply controller. Although the temperature is nominally controlled within a few degrees of this value, the long run durations allow for the possibility that actual long term changes in temperature occurred due to contamination ("poisoning") of the thermocouple. Pressures of the runs were 20, 25 and 30 kbars. Run durations were 50 hours (30 kb run) and 100 hours (20 and 25 kbar runs). The experiments were purely synthetic in nature in that no reversals, or other experimental procedures designed to demonstrate equilibrium were attempted. Run conditions and experimental procedure for syntheses conducted by Geiger and co-workers at the Technische Universität, Berlin are given in Appendix 5. Infrared spectroscopic procedures are the same as described in Chapters 1 and 4.

1.3 Results.

1.3.1 Run products.

Upon quenching, all three runs yielded well-formed, colorless garnet dodecahedra of pyrope composition together with excess water. Crystal sizes varied up to about 1 mm diameter, with most in the range of 100 μm to 500 μm. These crystals commonly contained turbid cores and clearer outer regions and were sometimes broken or fractured, presumably by decompression. The turbid regions are composed of fluid inclusions as well as birefringent inclusions which appear to be another mineral. Concentration of inclusions is also higher in sections of the crystal related to growing edges, resulting in a six-armed star shaped array of inclusions in some doubly polished cross sectional plates prepared for spectroscopic analysis (see Appendix 5, Fig.1.)

1.3.2 Spectroscopic analysis

Infrared spectra of the synthesized pyropes show the presence of absorptions due to O-H vibrations. The spectra are similar in their overall structure to those reported by Ackermann *et al.* (1983), although the signal to noise ratio is generally improved. An example is shown in Fig. 1. These spectra are characterized by a broad absorption near 3420 cm^{-1}, characteristic of liquid water, the intensity of which is approximately correlated with the density of fluid inclusions in the beam path and a sharper band near 3630 cm^{-1}. Subtraction of an appropriately scaled liquid water spectrum from the garnet spectrum (see Fig 1) reveals that the sharper 3630 cm^{-1} band is slightly asymmetric, or contains an unresolved component at the low-wavenumber side of the peak. Spectra taken in water

poor parts of the crystal confirm this structure (Appendix 5). In fact the second peak is resolved in spectra taken at 77 °K (Appendix 5, Fig. 5). In syntheses done in Germany, garnets produced from gel starting materials had IR spectra different from those produced from oxide mixes (described in Appendix 5). However, the garnets synthesized in Pasadena from gel have spectra identical to the garnets synthesized from oxide mixes in Germany. This difference may relate to the longer run times employed in the syntheses performed at Caltech (Appendix 5, Table 1).

The sharper band in the IR spectrum is believed to be due to OH bound in the garnet structure, as claimed by Ackermann *et al.* (1983), although this is very difficult to prove conclusively, because of the presence of inclusions in the garnets. Fig. 2 shows the results of an IR traverse done in garnet P29, grown by Geiger from oxide starting materials at 24 kbar and 950 °C. Each spectrum was obtained on a circular spot with diameter of 100 μm. Sample thickness was 535 μm. Intensity of the 3630 cm^{-1} band is plotted as a function of position in the garnet. This shows that the intensity of the 3630 cm^{-1} band is somewhat greater in the inclusion-rich areas of the crystal, but not as much as might be expected from the visible inclusion density if they alone were responsible for the absorption. Not shown on this figure, but evident from the spectra, is the general lack of correlation between the inclusion content and the presence of molecular water (generally low in this garnet), except in the crystal core, where both attain their highest concentrations. The intensity of the 3630 cm^{-1} band is high in areas where no inclusions are visible, and in clear sectors of the garnet is seen to change in intensity, decreasing toward the margin of the grain, with no change in observable inclusion density. Geiger *et al.* (1991) have pointed out the lack of OH bands in the IR spectrum of pyrope synthesized under nominally anhydrous conditions (Appendix 5, Fig.9) and the lack of a known hydrous mineral in the M-A-S-H compositional system with a corresponding IR spectrum in the OH region. Taken together, these observations

favor the structural OH interpretation for this band. Transmission electron microscopy may aid in ruling out inclusions as a source of the OH.

It may be that the factors responsible for increased inclusion content of the garnet (e.g., rapid crystal growth) are also responsible for increased incorporation of H defects in the garnet structure. Evidence that the OH component is linked to garnet growth, rather than to post-growth compositional readjustment is provided by the asymmetry of the OH zoning profiles. High inclusion densities define the probable cores of crystals, which are often displaced from the geometrical centers of the crystals, possibly because of growth interference from neighboring crystals. OH is typically highest in the crystal growth core, regardless of its proximity to the center of the grain (Fig.2) and may decrease to different concentrations on opposite sides of the same crystal. Sometimes two opposite margins of a polished plate may have the same OH concentration (Appendix 5, Fig.7). It may be significant that the run duration of garnet DB-31 showing the constant rim concentration of OH (Appendix 5, Fig. 7) was about three times longer than that of sample P-29 (Fig. 2), in which OH appears to decrease continuously to the margin of the grain.

1.4 Discussion

The variation in OH content shown in Fig. 2 and Appendix 5, Fig. 7 of individual pyrope crystals indicates a lack of equilibrium. A number of factors may be responsible for the observed zoning, including changes in run temperature, changes in water activity due to progressive Si-dissolution in the fluid, and variable garnet growth rate. Of these, the latter explanation seems particularly plausible, because it explains the high inclusion contents in the crystal cores. Given the problems experienced by other workers with achieving chemical equilibrium in hydrogarnets (albeit at lower temperatures) and the notorious

sluggishness of compositional adjustment (i.e., cation diffusion) in garnet, the OH contents of the garnets synthesized in this study and that of Geiger *et al.* (1991) should be interpreted with great caution. However, an important point can be made from these observations, namely that the hydrous component in pyrope garnet is not subject to equilibration over distances of tens to hundreds of μm on the time scales of these experiments (a few days) at temperatures of 900 - 1100 °C. It should be stressed that the OH substitution present in these synthetic samples may not be the same as that which occurs in natural pyrope garnets so that direct application to the kinetics of natural garnets may be inappropriate. Nevertheless, an important principle is established, namely that hydrous components in nominally anhydrous minerals are not necessarily rapidly equilibrating species, as they may be in olivine, for example (Mackwell and Kohlstedt 1990).

If the hydrous component in these pyrope garnets is incorporated via the hydrogarnet substitution, the following reaction may be written for the formation of a hydropyrope component. (It would be no surprise for OH incorporation proceeding via this mechanism to exhibit slow kinetics because of the required diffusion of Si in garnet.)

$$\underset{\text{garnet}}{Mg_3Al_2(SiO_4)_3} + \underset{\text{fluid}}{6H_2O} = \underset{\text{garnet}}{Mg_3Al_2(H_4O_4)_3} + \underset{\text{fluid}}{3SiO_2} \qquad (1)$$

This is an exchange reaction and the ratio of the equilibrium concentrations of the hydropyrope and pyrope components at some pressure and temperature is given by the following expression:

$$\frac{X^{gt}_{hpy}}{X^{gt}_{py}} = \frac{\gamma^{gt}_{hpy}}{\gamma^{gt}_{py}} \cdot \frac{\left(a^{fl}_{H_2O}\right)^6}{\left(a^{fl}_{SiO_2}\right)^3} \exp\left[\frac{-\Delta G^0_{P,T}}{RT}\right] \qquad (2)$$

in which X_i^j, γ_i^j and a_i^j represent respectively the mole fraction, activity coefficient and activity of component i in phase j, and $\Delta G^0_{P,T}$ is the standard state free energy change of reaction (1) at P and T. The above equation can be simplified with the approximation that for low OH concentrations, $a^{gt}_{py} = \gamma^{gt}_{py}.X^{gt}_{py} \approx 1$. Equation (2) indicates the desirability of maintaining constant activities of water and silica throughout the experiment. In the experiments reported here, both of these parameters were allowed to vary. Si is known to be highly soluble in aqueous fluids at high temperatures and pressures (Kennedy *et al.* 1962) and the probable dissolution of Si into water in these experiments results in decreased activity of water as well as a shift in the composition of the solid phases from the pyrope - H_2O join. This effect may be responsible for the high density of other mineral inclusions noted, among which Geiger has identified forsterite and quartz (Appendix 5). For a quantitatively rigorous determination of OH content of garnet as a function of water activity it would be desirable to buffer the activity of silica in the fluid by imposing, for example, quartz or coesite saturation. In fact, if the hydrogarnet substitution is not operative, and some other defect mechanism is responsible for OH incorporation in pyrope, it would be desirable to control the activities of MgO and Al_2O_3 as well. These issues, as well as the problems of achieving equilibrium, will need to be addressed in future quantitative studies aimed at calibrating pyrope as a hydrobarometer. First in priority would seem to be a demonstration that the observed OH component in these pyropes is not metastable.

For reasons outlined above, the quantitative relationship between OH and P, T or water activity was not pursued by Geiger *et al.* (1991). However, it is noted that OH contents determined at the margins of crystals exhibit a general tendency to increase with increasing pressure and decreasing temperature of synthesis. This results in a positive, but scattered

correlation of OH content with the fugacity of water in the experiments, calculated from the equation of state and method of fugacity coefficient determination of Saxena and Fei (1987). These calculations were done assuming a pure water fluid phase, which as discussed above, is probably inaccurate. A best fit to the plot of OH contents determined for the pyropes synthesized by Geiger in Germany (using the IR calibration outlined in Chapter 4) versus calculated fugacity of water in the experiments in the case of a pure fluid is shown in Fig. 3. As discussed in Chapter 3, this fit predicts water fugacities in equilibrium with pyrope megacrysts that are of the same order of magnitude as those calculated from co-magmatic olivines from the data of Bai and Kohlstedt (1992). The pyrope calibration may therefore be useful in an order-of-magnitude sense in predicting water fugacities from the OH content. Because of concerns over equilibrium and Si solubility, this relationship is precariously founded and should be used with caution.

1.5 Conclusion

OH-bearing pyrope garnets have been synthesized at pressures of 20 - 30 kbar and T = 1000 °C at Caltech, and by C. Geiger and coworkers in Germany at pressures from 20 - 50 kbar and T = 900 - 1100 °C and have been characterized by single-crystal FTIR spectroscopy. OH appears to be structurally incorporated in the garnet but is sometimes accompanied by liquid water which may reside in inclusions or fractures in the crystals. The structural OH component is often zoned in individual crystals and appears to be related to aspects of garnet growth. Lack of homogenization of OH during the course of the experiments indicates slow kinetics for the incorporation mechanism of this hydrous component. While this behavior is readily understandable for reaction mechanisms involving cation diffusion in garnet, it is different from rates observed for incorporation of H in olivine single crystals (Mackwell and Kohlstedt 1990), and may be different to the

behavior of hydrous components in natural garnets. OH contents of the outer zones of garnet crystals, which probably are most likely to approach the equilibrium OH content, show a broad positive correlation with calculated water fugacity during synthesis.

2. Ion-exchange experiments.

Müller (1988) reported the synthesis of essentially pure H feldspar ($HAlSi_3O_8$) with the sanidine structure (space group C2/m) by ion exchange of Na feldspar (high albite) with boiling H_2SO_4 under reflux conditions. It was found that sanidine was not subject to ion exchange in this manner, and the Na feldspar starting material was prepared by ion exchange (Na = K) of a natural low sanidine from the Eifel volcanic field, Germany in molten NaCl at 800 °C. In order to investigate the applicability of this technique to the synthesis of H-rich examples of other nominally anhydrous minerals, the experimental procedure described by Müller (1988) was duplicated as far as possible and a selection of minerals treated as described in that study. Synthesis of H-rich examples of nominally anhydrous minerals with spectroscopic similarity to natural samples would provide valuable samples for diagnostic structural techniques such as neutron diffraction or nuclear magnetic resonance spectroscopy that would elucidate the crystallographic position and structural role of the OH groups in these minerals. Typical concentrations of H in nominally anhydrous minerals are too low for such studies to be useful in most natural cases. Samples were held in boiling concentrated H_2SO_4 (T ~ 300 °C) in a water-cooled reflux condensor for up to 1 week. This treatment produced alteration of some sample surfaces, which was removed by polishing. None of the samples treated (garnet, olivine and pyroxene), including an omphacitic clinopyroxene with 6.5 wt. % Na_2O showed any change in the IR absorption spectrum of the grain interiors after treatment, and it is concluded that these materials are not susceptible to ion exchange to the extent of the

feldspars. A possible explanation is that in all the minerals treated here the cations play a structural role in linking Si-O chains or tetrahedra, whereas in the feldspars the Al, Si and O atoms form an independent framework not held together by cation polyhedra, and the cations are thus more free to move without disruption of the mineral structure. Müller *et al.* (1988) have also reported Li and H ion exchange of framework silicates with the b-quartz or keatite structures.

3. Heating experiments at atmospheric pressure

3.1 Introduction

A number of experiments designed to investigate the thermal stability of the hydrous component of natural nominally anhydrous minerals were performed. Skogby and Rossman (1989) and Ingrin *et al.* (1989) showed that pyroxenes are susceptible to changing H-content by heating in air, Ar, H_2 and under hydrothermal conditions. Intensities of the OH bands in pyroxene were typically reduced by heating in air or Ar and sometimes increased by heating in H_2, particularly in the case of ferric-iron rich clinopyroxenes. Substantial exchange of H by D in the structural OH groups in pyroxene was also achieved by Skogby and Rossman (1989) on relatively short time scales. The dehydroxylation mechanisms of amphiboles and micas have also been studied by several workers, e.g., Barnes 1930, Addison *et al.* 1962, Vedder and Wilkins 1969, Clowe *et al.*, 1988, Phillips *et al.* 1989. Substantial changes in the OH content of pyroxenes and amphiboles may occur without apparent breakdown of the mineral structure, and homogeneous redox reactions involving Fe^{2+} and Fe^{3+} have been proposed to operate in the gain and loss of H from these minerals. The existence of such redox reactions has potentially important implications for the stability of hydrous components in nominally

anhydrous minerals, because the incorporation or loss of H by such mechanisms may require only electron and proton migration. This is likely to be significantly faster than cation or oxygen diffusion in minerals and may give rise to orders -of-magnitude differences between the kinetics of reactions involving OH and those involving all other chemical components (except ionic valence changes) in minerals.

3.2 Experimental methods

In this study the behavior of OH in the following minerals in response to heating was investigated: pyrope garnet, augite, omphacite, enstatite, forsteritic olivine, zircon and kyanite. Doubly polished mineral plates were characterized by IR spectroscopy before heating. All spectroscopic investigations were done with unpolarized light and mineral samples were not crystallographically oriented, though of course the orientation of the sample with respect to the IR beam axis was constant before and after heating. Samples heated in air were placed in a ceramic crucible and held in a Lindberg bench furnace (P = 1 atm, air atmosphere) at temperatures varying from 200 °C to 1000 °C and times from 1 to about 100 hours. After removal from the furnace, samples were allowed to cool in air and the OH component re-examined by IR spectroscopy. In some of the high-temperature runs where the mineral surface was degraded or altered in some way, this outermost layer was removed by polishing, sometimes after spectroscopic characterization. Samples heated in vacuum were placed in Pyrex tubes on a vacuum extraction line, gently warmed to facilitate adsorbed surface water loss, then sealed in the evacuated tubes and heated in a furnace at 500 °C for 24 hours. Samples heated in Ar were placed in a quartz tube inside a furnace. The cool ends of the tube projecting beyond the furnace were sealed with rubber stoppers and commercial-grade Ar passed over the sample in a continuous stream through holes in the stoppers. All minerals examined were subject to H removal by the heat

treatment; individual mineral responses are described below. A summary of the heat treatments performed and the results obtained are presented in Table 1.

3.3 Results

3.3.1. Garnet.

Garnet megacryst MON-9 (Fig. 4) showed no significant change in OH content after heating in vacuum at 500°C for 24 hours. The same sample, heated in air at 600 °C for 24 hours showed a very slight (~5%) reduction in the intensity of the 3570 cm^{-1} OH band. Heating under the same conditions for a further 73 hours produced a total reduction in intensity of this band of about 50 % compared with the original untreated material. The intensity of the 3512 cm^{-1} band was unaffected by any of the above treatments. A previously untreated sample of MON-9 heated in air at 800 °C for 24 hours lost almost all of the 3570 cm^{-1} component, but retained most, if not all of the 3512 cm^{-1} component. The same result was produced by heating in Ar under these temperature-time conditions. The 3512 cm^{-1} component was removed from the garnet by heating at 1000 °C in air for three hours. Similar results to the above were obtained on the garnet megacryst LAC-40, which has a higher proportion of the 3512 cm^{-1} component in the starting material (Fig. 5). Heating this garnet at 425 °C for 33 hours after the 1000 °C treatment produced no change in the OH spectrum. It was noted that while heating to 800 °C produced little change in the appearance of the garnet, the sample was significantly degraded after the relatively short runs at 1000°C. This treatment produced a strongly iridescent surface layer. Microscopic examination of the surface revealed the pervasive development of small cracks in the sample to tens of microns depth. Surface iridescence appeared to nucleate on, and enhance the development of, surface scratches that presumably originated during polishing. It is

possible that the removal of the thermally more stable 3512 cm^{-1} component from the garnet is conditional on the development of these surface features, but this proposal has not been tested.

3.3.2. Clinopyroxene

An augite megacryst from Kilbourne Hole, KBH-2, and an omphacite HRV-147 from a Roberts Victor eclogite xenolith showed very little change in OH content on heating in vacuum at 500 °C. The augite exhibited a small decrease after 25 hours in air at 600 °C and was reduced to about 50% of the original intensity after a total of 97 hours at this temperature (sample thickness 0.21 mm). Both samples exhibited substantial decrease in OH content on heating at 800 °C for 24 hours, with almost all H being removed from the augite. Heating the augite sample in Ar at 800 °C for 24 hours also removed all OH. These results are in agreement with the observations of Skogby and Rossman (1989) and Ingrin *et al.* (1989).

3.3.3 Enstatite

An aluminous enstatite (KBH-1) from a Kilbourne Hole spinel lherzolite was completely dehydrated after heating at 1000 °C for 24 hours. This is the material used for quantitative calibration of the OH band intensities in orthopyroxene (Chapter 4).

3.3.4. Olivine

IR spectra of olivine sample KLV23.2, heated progressively from 200 °C to 1000 °C are shown in Fig. 7. Olivine shows no change in the spectrum from room temperature to 600

°C. At 800 °C, the bands began to decrease in intensity and after 14 hours the sample suffered considerable oxidation, forming a red zone, perhaps caused by hematite precipitation, which extended some 10 - 20 μm into the olivine. Substantial OH remained in the sample after 14 hours at 800 °C. Heating for one hour at 1000 °C. produced a red zone some 70 -80 μm thick at the olivine surface, and OH intensity was somewhat reduced. Unlike garnet, OH only appeared to be lost from olivine with noticeable destruction of the mineral outer surfaces. It would appear that H loss from olivine proceeds more slowly than for pyroxenes in these experiments.

3.3.4. Zircon

IR spectra of zircon sample ROM188.z2, heated progressively from 200 °C to 800 °C are shown in Figs 8a and 8b. Zircon shows a different behavior from the other minerals in that the OH spectrum responds to heating at lower temperatures. No change in the spectrum is seen after heating at 200 °C, but after one hour at 400 °C, the intensities of the two sharp OH bands in the spectrum (one in each of the two polarization directions) are seen to increase by about a factor of two. This appears to be at the expense of a broader absorption which extends from 3200 to 3500 cm^{-1}. Further heating produces no change in the OH spectrum until 800 °C, when intensities of the OH bands decline substantially. A band at 3200 cm^{-1} which absorbs light vibrating perpendicular to the c axis increases more or less continuously in intensity as temperature is raised. Woodhead *et al* 1991 have argued that this band is not due to OH, but results from lattice vibrational modes reconstituted from the metamict state during thermal annealing. The same explanation can be offered for the behavior of OH, that is, radiation damage results in some destruction of structurally incorporated OH sites to form random OH groups or possibly water molecules. During thermal annealing the structure is restored and OH groups return to their normal

crystallographic sites. The U content of kimberlite zircons is usually low (a few tens of ppm at most) so that although these samples are some 10^8 years old they are relatively undamaged.

3.3.5. Kyanite

The kyanite sample FSM-15 showed very similar response to the omphacite under the same heating conditions (see above), with the original intensity of the OH bands decreasing to about one third after 24 hours in air at 800 °C.

4. Hydrothermal experiments

Two hydrothermal experiments were conducted to investigate the effects of elevated water pressures on the incorporation of OH in garnet. Spectroscopically characterized polished mineral plates were enclosed in crimped, but unsealed $Ag_{25}Pd_{75}$ alloy capsules and run in a rapid quench cold-seal pressure vessel at 800 °C and 600 bars using water as a pressure medium. In these runs the fugacities of fluid species were not controlled, but the fugacity of oxygen is believed to be buffered by the Ni-alloy bomb and its oxidation products so as to lie close to fO_2 defined by the Ni-NiO buffer. For a fluid phase consisting of pure water this defines the fugacities of all fluid components. One 2 hour double-capsule buffered run was attempted with an Fe-FeO buffer enclosed in an outer gold capsule surrounding an inner $Ag_{25}Pd_{75}$ capsule containing the samples, but the starting materials were destroyed (crushed) during the run and could not be examined spectroscopically.

Three different natural pyrope garnet starting materials were used in these experiments. These were garnet MON-9 that was previously untreated and showed the characteristic

two-band spectrum, garnet LAC-40 which had been dehydrated by heating in air at 800 °C for 24 hours followed by 3 hours at 1000°C, and sample KM-1493, a naturally OH-free garnet megacryst. Spectra of these materials before and after hydrothermal treatment are illustrated in Figs 4-6. Compositions of these garnets are given in Chapter 1 and are quite similar. After 48 - 60 hours of hydrothermal treatment the OH contents of both of the previously untreated samples were unchanged, that is the OH-free garnet remained OH-free and the OH-bearing sample MON-9 retained its original complement of OH with the same spectral characteristics. A thin coating of fine crystals including at least one hydrous mineral grew on the surface of the garnets (Figs 5e and 6b), but removal of some 25 μm of material from each surface of the plate revealed the garnet beneath this to be unchanged (Figs 4f and 6c). In contrast to the above, the dehydrated sample LAC-40 showed the growth of an OH band at 3570 cm^{-1}, clearly distinguishable from the surface hydrous minerals, after 48 hours hydrothermal treatment (Fig. 5e and f). The hydrothermally treated plate was 0.47 mm thick and a traverse of eight 35 μm diameter sized spots across the width of the plate revealed that the concentration was essentially constant from one flat surface of the plate to the other. Thus 48 hours at 800 °C was sufficient time to homogenize the garnet with respect to OH content. It is noteworthy that although the original LAC-40 sample prior to dehydration in air contained prominent OH bands at both 3570 and 3512 cm^{-1}, only the 3570 cm^{-1} band was restored during the hydrothermal treatment (Fig 5f). Furthermore, the intensity of this band after hydrothermal treatment was somewhat greater (by about a factor of three) than in the original starting material.

5. Discussion and a model for OH incorporation in natural pyrope garnet.

The ready removal and hydrothermal replacement of the H characterized by O-H stretching vibration at 3570 cm^{-1}, together with the observation made in the previous chapter that H

appears to be liberated from garnet (and pyroxenes) as H_2 suggests that a redox reaction such as the following may be responsible for loss of this component of H:

$$2Fe^{2+} + 2OH^- = 2Fe^{3+} + 2O^{2-} + H_2.$$

It is a persistent problem in the study of the hydrous component in minerals such as pyralspite garnets that the concentrations of H are too low for structural or crystal-chemical arguments to be particularly useful in placing constraints on the chemical association of the H with other components of the garnet. For example, predictions may be (and commonly are) made about the distribution of various cations over the three sites in garnet, but these cannot be expected to be definitive or exclusive at the tens of ppm levels. These concentrations are within the realm of equilibrium defect concentrations and it could be expected that most of the common cations may be present at these concentrations in any of the sites. In principle, the change in oxidation state of Fe is measurable spectroscopically, but the changes expected due to H-loss by reaction (2) above (less than 1% relative) would not be detectable under normal operating conditions. If removal of H from the garnet is accompanied by oxidation of Fe^{2+}, then the ease with which the 3570 cm^{-1} band OH is removed suggests that this may be accompanied by formation of Fe^{3+} in the octahedral site, where it is most readily accommodated:

$$[Fe^{2+}O_5OH]^{VI} = [Fe^{3+}O_6]^{VI} + {}^1/_2H_2.$$

The presence of octahedral Fe^{2+}, available for oxidation in concentrations at the level of a few hundred ppm seems quite plausible in these garnets and has been documented elsewhere (Amthauer *et al.* 1977). The proposed mechanism may be testable by investigating the kinetics of dehydrogenation as a function of the concentration of

octahedral Fe^{2+}, for example in hydrous titanian andradites. Although this mechanism does not necessarily imply any structural connection between octahedral Fe^{2+} and OH in the garnet, this would facilitate the process. The $[Fe^{2+}]VI$ - OH association can also be rationalized on crystal chemical grounds in that the charge deficiency created by the substitution of Fe^{2+} for Al^{3+} is compensated locally by an interstitially situated H.

The greater thermal stability of the OH band at 3512 cm^{-1} implies a different dehydrogenation mechanism for this component. In chapter 3 the correlation of this band with Ti substitution in garnet was demonstrated. The substitution of the highly charged Ti^{4+} cation into the garnet structure requires compensating charge balance (Ti^{4+} in the tetrahedral site in garnet is not favored because of size constraints and is preceded by Al^{3+} and Fe^{3+} in priority for this site - Huggins *et al* . 1977). This may involve $[M^{2+}]^{VI}$ substitutions (Huckenholz 1969), $[Na^{+}]^{VIII}$ substitution (Reid *et al.* 1976) or Fe-Ti charge transfer (Huggins *et al.* 1977, Platonov *et al.* 1991). If the OH is directly coupled to Ti in some form of charge compensating substitution, or in a position that facilitates electron transfer between Fe and Ti, then its removal from the local environment may be expected to encounter some resistance because of charge balance requirements. In fact the high temperatures required for its removal may result from a demand for some degree of cation rearrangement and possibly disruption of the garnet structure. An example of a possible reaction is:

$$[Ti^{4+}O_5OH]^{VI} + [Fe^{2+}]^{VIII} + [Mg^{2+}]^{VI} = [Ti^{4+}O_6]^{VI} + [Fe^{3+}]^{VI} + [Mg^{2+}]^{VIII} + {}^1/_2H_2.$$

The vibrational frequencies of the two bands are qualitatively in agreement with the above model in that the more highly charged cation would tend to draw electron density from the

O-H bond causing a decrease in vibration frequency and displacement of the OH band position in the IR spectrum to lower wavenumber. This effect is known to occur in amphiboles, with Ti^{4+} substitution producing a substantial shift in absorption frequency (~ 80 cm^{-1}) (Hawthorne 1981).

Implications for interpretation of OH in natural samples.

That the OH content of garnet is apparently unresponsive to hydrothermal treatment in the absence of previous heating for both naturally low-OH (KM-1493) and high-OH (MON-9) starting materials suggests that the capacity of these minerals to incorporate OH may be set by their original growth conditions, that is, the ability to incorporate substantial H may require original crystal growth in a hydrous environment. This type of behavior has been recorded for OH in olivine by Bai & Kohlstedt (1992a,b), who demonstrate that substantially greater OH concentrations are introduced under a given set of conditions into olivines previously annealed under "wet " conditions compared with those previously annealed "dry." The implications of this observation for the interpretation of the OH contents of natural mantle-derived mineral samples such as those erupted in volatile rich environments like kimberlites is that it may not be possible to elevate the OH content of a mineral such as garnet or olivine above that which it originally contained in the mantle. In such a view, the concentrations recorded in these minerals would be minimum values, given the possibility that some dehydration may have occurred. It is possible, however, that dehydration requires high external oxygen fugacities which can overcome the intrinsic buffering capacity of the mineral, which may itself be quite substantial in the case of garnets with high concentrations of both Fe^{2+} and Fe^{3+} compared to OH. Changes in external fH_2 may be insufficient to disturb the intra-mineral redox state, a change which is required for H incorporation or loss by this mechanism. Thus, despite indications that H

can move rapidly through garnet to form OH groups or be driven off as H_2, it is not obvious that the OH content of this mineral will readjust rapidly to changes in external fO_2 and fH_2. If such readjustment does occur, it would appear to be limited by the pre-existing crystal chemistry. The general absence of zoning in OH content of large mineral samples from kimberlites argues either for lack of disturbance or for rapid homogenization, while the preservation of the systematics described and discussed in chapters 1 and 3 appears to favor the former option.

Conclusions and summary

Synthetic pyropes containing what appears to be structurally bound OH have been synthesized at temperatures up to 1100 °C (Geiger *et al.* 1991) suggesting that this particular form of OH is stable to high temperatures. The OH component of natural pyropes, which may be chemically different to that in the pure synthetic mineral, is "stable" at 800 °C at 600 bars P_{H_2O} with respect to the rest of the garnet structure (the whole garnet is metastable under these conditions, but it has been demonstrated that reactions involving the hydrous component under these conditions are not kinetically inhibited.) Hydrothermal experiments on olivine (Mackwell and Kohlstedt 1990, Bai and Kohlstedt 1992a,b) demonstrate stability of OH in this mineral to 1300 °C under hydrothermal conditions. All nominally anhydrous minerals investigated here lose a proportion of their OH component on heating in air or argon at temperatures of 600 °C and above. This dehydration may be complete given sufficient time at this temperature and is accomplished in less than 3 hours at 1000°C for samples of several hundred micrometers thickness. It is proposed that much of the H is lost from garnet by redox reactions involving oxidation of Fe^{2+}, as previously concluded by others for pyroxenes, amphiboles and micas. These results suggest that, given appropriate conditions of f_{O2} and f_{H_2O}, OH in many nominally

anhydrous minerals is stable to temperatures encountered in the upper mantle and probably above the maximum thermal stability of many hydrous minerals. Although H is mobile in these minerals compared with other chemical species, and can be quite easily exchanged with D in pyroxenes, for example, changing the absolute OH content may require specific external conditions. As a rule, increasing the OH content above that set during crystallization appears to require structural rearrangement of the mineral. Use of the OH content of natural nominally anhydrous mineral samples to infer geological conditions appears feasible, but requires a deeper understanding of the reaction mechanisms and kinetics of the hydrous component of these minerals to be conclusive.

References

Ackermann, L., Cemic, L. and Langer, K. 1983 Hydrogarnet substitution in pyrope: A possible location for "water" in the mantle. *Earth planet .Sci .Lett.* **62**, 208-214

Addison, C. C., Addison, W. E., Neal, G. H. and Sharp, J. H. 1962 Amphiboles: Part 1. The oxidation of crocidolite. *J. Chem. Soc.* **1962**, 1468-1471.

Aines, R. D. and Rossman, G. R. 1984a The hydrous component in garnets: Pyralspites. *Amer. Mineral.* **69**, 1116-1126

Amthauer, G., Annersten, H. and Hafner, S. S. 1977. The Mössbauer spectrum of ^{57}Fe in titanium-bearing andradites. *Phys. Chem. Minerals.* **1**, 399-413.

Bai, Q. and Kohlstedt, D. L. 1992a Substantial hydrogen solubility in olivine and implications for water storage in the mantle. *Nature* **357**, 672-674.

Bai, Q. and Kohlstedt, D. L. 1992b Effects of chemical environment on the solubility and incorporation mechanism for hydrogen in olivine. submitted to *Phys. Chem. Minerals.*.

Barnes, V. E. 1930 Changes in hornblende at about 800°C. *Amer. Mineral.* **15**, 393-

Basso, R. and Cabella, R. 1990 Crystal chemical study of garnets from metarodingites in the Voltri Group metaophiolits (Ligurian Alps, Italy) *Neues Jahrb. Mineral. Mh.* **1990**, 127-136.

Basso, R., Della Giusta, A. and Zefiro, L. 1981 A crystal chemical study of a Ti-containing hydrogarnet. *Neues Jahrb. Mineral. Mh.* **1981**, 230-236.

Basso, R., Della Giusta, A. and Zefiro, L. 1983 Crystal structure refinement of plazolite, a highly hydrated natural grossular. *Neues Jahrb. Mineral. Mh.* **1983**, 251-258.

Basso, R., Cimino, F. and Messiga, B. 1984a Crystal chemistry of hydrogarnets from three different microstructural sites of a basaltic metarodingite from the Voltri Group (Western Liguria, Italy.) *Neues Jahrb. Mineral. Abh.* **148**, 246-258.

Basso, R., Cimino, F. and Messiga, B. 1984b Crystal chemical and petrological study of hydrogarnets from a Fe-gabbro metarodingite (Gruppo di Voltri, Western LIguria, Italy). *Neues Jahrb. Mineral. Abh.* **150**, 247-258.

Begley, A. B. and Sclar, C. B. 1984 Experimental evidence for the existence of hydropyrope. *Eos* **65**, 1091.

Birkett, T. C.and Trzcienski, W. E., Jr. (1984) Hydrogarnet: multi-site hydrogen occupancy in the garnet structure. *Canad. Mineral.* **22**, 675-680

Burnham, C. W., Holloway J. R.and Davis, N. F. 1969. Thermodynamic properties of water to 1000°C and 10,000 bars. *Geol. Soc. Amer. spec. Paper* **132**, 96pp.

Carlson, E. T. 1956 Hydrogarnet formation in the system lime-alumina-silica-water. *J. Res. Natl. Bur. Stds.* **56**, 327-335.

Cho, H. and Rossman, G. R. Single crystal NMR studies of low-concentration hydrous species in grossular. Ms to be submitted to *Amer. Mineral.*

Clowe, A. C., Popp, R. C. and Fritz, S. J. 1988 Experimental investigation of the effect of oxygen fugacity on ferric-ferrous ratios and unit cell parameters of four natural clinoamphiboles. *Amer. Mineral.* **73** : 487-499.

Flint, E. P. McMurdie, H. F. and Wells, L. S. 1941 Hydrothermal and X-ray studies of the garnet-hydrogarnet series and the relationship of the series to the hydration products of Portland cement. *J. Res. Natl. Bur. Stds.*, **26**, 13-33.

Foreman, D. W. 1968 Neutron and X-ray diffraction study of $Ca_3Al_2(O_4D_4)_3$, a garnetoid. *J. Chem. Phys.* **48**, 3037-3041.

Geiger, C. A., Langer, K., Bell, D. R., Rossman, G. R. and Winkler, B. 1991. The hydroxide component in synthetic pyrope. *Amer. Mineral.* **76**, 49-59.

Gustafson, W. J. 1974 The stability of andradite, hedenbergite and related minerals in the system Ca-Fe-Si-O-H. *J. Petrol.* **15**, 455-496.

Hawthorne 1981 Amphibole spectroscopy. In. D. R. Veblen (ed) *Amphiboles and other hydrous pyriboles - mineralogy. Mineralogical Society of America Reviews in Mineralogy* **9A**, 103-139.

Hsu, L. C. 1968 Selected phase relationships in the system Al-Mn-Fe-Si-O-H: A model for garnet equilibria. *J. Petrol.* **9**, 40-83.

Hsu, L. C. 1980 Hydration and phase relations of grossular-spessartine garnets at P_{H_2O} = 2 kbar. *Contrib. Mineral. Petrol.* **71**, 407-415.

Huckenholz, H. G. 1969 Synthesis and stability of Ti-andradite *Amer. J. Sci.* **267A**, 209-232.

Huckenholz, H. G. and Fehr, K. T. 1982 Stability relationships of grossular + quartz + wollastonite + anorthite. II. The effect of grandite - hydrograndite solid solution. *Neues Jahrb. Mineral. Abh.* **145**, 1-33.

Huckenholz, H. G., Hölzl, E. and Linhuber, W. 1975 Grossularite, its solidus and liquidus relations in the CaO-Al_2O_3-SiO_2-H_2O.system up to 10 kbar. *Neues Jahrb. Mineral. Abh.* **124**, 1-46.

Huggins, F. E., Virgo, D. and Huckenholz, H. G. 1977. Titanium-containing silicate garnets, I. The distribution of Al, Fe^{3+} and Ti^{4+} between octahedral and tetrahedral sites. *Amer . Mineral.* **62**, 475-490.

Ingrin, J., Latrous, K., Doukhan, J. C. and Doukhan, N. 1989. Water in diopside : an electron microscopy and infrared spectroscopy study. *Eur.J. Mineral.* **1**: 327 - 341.

Ito, J. and Frondel, C. 1967 New synthetic hydrogarnets. *Amer. Mineral.* **52**, 1105-1109.

Kennedy, G. C., Wasserburg, G. J., Heard, H. C. and Newton, R. C. 1962 The upper triple phase region in the system SiO_2-H_2O. *Amer. J. Sci.* **260**, 501-521.

Kobayashi, S. and Shoji, T. 1987 Infrared spectra and cell dimensions of hydrothermally synthesized grandite-hydrograndite series. *Mineral. J.* **13**, 490-499.

Kühberger, A., Fehr, T., Huckenholz, H. G. and Amthauer, G. 1989. Crystal chemistry of a natural schorlomite and Ti-andradites synthesized at different oxygen fugacities. *Phys. Chem. Minerals.* **16**, 734-740.

Lager, G., Armbruster, T., Rotella, F. J. and Rossman, G. R. 1989 OH substitution in garnets : X-ray and neutron-diffraction, infrared, and geometric-modeling studies. *Amer. Mineral.* **74**, 840- 851

Mackwell, S. J. and Kohlstedt, D. L. 1990 Diffusion of hydrogen in olivine: implications for water in the mantle. *J. geophys. Res.* **95**, 5079-5088

Matthes, S. 1961 Ergebnisse zur Granatsynthese und ihre Beziehungen zur natürlichen Granatbildung innerhalb der Pyralspit-Gruppe. *Geochim. Cosmochim. Acta* **23**, 233-294.

Müller, G. 1988 Preparation of hydrogen and lithium feldspars by ion exchange. *Nature*, **332**, 435-436.

Müller, G. Hoffman, M and Neeff, R. 1988 Hydrogen substitution in lithium-aluminosilicates. *J. Mater. Sci.* 1779-1785.

Pabst, A. 1937 The crystal structure of plazolite. *Amer. Mineral.* **22**, 861-868.

Passaglia, E. and Rinaldi, R. 1984 Katoite, a new member of the $Ca_3Al_2(SiO_4)_3$ - $Ca_3Al_2(OH)_{12}$ series and a new nomenclature for the hydrogrossular group of minerals. *Bull. MIneral.* **107**, 605-618.

Phillips, M. W., Popp, R. K. and Clowe, C. A. 1988 Structural adjustments accompanying oxidation-dehydrogenation in amphiboles. *Amer. Mineral.* **73** : 500-506.

Phillips, M. W., Draheim, J. E., Popp, R. K., Clowe, C. A.and Pinkerton, A. A. 1989. *Amer. Mineral.* **74**, 764.

Pistorius, C. W. F. T. and Kennedy, G. C. 1960 Stability relations of grossularite and hydrogrossularite at high temperatures and pressures. *Amer. J. Sci.* **258**, 247-257.

Platonov, A. N., Langer, K., Matsuk, S. S., Taran, M. N. and Hu, X. 1991 Fe^{2+}-Ti^{4+} charge-transfer in garnets from mantle eclogites. *Eur. J. Mineral.* **3**, 19-26.

Reid, A. M., Brown, R. W., Dawson, J. B. Whitfield, G. G. and Siebert, J. C. 1976. Garnet and pyroxene compositions in some diamondiferous eclogites. *Contrib. Mineral. Petrol.* **58**, 203-220.

Rossman G. R. and Aines, R.D. 1991 The hydrous components in garnets : grossular-hydrogrossular. *Amer Mineral* **76**, 1153-1164

Roy, D. M. and Roy, R. 1957 System CaO-Al_2O_3-SiO_2-H_2O. VI. The grossularite - $3CaO.Al_2O_3.6H_2O$ join. *Bull. Geol. Soc. Amer.* **68**, 1788.

Sacerdoti, M. and Passaglia, E. 1985 The crystal structure of katoite and implications within the hydrogrossular group of minerals. *Bull. Mineral.* **108**, 1-8.

Schiffman, P. and Liou, J. G. 1980 Synthesis and stability relations of Mg-Al pumpellyite, $Ca_4Al_5MgSi_6O_{21}(OH)_7$. *J. Petrol* **21**, 441-474.

Saxena, S. K. and Fei, Y. 1987. High pressure and high temperature fluid fugacities. *Geochim. Cosmochim. Acta.* **51**, 783-791.

Schreyer, W. and Seifert, F. 1969 High pressure phases in the system $MgO-Al_2O_3-SiO_2-H_2O$. *Amer. J. Sci.* **267A**, 407-443.

Shoji, T. 1974 $Ca_3Al_2(SiO_4)_3$ - $Ca_3Al_2(O_4H_4)_3$ series garnet: composition and stability. *J. Mineral. Soc. Japan* **11**, 359-372.

Shoji, T. 1975 Phase relations in the system $CaO-Fe_2O_3-SiO_2-H_2O$. *J. Mineral. Soc. Japan* **12**, 143-156.

Skogby, H. S. and Rossman, G. R. 1989 OH- in pyroxene : An experimental study of incorporation mechanisms and stability. *Amer. Mineral.* **74** : 1059-1069.

Vedder, W. and Wilkins, R. W. T. 1969 Dehydroxylation and rehydroxylation, oxidation and reduction of micas. *Amer. Mineral.* **54** : 482-509.

Woodhead, J. A., Rossman, G. R. and Thomas, A. P. 1991 Hydrous species in zircon. *Amer. Mineral.* **76**, 1533-1546.

Yoder, H. S., Jr. 1950 Stability relations of grossularite. *J. Geol.* **58**, 221-253.

Fig. 1. Single crystal infrared spectra of OH-bearing pyrope (run no. DB-30) synthesized from gel of composition $Mg_3Al_2Si_3O_{12}$ at 25 kbars and 1000°C for 100 hours in the presence of excess water. (a) Spectrum showing two bands; a sharp band that is assigned to structurally-bound OH at 3630 cm_{-1} and a broader band at 3420 cm^{-1} assigned to liquid water in cracks or inclusions within the garnet. (b) The same spectrum but with the spectrum of liquid water, obtained from a film of water held between two glass plates, subtracted. The sharp band at 3630 cm^{-1} is assigned to structural OH in the garnet and the absorptions below 3300 cm^{-1} are due to hydrocarbon and other contamination on the sample surface. Spectra normalized to 1 mm thickness..

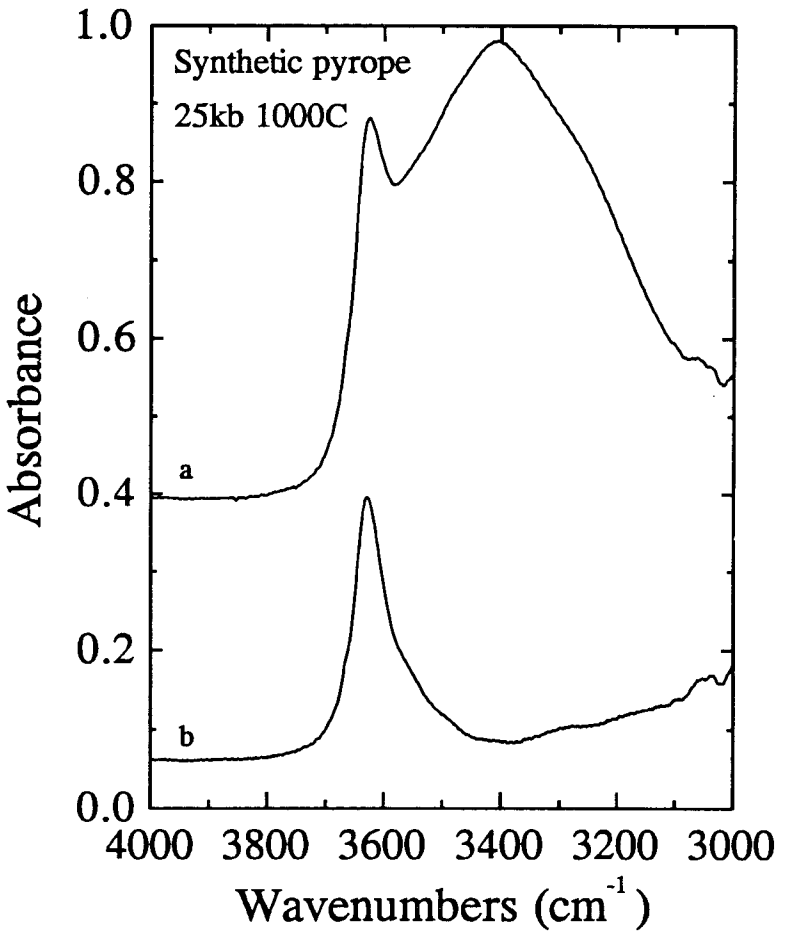
Synthetic pyrope
25kb 1000C
a
b
Absorbance
1.0
0.8
0.6
0.4
0.2
0.0
4000
3800
3600
3400
3200
3000
Wavenumbers (cm-1)

Fig. 1

Fig. 2. Variation in intensity of the band at 3630 cm^{-1}, assigned to vibration of structurally-bound OH groups, as a function of position in the synthetic pyrope P-29, grown from oxide starting materials by C. A. Geiger. Plotted points are result of three core to rim traverses on a single polished plate of one crystal using a 100 μm diameter aperture. Solid cicles represent traverses within inclusion-rich (turbid) sectors of the crystal and open circles are for a traverse in an inclusion-poor (clear) sector. These sectors are illustrated in Fig. 1 of Geiger *et al.* 1991 (Appendix 1.). The inclusion-rich core of the crystal is assigned a value of 0 μm on the abscissa and the position of the edge of the grain for each traverses is shown by the arrows. Sample thickness 535 μm, but absorption intensities are normalized to a thickness of 1 mm.

Fig. 2

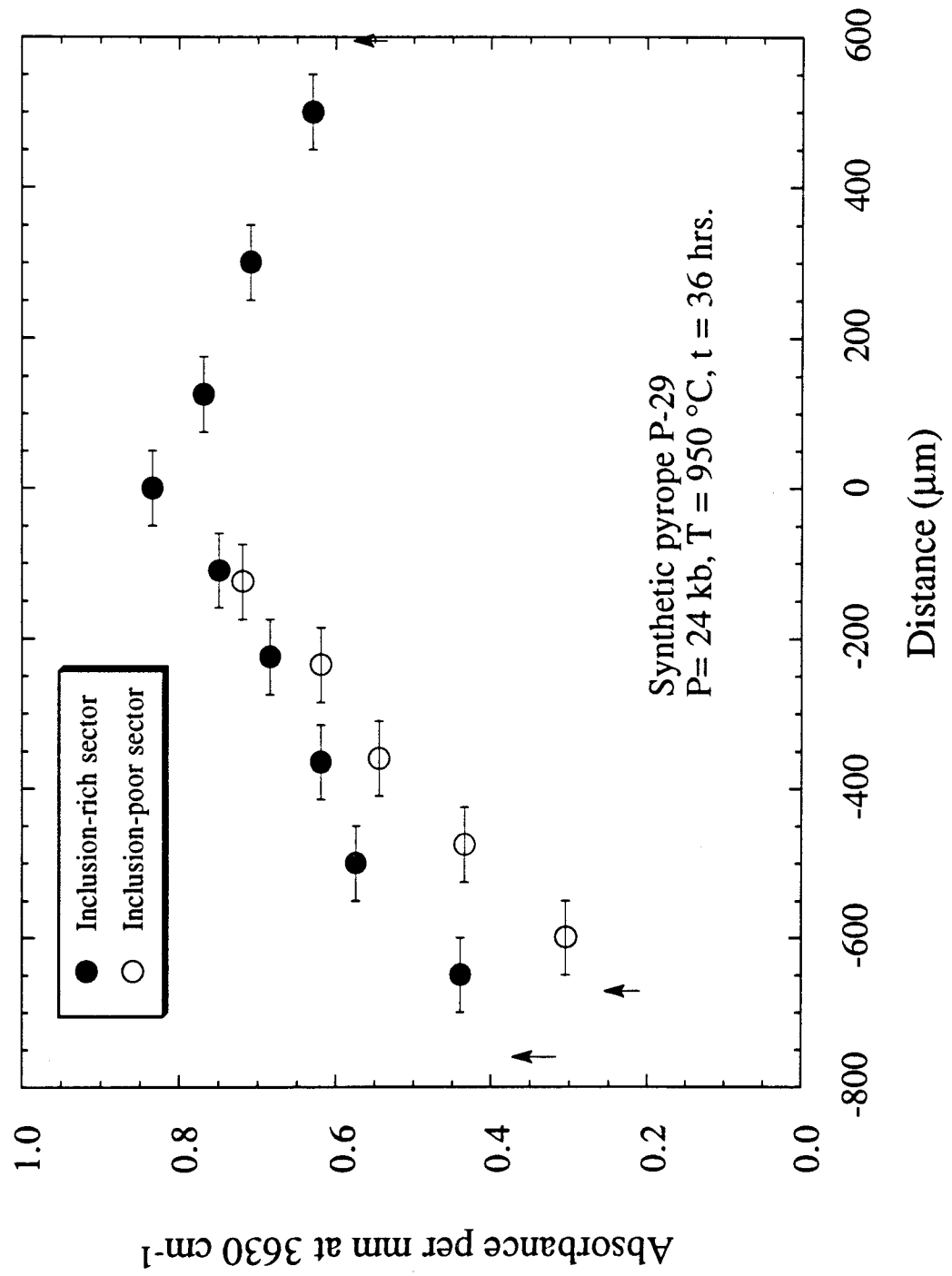
Absorbance per mm at 3630 cm-1
1.0
0.8
0.6
0.4
0.2
0.0
-800
-600
-400
-200
0
200
400
600
Distance (μm)
Inclusion-rich sector
Inclusion-poor sector
Synthetic pyrope P-29
P= 24 kb, T = 950 °C, t = 36 hrs.

Fig. 3. OH content (expressed as ppm H2O) of synthetic pyropes grown by Geiger and co-workers as a function of the calculated fugacity of water during synthesis, assuming the fluid to be composed of pure water. The OH contents are derived from measurements of the linear absorbance per mm of the band at 3630 cm^{-1}, from which integrated absorbances are calculated assuming a constant relationship of linear absorbance to integrated absorbance for this band, measured on one sample. The calibration for pyrope garnet presented in Chapter 4 was used to determine OH concentration from the integrated absorbances. Water fugacities were calculated from the equation of state of Saxena and Fei (1987), using fugacity coefficients calculated from the 5 kbar data of Burnham *et al.* (1969), as set out in Saxena and Fei (1987).

Fig. 3

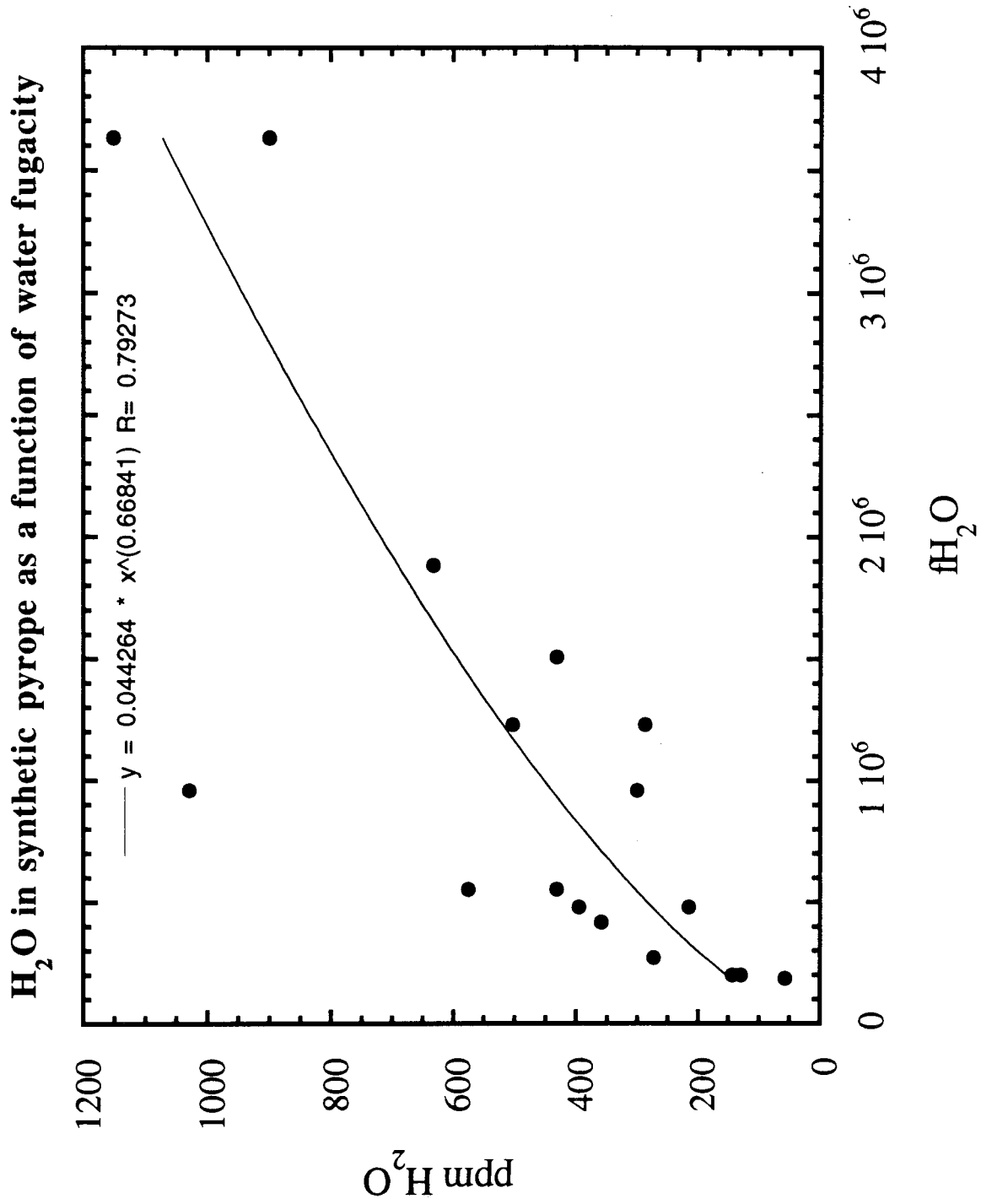
H2O in synthetic pyrope as a function of water fugacity
y = 0.044264 * x^(0.66841) R= 0.79273
ppm H2O
0
200
400
600
800
1000
1200
0
1 10^6
2 10^6
3 10^6
4 10^6
fH2O

Fig. 4. Unpolarized single-crystal IR spectra of OH in natural pyrope MON-9 before and after heating and hydrothermal treatment. Heat treatments for samples of same thickness are cumulative, i.e., the same sample is progressively subjected to higher temperatures. All spectra normalized to 1 mm thickness.

(a) Untreated sample 0.268 mm.

(b) After heating at 500 °C in vacuum (~10^{-3} torr) for 24 hrs. 0.268 mm.

(c) After heating at 600 °C in air for 24 hrs. 0.318 mm.

(d) After heating at 600 °C in air for a further 73 hrs. (97 hrs. total) 0.318 mm.

(e) After heating at 800 °C in air for 24 hrs. 0.268 mm

(f) After hydrothermal treatment at 800 °C and 600 bars P_{H2O} at fO2 ~NNO for 60 hrs. No pre-treatment. 0.358 mm.

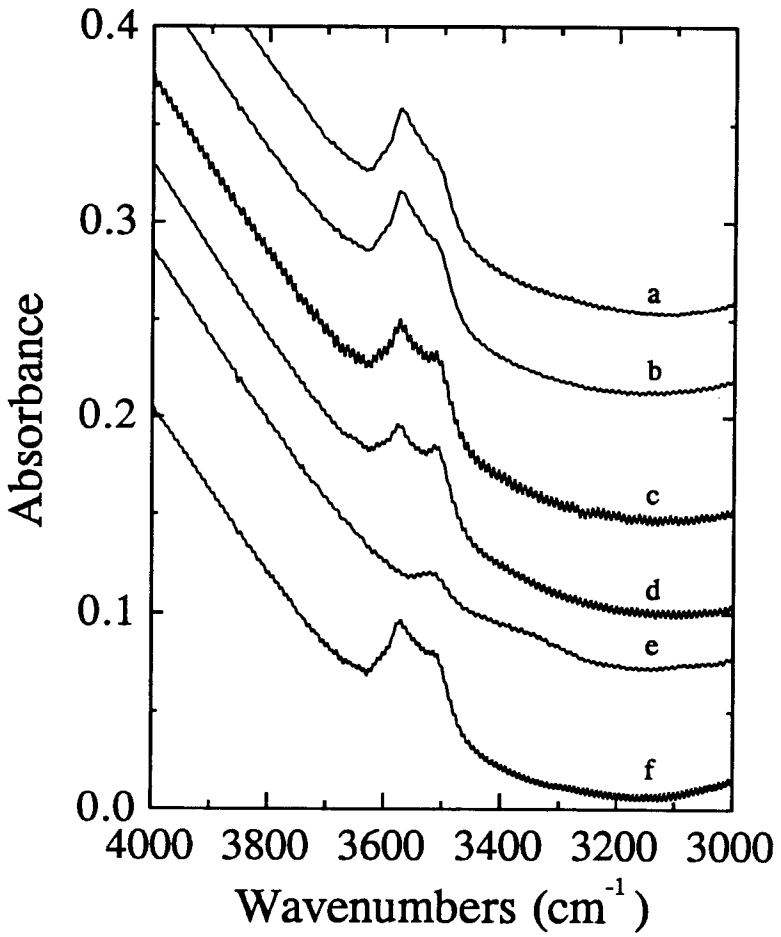
0.4
0.3
0.2
0.1
0.0
Absorbance
a
b
c
d
e
f
4000 3800 3600 3400 3200 3000
Wavenumbers (cm-1)

Fig. 4

Fig. 5. Unpolarized single-crystal IR spectra of OH in natural pyrope LAC-40 before and after heating and hydrothermal treatment. A single fragment 0.471 mm thick was subjected to treatment in the order that the spectra are presented, i.e., (a) through (f). Spectrum (f) was measured on the sample after polishing to a thickness of 0.370 mm to remove the coat of hydrous minerals evident from spectrum (e). All spectra normalized to 1 mm thickness, except for (e) which is plotted at 0.5 mm thickness for convenience. Spectra have been arbitrarily shifted on the vertical scale for ease of plotting.

(a) Untreated

(b) 800 °C in air, 24 hrs.

(c) 1000 °C in air, 3 hrs.

(d) 425 °C in air, 33 hrs.

(e) 800 °C, 600 bars P_{H2O} at f_{O2} ~Ni-NiO for 48 hrs. Surface coat retained

(f) 800 °C, 600 bars P_{H2O} at f_{O2} ~Ni-NiO for 48 hrs. Surface coat removed. Spectrum taken with beam path parallel to original surface, in the centre of the grain. This represents the volume of sample furthest from the grain surface exposed to hydrothermal treatment.

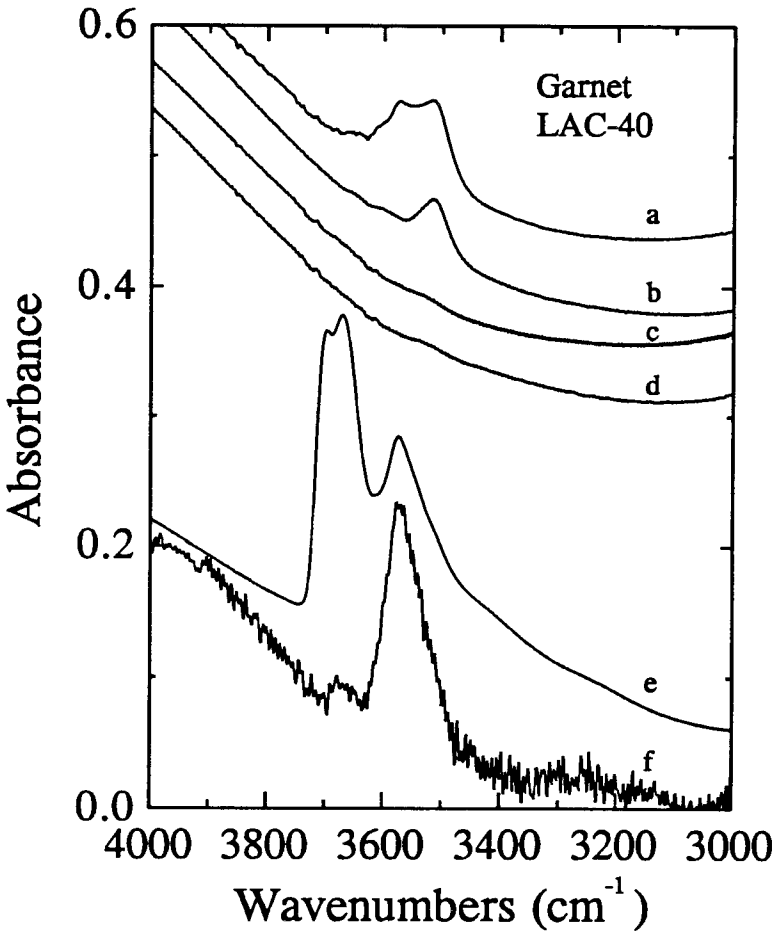
Garnet
LAC-40
a
b
c
d
e
f
Absorbance
0.6
0.4
0.2
0.0
4000
3800
3600
3400
3200
3000
Wavenumbers (cm-1)

Fig. 5

Fig. 6. Unpolarized single-crystal IR spectra of OH in natural pyrope KM-1493 before and after heating and hydrothermal treatment. All spectra normalized to 1 mm thickness.

(a) Untreated. 0.350 mm.

(b) 800 °C, 600 bars P_{H2O} at f_{O2} ~Ni-NiO for 48 hrs. No pre-treatment, surface coat retained. 0.350 mm.

(c) 800 °C, 600 bars P_{H2O} at f_{O2} ~Ni-NiO for 48 hrs. No pre-treatment, surface coat removed by polishing. Beam path same direction as (b). 0.324 mm thick.

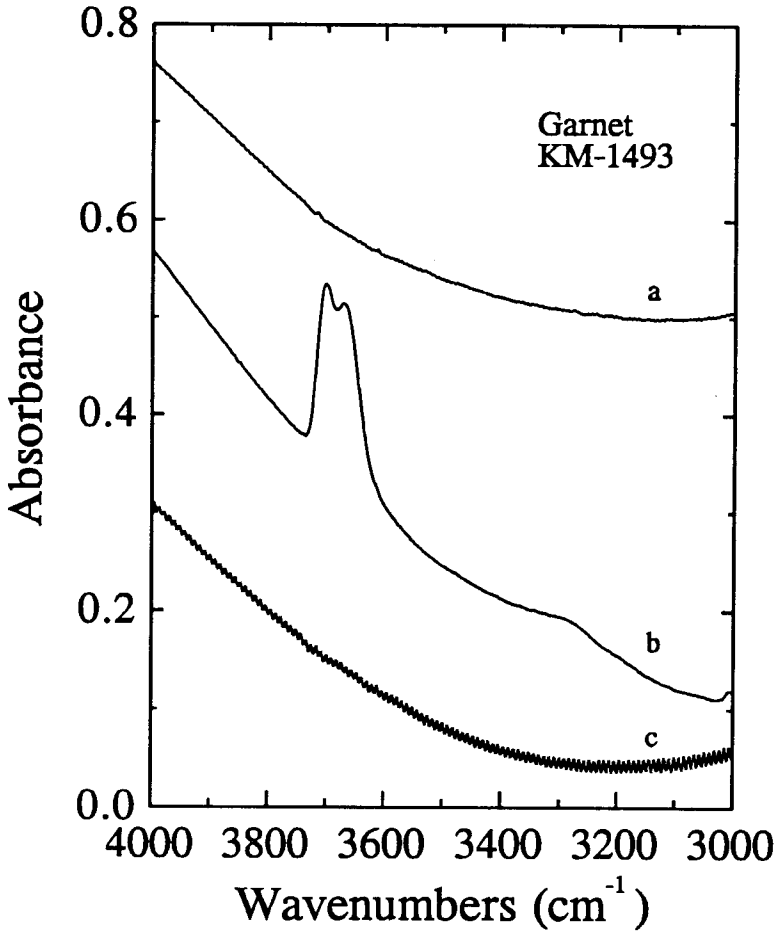
Garnet
KM-1493
a
b
c
Absorbance
0.0
0.2
0.4
0.6
0.8
4000
3800
3600
3400
3200
3000
Wavenumbers (cm-1)

Fig. 6

Fig. 7. IR spectra of olivine sample KLV-23.2 polarized parallel to γ ([100]). Spectra represent progressive (cumulative) treatment of a single fragment, originally 0.381 mm thick. Spectra (a) through (e) are normalized to 1 mm thickness. Heating at 800 °C and above produces surface oxidation which was removed by polishing before collection of spectra (f) and (g). These two spectra are not normalized to 1mm thickness, but are plotted as 0.864 mm and 0.535 mm respectively, the equivalent thicknesses represented by the material remaining after polishing. Normalization of these spectra to 1mm would overestimate the total amount of OH remaining in the sample because too much weight would be given to OH concentrations at the core of the grain (material containing very little or no OH has been removed by polishing).

(a) Untreated 0.381 mm.

(b) 200 °C, air, 1hr. 0.381 mm

(c) 400 °C, air, 1 hr. 0.381 mm.

(d) 600 °C, air, 1.5 hr. 0.381 mm

(e) 800 °C, air, 2 hr. 0.381 mm (surface tarnish not removed).

(f) 800 °C, air, further 12 hr. 0.329 mm.

(g) 1000 °C, air, 1 hr. 0.204 mm.

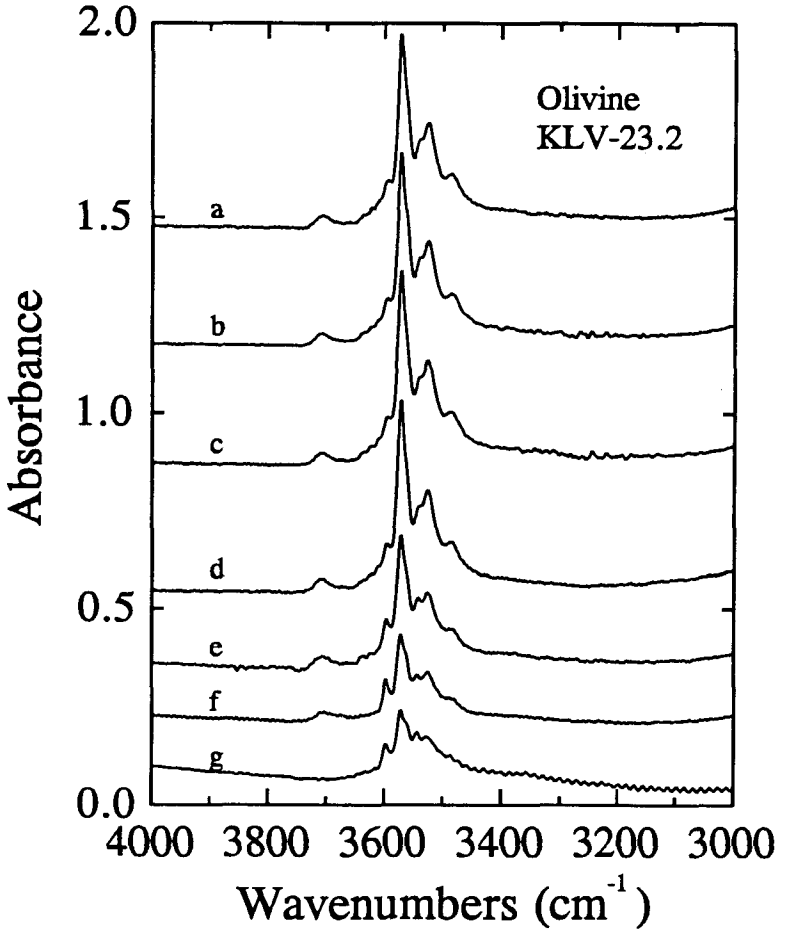
Olivine
KLV-23.2
a
b
c
d
e
f
g
Absorbance
2.0
1.5
1.0
0.5
0.0
4000
3800
3600
3400
3200
3000
Wavenumbers (cm-1)

Fig. 7

Fig. 8a. IR spectra of zircon sample ROM188.z1 polarized parallel to c ([001]). Spectra represent progressive (cumulative) treatment of a single fragment, 0.410 mm thick. Spectra are normalized to 1 mm thickness.

(a) Untreated

(b) 200 °C, air, 2 hrs.

(c) 400 °C, air, 1 hr.

(d) 500 °C, air, 9 hrs.

(e) 650 °C, air, 1 hr.

(f) 800 °C, air, 3 hrs.

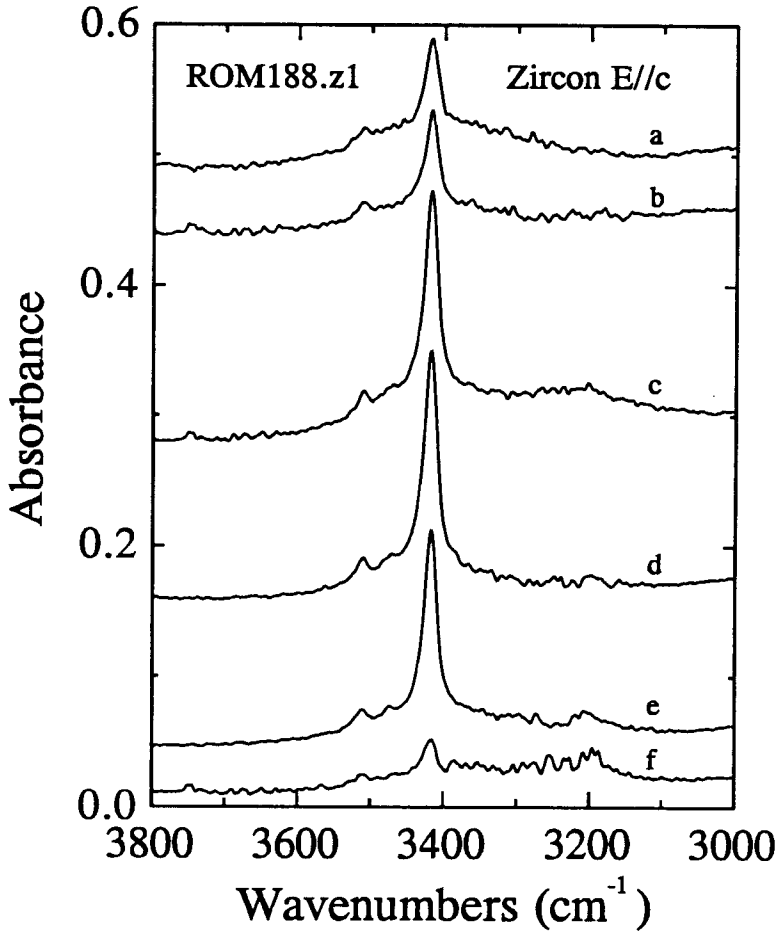
ROM188.z1
Zircon E//c
a
b
c
d
e
f
Absorbance
0.6
0.4
0.2
0.0
3800
3600
3400
3200
3000
Wavenumbers (cm-1)

Fig. 8a

Fig. 8b. IR spectra of zircon sample ROM188.z1 polarized perpendicular to c. Spectra represent progressive (cumulative) treatment of a single fragment, 0.410 mm thick. Spectra are normalized to 1 mm thickness.

(a) Untreated

(b) 200 °C, air, 2 hrs.

(c) 400 °C, air, 1 hr.

(d) 500 °C, air, 9 hrs.

(e) 650 °C, air, 1 hr.

(f) 800 °C, air, 3 hrs.

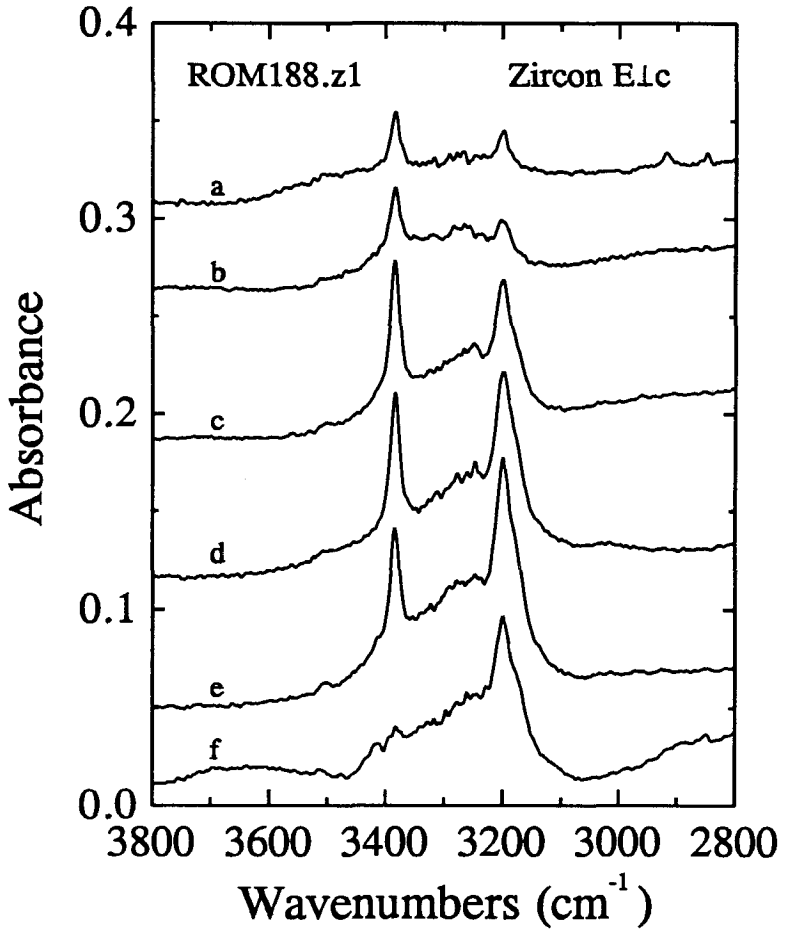
ROM188.z1
Zircon E⊥c
a
b
c
d
e
f
Absorbance
0.0
0.1
0.2
0.3
0.4
3800
3600
3400
3200
3000
2800
Wavenumbers (cm-1)

Fig. 8b

Chapter 6. Summary discussion

Introduction

The aims of this study, as set out in the introduction, were "to investigate the role of OH-bearing, nominally anhydrous minerals as reservoirs of H in the Earth's mantle, to examine their potential use as petrogenetic indicators in certain mantle settings and to elucidate selected aspects of the geochemical principles governing H incorporation in these phases." In this section these aims are reviewed, and some speculations entertained.

The role of nominally anhydrous minerals as reservoirs of H in the mantle.

This study has revealed that trace H is a ubiquitous component in mantle silicate minerals, present in concentrations from a few ppm to about 0.1 wt.% H_2O, with only certain garnet and rare olivine samples not containing detectable OH. The water content of the mantle has been a subject of considerable speculation, but is likely to be heterogeneous on a variety of scales. For this reason, the relative importance of nominally anhydrous minerals for the geochemistry of H is likely to vary considerably from one part of the mantle to another. This view was recently expressed as a general principal for all phases with regard to water storage in the mantle (Thompson 1992). In this context, the contribution of this study has been to illustrate the *capacity* of nominally anhydrous minerals to influence H geochemistry by demonstrating concentrations in certain minerals. Determining how these concentrations are likely to vary in the mantle in response to the pressure, temperature and local water activity is the next and critical step in establishing a quantitative description of the role of nominally anhydrous minerals in mantle H geochemistry.

Because of the sampling bias, the only mantle region for which the measurements presented here arguably give representative water contents is the continental lithosphere. Unfortunately this region, being relatively cold, is conducive to the growth of hydrous minerals such as phlogopite and amphibole, which will probably dominate the H budget. An additional problem is that the xenolith samples are by definition derived from areas of magmatic (typically volatile-rich) activity in which it could be argued that original H contents in mantle rocks are rapidly overprinted. Similar, though perhaps slightly less severe problems attend many tectonically emplaced mantle sections in the crust. If direct samples are not very helpful, can any predictions then be made about where nominally anhydrous minerals assume importance?

Because OH contents in "anhydrous" minerals are far lower than in other hydrous phases, it stands to reason that their importance will be greatest in regions of the mantle where these other phases are not present. This is likely to be in regions of the mantle that are hot and water-poor. Evidence from experiments (Bai and Kohlstedt 1992) and from analysis of natural samples (e.g., megacrysts and high-T peridotites, this study) indicates that the hydrous component in these minerals is stable to high temperatures ($\geq$ 1300 °C). Because most hydrous minerals with any appreciable thermal stability appear to contain K, nominally anhydrous minerals are potentially more important in K-poor parts of the mantle. However, hydrous K-bearing phases may be less important than sometimes suggested because of the probability of accommodation of large amounts of K in clinopyroxene at high pressures (Erlank & Kushiro 1970, Harlow & Veblen 1991). It might therefore be expected that nominally anhydrous minerals would be important in average, or ambient mantle, whereas other phases assume importance in cold regions or where sharp chemical heterogeneities are preserved. These two conditions are probably met simultaneously in some regions of the mantle, obvious examples being cratonic

lithospheric mantle and subducting oceanic crust. There is no evidence to suggest that OH in nominally anhydrous minerals decreases at higher pressures; if anything the contrary is indicated by the relationship between water fugacity and OH in olivine reported by Bai and Kohlstedt (1992), in that high water fugacities are more readily attained at high pressures. Recent high-pressure experimental studies on wadsleyite (ß-Mg_2SiO_4) (McMillan *et al.* 1991, Young *et al.*, 1992) have revealed substantial OH contents as predicted by Smyth (1987). Thompson (1992) has discussed the implications of rising mantle material intersecting the 400 km seismic discontinuity.

Consideration of a hypothetical isobaric T-X phase diagram in the general system A - H_2O predicts that low concentrations of water in nominally anhydrous minerals are likely to cause melting at temperatures only slightly below the dry melting temperatures of these minerals, but the contrast with the solidus temperature in the absence of the solubility of trace OH in the minerals is dramatic. Where the presence of a few hundred ppm water would cause melting in the absence of a hydrous component in the mineral, and therefore water "storage" in a melt, the presence of solid solution may prevent melting to substantially higher temperatures. The extent to which this is accomplished depends on the extent of solid solution towards the hydrous component. If the nominally anhydrous minerals are close to saturation, then melting will occur at temperatures close to the vapor-saturated solidus. With the apparent demise of several dense hydrous magnesium silicates as water storage candidates (Wunder and Schreyer 1992) and the above comments on melting behavior, the concept of a water line in the upper mantle, above which water is present as a fluid (Liu 1987) or a melt (Thompson 1992) may be inappropriate, particularly in typical MORB-source type upper mantle in terms of water content.

These considerations suggest that nominally anhydrous minerals may be the dominant hydrous phases in depleted, relatively water-poor mantle. OH concentrations predicted from bulk or mineral-melt D_{H_2O} to be residual in the nominally anhydrous mantle after melting and extraction of primary arc basalt (~ 1-2 wt.% H_2O) from a hydrous mantle wedge are on the order of 100 - 200 ppm. If this material re-supplies the depleted mantle with water, then for the nominally anhydrous minerals to account entirely for the steady-state water cycle in the Earth, in which water is degassed at ocean ridges and returned to the mantle at subduction zones, would require the generation of arc basalt at a rate comparable to that of oceanic ridge basalt, corrected for systematic degrees of partial melting that may exist between the two. However, it is not necessarily to be expected that this residue would be a suitably "fertile" source in terms of basaltic components for MORB production. The existence of incompatible element and water enriched mantle domains, which may result from recycled material, suggest that other mechanisms are available to recycle water, though it is interesting to note that the ratio of water measured in nominally anhydrous minerals in eclogite to that in peridotite is similar to the ratio of water in enriched versus depleted basalt sources (~2:1)

Neither measurement of OH content in nominally anhydrous minerals, nor experimental studies of mineral stabilities constrain the water content of the mantle. That goal would appear to be best attained by careful measurement of the water content of basalts and by geochemical modeling. The role that nominally anhydrous minerals play can be best evaluated by identification of the incorporation mechanisms of H and the experimental determination of their H contents under predicted mantle conditions. This study has not addressed the importance of H in minerals for physical properties of the mantle, such as rheology, conductivity or mineral ionic diffusivities, but these are issues that bear

integration into an overall model for the fundamental mechanisms of trace H incorporation.

Nominally anhydrous minerals as petrogenetic indicators.

This study has presented a large body of data which indicate a correlation between the OH content of nominally anhydrous minerals and their petrogenetic history. In chapter 1 a number of conclusions about the petrogenesis of various mantle assemblages were drawn from the OH content of their garnets. Chapter 3 examined several minerals from a single association in detail. In all of these observations there is a self-consistency which is compelling, namely that the OH contents of these minerals undoubtedly record petrologic information from the mantle. However, there has always been the nagging doubt that the information being conveyed by the measured OH contents is not about their mantle OH contents, but about some other aspect of their crystal chemistry which determines the OH content of the mineral when it is subjected to an imposed set of volatile fugacities (fO_2, fH_2, fH_2O in particular) in the crustal emplacement environment. Such aspects could include the original OH content, but may also contain effects of cation vacancies, redox state and the like. Cause for concern in this area derives from observations on the behavior of H in nominally anhydrous minerals in experimental systems, for example, the extreme rapidity with which the OH content of olivine may be changed in a hydrothermal environment (Mackwell and Kohlstedt 1990), the ease with which Fe^{3+} bearing pyroxenes can be induced to display OH bands in the IR spectrum after heating in a stream of H_2 (Skogby and Rossman 1989, Skogby, in prep) and the general lability of OH in these minerals in oxidizing environments at moderate temperatures. Loss of OH due to heating on eruption has been proposed to account for low OH contents of basalt-hosted olivines (Miller *et al.* 1987) and was hinted at in

chapter 1 as a possible explanation for differences in OH contents in garnet megacrysts from basalts and kimberlites. Furthermore, the general uniformity in OH content of mantle clinopyroxenes (most variation is within a factor of two to three) is somewhat troubling, particularly in when their coexisting minerals are highly variable and often totally OH-free (eclogites).

This issue has been addressed at several points in the thesis, but it seems worthwhile to compile some of the evidence for the preservation of actual mantle OH (the possibility that it is isotopically exchanged is discussed in Appendix 1). It can be said in advance that I am not aware of any argument which would prove the case. There are also, however, few arguments against, which cannot be countered or rationalized. All observations to date are consistent with the hypothesis that the OH contents of these minerals are preserved intact from the mantle. As stated above, the weight of self consistent petrological data is a strongly persuasive point. High water fugacities calculated from the Monastery megacryst olivines with petrographic evidence for annealing in lower fH_2O samples are inconsistent with water in the crust. The similarity of behavior of H and K in clinopyroxene megacrysts argues for no resetting of H in the crust, because K cannot be similarly reset. Hydrothermal experiments failed to alter the OH content of garnets (this study) and pyroxene (Skogby and Rossman 1989). The low OH contents of basalt-hosted olivines and garnets cited as possibly due to dehydration also appear to be consistent with their conditions of origin, if they have not experienced high water activities. Strong oxidation or reduction appears to be required in order to change a mineral's OH content. Removal and addition of OH in some minerals may require structural rearrangement.

Acceptance of the general rule that OH in these minerals has not been substantially disturbed is concluded to be a reasonable working hypothesis, but that it is worth considering the alternative in any case where this may seem appropriate. Further experimental work will help to define the conditions under which this assumption is likely to be valid.

Even with this assumption, however, it appears from the partitioning data presented in Chapter 3 that the quantitative calibration of the OH contents of these minerals as hydrobarometers will be a complex task. The simple relationship described by Bai and Kohlstedt (1992) between f_{H_2O} and H content of olivine was determined on an olivine of one composition. The possibility that OH content is coupled with minor element substitution, even in olivine, means that the extrapolation of this calibration to natural systems may be problematic, especially if H is coupled to other trace elements (e.g., Ti) which can vary enormously in concentration. The existence of multiple OH sites in minerals also poses problems and it may be necessary to treat each independent peak in the OH spectrum as a separate type of OH, with its own partitioning behavior, not to mention molar absorption coefficient. Nevertheless, the conclusion of this study is that useful petrogenetic information is retrievable from these minerals. Just how far back in the sample's mantle history is decipherable remains to be determined, and may vary from one mineral to another.

Geochemical principles governing OH incorporation in these phases.

Much of this aspect has been touched on in the previous section, but it is indeed the least covered aim in this thesis. The following points summarize some of the principles "established" in this study.

1. OH content of minerals such as garnet and olivine, and perhaps less certainly pyroxenes, are set during crystallization of the mineral and depend on the activity of water, physical variables such as P and T, and the activities of various chemical components, among which Ti seems to be significant. It may be that cation substitutions that require charge compensation are susceptible to coupling with H, as suggested by Vlassopoulos *et al.* (1992) for rutile. There is at present no evidence for hydrogarnet type substitutions in the orthosilicates, though these cannot usually be expressly ruled out. It can be expected that models for OH incorporation based on pure system defect equilibria may prove inadequate in describing phenomena in natural minerals.

2. It is conceivable that this OH content may be reset in the mantle, for example by a metasomatic event. In pyroxenes from coarse peridotites, where high OH contents are often accompanied by development of amphibole lamellae and suggest action of a hydrous fluid, this may occur more readily than in garnets which are often not notably richer in OH in phlogopite-bearing peridotites, though they may sometimes be.

3. OH in these minerals can be removed by heating in an oxidizing environment, and can be replaced by hydrothermal treatment in garnets, olivine and pyroxenes, though not necessarily in precisely the same sites and at the same concentrations as prior to removal. Hydrothermal treatment of garnet and pyroxene without annealing generally does not change the OH content substantially. In these situations, H gain and loss is believed to proceed via homogeneous redox reactions.

4. IR spectra of the same mineral species are generally similar, but display some composition-dependent variability. This indicates that the OH groups generally populate the same crystallographic sites in these minerals. Large variations in spectral patterns, such as those described for grossular garnets (Rossman and Aines 1991) or olivines (Miller *et al.* 1987) are not observed.

Analytical concerns.

Despite the advances made in calibration of the IR technique, precise and accurate analysis of H by independent methods at the 10 -500 ppm H_2O level remains a challenge. These calibrations are often enormously tedious, which is discouraging when one considers the range of infrared spectra that must be calibrated. It is anticipated that high vacuum, high sensitivity ion microprobe and other micro-analytical methods may be preferable to IR spectroscopy for quantitative analysis in the long run, though the calibration problems can be expected to be severe in these instruments too. The spectroscopic technique is invaluable as a probe into the molecular level interactions and micro-chemical environment of the OH groups, but this sensitivity to structural information is part of the quantitative downfall. Ideally the two techniques should be combined for maximum information.

Future directions.

There appears to be little need for further surveys of the H content of mantle minerals, other than specific studies aimed at establishing regional geochemical trends. Even in these cases it would be desirable to establish a firmer basis for quantitative interpretation of observed variations. From a mineralogical point of view, it will be interesting to establish the relationship of trace OH to stoichiometric OH in minerals through the gray area of micro-phase mineralogy. The importance of submicroscopic domains of hydrous minerals stabilized within anhydrous hosts, e.g., brucite or titanoclinohumite lamellae in olivine has yet to be evaluated. For the nominally anhydrous minerals, we would ultimately like to know precisely where the H is located, what controls its abundance

under specified conditions, the kinetics and H-isotopic fractionations of the reactions involving hydrous components and the stability of trace structural OH with respect to other forms of H.

With current technology, solving the structural problems by neutron diffraction, NMR and other spectroscopic techniques requires particularly OH rich samples. Natural samples are rarely sufficiently hydrous for these purposes and synthetic samples offer the advantage of isotopic labeling and elimination of impurity effects such as arise from paramagnetic ions. The onus will be to demonstrate correspondence between synthetic and natural examples.

Experimental studies investigating the concentration of OH as a function of P, T, X, f_{O_2}, f_{H_2O} etc. are critical if these minerals are to be used in a quantitative sense in earth science. Due to the large number of variables which appear to affect the concentration of trace structural OH, these experiments will be difficult to do in a well-controlled way. As in the structural studies, the connection of the synthetic to the natural system must be appraised. Attention to structural aspects of OH incorporation is important in these studies too, and it is critical that bulk analytical techniques such as SIMS be complemented by spectroscopic studies. As an illustration, it is not clear that any of the large number of experimental studies on hydrogarnets reported in Chapter 5 are at all relevant to trace OH in garnets. Two types of experiments are important in the immediate future: (i) low-pressure hydrothermal studies in which P, T and, especially, volatile activities can be adequately controlled, with sufficiently large crystals grown or equilibrated so that they can be well characterized and (ii) very-high pressure (multi-anvil type apparatus) experiments that can investigate the pressure dependence of the solubility of hydrous components in minerals, and the equilibrium phase assemblages in hydrous

mantle or model mantle compositions. Some very low pressure experiments might also be interesting in evaluating the role of this form of H in planetary accretion. Thermodynamic modeling of trace OH in minerals may prove to be useful in its predictive capacity, but ultimately it is the experimental studies which will provide the definitive data.

Isotope fractionation experiments are important because these minerals have the capability, like oxygen isotopes, to track the passage of fluids through anhydrous mineral assemblages. Kinetic studies of D/H exchange will be necessary to delineate the circumstances under which D/H in these minerals can provide useful information. Further isotopic analysis of H in anhydrous minerals is necessary in the near future to confirm the observations made in Appendix 1 on limited samples under marginal analytical conditions.

In summary, there is a large amount of work to be done to exploit the potential of trace structural OH in minerals, presenting many technological challenges. The importance of H and the ubiquity of this phenomenon ensure a wide range of applications to problems in earth science.

References

Bai, Q & Kohlstedt, D. L. 1992. Substantial hydrogen solubility in olivine and implications for water storage in the mantle. *Nature* **357,** 672-674.

Erlank, A. J. and Kushiro, I. 1970. Potassium contents of synthetic clinopyroxenes at high temperatures and pressures. *Carnegie Insy. Washington Yearb.* **68,** 233-236.

Harlow, G. E. and Veblen, D. R. 1991. Potassium in clinopyroxene inclusions from diamonds. *Science* **251,** 652-655.

Liu, L.-G. 1987 Effects of H_2O on the phase behaviour of the forsterite-enstatite system at high pressures and temperatures and implications for the Earth. *Phys. Earth planet. Int.* **49,** 142-167.

Mackwell, S. J. & Kohlstedt, D.L. 1990. Diffusion of hydrogen in olivine: implications for water in the mantle. *J. geophys. Res.* **95,** 5079-5088.

McMillan, P. F., Akaogi, M., Sato, R. K. Poe, B and Foley, J. 1991. Hydroxyl groups in ß-Mg_2SiO_4. *Amer. Mineral.* **76,** 354-360.

Miller, G. H., Rossman, G. R. & Harlow, G. E. 1987. The natural occurrence of hydroxide in olivine. *Phys. Chem. Minerals* **14,** 461-472.

Rossman, G. R. and Aines, R. D. 1991 The hydrous components in garnets : grossular-hydrogrossular. *Amer. Mineral.* **76,** 1156-1164.

Skogby, H. S. and Rossman, G. R. 1989 OH- in pyroxene : An experimental study of incorporation mechanisms and stability. *Amer. Mineral.* **74** : 1059-1069.

Skogby, H. S. in prep. Hydroxyl incorporation in synthetic clinopyroxenes.

Smyth, J. R. 1987 ß-Mg_2SiO_4.: a potential host for water in the mantle? *Amer. MIneral.* **72,** 1051-1055.

Thompson, A. B. 1992 Water in the Earth's upper mantle. *Nature* **358,** 295-302.

Vlassopoulos, D., Rossman, G, R. and Haggerty, S. E 1992 Coupled substitution of H and minor elements in rutile and implications of high OH contents in Nb-Cr rutile from the upper mantle. ms submitted.

Wunder, B. and Schreyer, W. 1992 Metastability of the 10Å phase in the system MgO-SiO_2-H_2O (MSH). What about hydrous MSH phases in subduction zones? *J. Petrol.* **33,** 877-889.

Young, T. E., Green, H. W. II, Hofmeister, A. M. and Walker, D. 1992 Infrared spectroscopic investigation of hydroxyl in nd coexisting olivine: implications for mantle evolution and dynamics. *Phys. Chem. Minerals,* in press.

Appendices

Appendix 1

The isotopic composition of hydrogen in nominally anhydrous mantle minerals.

by

David R. Bell and Phillip D. Ihinger

Nominally anhydrous minerals of the Earth's mantle are a potentially important reservoir for hydrogen in the Earth's interior due to their capability to incorporate hydroxyl in trace quantities. Here we present measurements of the isotopic composition (D/H ratio) of hydrogen from upper-mantle derived garnet, enstatite and augite which, together with predictions of fractionation behavior from IR spectroscopic systematics, suggest that the D/H ratio of this reservoir of hydrogen may differ from that of other mantle H in being relatively depleted in deuterium.

Knowledge of the isotopic composition of hydrogen in various reservoirs on Earth provides, in principle, a valuable tool with which to investigate how water has behaved during the accretion and geological evolution of the planet. While water in the crust and hydrosphere is relatively well characterized in terms of mass and δD, the amount and isotopic composition of hydrogen in the Earth's deeper interior are poorly known. It has been a common practise to consider deep-seated H in terms of a "mantle" value or limited range of values of δD (Sheppard and Epstein 1970, Boettcher and O'Neil 1980, Kyser and O'Neil 1984, Kyser 1990). The coincidence of these mantle values (-60‰ to -80‰ relative to Standard Mean Ocean Water) with the common range of primary δD values in igneous rocks as well as many sedimentary and metamorphic rocks in the Earth's crust has led to the idea (Taylor 1977, Taylor and Sheppard 1986) that the outermost part of the silicate Earth has been homogenized in terms of δD by recycling processes and is in a steady state. The mantle δD is thus determined by partitioning of H and D between rocks and the hydrosphere near the Earth's surface, and is effectively buffered by the large mass of water in the oceans relative to that in the shallow mantle. It is, however, not clear to what depths in the Earth this mechanism operates.

There is a growing body of evidence (Poreda 1985, Poreda *et al.* 1986, Dobson and O'Neil 1986, Hochstaedter *et al.* 1990, Chaussidon *et al.* 1991)) suggesting that hydrogen (water) in the Earth's interior is isotopically heterogeneous, and that separate reservoirs of hydrogen may exist which are characterized by different D/H ratios. It is now more or less accepted that the mantle near subduction zones is enriched in D, but a uniform δD of about -80 ‰ has been suggested for the remainder of the mantle by Kyser (1986). Data from Poreda *et al.* 1986 suggest otherwise. Unfortunately, several factors conspire to blur the interpretation that can be attached to measurements of δD on hydrogen in mantle-derived hydrous minerals and volcanic glasses. These relate to the susceptibility of the original δD to disturbance by exchange or contamination with the large concentrations of H near the Earth's surface, facilitated by rapid kinetics, and the large fractionations in D/H ratio between phases which accompany chemical reactions and physical processes in geology. These factors make it difficult (but not impossible) to prove beyond doubt that true, large scale heterogeneities in mantle δD exist. Nevertheless, in view of what could be learned about water on Earth, and also about the origin of coupled chemical heterogeneities in the mantle (Poreda *et al.* 1986), it would seem prudent to consider the possibility of these variations seriously.

Measurements of δD of mantle-derived H have to date concentrated mostly on hydrous minerals (phlogopite and amphibole) in rocks of mantle origin such as massif peridotites (Javoy 1980) and xenoliths in volcanic eruptions (Sheppard and Epstein 1970, Kuroda *et al.* 1975, 1977, Sheppard and Dawson 1975, Boettcher and O'Neil 1980, Deloule *et al.* 1991) as well as on basaltic lavas, quenched to glass on the ocean floor. Mantle H is not restricted to residence in stoichiometrically hydrous minerals, and may also occur in a fluid or melt phase (Wyllie 1970). It has recently been suggested (Bell and Rossman 1992) that, in addition to these repositories, the common, nominally anhydrous mantle minerals

are an important reservoir of H in the Earth's interior, possibly dominating the H budget of the depleted upper mantle. The identification of this new reservoir of H may have important implications for the Earth's water cycle.

In order to examine the potential for nominally anhydrous minerals to constitute an isotopically distinct reservoir of H in the mantle, we have measured the D/H ratios of hydrogen extracted from pyrope garnet, enstatitic orthopyroxene and subcalcic diopsidic augite (clinopyroxene) of upper mantle origin. These minerals can accommodate several hundred parts per million of water by weight in certain circumstances (Aines and Rossman 1984a,b, Skogby *et al.* 1990, Smyth *et al.* 1990, Bell and Rossman 1992b).

Analytical methods and samples

D/H ratios were determined as a follow-up to a study designed to calibrate an infrared spectroscopic technique for quantitative analysis of H in mantle minerals (Chapter 4). Details of the sample preparation procedure, in which particular attention was paid to excluding H other than that bound in the nominally anhydrous phases of interest, are given in that study. Two key aspects of the study were (i) the infrared spectroscopic characterization and quantitative measurement of the OH in the mineral samples both prior to and after extraction and (ii) the selection of suitable large clean crystals and their subsequent careful purification to yield inclusion- and crack-free gem quality mineral fragments (≥99.95% pure).

Samples. The garnet, MON-9, is a megacryst from the Monastery Mine kimberlite, South Africa measuring some 10 cm in diameter. This kimberlite is well known for its spectacular suite of megacrysts, or "discrete nodules," and the present sample, while larger

than most garnets from that locality, is not exceptional. This sample contains 56 ppm H_2O, which is approximately in the middle of the range of water contents of Monastery garnet megacrysts (Bell and Rossman 1992b). The origin of these megacrysts has been ascribed to crystallization from a magma in the upper part of the asthenospheric mantle (Nixon and Boyd 1973) or lower lithosphere (Gurney *et al.* 1979), possibly in a stockwork of veins (Harte and Gurney 1981). Pressure of crystallization is estimated at 53 kb kb (Moore 1986). Various minerals from the Monastery kimberlite have been the subject of H-isotope studies by Sheppard and Epstein (1970), Sheppard and Dawson (1975) and Boettcher and O'Neil (1980).

The clinopyroxene PMR-53 is a subcalcic augite megacryst from the Premier Mine, South Africa, similar to other clinopyroxene megacrysts commonly found in kimberlites. Megacrysts from the Premier Mine have been described by De Bruin (1991) and δD values of Premier Mine materials are reported by Sheppard and Dawson 1975 and Boettcher and O'Neil 1980.

The orthopyroxene sample KBH1.opx is a mineral separate prepared from a Cr-diopside series (Type I) spinel lherzolite from the unconsolidated tuff ring of the basanite maar at Kilbourne Hole, New Mexico. Microscopic examination of several hundred grams of coarsely crushed material from this xenolith has revealed no trace of primary hydrous minerals.

Analytical Procedure Polarized infrared spectra were collected on crystallographically-oriented and polished plates of the pyroxenes, and unpolarized spectra of the garnet were collected, using a Nicolet 60SX Fourier Transform IR spectrometer before and after extracton. Three separate aliquots of different mass of each of the pyroxene samples and

two of the garnet sample were analyzed. In addition, the procedure was repeated on an empty crucible to determine the line blank of 3 μmoles of H2. Aliquots were loaded into clean, but untreated Pt crucibles after weighing and degassed at 150 - 200 °C for three hours. Hydrogen was extracted by heating the sample in an induction furnace under vacuum, converted to water by reacting with CuO at 500 °C, purified cryogenically, converted back to H_2 over hot Uranium and collected after volumetric measurement in a calibrated Hg manometer. H released during the low temperature degassing step was mostly in the form of water. The temperature was raised incrementally to just below the sample melting point, with proportions of reduced and oxidized gases being monitored semiquantitatively. Above approximately 500 °C, H was released from the samples as H_2.

Infrared spectroscopy was used to determine the amount of residual hydrogen in the mineral grains (which were not melted in order to preserve short diffusion distances) after extraction. This analysis, which was performed on the largest grains and therefore provides a maximum estimate for possible residual OH, revealed that following average degree of dehydrogenation: clinopyroxene >99%, orthopyroxene ≥83%, garnet ≥95%. The D/H ratios of the collected H_2 gas samples were determined by mass spectrometry (by PDI) with a precision of ±2‰ for most samples but with somewhat greater errors for the smallest (≤ 4 μmol) samples.

Results

Sample aliquot masses, H_2 yields and H-isotopic composition of the extracted gases are reported in Table 1. δD values are shown as a function of H yield in Fig. 1. All extractions resulted in H yield that were remarkably proportional to the aliquot masses, giving precise OH concentrations for IR calibration (Chapter 3) and demonstrating

consistency of the line blank In addition, analysis of a spectroscopically anhydrous garnet produced a comparable blank level of 4.98 μmoles which was somewhat higher than the line blank because of prior HF acid treatment of the crucible (not done in all other analyses). This indicates efficient screening of extraneous H during sample preparation and minimal contamination during sample handling and loading. Despite these precautions, the extremely low OH concentrations in the minerals imply that for the smallest aliquots of garnet and orthopyroxene, a large proportion of the H finally collected and analyzed is derived from the blank. Much of this blank is believed to derive from atmospheric moisture adsorbed onto the crucible and quartz sample vessel walls and is therefore of highly variable isotopic composition. The true D/H ratios of these low-mass samples are therefore extremely uncertain (Figure 1). However, for larger sample masses, particularly of clinopyroxene, the blank comprises only a small fraction of the total and does not influence the measured composition to a significant degree.

Discussion

All of the more reliably determined δD values lie in the range between -100 and -130 ‰ . In figure 2 these values are compared to δD values of other mantle minerals and of oceanic basalts. It can be seen that the nominally anhydrous mineral δD values are depleted in deuterium relative to the majority of mantle derived materials. The limited sampling does not allow firm statements to be made, but the data do suggest that these minerals may be characterized by distinctively light δD values. Precisely what these δD values represent is not immediately obvious and we consider several possible processes that could have contributed to the measured δD.

(1) *On-line fractionation and contamination*

We have already expressed our opinion that the H collected and analyzed isotopically does not derive from forms of H other than that which is structurally bound in the nominally anhydrous minerals, that is, it does not derive from fluid inclusions or alteration phases along cracks. However, it is necessary to examine to what extent the D/H ratio of the samples can be fractionated by effects introduced from the extracton line.

The error bars in Fig. 1 provide an estimate of the uncertainty in the isotopic composition of the sample δD caused by uncertainty in the composition of the blank. Based on measurements of the isotopic composition of the blank on various occasions over the past year we assigned a somewhat arbitrary uncertainty of $\pm$ 40 ‰ to the blank.

Although the essentially all hydrogen was extracted from the clinopyroxene samples, IR spectroscopic analysis revealed some residual OH in both the orthopyroxene and garnet. The precise amount is difficult to quantify, because the amount remaining depends on the grain size, which spanned a substantial range for each mineral. Our analyses of residual OH were made on the thickest, and therefore most OH-rich mineral fragments and are thus likely to underestimate the degree of extraction. This is compounded by the polishing procedure for IR analysis, which removes the most OH-depleted crystal exteriors and artificially elevates their apparent OH concentrations. The fact that most of the OH appears to leave the sample as H_2 suggests that incomplete extraction will yield a value more deuterium-depleted than the bulk, because H_2 discriminates against deuterium relative to water or OH.

The small volumes of gas involved in these extractions are known to be subject to some on line fractionation due to so-called "memory effects." These effects, which depend on the

volume of the sample under consideration and the isotopic composition of the previous sample to be extracted have been calibrated for the present extraction line by analysis of small quantities of gas of known isotopic composition. Data presented in Fig.1 have not been corrected for this effect

(2) *Mantle processes.* If the measured δD values represent the isotopic composition of H in these samples as they existed in the mantle, then the results suggest an isotopically distinct form of H in the mantle. These isotopic compositions are nevertheless not unique, and even lighter values have been reported for amphiboles from kimberlite-hosted xenoliths by Kuroda *et al.* (1975,1977) and Kyser (O'Neil, pers. comm.). The striking aspect of our data set is however that all three samples (from diverse localities and host rocks) record low δD. If these values are indeed primary, then their distinctive δD values are likely to reflect principally the large *fractionation* between the local ambient mantle H reservoir and the nominally anhydrous minerals. This is likely because all three samples derive from hydrous environments in the mantle, where a greater sink of H than the nominally anhydrous minerals (e.g., melt, hydrous fluid or hydrous mineral) is likely to exist. The high OH content of the kimberlitic megacryst environment is readily confirmed by the presence of phlogopite and a general enrichment in incompatible elements (Eggler *et al.* 1979, Boyd and Nixon 1973, Gurney *et al.* 1979, Harte 1983). While the spinel lherzolite from Kilbourne Hole has probably experienced a largely anhydrous history, there is strong evidence that the mantle environment from which such xenoliths were derived has been generally perturbed by the overall magmatic event resulting ultimately in transport to the surface (Wilshire 1987). This is supported by the relatively high OH concentrations in both ortho- and clinopyroxene from this xenolith (Bell and Rossman 1992a).

Two lines of evidence suggest that nominally anhydrous minerals may be depleted in D relative to coexisting hydrous phases. Firstly, the fundamental stretching frequencies of the OH bonds in nominally anhydrous minerals are typically substantially lower than those in hydrous silicates such as micas and amphiboles. It has been shown that a negative correlation exists between the fundamental OH stretching frequency of a given mineral and $\Delta_{mineral\text{-}H_2O}$ (Dobson *et al.* 1989). Weighted mean of the infrared absorption frequencies for OH is near 3560 cm^{-1}, 3500-3550 cm^{-1}, and 3300 cm^{-1} for the garnet, clinopyroxene and orthopyroxene samples respectively. Amphibole OH stretching frequencies are typically greater than 3650 cm^{-1} and in phlogopite occur at 3660 - 3710. cm^{-1}. Although the correlation is not tightly constrained, these data would predict, for example, a $\Delta_{gt\text{-}phl}$ of about 15 ‰ and $\Delta_{opx\text{-}H_2O}$ of ~ -60 ‰. Secondly, in support of this, it has been observed that phlogopite megacrysts from the Monastery Mine show a relatively narrow range of δD between -58 and -65 ‰ (Sheppard and Epstein 1970, Sheppard and Dawson 1975, Boettcher and O'Neil 1980). If garnet and phlogopite both derive their H from the same reservoir (they may be broadly co-magmatic), i.e., they are in approximate isotopic equilibrium, then the IR stretching frequencies predict that garnet would be isotopically lighter than phlogopite, although the observed fractionation is somewhat greater than that predicted. It is possible that the approximately 40‰ depletion in D relative to phlogopite represents the equilibrium D/H fractionation between the two minerals.

(3) Isotopic exchange associated with eruption and crustal residence

Although it has been argued that most nominally anhydrous minerals in xenoliths retain their OH contents from the mantle (this work; chapters 1, 3 and 6), H may be subject to isotopic exchange in the environment of emplacent. It is commonly observed that such minerals can be partially deuterated by hydrothermal treatment in the laboratory on

relatively short time scales (hours to days) (Skogby and Rossman 1989). The hydrous environment of diatreme and hypabyssal facies kimberlite emplacement in the crust provides ample opportunity for exchange with circulating deuteric fluids or meteoric water. The presence of such fluids is indicated by petrographic criteria such as primary serpophite and extensive serpentinization of olivine. Sheppard and Dawson (1975) have demonstrated the involvement of local meteoric water in the serpentinizing fluids. Matrix phlogopite and serpentine have δD values of -85 to -105 ‰ in southern African kimberlites (Sheppard and Dawson 1975), values which are similar to, but somewhat heavier than, the nominally anhydrous minerals. With the type of D/H fractionations expected for the nominally anhydrous minerals based on their IR stretching frequencies, the δD values for the clinopyroxene and garnet (the samples from kimberlite) are more or less those expected to be in equilibrium with the meteoric-hydrothermal fluids that produced the serpentinization. Thus the δD values of these minerals are ambiguous, possibly reflecting either mantle or crustal H exchange. This could be tested by analysis of H in nominally anhydrous megacrysts from kimberlites erupted at high latitudes (such as the Somerset Island province), where the meteoric-hydrothermal fluids would be expected to have extreme isotopic compositions.

Perhaps less opportinuity for exchange in the crust is afforded to the spinel-lherzolite orthopyroxene from Kilbourne Hole. This xenolith was recovered from the unconsolidated ejecta ring formed during explosive development of the maar. Groundwater has no doubt percolated through this material and the xenolith, but temperatures may have been very low. Amphibole samples from the southwestern U.S. are strongly heterogeneous in δD (Boettcher and O'Neil 1980, Dyar *et al.* 1992) and OH in orthopyroxene may be affected by similar processes that caused this large variation. In particular, loss of H_2 during heating may account for some of the variation observed.

Implications of low δD in nominally anhydrous minerals

If nominally anhydrous minerals are D-depleted relative to other hydrous phases, as suggested by the stretching frequencies of their OH bands in the IR spectra, and as indicated by the analyses presented here, then their role in the geochemistry of H should be fingerprinted by low values of δD. Bell and Rossman (1992a) and Chapter 6 of this study have suggested that these minerals may be the dominant reservoir of H in the depleted (MORB-source) mantle. It can be seen from studies of arc and back-arc basin basalts (Fig. 2b) that the isotopic compositions of H in subduction related lavas are significantly D-enriched relative to MORB, having δD similar to that of the subducting oceanic lithosphere. If nominally anhydrous minerals that are residual in the mantle after extraction of the hydrous subduction-related melts are D-depleted relative to H in the lavas, as might be expected from their predicted sense of isotopic fractionation, then this residue might be expected to have an isotopic composition of H similar to that of MORB. The connection between mantle residua of subduction-related melting and the MORB source in terms of water content and the role of nominally anhydrous minerals has been alluded to in chapters 2 and 6, and is consistent with this explanation for the isotopic composition of H in MORB.

Summary and concluding remarks

The isotopic composition of H recorded by nominally anhydrous minerals containing trace quantities of OH is different from the commonly encountered range of δD in mantle-derived minerals and volcanic glasses. If these isotopic compositions have been preserved during eruption and transport of the xenoliths then nominally anhydrous minerals appear to represent an isotopically distinct (deuterium-depleted) reservoir of mantle H.

Fractionations involving the nominally anhydrous minerals may be responsible for some of the apparent H-isotope heterogeneity in oceanic basalts, and may produce H isotopic zoning in the mantle if the P-T stability range of these minerals differs from that of hydrous minerals. It is, however, quite possible that the samples analyzed here have exchanged hydrogen during and after their ascent from the mantle, and that the low δD values reflect interaction with a component of meteoric water-derived hydrogen. This question will hopefully be resolved by determination of the relevant mineral-water fractionations of D/H for the nominally anhydrous minerals, by an increased understanding of the mobility of H in these mineral systems during eruption processes and by further analysis of carefully selected samples which can discriminate between local meteoric and magmatic waters.

References

Aines RD, Rossman GR (1984a) The hydrous component in garnets: Pyralspites. *Amer Mineral* **69**, 1116-1126

Aines RD, Rossman GR (1984b) Water content of mantle garnets. *Geology* **12,** 720-723

Bell, D. R., Ihinger, P. D., Rossman, G. R., Epstein, S. 1992. Calibration of an infrared spectroscopic technique for quantitative analysis of hydroxyl in garnet and pyroxene. To be submitted to *Amer Mineral.*

Bell, D. R. & Rossman, G. R. 1992a. The distribution of hydroxyl in garnets from the sub-continental mantle of southern Africa. *Contrib. Mineral. Petrol.* **111**, 161-178.

Bell, D. R. & Rossman, G. R. 1992b. Water in Earth's mantle; the role of nominally anhydrous minerals. *Science* **255**, 1391-1397.

Chaussidon, M., Sheppard, S M. F. and Michard, A. (1991) Hydrogen, sulphur and neodymium isotope variations in the mantle beneath the EPR at 12° 50' N. In: Taylor, H. P., Jr., O'Neil, J. R. and Kaplan, I. R. (eds) *Stable isotope geochemistry: a tribute to Samuel Epstein. Geochemical Society spec Publ.* **3,** 325-337.

Craig, H. and Lupton, J. E. (1976) Primordial neon, helium and hydrogen in oceanic basalts. *Earth planet. Sci. Lett.* **31**, 369-385.

Deloule, E., Albarede, F. and Sheppard, S. M. F. (1991) Hydrogen isotope heterogeneities in the mantle from ion probe analysis of amphiboles from ultramafic rocks. *Earth Planet. Sci. Lett.* **105,** 543-553.

Dobson, P. F., Epstein, S. and Stolper, E. M. (1989) Hydrogen isotope fractionation between coexisting vaporand silicate glasses and melts at low pressure. *Geochim. Cosmochim. Acta. 53,* 2723-2730.

Dobson, P. F. and O'Neil, J. R. (1987) Stable isotope compositions and water contents of boninite series volcanic rocks fom Chichi-jima, Bonin Islands, Japan. *Earth planet. Sci. Lett.* **82**, 75-86.

Dyar, M. D., McGuire, A. V. and Mackwell, S. J. (1992) Fe3+/H+ and D/H in mantlle kaersutites.

Eggler, D. H., McCallum, M. E. and Smith, C. B. (1979) Megacryst assemblages in kimberlite from northern Colorado and southern Wyoming: Petrology, geothermometry-barometry and areal distribution. In: Boyd FR, Meyer HOA (eds.) *The Mantle Sample: Inclusions in Kimberlites and Other Volcanics.* AGU, Washington, pp. 213-226

Garcia, M. O., Muenow, D. W., and Aggrey, S. E. (1989) Major element, volatile and stable isotope geochemistry of Hawaiian submarine tholeiitic glasses. *J. geophys. Res.* **94**, 10525-10538.

Gurney, J.J., Jakob, W.R.O. and Dawson, J.B. (1979) Megacrysts from the Monastery kimberlite pipe, South Africa. In: Boyd FR, Meyer HOA (eds.) *The Mantle Sample: Inclusions in Kimberlites and Other Volcanics.* AGU, Washington, pp. 227-243

Harte, B. (1983) Mantle peridotites and processes - the kimberlite sample. In : Hawkesworth CJ, Norry MJ (eds) *Continental basalts and mantle xenoliths.* Shiva, Cheshire, pp. 46-91

Harte, B. and Gurney, J.J. (1975) Evolution of clinopyroxene and garnet in an eclogite nodule from the Roberts Victor kimberlite pipe, South Africa. *Phys Chem Earth* **9,** 367-388

Harte, B. and Gurney, J. J. (1981) The mode of formation of chromium-poor megacryst suites from kimberlites. *J Geol* **89,** 749-753

Hochstaedter, A. G., Gill, J. B., Kusakabe, M., Newman, S., Pringle, M., Taylor, B. and Fryer, P. (1990) Volcanism n the Sumisu Rift, I. Major element, volatile and stable isotope geochemistry. *Earth planet. Sci. Lett.* **100**, 179-194.

Javoy, M. 1980 $^{18}O/^{16}O$ and D/H ratios in high temperature peridotites. *Colloques International du CNRS* **272,** 279-287.

Kuroda, Y., Suzuoki, T., Matsuo, S. and Aoki, K.-I. (1975) D/H ratios of the coexisting phlogopite and richterite from mica nodules and a peridotite in South African kimberlites. *Contrib. MIneral. Petrol.* **52,** 315-318.

Kuroda, Y., Suzuoki, T. and Matsuo, S. (1977) Hydrogen isotope composition of deep seated water. *Contrib. Mineral. Petrol.* **60**, 311-315.

Kyser, T. K. (1986) Stable isotope variations in the mantle. In: Valley, J. W., Taylor, H. P., Jr.,and O'Neil, J. R. (eds) *Stable isotopes in high temperature geological processes. Mineralogical Society of America Reviews in Mineralogy* **16**, 141-164.

Kyser, T. K. (1990) Stable isotopes in the continental lithospheric mantle. In. Menzies, M. A. and Hawkesworth, C. J. (eds) *Continental Mantle.* Oxford University Press, Oxford. pp. 127-156.

Kyser, T. K. and Javoy, M. (1981) Stable isotope relations in the Loihi seamount. *EOS, Trans. Amer. geophys Union* **62**, 1083.

Kyser, T. K. and O'Neil, J. R. (1984) Hydrogen isotope systematics of submarine basalts. *Geochim. Cosmochim. Acta* **48**, 2123-2133.

Kyser, T. K., Cameron, W. E. and Nisbet, E. G. (1986) Boninite petrogenesis and alteration history: Constraints from stable isotope compositionso of boninites from Cape Vogel, New Caledonia and Cyprus. *Contrib. Mineral. Petrol.* **92**, 1-5.

Nixon PH, Boyd FR (1973b) The discrete nodule (megacryst) association in kimberlites from northern Lesotho. In: Nixon PH (ed.) *Lesotho Kimberlites.* Lesotho National Development Corporation, Maseru, pp. 67-75

Poreda, R. (1985) Helium-3 and deuterium in back-arc basalts: Lau Basin and the Mariana Trough. *Earth planet. Sci. Lett.* **73**, 244-254.

Poreda, R., Schilling, J.-G. and Craig, H. (1986) Helium and hydrogen isotopes in ocean-ridge basalts north and south of Iceland. *Earth planet. Sci. Lett.* **78**, 1-17.

Rison, W. and Craig, H. Loihi seamount: Mantle volatiles in the basalts. *EOS, Trans. Amer. geophys Union* **62**, 1083.

Sheppard, S. M. F. and Dawson, J. B. (1975) Hydrogen, carbon and oxygen isotope studies of megacryst and matrix minerals from Lesothan and South African kimberlites. *Phys. Chem Earth* **9**, 747-763.

Sheppard, S. M. F. and Epstein, S. (1970) D/H and $^{18}O/^{16}O$ ratios of minerals of possible mantle or lower crustal origin. *Earth planet. Sci. Lett.* **9**, 232-239.

Sheppard, S. M. F. and Harris, C. Hydrogen and oxygen isotope geochemistry of Ascension Island lavas and granites: variation with crystal fractionation and interaction with sea water. *Contrib. Mineral. Petrol.* **91**, 74-81.

Skogby H. S., Bell, D. R. and Rossman, G. R. (1990) Hydroxide in pyroxenes; variations in the natural environment. *Amer. Mineral.* **75**, 764-774

Skogby H. S., Rossman, G. R. (1991) The intensity of amphibole OH bands in the infrared absorption spectrum. *Phys. Chem. Minerals* **18**, 64-68

Smith, D.and Boyd, F. R. (1987) Compositional heterogeneities in a high temperature lherzolite nodule and implications for mantle processes. In: Nixon PH (ed) *Mantle xenoliths.* John Wiley & Sons, Chichester, pp. 551-561

Smyth J. R., Bell, D. R. and Rossman, G. R. (1991) Hydroxyl in upper mantle clinopyroxenes. *Nature* **35**, 732-735

Taylor, H. P., Jr. (1977) Water/rock interaction and the origin of H_2O in granitic batholiths. *J. geol. Soc. London* **133**, 509-558.

Weis, D., Demaiffe, D., Cauet, S. and Javoy, M. (1987) Sr, Nd, O and H isotopic ratios in Ascension Island lavas and plutonic inclusions; cogenetic origin. *Earth planet. Sci. Lett.* **82**, 255-268.

Wyllie, P. J. (1970) Ultramafic rocks and the upper mantle. *Mineral. Soc. Amer. spec. Paper* **3**, 3-32

Sample	Extrct wt	µmoles H2O	µmoles CO2	∂D	µmoles H2O	µmoles CO2	∂D	prev ∂D	memory	mem crct	µmole	µmole	µmole	µmole	∂D smpl	∂D smpl
	(mgrams)	obs LT	obs LT	obs LT	obs HT	obs HT	obs HT	High Temp	blank	∂D HT	H2O LT	H2O HT	CO2 LT	CO2 HT	bl=-140	bl=-110
blank	0	1.13	0.25	NA	2.97	1.7	-111.3									
augite																
PMR.53.500	500	3.1	0.15	NA	10.44	1.88	-100.2	NA			2.0	7.5	-0.1	0.2	-84.4	-96.4
PMR.53b.1000	1000.2	4.51	0.37	-84.85	20.45	4.06	-118.8	-84.9	1.84	-122.2	3.4	17.5	0.1	2.4	-119.2	-124.3
PMR.53.1000	1000	4.02	*.4	-113.2	18.03	2.92	-111.5	-113.2	1.62	-111.3	2.9	15.1	0.2	1.2	-105.7	-111.6
PMR.53.200	200	1.38	0.26	NA	5.43	1.67	-129.6	NA			0.3	2.5	0.0	0.0	-117.1	-153.4
KBH-2.1000	1000	3.85	0.61	SNA	41.59	21.63	-107.4	SNA			2.7	15.0	0.4	19.9	-270.0	-275.9
KBH-2.2000	2039.3	1.95	NSOA	NA	47.24	7.5	-79.7	NA			0.8	44.3	-	5.8	-75.7	-77.7
opx																
KBH-1.1300	1300	4.12	0.54	-106.1	16.38	2.9	-114.4	-106.1	1.47	-115.2	3.0	13.4	0.3	1.2	-109.7	-116.4
KBH-1.650	650	3	0.39	-154	9.76	2.05	-113.4	-154	0.88	-109.4	1.9	6.8	0.1	0.4	-96.0	-109.1
KBH-1.200	200	1.64	0.3	NA	5.06	1.55	-89.8	NA			0.5	2.1	0.1	-0.2	-18.5	-61.1
garnet																
MON-9.1000	1000	4.48	0.44	-99.2	6.95	2.66	-115.7	-98.6	0.62	-117.4	3.4	4.0	0.2	1.0	-100.5	-122.9
MON-9.1800	1800	5.15	0.61	-116.62	14.21	0.93	-78.3	-116.7	1.28	-74.5	4.0	11.2	0.4	-0.8	-57.2	-65.1
MON-9.3000	3000	4.3	0.54	-91.31	12.16	4.29	-110.7	-91.3	1.09	-112.6	3.2	9.2	0.3	2.6	-103.8	-113.5
KLV-18.1800	1809	11.79	1.24	NA	18.94	7.83	-80.7	NA			10.7	16.0	1.0	6.1	-69.7	-75.3
KM-1493.18	1799	4.49	0.21	-132.3	4.79	3.22	-124.2	-132.3	0.43	-123.4	3.4	1.8	0.0	1.5	-96.3	-145.3

Table 1. Isotopic compositions and yields of H2 and CO2 for all samples extracted (compiled by PDI)

Fig. 1. Isotopic composition of H in nominally anhydrous minerals as a function of the high-temperature yield of H_2. Error bars are based on the fraction of the blank contribution (3 μmol) to each sample and an assigned uncertainty in the blank.

Fig. 1. The isotopic composition of H in nominally anhdrous mantle minerals

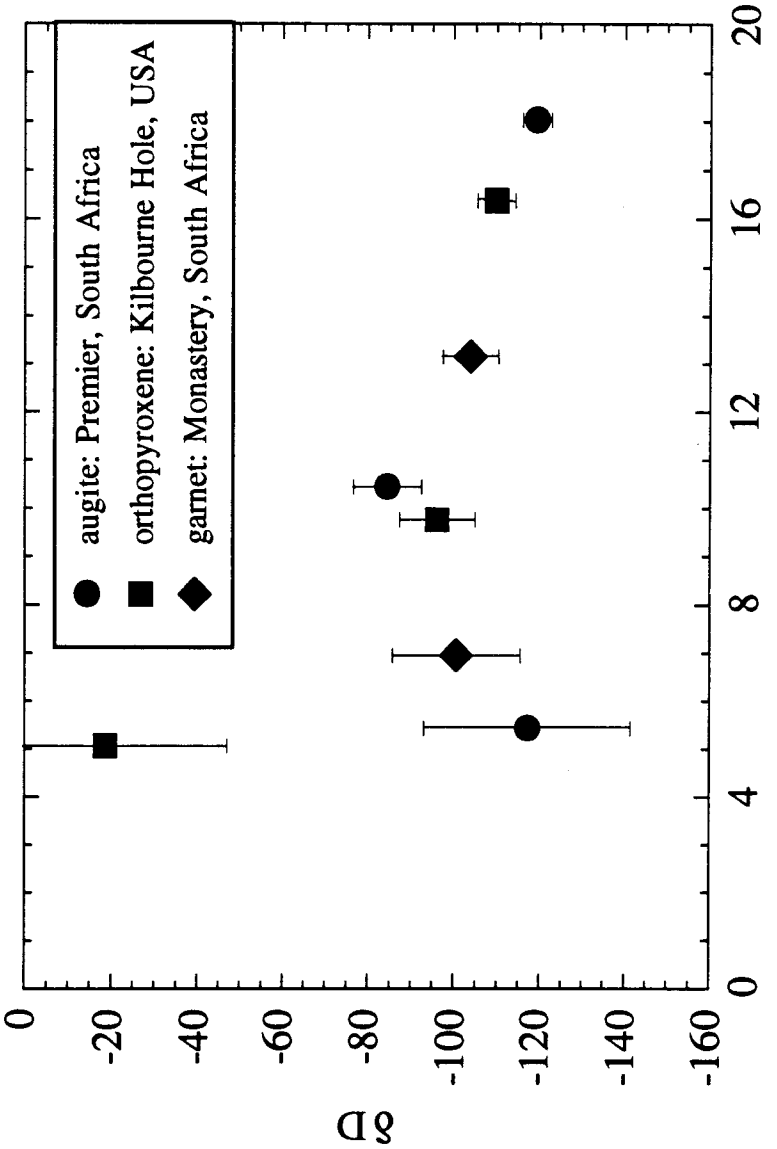

Fig. 2. Frequency distribution of isotopic compositions of H in (a) minerals of mantle origin, including the nominally anhydrous minerals analyzed in this study, and (b) glassy oceanic lavas. Open and solid bars for Hawaii indicate the datasets of Garcia *et al.* (1989) and Kyser and O'Neil (1984), respectively.

Fig. 2a. δD in Mantle Minerals

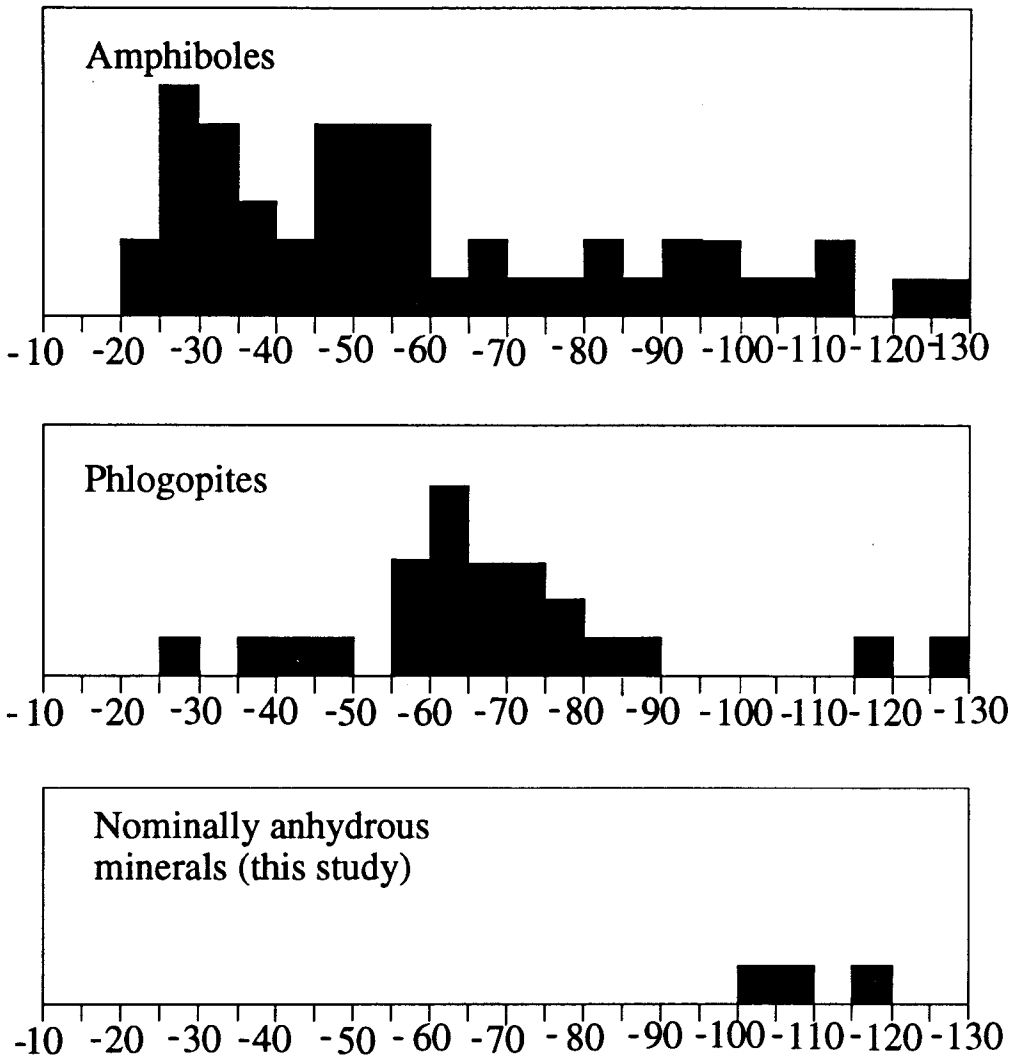

Fig. 2b. δD in Oceanic Basalts

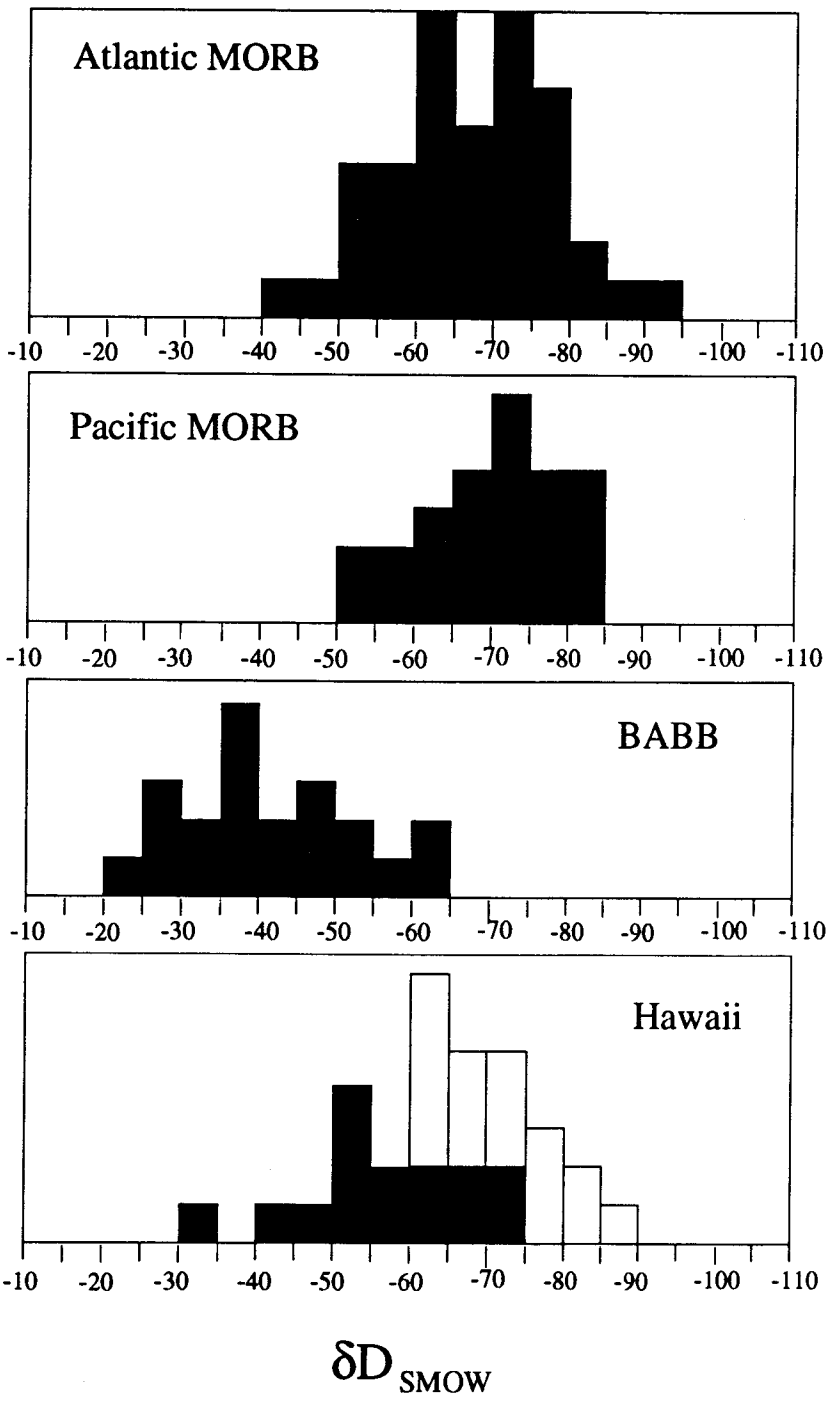

Appendix 2

Water in mantle minerals.

Nature **357**, 646-647.

characteristics of the electrode/silicon interface as the transition reaches each electrode: the rectifying Schottky barrier is replaced by an ohmic metal-to-metal interface.

Independently and very recently, Gilman reviewed[13] MNM transitions in a range of semiconductors and insulators and showed some striking correlations between the experimental 'metallization pressures' and values calculated from the polarization catastrophe model. He predicts that many such transitions should be observable under indenters, and speculates whether plastic shear may play a role in the MNM transition. He also suggests that, alternatively, 'metallization' and dislocation motion may both be correlated with the excitation of bonding electrons into antibonding states, and offers some supporting evidence from the literature.

In the meantime, Pirouz *et al.*[14] have been conducting a separate series of experiments to study the partial transformation of diamond-cubic silicon to a diamond-hexagonal form by indentation at 400–650 °C (Clarke, Pharr and colleagues' experiments were at room temperature). They show that this process is martensitic (shear-induced); here the deviatoric stress component under an indenter is crucial. But the authors have apparently not looked for an MNM transition in the hexagonal silicon.

There remains the question of how the amorphous, conducting phase[2] arises. Conventional pressurization experiments have hitherto shown no sign of it. This is addressed in Pharr's latest contribution[6]. He marshals the extensive published evidence to show that silica, ice and several semiconductors other than silicon become amorphous under pressure. Indeed, non-hydrostatic stresses, at the edge of an indentation, help give silica two distinct pressure-induced amorphous phases. And it is also clear that thin amorphous silicon films can undergo an abrupt MNM transition under hydrostatic pressure[15] (just as unpressurized amorphous silicon 'melts' to produce a denser, metallic melt). Perhaps silicon will amorphize only under a combination of hydrostatic and deviatoric stresses. Pharr simply concludes that "at some point in the transformation, an amorphous phase is formed". As people are wont to say in grant proposals, more research is clearly needed. □

Robert W. Cahn is in the Department of Materials Science and Metallurgy, University of Cambridge, Pembroke Street, Cambridge CB2 3QZ, UK.

1. Huff, N. R. in *Concise Encyclopedia of Semiconducting Materials and Related Technologies* (eds Mahajan, S. & Kimerling, L.) 478–492 (Pergamon, Oxford, 1992).
2. Clarke, D. R., Kroll, M. C., Kirchner, P., Cook, R. F. & Hockey, B. J. *Phys. Rev. Lett.* **60**, 2156–2159 (1988).
3. Pharr, G. M., Oliver, W. C. & Clarke, D. R. *J. electron. Mater.* **19**, 881–887 (1990).
4. Pharr, G. M., Oliver, W. C. & Harding, D. S. *J. Mater. Res.* **6**, 1129–1130 (1991).
5. Pharr, G. M. *et al. J. Mater. Res.* **7**, 961–972 (1992).
6. Pharr, G. M. in *Thin Films: Stresses and Mechanical Properties III* (eds Nix, W. D. *et al.*) (Materials Research Society, Pittsburgh, in the press).
7. Mott, N. F. *Proc. Phys. Soc.* **A62**, 416 (1949).
8. Cottrell, A. *An Introduction to the Modern Theory of Metals*, 16–20 (Institute of Metals, London, 1988).
9. Edwards, P. P. & Sienko, M. J. *Phys. Rev.* **B17**, 2575–2581 (1978).
10. Edwards, P. P. & Sienko, M. J. *Int. Rev. phys. Chem.* **3**, 83 (1983).
11. Gerk, A. P. & Tabor, D. *Nature* **271**, 732 (1978).
12. Gridneva, I. V., Milman, Y. V. & Trifilov, V. I. *Phys. Stat. Sol.* **14**, 177 (1972).
13. Gilman, J. J. *J. Mater. Res.* **7**, 535–538 (1992).
14. Pirouz, P., Chaim, R., Dahmen, U. & Westmacott, K. H. *Acta metall. Mater.* **38**, 313–322; 323–328; 329–336 (1990).
15. Shimomura, O. *et al. Phil. Mag.* **29**, 547 (1974).

EARTH SCIENCES

Water in mantle minerals

David R. Bell

NEW experiments suggest that olivine, probably the most abundant mineral in the Earth to a depth of 400 km, can incorporate substantial amounts of hydrogen under water-rich, high-pressure conditions. This work, reported by Bai and Kohlstedt on page 672 of this issue[1], addresses two basic questions facing those looking at the role of water in the evolution of the Earth: how much is there and where is it stored?

Geologists recognize that dynamic physical and chemical processes in the Earth's interior — such as those which dictate the distribution of the continents, control the generation and eruption of magmas, and perhaps lead to the accumulation of the atmosphere and oceans themselves — can be strongly influenced by the presence of water. Since the suggestion[2] that a protracted degassing of the Earth's interior gave rise to the atmosphere and oceans, the search has been on for suitable host phases for mantle hydrogen. Although current opinion favours early, perhaps catastrophic release of volatiles from the Earth's interior, the identity of H storage sites remains important for understanding water recycling and for predicting the behaviour of H during processes deep in the Earth. This knowledge should give a better appreciation of how the evolution of the atmosphere and oceans is linked to processes in the Earth's interior.

The presence of hydrous minerals such as amphiboles and micas in mantle-derived xenoliths (accidental rock fragments transported to the surface in volcanic eruptions) provides clear evidence of water storage in the upper mantle. Unfortunately, it is difficult to generalize these local observations, because the mantle is known to be heterogeneous, especially under the continents whence many of the xenoliths are derived. Many of the observed hydrous minerals may be local phenomena generated by relatively small-scale magmatic events, thereby not representing the mantle at large. As we don't have direct access to most of the mantle, our understanding must rely heavily on laboratory studies.

Experimental phase-equilibrium studies which simulate conditions in the Earth's interior can place powerful constraints on the expected phase assemblages in the upper mantle. Studies on compositions in the mantle-analogue system, MgO–SiO_2–H_2O, have produced a number of hydrous phases which are candidates for storing water in the mantle. However, many of these phases are apparently not stable at the high temperatures of average mantle and thus would be restricted to anomalously cold regions such as subducting slabs.

Minor components not accounted for in simple synthetic systems may stabilize small quantities of hydrous phases, which, because of the generally water-poor nature of the mantle (probably 0.01–0.1 per cent H_2O by weight), may be relatively important water reservoirs. Experimental studies on micas and amphiboles have revealed that certain compositional variants of these phases (particularly those rich in potassium and fluorine) are stable well into upper-mantle pressure and temperature conditions. Similarly, titanium seems to stabilize several of the humite group minerals (structures composed of alternating layers of olivine and brucite $[Mg(OH)_2]$) to mantle pressures and temperatures[3].

In general, the incompatible-element content of the upper mantle is low, and large concentrations of K, Ti or F-rich hydrous minerals cannot be supported. As a result, such hydrous minerals may be restricted to areas locally enriched in these elements, with the nature of the water storage sites depending on the scale of mantle chemical heterogeneities.

Here at Caltech, Rossman and co-workers have found small, but virtually ubiquitous quantities of H in the common, nominally anhydrous mantle minerals, such as olivine, garnet and the pyroxenes (see ref. 4). Hydrogen is bound in the mineral structure as hydroxyl groups (OH). Concentrations vary from less than 1 part per million (p.p.m.) up to 0.1 per cent H_2O by weight. The effect on the transport properties of the host phase[5], with its attendant implications for mantle rheology,

have motivated a number of studies of the olivine–H_2O system, including the present one by Bai and Kohlstedt. The nominally anhydrous minerals are the dominant constituents of the mantle, so they are potentially important reservoirs of H in the Earth's interior.

Hydrogen concentrations measured in minerals from natural mantle samples suggest OH-bearing capacities sufficient to account for the water content[6,7] of the depleted upper mantle (about 100–200 p.p.m.). Although the measurements on natural samples are valuable in demonstrating the ability of these phases to store OH, the concentrations are not easily generalized to average mantle. Because of the low H concentrations, relatively little is known about the substitution mechanisms by which OH is incorporated in these phases, where it sits in the mineral structure or how the concentrations are affected by pressure, temperature and a host of extensive parameters encountered in the mantle.

Bai and Kohlstedt have taken the first step in erecting a quantitative experimental framework for the understanding of the behaviour of H in this reservoir. Their study demonstrates that the hydrous component in olivine is stable to a temperature of 1,300 °C at relatively low pressure, thereby exhibiting considerably greater thermal stability than most hydrous magnesium silicates. If the hydrous components of other nominally anhydrous minerals, in particular pyroxenes, which appear[4] to contain the most OH of the common mantle minerals, behave similarly then these minerals may be able to store H under conditions where most stoichiometrically hydrous minerals break down.

It will be important to investigate the effect of pressure on the solubility of H in olivine and other mantle minerals, as Bai and Kohlstedt's experiments were conducted at pressures of the uppermost crust, and require considerable extrapolation to the mantle regime. As OH concentrations in olivine appear to be linked with certain point defects, it remains to be seen if saturation effects or other substitution mechanisms come into play at high water fugacities and perturb the reported systematics. □

David R. Bell is in the Division of Geological and Planetary Sciences, California Institute of Technology, Pasadena, California 91125, USA.

1. Bai, Q. & Kohlstedt, D. L. *Nature* **357**, 672–674 (1992).
2. Rubey, W. W. *Geol. Soc. Am. Bull.* **62**, 1111 (1951).
3. Khodyrev, O. Y., Agoshkov, V. M. & Slutskiy, A. B. *Trans. USSR Acad. Sci.* **312**, 255–258 (1990).
4. Bell, D. R. & Rossman, G. R. *Science* **255**, 1391–1397 (1992).
5. Mackwell, S. J., Kohlstedt, D. L. & Paterson, M. S. *J. geophys. Res.* **90**, 11319–11333 (1985).
6. Michael, P. *Geochim. Cosmochim. Acta* **52**, 555 (1988).
7. Dixon, J. E., Stolper, E. M. & Delaney, J. R. *Earth planet. Sci. Lett.* **90**, 87–104 (1988).

Appendix 3

Hydroxide in pyroxene: Variations in the natural environment.

by

H. S. Skogby, D. R. Bell and G. R. Rossman

The American MIneralogist **75**, 764-774

American Mineralogist, Volume 75, pages 764–774, 1990

Hydroxide in pyroxene: Variations in the natural environment

HENRIK SKOGBY,* DAVID R. BELL, GEORGE R. ROSSMAN
Division of Geological and Planetary Sciences, California Institute of Technology, Pasadena, California 91125, U.S.A.

ABSTRACT

A suite of 51 pyroxenes from a wide range of geological environments was examined with infrared spectroscopy. Small amounts of OH occur in nearly all the samples, suggesting that OH groups are a minor component of most pyroxenes. The OH concentrations vary (0.002–0.12 wt% OH) as a function of geological setting with the greatest amounts occurring in mantle-derived samples. The intensities of certain OH absorption bands are somewhat correlated with pyroxene composition, in particular with the presence of trivalent cations. This suggests that crystal chemical or compositional factors also control the OH incorporation. The OH incorporated in the pyroxene structure is easily distinguishable from OH owing to amphibole lamellae, which usually occur in diopsides and often in orthopyroxenes. OH in pyroxene is probably a function of the activity of hydrous components during crystallization but may also depend on postcrystallization changes in the geological environment.

INTRODUCTION

Pyroxenes ideally are anhydrous, although in a few instances a small content of hydroxide has been identified (Wilkins and Sabine, 1973; Beran, 1976). Some of the OH is present in submicroscopic amphibole lamellae or other biopyribole lamellae, as seen in electron microscopy studies (Veblen and Buseck, 1981). Ingrin et al. (1989) showed that OH also occurs in diopsides that do not contain amphibole lamellae. The non-amphibole OH may be present on the O sites in the pyroxene structure, with cation substitutions or vacancies compensating for the charge of the H^+ ion (Beran, 1976). We have demonstrated that pyroxenes with tetrahedral Fe^{3+} are capable of incorporating H in laboratory experiments (Skogby and Rossman, 1989). However, the generality of the occurence of OH in pyroxenes has not been explored, and the relationship between OH concentration and geological provenance has not been established. There is a special interest in the study of mantle-derived pyroxenes because of the comparatively high OH content of coexisting phases (Miller et al., 1987; Aines and Rossman, 1984) and the possible effects of hydrous pyroxenes on physical properties of the mantle.

The aim of this investigation was to survey the occurrence of OH in a wide range of pyroxenes from different geological environments and to determine if there are significant natural variations in the OH content of the pyroxenes.

EXPERIMENTAL METHODS

Pyroxenes from a wide range of geological environments have been studied, including samples from metamorphic, volcanic, pegmatitic, and mantle-derived rocks. Sample types, localities, and geological environments are listed in Table 1. We examined samples ranging from essentially gem quality to turbid or altered, as well as samples with abundant inclusions.

Sample preparation consisted of orienting single crystals by morphology and interference figures, followed by cutting and doubly polishing to a typical thickness of 0.2–1.0 mm. The orientation of most samples was confirmed by IR reflectance spectroscopy. A few samples (nos. 34, 35, and 43) were available only in small amounts and could not be oriented by these methods.

Polarized spectra in the infrared region were obtained with a Nicolet 60SX Fourier transform IR spectrophotometer using a $LiIO_3$ polarizer. The three optical directions were measured on (100) and (010) sections of most samples, but (001) and a* sections were also studied for a few samples. For the orthopyroxenes, the orientation convention α = (E//b, b ~ 8.9 Å), β = (E//a, a ~ 18 Å), γ = (E//c, c ~ 5.2 Å) was used where E is the vibration direction of the incident electric vector. Unpolarized spectra were measured on the few unoriented samples (nos. 34 and 35) and on a polycrystalline sample (no. 43). A beam-path free from inclusions was carefully sought, but in some cases inclusions were impossible to avoid.

To test the influence of visible inclusions on the OH spectra, spectra were obtained from samples with both clear and included regions, which were masked to isolate each region. If the inclusions were amphibole lamellae, the OH pattern of amphiboles was readily apparent. Oth-

* Present address: Uppsala University, Institute of Geology, Department of Mineralogy and Petrology, Box 555, S-751 22 Uppsala, Sweden.

0003-004X/90/0708-0764$02.00

TABLE 1. Sample types, localities, and ranked OH contents for pyroxenes

Sample no.	Locality	OH abundance: OH pfu*	OH abundance: Wt% OH	Geological environment	Reference no.
47 omphacite	Roberts Victor Mine, S. Africa	0.016	0.12	eclogite xenolith in kimberlite	HRV 147 (Hatton, 1978)
20 augite	Kilbourne Hole, NM	0.014	0.10	xenolith in basalt	GRR 1656 (from S. Huebner)
30 aegirine	Caithness, Scotland	0.012	0.088	authigenic, sediment	GRR 572 (Fortey and Michie, 1978)
13 diopside**	Sydenham, Ontario	0.012	0.085	high-grade pyroxeneite	GRR 1620
17 augite	Hopi Butte, AZ	0.0095	0.073	xenocryst in mantle diatreme	GRR 1646
16 diopside	Garnet Ridge, AZ	0.0093	0.073	xenocryst in mantle diatreme	GRR 1648
7 diopside	Maui, Hawaii	0.0087	0.066	megacryst in basalt	CIT 3477
32 enstatite	India	0.0083	0.066	metamorphic	GRR 1650b
48 enstatite	Premier Mine, S. Africa	0.0061	0.050	megacryst in kimberlite	PMR 54
33 enstatite	India	0.0061	0.050	metamorphic	GRR 1650a
50 diopside	Akhmat, Soviet Union	0.0057	0.045	metamorphic?	CIT 13123
40 diopside	Elephant Butte, NM	0.0047	0.037	xenolith in basalt	GRR 1645
1 spodumene	Pala, CA	0.0043	0.041	granitic pegmatite	GRR 1659
3 diopside	Outokumpu, Finland	0.0036	0.028	metamorphic	CIT 8085
9 augite	Cedar Butte, OR	0.0035	0.027	volcanic	GRR 583
46 augite	Kangan, Andra Pradish, India	0.0032	0.026	volcanic?	GRR 1660 (from S. Huebner)
6 diopside	Binntal Vallis, Switzerland	0.0032	0.025	metamorphic	GRR 472
37 enstatite	Chichijima, Bonin Islands, Japan	0.0026	0.022	boninite lava	DB 82 (Dobson, 1986)
45 aegirine	synthetic	0.0025	0.018	synthetic, hydrothermal	GRR 264 from WA Dollase (GAW-1)
5 diopside	Mount Bity, Madagascar	0.0023	0.018	metamorphic	GRR 637
39 hedenbergite	Nordmarken, Sweden	0.0022	0.016	metamorphic	NMNH 16168
18 enstatite	Alpine, TX	0.0020	0.016	lower crustal	ALP1 (Duba et al., 1979, from S. Huebner)
12 diopside**	Sinnidal, Norway	0.0019	0.015	metamorphic	GRR 1621
8 aeg.-aug.	Magnet Cove, AR	0.0019	0.014	nepheline syenite pegmatite	CIT 349
10 diopside	Obersulzbach, Austria	0.0018	0.014	metamorphic	CIT 2593
51 augite	Juan de Fuca Ridge	0.0016	0.012	gabbroic xenolith in basalt	5-0 (Dixon et al., 1986)
19 enstatite	Kyogle, Australia	0.0014	0.011	basalt xenolith	GRR 1655 (from S. Huebner)
28 diopside	Vesuvius, Italy	0.0012	0.009	rhyolitic pumice	GRR 205 (NMNH C2429)
2 diopside	Rajasthan, India	0.0010	0.008	metamorphic	CIT 11221
38 enstatite	Zabargad, Egypt	0.0008	0.007	low-P metamorphic	GRR 649 (AMNH 49033)
21 diopside	Kauai, Hawaii	0.0007	0.006	oxidized alkali picrite	GRR 603 (Johnston and Stout, 1984)
31 enstatite**	Bamble, Norway	0.0007	0.006	megacryst	GRR 40
4 diopside	Natural Bridge, NY	0.0006	0.005	calcite vein	CIT 2135
36 enstatite**	Nain, Labrador	0.0006	0.005	megacryst, anorthosite	GRR 1616 (Veblen and Bish, 1988)
35 esseneite	Buffalo, WY	0.0005	0.004	buchite	I-90 (Foit et al., 1987)
41 diopside*	Magog, Ontario	0.0005	0.004	metamorphic	GRR 1649
14 diopside	DeKalb, NY	0.0003	0.003	metamorphic limestone	GRR 664
29 aegirine	Mount Saint Hilaire, Quebec	0.0002	0.002	nepheline syenite	CIT 8449
25 aegirine**	Magnet Cove, AR	0.0002	0.001	nepheline syenite pegmatite	CIT 11832
34 fassaite	Angra dos Reis meteorite	not detected		meteorite	GRR 290 (Keil et al., 1976)
44 diopside	synthetic	not detected		synthetic, KVO_3 flux	GRR 510 from J. Ito
11 hedenbergite	Harroult, Ontario	not determined†		metamorphic?	CIT 6859
15 diopside	Oka, Quebec	not determined†		metamorphic?	UCLA MS2824
22 hedenbergite**	Waldo Mine, NM	not determined†		metamorphic?	CIT 8308
23 hedenbergite**	Rio Marine, Elba, Italy	not determined†		metamorphic?	CIT 7494
24 hedenbergite**	Silver City, NM	not determined†		metamorphic?	UCLA MS2955
26 aegirine	Wausau, WI	not determined†		granitic rock	CIT 8193
27 omphacite	Möre, Norway	not determined†		eclogite	CIT 7491
42 clinoenstatite**	Chichijima, Bonin Islands, Japan	not determined†		boninite lava	MD-57 (Dobson, 1986)
43 omphacite	Burma (?)	not determined†		jade	GRR 814
49 omphacite	Roberts Victor Mine, S. Africa	not determined†		eclogite xenolith in kimberlite	390/4 (Hatton, 1978)

Note: OH concentrations were calculated using a molar absorptivity of ϵ = 150 liter/mole-cm and summed intensities for pyroxene bands in the three optical directions. NMNH = National Museum of Natural History, Smithsonian Institution. CIT = California Institute of Technology Mineral Reference Collection. AMNH = American Museum of Natural History, New York.

* Per formula unit, XYZ_2O_6.

** Visible evidence for turbidity or alteration in volume of measurement.

† OH concentration could not be determined because sample could not be oriented or was polycrystalline.

erwise, the inclusions did not contribute to the spectroscopic data, indicating that they were generally anhydrous phases.

The OH concentrations in the samples were calculated from the intensities of the OH bands according to Beer's law: Absorbance = ϵ × path length × OH concentration. The molar absorptivity (ϵ) was estimated by a number of methods described in the results section, assuming the

TABLE 2. Structural formulae of pyroxenes analyzed by electron microprobe

	1 sp	2 di	3 di	4 di	5 di	6 di	7 di	8 ae-aug	9 aug	10 di	12 di	13 di	14 di
Si	1.992	2.006	1.990	1.961	1.981	1.979	1.731	1.986	1.884	1.994	1.997	1.981	2.012
$^{[4]}$Al	0.008	0.000	0.010	0.039	0.007	0.021	0.269	0.014	0.116	0.006	0.003	0.019	0.000
$^{[6]}$Al	0.997	0.016	0.023	0.017	0.000	0.007	0.096	0.017	0.048	0.019	0.052	0.027	0.013
Ti	0.000	0.000	0.000	0.003	0.000	0.000	0.047	0.014	0.026	0.000	0.002	0.001	0.000
Fe^{3+}	0.000	0.000	0.000	0.044	0.043	0.054	0.122	0.622	0.027	0.040	0.036	0.068	0.000
Cr	0.000	0.000	0.019	0.000	0.000	0.000	0.008	0.001	0.015	0.000	0.001	0.001	0.000
Mg	0.000	0.916	0.861	0.746	0.908	0.799	0.720	0.182	0.875	0.713	0.824	0.485	0.970
Fe^{2+}	0.001	0.069	0.089	0.171	0.040	0.107	0.106	0.120	0.171	0.213	0.126	0.413	0.016
Mn	0.000	0.002	0.002	0.004	0.003	0.006	0.004	0.012	0.004	0.021	0.001	0.025	0.000
Ca	0.001	0.971	0.976	0.987	1.009	0.989	0.846	0.377	0.810	0.941	0.867	0.900	0.971
Na	0.005	0.020	0.030	0.028	0.009	0.038	0.051	0.655	0.024	0.053	0.091	0.080	0.017

	28 di	29 ae	30 ae	31 en	32 en	33 en	34** fas	35 ess	36† en	37 en	38 en	39 hd	40 di
Si	1.801	2.007	1.995	2.004	2.001	1.999	1.728	1.360	1.93	1.984	1.976	1.980	1.926
$^{[4]}$Al	0.199	0.000	0.000	0.000	0.000	0.001	0.272	0.636	0.07	0.016	0.024	0.006	0.074
$^{[6]}$Al	0.069	0.041	0.000	0.004	0.032	0.017	0.161	0.000	0.04	0.000	0.017	0.000	0.007
Ti	0.032	0.010	0.000	0.000	0.002	0.000	0.059	0.029	0.00	0.001	0.001	0.000	0.014
Fe^{3+}	0.081	0.804	0.980	0.000	0.000	0.000	0.000	0.605	0.00	0.008	0.005	0.041	0.039
Cr	0.002	0.000	0.001	0.001	0.000	0.000	0.005	0.000	0.01	0.009	0.001	0.000	0.014
Mg	0.739	0.016	0.003	1.698	1.525	1.730	0.568	0.339	1.49	1.718	1.975	0.416	0.954
Fe^{2+}	0.123	0.073	0.000	0.283	0.417	0.238	0.223	0.026	0.45	0.222	0.000	0.502	0.066
Mn	0.004	0.028	0.000	0.000	0.008	0.005	0.002	0.004	0.01	0.004	0.000	0.064	0.003
Ca	0.933	0.142	0.001	0.010	0.015	0.009	0.968	0.982	0.01	0.038	0.000	0.984	0.889
Na	0.018	0.878	1.019	0.000	0.000	0.000	0.002	0.017	0.00	0.000	0.001	0.007	0.014

Note: The formulae are normalized to four cations.
* 18, 19, and 20: Analyses provided by J.S. Huebner.
** 34: Analysis from Hazen and Finger (1977).
† 36: Analysis from Veblen and Bish (1988).
‡ 0.011 K also present in sample.

species OH expressed in mol/L. Absorbances were calculated by summing the peak height in the three optical directions for all peaks assumed to be caused by intrinsic (pyroxene) OH as

$$\mathrm{Abs}_{\mathrm{sum}} = \sum_{i=1}^{n} (\mathrm{Abs}_i(\alpha) + \mathrm{Abs}_i(\beta) + \mathrm{Abs}_i(\gamma)).$$

For a few samples where spectra in all three optical directions could not be obtained, the OH concentration was estimated by comparison with spectra of other samples.

The samples were analyzed with a JEOL 733 electron microprobe at 15 kV accelerating potential and 15 nA Faraday cup current. Data were corrected as described in Skogby and Rossman (1989). Structural formulas of the samples normalized to four cations are in Table 2.

RESULTS

IR spectroscopy

Narrow absorption bands occur in the 3000–3700 cm^{-1} region of the infrared spectra of nearly all samples. Both OH and H_2O absorb in this region. In nearly all cases, the absence of a water combination band near 5200 cm^{-1} indicates that the absorbing species is hydroxide ion. The only exceptions were altered or fibrous samples that showed evidence of the much broader band of liquid H_2O. The OH^- ion is present in all our natural samples, except the meteoritic fassaite (no. 34). The spectroscopic features (band position, intensity, polarization) vary among samples depending on composition, geologic environment, and locality. The polarized spectra obtained on oriented sections show that all bands are pleochroic, which means that the OH dipoles giving rise to these bands are crystallographically oriented.

For purposes of classification, the OH^- absorption bands in pyroxenes have been divided into two classes (Skogby and Rossman, 1989). The first class occurs at higher wavenumbers (approximately 3675 cm^{-1}) in the spectra of many pyroxenes and resembles the sharp peaks in amphibole spectra. These bands, referred to here as amphibole bands, are most prominent in the spectra of somewhat altered pyroxenes and in samples with visible amphibole lamellae. They are weaker or absent in gem-quality pyroxenes. The second class occurs at lower wavenumbers in the spectra of all hydrous pyroxenes, consisting of broader absorptions, which we call pyroxene bands. They are also present in the spectra of gem-quality samples and are not associated with foreign phases.

The pyroxene bands occur between 3000–3640 cm^{-1} and for clinopyroxenes can be further divided into two groups, based on pleochroic behavior (Table 3). Three bands may occur around 3350, 3450, and 3525 cm^{-1} and have the pleochroism $\gamma > \alpha = \beta$. Another band is usually present at 3620–3640 cm^{-1} with $\alpha = \beta$, $\gamma = 0$. For different samples there is a large range of absorption intensities per unit thickness, suggesting large variations in OH concentration.

TABLE 2—*Continued*

16 di	17 aug	18* en	19* en	20* aug	21 di	25 ae
1.983	1.841	1.815	1.915	1.776	1.710	2.002
0.017	0.159	0.185	0.085	0.224	0.228	0.000
0.109	0.084	0.089	0.068	0.160	0.049	0.025
0.001	0.039	0.014	0.004	0.041	0.062	0.030
0.007	0.054	0.075	0.000	0.072	0.245	0.760
0.063	0.008	0.001	0.009	0.000	0.000	0.001
0.807	0.824	1.367	1.538	0.732	0.748	0.053
0.037	0.131	0.380	0.305	0.155	0.013	0.111
0.002	0.003	0.006	0.004	0.003	0.004	0.015
0.810	0.792	0.058	0.062	0.745	0.882	0.152
0.164	0.065	0.010	0.010	0.092	0.059	0.851

41 di	43 omp	45 ae	47‡ omp	48 en	50 di	51 aug
1.967	2.005	1.976	1.969	1.977	2.012	1.927
0.007	0.000	0.015	0.031	0.023	0.000	0.073
0.000	0.567	0.000	0.558	0.014	0.011	0.031
0.001	0.006	0.001	0.008	0.007	0.002	0.015
0.060	0.000	0.978	0.000	0.003	0.000	
0.001	0.000	0.001	0.002	0.003	0.019	0.008
0.776	0.407	0.002	0.425	1.734	0.947	0.951
0.152	0.032	0.000	0.058	0.191	0.032	0.187
0.014	0.003	0.000	0.001	0.004	0.002	0.006
1.020	0.396	0.000	0.478	0.033	0.950	0.798
0.003	0.583	1.026	0.459	0.011	0.025	0.016

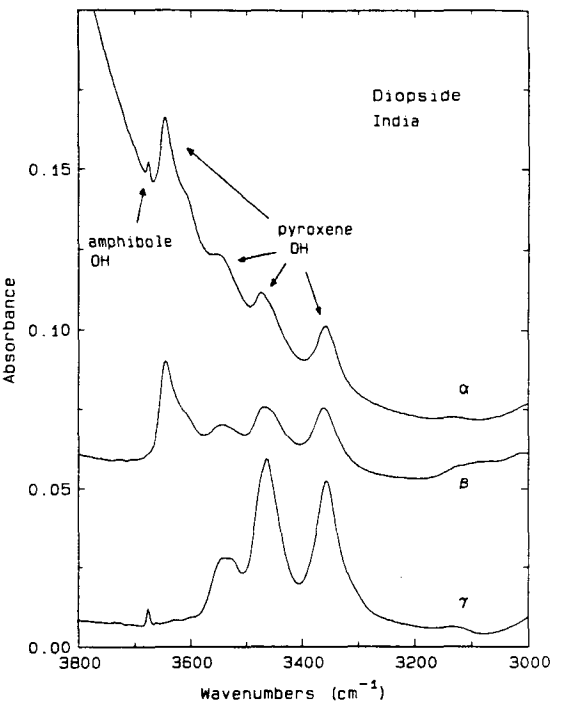

Fig. 1. Polarized IR spectra (α, β, γ) of diopside from India (no. 2). Spectra normalized to 1 mm thickness. Note weak amphibole band at 3675 cm^{-1}; other bands are referred to as pyroxene bands.

Diopside-hedenbergite

Diopside spectra usually have four pyroxene bands (Fig. 1). Three bands occur close to 3355, 3460, and 3535 cm^{-1} in most samples, with the pleochroism $\gamma > \alpha = \beta$. A fourth band occurs at 3645 cm^{-1} with $\alpha = \beta$ and $\gamma = 0$. The band at 3460 cm^{-1} is usually the strongest in the spectrum. The position and pleochroism of the absorption bands are similar for different samples, but the absolute intensities vary strongly (Fig. 2). Bands that are attributed to amphibole are present in the spectra of most diopsides. Spectra obtained from a synthetic diopside grown by J. Ito from a KVO_3 flux (no. 44) show neither pyroxene nor amphibole absorption bands, demonstrating that these bands arise from something other than the lattice vibrations of pyroxene itself.

Hedenbergite spectra are similar to diopside spectra, with two absorption bands at 3440 and 3520 cm^{-1} and a weak 3640 cm^{-1} band. Some spectra have several sharp amphibole peaks, resembling spectra of amphiboles of intermediate actinolite-grunerite compositions (Burns and Strens, 1966). A broad band at 3200–3700 cm^{-1} caused by molecular water occurs in the spectra of some altered hedenbergites.

Augite

Three pyroxene bands are usually present in augite spectra (Fig. 3). Two occur at 3465 and 3520 cm^{-1} with

TABLE 3. General properties of pyroxene absorption bands

Sample	Wavenumber [cm^{-1}] 3620–3640	3520–3535	3450–3465	3350–3355
Diopside	$\alpha = \beta, \gamma = 0$	$\gamma > \alpha = \beta$	$\gamma > \alpha = \beta$	$\gamma > \alpha = \beta$
Hedenbergite	$\alpha = \beta, \gamma = 0$	$\gamma > \alpha = \beta$	$\gamma > \alpha = \beta$	—
Augite	$\alpha = \beta, \gamma = 0$	$\gamma > \alpha = \beta$	$\gamma > \alpha = \beta$	—
Aegirine-augite	$\alpha > \beta > \gamma$	—	—	—
Compositional association	M^{3+}	Fe^{2+}	Fe^{2+}, Mg	Mg
Thermal stability*	most stable	unstable	stable	unstable
Reequilibration**	increase	decrease	increase	decrease

* Thermal stability refers to heating experiments performed on diopsides and aegirine-augite in air or H_2 at one atmosphere pressure (Skogby and Rossman, 1989).

** Reequilibration refers to hydrothermal experiments performed on diopsides at 600–800 °C and 1–2 kbar pressure.

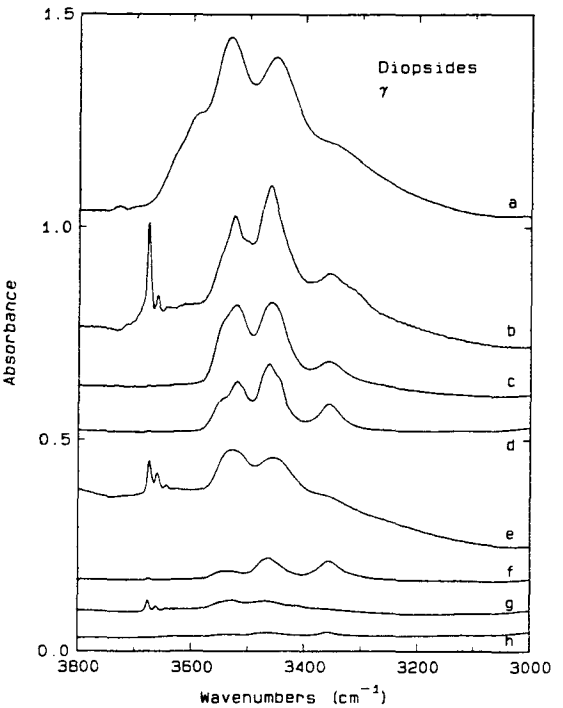

Fig. 2. IR spectra of diopsides in γ-polarization plotted for 1 mm thickness, (a) no. 16, Garnet Ridge, AZ, (b) no. 3, Outokumpu, Finland, (c) no. 6, Binntal Vallis, Switzerland, (d) no. 5, Mount Bity, Madagascar, (e) no. 12, Sinnidal, Norway, (f) no. 2, Rajasthan, India, (g) no. 4, Natural Bridge, NY, (h) no. 14, DeKalb, NY.

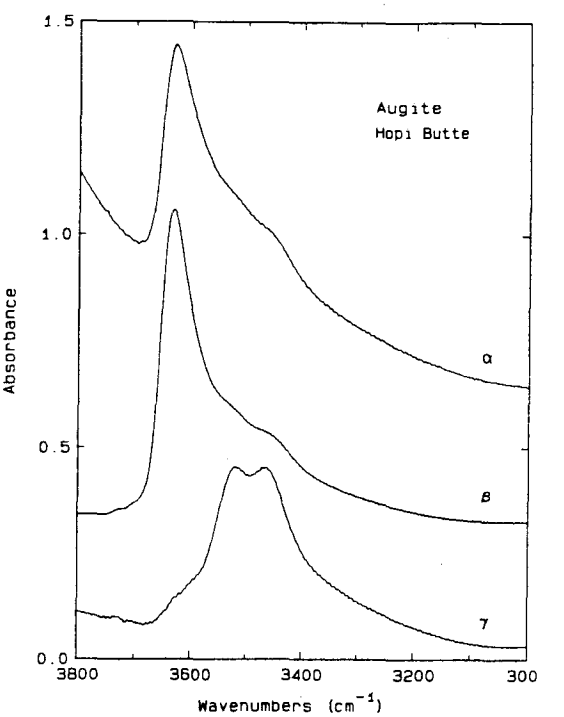

Fig. 3. Polarized spectra of augite (no. 17, Hopi Butte) normalized to 1 mm thickness.

the pleochroism $\gamma > \alpha = \beta$, and a third band, usually the strongest, occurs at 3635 cm^{-1} with $\alpha = \beta$, $\gamma = 0$. In contrast to diopside, there is no band around 3355 cm^{-1}. The absorption bands in augite spectra are usually broader than in diopside spectra. Amphibole bands have not been detected in augite spectra.

Aegirine and aegirine-augite

Two absorption bands may occur in the spectra of aegirine and aegirine-augite: one band at 3620–3650 cm^{-1} (Fig. 4), and another band which is sometimes present around 3550 cm^{-1}. In contrast to the 3630–3640 cm^{-1} band in augite and diopside, the corresponding band in aegirine has an absorption component in the γ direction. This may be caused by the γ and α directions having different angles, with the c axis in the (010) plane in aegirines and diopside-augites. Spectra of an authigenic aegirine sample of almost exact end-member composition (Fortey and Michie, 1978) have a strong band at 3555 cm^{-1} in all the three optical directions. Spectra of a synthetic aegirine sample (no. 45) provided by W. A. Dollase and grown by hydrothermal methods have rather sharp bands at 3675 cm^{-1} (probably amphibole), 3620 cm^{-1}, 3555 cm^{-1}, and 3485 cm^{-1} in its spectrum.

Omphacite

Only one well-oriented omphacite sample has been studied. Its spectrum (Fig. 5) is similar to spectra of pyroxenes in the diopside-hedenbergite series, but the absorption bands are considerably stronger. Bands occur at the same wavenumbers in spectra of two other unoriented omphacites. No amphibole bands were detected in any of the omphacite samples.

Orthopyroxene

Orthopyroxene spectra differ from clinopyroxene spectra. Prominent bands may occur at 3410, 3510, and 3560 cm^{-1} and are often sharper than clinopyroxene bands (Fig. 6). The pyroxene bands have the pleochroism $\gamma > \alpha \sim \beta$. Amphibole bands occur in some samples, with the strongest absorbance in the β direction. The spectra of two anorthosite megacryst samples (Labrador and Bamble) are dominated by a strong amphibole band around 3660 cm^{-1} in the β direction (but which are weak in the γ direction in Fig. 6). Both of these samples are known from electron microscopy studies to contain thin lamellae of clinoamphibole (Veblen and Bish, 1988).

Disordered pyribole and jimthompsonite

Electron microscopy studies have shown that pyroxenes may contain not only submicroscopic amphibole lamellae but also disordered pyribole and the triple-chain

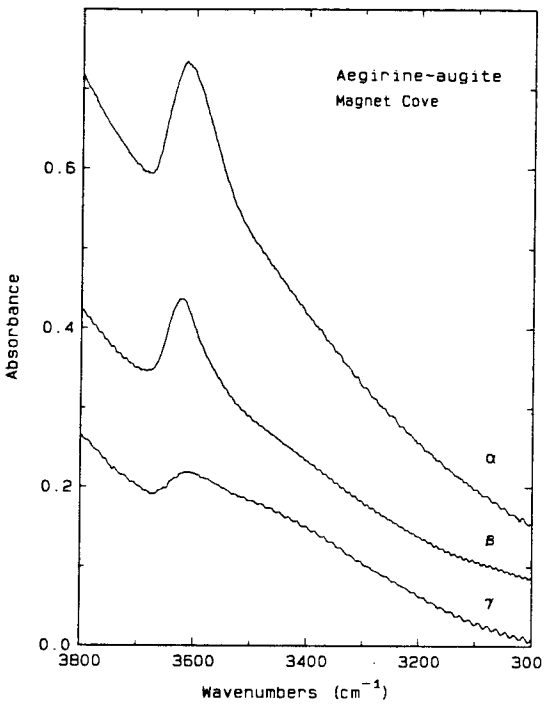

Fig. 4. Polarized spectra of aegirine-augite (no. 18, Magnet Cove) normalized to 1 mm thickness.

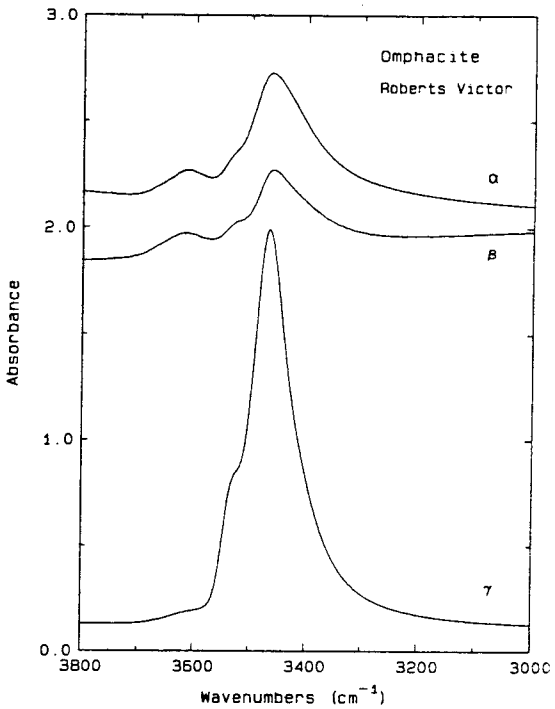

Fig. 5. Polarized spectra of omphacite (no. 47, Roberts Victor, South Africa) normalized to 1 mm thickness.

analogue of amphibole, jimthompsonite (Veblen and Buseck, 1981). The IR patterns of these phases are not known, and the possibility exists that they cause some of the OH bands in pyroxene spectra. To resolve this uncertainty, we measured IR spectra of a jimthompsonite sample provided by J. L. Rosenfeld. Spectra of both jimthompsonite and anthophyllite were obtained on a thin section using unpolarized light and microscope spectroscopic methods. The phases were identified by their typical cleavage angles of 38° for jimthompsonite and 55° for anthophyllite. The spectrum of jimthompsonite is very similar to that of anthophyllite, with sharp bands occurring around 3660 cm^{-1} (Fig. 7). Because the structural environment about OH in the disordered pyriboles and jimthompsonite are similar, we are confident that the pyroxene bands are not caused by jimthompsonite or related disordered pyriboles.

OH concentration

IR spectroscopy provides a very sensitive method for detecting trace amounts of OH in minerals but is not intrinsically self-calibrating. In order to calibrate the spectroscopy data, an independent method of water analysis is required. Wilkins and Sabine (1973) measured H_2O concentrations in diopside from Tyrol, Austria, by dehydration and P_2O_5, coloumetry, and presented an unpolarized spectrum obtained on a (110) section. To compare these data to our polarized spectra, we measured unpolarized spectra on (110) sections of two diopsides (India and Ural) that have OH patterns similar to the Tyrol sample. The resulting OH concentrations and molar absorptivities are in Table 4. The most OH-rich pyroxenes have OH contents approaching those of some mantle-derived amphiboles (e.g., kaersutite B-CH-5-A; Boettcher and O'Neil, 1980).

We also tried a number of other methods to calibrate the pyroxene OH bands: A nuclear profiling method (Rossman et al., 1988) was used to determine the OH content in three of the pyroxene samples (Table 4). Molar absorptivities for some hydrous minerals (amphiboles, micas, and tourmaline; Skogby and Rossman, in preparation) with stoichiometric OH contents were determined and applied to the pyroxene data. The calibration of Paterson (1982), derived primarily from glasses using inte-

Table 4. Estimated molar absorptivities

No. sample	Wt% OH	Abs/mm	ϵOH
50 diopside, Ural*	0.047	1.37	164
2 diopside, India*	0.010	0.24	138
20 augite, Kilbourne Hole**	0.102	2.86	151
48 enstatite, Premier**	0.096	1.31	70

Note: ϵ-values were calculated assuming the species OH according to absorbance = ϵ × path × concentration, where path is in cm and concentration is in mol/L.

* OH estimated by comparison with data of Wilkins and Sabine (1973).

** Water content determined by R. Livi using nuclear profiling analysis.

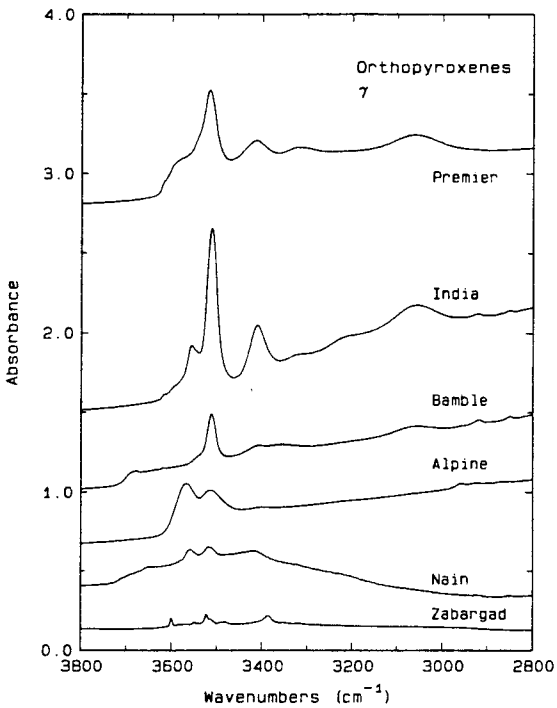

Fig. 6. Spectra of orthopyroxenes in γ-polarization plotted for 1 mm thickness. From top to bottom: no. 22, Premier Mine; no. 32, India; no. 18, Bamble; no. 18, Alpine; no. 20, Nain; no. 21, Zabargad. Amphibole bands occur in the β spectra of the samples from Nain, India, and Bamble.

grated molar absorptivities, was also tried. The OH concentrations obtained from the different calibration methods show considerable scatter, but most methods give values within a factor of two of the calculation of Wilkins and Sabine's data. For purposes of estimating the OH contents and variation among samples (Table 1), we used $\epsilon = 150$ mol^{-1} cm^{-1}. As better calibrations are established, the values in Table 1 may need revision.

Discussion

In assessing the OH content of pyroxenes, it is convenient to think in terms of two types of controlling factors. These may be broadly classed as external and internal in character. The internal controls are structural limitations imposed by crystal chemistry and refer to the degree to which pyroxene of a particular composition can accommodate OH. External controls are factors such as f_{H_2O}, f_{H_2}, a_{OH^-}, or other characteristics of the petrological environment that may result in pyroxene of a given composition having varying OH amounts. It is not easy to establish which factor exerts the dominant influence, since the internal and external parameters are often correlated. In the following discussion we attempt to evaluate the relative roles of these factors in producing the OH variability in our sample set.

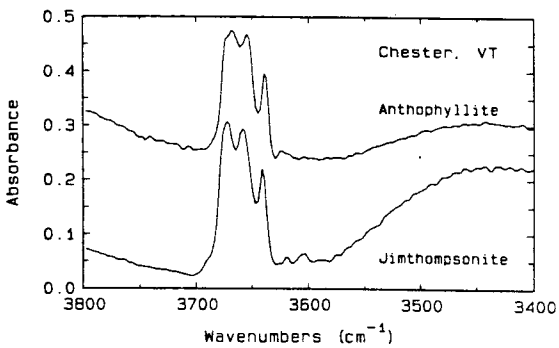

Fig. 7. Unpolarized spectra of coexisting anthophyllite (top) and jimthompsonite (bottom). Spectra were obtained from a thin-section cut perpendicular to the c axis. Sample thickness 30 μm. The broad band centered around 3400 cm^{-1} is due to the glue in the thin section and does not represent sample absorption. Band positions for the jimthompsonite are 3672, 3657, and 3641 cm^{-1}.

External factors

The OH concentrations of pyroxenes vary significantly from one geological environment to another (Table 1). Although much scatter in OH concentration exists in samples of similar paragenesis, several useful observations can be made from the broad trends displayed. It is encouraging to note that the weakest OH spectra are from anhydrous environments, namely the meteoritic and flux-grown synthetic samples. This is circumstantial evidence that OH in pyroxenes reflects some aspect of volatile activity in the geological environment and is not influenced by superficial processes such as atmospheric contamination. There is a general tendency for the samples from higher pressure environments to contain higher concentrations of OH. Thus, crustal pyroxenes from metamorphic environments are highly variable in OH content (0.003–0.085 wt% OH), with the greatest amounts occurring in samples from high-grade rocks. This is taken to the extreme in mantle-derived materials, which are consistently among the most hydrous of our samples. The most hydrous pyroxene is an omphacite from an eclogite xenolith in kimberlite of the Roberts Victor Mine, South Africa. This sample, with 0.12 wt% OH, has, by analogy with other Roberts Victor eclogites, an estimated pressure of origin in the range 35–55 kbar (Hatton, 1978; Basu et al., 1986). It seems unlikely that all these high-pressure pyroxenes have crystallized in water-rich environments. We therefore suspect that their OH-rich characteristics could be linked to an internal aspect associated with the high-pressure environment, for example, their more aluminous nature.

Ingrin et al. (1989) and Skogby and Rossman (1989) have shown that OH may be rapidly removed and then reintroduced into pyroxenes by heating and hydrothermal treatment at low pressures. It may be important to note that all our mantle pyroxenes (which are uniformly

OH-rich) were found as xenoliths or xenocrysts erupted in alkaline volcanic rocks. These host magmas are typically volatile-rich, and the OH content of the included pyroxenes may be influenced during their transport to the surface. It might be instructive to compare the OH content of xenolithic pyroxenes of both crustal and mantle origin in such eruptives.

Pyroxenes from crustal volcanic and plutonic igneous rocks are also highly variable in OH content. Spodumene from a granitic pegmatite (no. 1) and an enstatite (no. 37) phenocryst that crystallized at about 2 kbar from a hydrous boninite magma (Dobson, 1986) both contain appreciable OH contents, 0.04 and 0.02 wt%, respectively. Pyroxenes from syenitic rocks (nos. 8, 25, and 29), anorthosite (no. 36) and a rhyolite (no. 28) are poorer in OH. One of the most OH-rich samples is an aegirine of essentially end-member composition (no. 30), believed to be of sedimentary authigenic or diagenetic origin (Fortey and Michie, 1978). The high OH content of this sample shows that such concentrations are not restricted to pyroxenes from high-pressure environments (at least not in aegirines). The presence of coexisting pyrite suggests relatively reducing conditions in the sediment. Pyroxenes that have formed in anomalously oxidizing environments (buchite and oxidized alkali picrite, sample nos. 35 and 21, respectively) are very poor in OH, suggesting that f_{O_2} may also play a role.

Consideration of the above geologic factors leads us to suggest that the OH content of pyroxenes is some function of the activity of hydrous species. After crystal growth, changes in the f_{O_2} and f_{H_2} may affect the final OH concentration. Complicating this relationship are crystal chemistry effects that modify the proportionality between pyroxene OH content and external f_{H_2O} (i.e., activity coefficient of the hydropyroxene component).

Internal factors

The relatively high OH concentrations detected (up to 0.016 OH per formula unit) suggest that the incorporation of H is associated with, and its charge balanced by, the minor elements (e.g., Al, Cr, Fe^{3+}, Na) or vacancies, rather than by trace elements that are unlikely to be present in adequate amounts. Since the OH band positions and relative intensities of the OH-poor samples closely match those of OH-rich samples, the substitutional mechanisms are likely to be the same.

The IR patterns obtained for the different types of clinopyroxenes show clear compositional dependence. Spectra of aegirine-augites are dominated by the 3620–3640 cm^{-1} band (Fig. 4), whereas spectra of Al-poor diopsides are dominated by the bands around 3450, 3525, and 3350 cm^{-1} (Fig. 1). Augite spectra have a more even intensity distribution between the two groups of bands (Fig. 3).

The correlation between chemical composition and OH-band intensity was systematically examined, including correlations among OH-band intensities and the concentration of single elements and sets of elements. A few correlations were found for clinopyroxenes, but no correlations were found for the less chemically variable orthopyroxenes.

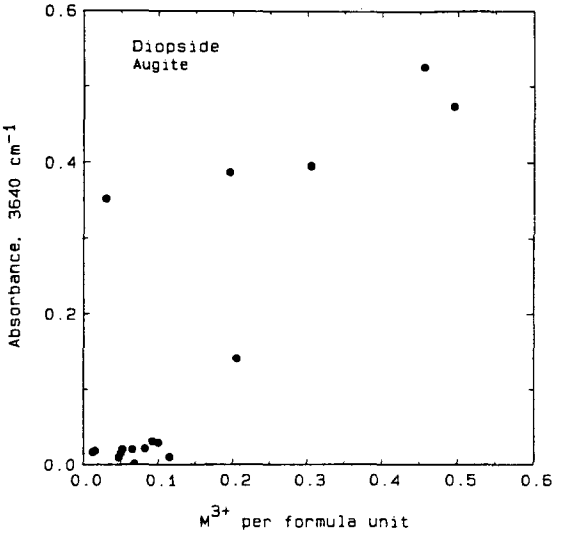

Fig. 8. Summed absorbance per mm thickness in the three optical directions of the band at 3620–3640 cm^{-1} plotted versus Al + Cr + Fe^{3+} per formula unit. Data represent diopside-hedenbergites, augites, and aegirine-augites.

The correlation between the summed absorbance intensity of the 3620 to 3640 cm^{-1} bands in the three optical directions and the sum of trivalent ions (mostly Al) for diopsides-hedenbergites and augites is displayed in Figure 8. The weak correlation found might be due to a spatial association of the OH causing this band with trivalent ions. Alternatively, the geochemical environment in which high-Al pyroxenes grows might favor incorporation of OH in the pyroxene structure. The clustering of samples close to the origin indicates that Al-poor samples seldom have strong 3640 cm^{-1} bands. For Fe^{3+}-rich samples, this band shifts towards 3620 cm^{-1}.

Figure 9 shows the sum of the intensities of the two bands occurring around 3525 and 3450 cm^{-1} versus the Fe^{2+} concentration for crustal diopsides-hedenbergites. The somewhat triangular-shaped distribution (no samples plot in the upper left corner) suggests that Fe^{2+}-rich samples can accommodate more OH than Fe^{2+}-poor samples. The samples with high Fe^{2+} contents and low OH concentration may have formed under conditions unfavorable for OH incorporation (e.g., low f_{H_2O} and f_{H_2}).

The band at 3350 cm^{-1} seems to be connected with Mg; it occurs only in spectra of diopsides with Mg/(Mg + Fe) > 0.80. The intensity of the band relative to the other bands increases with increasing Mg content.

The variable OH saturation of pyroxenes caused by equilibration in different geological environments is likely to obscure possible correlations such as those investigated above. In order to reduce this source of variability,

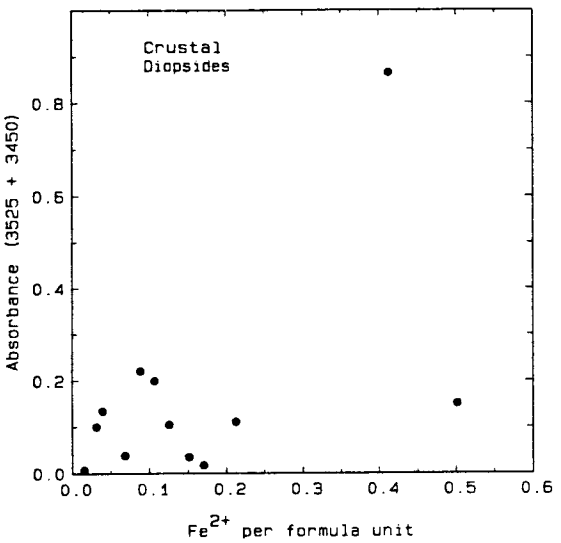

Fig. 9. Summed absorbance per mm thickness in the three optical directions of the bands at 3525 and 3450 cm^{-1} plotted versus Fe^{2+} per formula unit. Data represent crustal diopsides and hedenbergites.

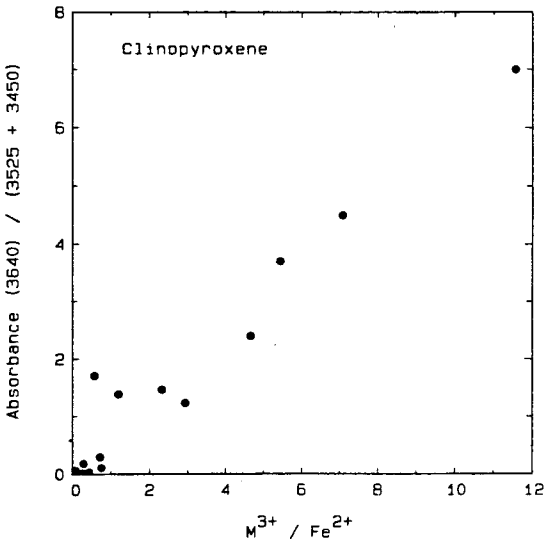

Fig. 10. Ratio of summed absorbance for the bands around 3450 and 3525 cm^{-1} plotted versus the ratio $(Al + Cr + Fe^{3+})/Fe^{2+}$. Data represent hedenbergites, augites, aegirine-augites, and diopsides with Fe >0.10 per formula unit.

we examined the correlation between the ratio of individual band intensities and the ratio of the cation concentrations with which the bands appear to be associated. In Figure 10, the ratio $(Al + Cr + Fe^{3+})/Fe^{2+}$ is plotted versus the ratio $(Abs_{3620-3640}/(Abs_{3525} + Abs_{3450})$ for diopside-hedenbergites, augites, and aegirine-augites. Diopsides with Fe < 0.10 per formula unit were excluded from the plot because of the large error in $(Al + Cr + Fe^{3+})/Fe^{2+}$ for the Fe-poor samples. The correlation of the ratios is consistent with a correlation of trivalent ions with the band in the 3620 to 3640 cm^{-1} region, and a correlation of Fe^{2+} with the bands at 3450 and 3525 cm^{-1}, independent of total OH concentration.

The correlations between composition and absorbance intensities are in Table 3. Also listed are the thermal stability and reequilibration behavior of the OH ions giving rise to the bands (Skogby and Rossman, 1989). These pyroxene bands can be divided into two groups: one occurring at 3620 to 3640 cm^{-1} associated with trivalent ions, having the pleochroism $\alpha = \beta$, $\gamma = 0$, and a relatively stable thermal behavior. The second group consists of the three bands around 3525, 3460, and 3350 cm^{-1} associated with divalent ions, having the pleochroism $\gamma > \alpha = \beta$ and a more complex thermal behavior.

The distribution of OH band intensity in omphacite is especially interesting because the structure can be regarded as a solid solution of jadeite and diopside. As seen from the omphacite spectra (Fig. 5), the bands at 3525 and 3460 cm^{-1} dominate the spectra, suggesting that OH preferably enters the diopside environment.

OH orientation

The pleochroic behavior of the OH bands in spectra of the Indian diopside is summarized in Table 5. The pyroxene band at 3645 cm^{-1} is due to dipoles inclined to the (001) plane, closer to the b axis than the a axis, which is in agreement with the findings of Beran (1976), who suggested that the OH dipole was present in the O(2) position pointing towards O(3). The O(2) position is the most favorable for OH substitution, since it is highly underbonded (Cameron and Papike, 1980). If Al substitutes for Si, it will increase the underbonded character of the O(2) even further, making OH substitution at the O(2) site more favorable. However, the intensity of the 3645 cm^{-1} band correlates better with total Al than tetrahedral Al.

The pleochroism of the pyroxene bands at 3355, 3460, and 3535 cm^{-1} corresponds to an OH dipole orientation in the (100) plane close to the c axis. These bands may also be caused by OH dipoles present at O(2) positions, pointing in another direction. The pyroxene bands in orthopyroxene spectra usually have the strongest absorption in the γ polarization, as observed by Beran and Zemann (1986).

Amphibole bands

The sharp bands around 3675 cm^{-1} observed in most diopside-hedenbergite spectra and in some orthopyroxene spectra most likely are due to submicroscopic amphibole lamellae. These bands are prominent in the spec-

TABLE 5. Pleochroism of OH absorption bands in spectra of the India diopside (no. 2)

Section	E‖	[cm⁻¹] 3645	3535	3460	3355
(001)	a*	0.71	0.00	0.04	0.03
(001), (100)	b* = β**	1.00	0.36	0.28	0.27
(100)	c*	0.29	1.00	1.00	1.00
⊥c	a*	0.32	0.00	0.04	0.00
(010)	α**	0.59	0.44	0.28	0.30
(010)	γ**	0.00	0.89	0.96	0.62

Note: The intensities are normalized to the maximum absorbance observed for the individual bands.
* a, b, and c are crystallographic directions.
** α, β, and γ are optical extinction directions.

TABLE 6. Estimation of amphibole lamellae in pyroxene by IR spectroscopy

No. sample	Geological environment	ΣA (3675)/ mm	Vol-ppm amphibole	amph : pyx
	Diopsides			
3 Finland	metamorphic	0.602	1200	1:830
13 Ontario	high-grade metamorphic	0.520	1000	1:960
12 Norway	metamorphic	0.246	490	1:2000
41 Ontario	metamorphic	0.071	140	1:7000
4 New York	metamorphic	0.040	80	1:12000
10 Austria	metamorphic	0.022	44	1:23000
39 Sweden	metamorphic	0.019	38	1:26000
2 India	metamorphic	0.0093	19	1:54000
5 Madagascar	metamorphic	0.0072	14	1:69000
6 Switzerland	metamorphic	0.0060	13	1:83000
	Orthopyroxenes			
31 Norway	megacryst	1.34	2700	1:370
36 Labrador	megacryst	1.20	2400	1:420
33 India	metamorphic?	0.093	186	1:5400
32 India	metamorphic?	0.0118	24	1:42000

Note: ΣA(3675)/mm denotes the summed absorbance for the three optical directions per mm. The amount of amphibole lamella was calculated from the summed absorbances assuming an absorbance of the OH bands of 500-mm thickness, derived from spectra of pure tremolite and actinolite (Skogby and Rossman, in preparation).

tra of two orthopyroxenes (nos. 36 and 31) previously shown to contain abundant submicroscopic amphibole lamellae (Veblen and Bish, 1988). Previously, Ingrin et al. (1989) reported a weak absorption band at 3675 cm⁻¹ in the spectrum of a diopside that contained submicroscopic amphibole lamellae.

The pleochroism of the sharp amphibole bands occurring around 3675 cm⁻¹ in many pyroxene spectra is somewhat different compared to the pleochroism we determined for OH bands in amphibole ($\alpha \sim \gamma$, $\beta = 0$ in clinopyroxenes, $\alpha > \gamma$, $\beta = 0$ in clinoamphiboles). Clinoamphibole lamellae in clinopyroxene usually are parallel to (010) and share crystallographic axes with the host structure (Veblen and Buseck, 1981). However, the extinction angles in (010) sections are different in monoclinic pyroxenes and amphiboles ($\mathbf{c} \wedge Z = 38$–$43°$ in diopside; $\mathbf{c} \wedge Z = 14$–$15°$ in tremolite). The polarization of the incident light will therefore be mixed in the submicroscopic amphibole lamellae, resulting in a more even intensity distribution in the α and γ directions.

Since amphiboles have very strong absorption bands (absorbance = ~500/mm thickness in tremolite-actinolite, Skogby and Rossman, in preparation), IR spectroscopy provides a very sensitive means of measuring concentrations of submicroscopic amphibole lamellae in pyroxenes. A summed thickness of amphibole lamellae in the pyroxene of less than 5 nm will be detectable under favorable conditions of sharp bands, as is the case for tremolite. An estimate of concentration of amphibole lamellae in our pyroxenes is in Table 6. Amphibole lamellae were detected in most metamorphic diopsides. Visible lamellae were not present in these samples. However, a few samples were too dark to offer a clear view of the beam path, so it is possible that visible amphibole lamellae escaped detection in these samples.

SUMMARY

All natural pyroxenes examined in this study, with the exception of a single meteoritic fassaite, contain detectable levels (>0.001 wt%) of structurally-bound hydroxyl. We conclude that OH-bearing pyroxenes are common in terrestrial geological environments.

The hydroxyl concentration varies as a function of geological environment, being greatest in samples of high pressure origin.

Initial OH contents of pyroxenes are probably a function of the thermodynamic activity of OH, subject to an upper limit imposed by the pyroxene crystal chemistry. Subsequent changes in external factors such as f_{O_2} and f_{H_2} may cause changes in the OH content.

The observed range of OH concentrations is presently estimated to be <0.001 to 0.12 wt% OH. This may be adjusted slightly as more accurate calibrations of the infrared technique are performed on a wider range of pyroxene compositions. Ranges of OH contents of orthopyroxenes and clinopyroxenes overlap considerably.

Infrared absorption spectra of the OH in pyroxenes comprise several bands (the pyroxene bands). In clinopyroxenes, the relative intensities of these bands correlate to some degree with composition.

Comparatively sharp absorptions at high wavenumber are due to OH in amphibole lamellae (the amphibole bands), which can be detected at levels equivalent to 5 unit cells in thickness. Amphibole lamellae have not been detected in mantle-derived pyroxenes in this study.

Although we have characterized the pleochroism of the OH absorptions and noted the influence of certain cations on band intensities, little is known about the actual site or sites of the OH groups in the pyroxene lattice. Furthermore, no direct substitutional mechanisms for the OH component have as yet been identified.

ACKNOWLEDGMENTS

We thank the following individuals for providing samples for this study: J.E. Dixon, P. Dobson (Caltech), W.A. Dollase (UCLA), J. Ito (Univ. Chicago), F.F. Foit (Univ. Washington), J.J. Gurney (Univ. Cape Town),

G. Harlow (Amer. Museum Natl. History, NY), D. Johnston (Univ. Oregon), J.L. Rosenfeld (UCLA), J.S. White (Smithsonian Institution), and J.S. Huebner (USGS, Reston, VA) who also provide microprobe analyses of his samples. R. Livi (Porto Alegre) is especially thanked for providing the H analyses by nuclear reaction analyses. The study was supported by the National Science Foundation, Grants EAR 86-18200 and EAR 88-16006, a Harry Crossley Foundation scholarship to D.R.B., and by the Knut and Alice Wallenberg Foundation through a postdoctoral fellowship to H.S. This is contribution number 4782 of the Division of Geological and Planetary Sciences, California Institute of Technology.

References cited

Aines, R.D., and Rossman, G.R. (1984) Water content of mantle garnets. Geology, 12, 720–723.

Basu, A.R., Ongley, J.S., and MacGregor, I.D. (1986) Eclogites, pyroxene geotherm, and layered mantle convection. Science, 233, 1303–1305.

Beran, A. (1976) Messung des Ultrarot-Pleochroismus von Mineralen. XIV. Der Pleochroismus der OH-Streckfrequenz in Diopsid. Tschermaks Mineralogisches und Petrologisches Mitteilungen, 23, 79–85.

Beran, A., and Zemann, J. (1986) The pleochroism of a gem-quality enstatite in the region of the OH stretching frequency, with a stereochemical interpretation. Tschermaks Mineralogisches und Petrologisches Mitteilungen, 35, 19–25.

Boettcher, A.L., and O'Neil, J.R. (1980) Stable isotope, chemical, and petrographic studies of high-pressure amphiboles and micas: Evidence for metasomatism in the mantle source regions of alkali basalts and kimberlites. American Journal of Science, 280A, 594–621.

Burns, R.G., and Strens, R.G.J. (1966) Infrared study of the hydroxyl bands in clinoamphiboles. Science, 153, 890–892.

Cameron, M., and Papike, J.J. (1980) Crystal chemistry of silicate pyroxenes. In C.T. Prewitt, Ed., Pyroxenes. Mineralogical Society of America Reviews in Mineralogy, 7, 1–93.

Dixon, J.E., Clague, D.A., and Eissen, J.P. (1986) Gabbroic xenoliths and host ferrobasalt from the southern Juan de Fuca Ridge. Journal of Geophysical Research, 91B, 375–3820.

Dobson, P.F. (1986) The petrogenesis of the volcanic rocks of Chichi-Jima, Bonin Islands, Japan. Ph.D. thesis, Stanford University.

Duba, A., Dennison, M., Irving, A.J., Thornber, C.R., and Huebner, J.S. (1979) Electrical conductivity of aluminous orthopyroxene (abs.). Tenth Lunar and Planetary Science Conference, p. 318–319. Lunar and Planetary Institute, Houston, Texas.

Foit, F.F., Hooper, R.L., and Rosenberg, P.E. (1987) An unusual pyroxene, melilite, and iron oxide mineral assemblage in a coal-fire buchite from Buffalo, Wyoming. American Mineralogist, 72, 137–147.

Fortey, N.J., and Michie, U.McL. (1978) Aegirine of possible authigenic origin in Middle Devonian sediments in Caithness, Scotland. Mineralogical Magazine, 42, 439–442.

Hatton, C.J. (1978) The geochemistry and origin of xenoliths from the Roberts Victor Mine. Ph.D. thesis, University of Cape Town, South Africa.

Hazen, R.M., and Finger, L.W. (1977) Crystal structure and compositional variation of Angra dos Reis fassaite. Earth and Planetary Science Letters, 35, 357–362.

Ingrin, J., Latrous, K., Doukhan, J.C., and Doukhan, N. (1989) Water in diopside: An electron microscopy and infrared spectroscopy study. European Journal of Mineralogy, 1, 327–341.

Johnston, A.D., and Stout, J.H. (1984) A highly oxidized ferrian salite-, kennedyite-, forsterite-, and rhönite-bearing alkali gabbro from Kauai, Hawaii and its mantle xenoliths. American Mineralogist, 69, 57–68.

Keil, K., Prinz, M., Hlava, P.F., Gomes, C.B., Curvello, W.S., Wasserburg, G.J., Tera, F., Papanastassiou, D.A., Huneke, J.C., Murali, A.V., Scheinin, N.B., and Clayton, R.N. (1976) Progress by the consorts of Angra dos Reis. In Lunar Science VII, Lunar Science Institute, Houston, Texas, p. 443–445.

Miller, G.H., Rossman, G.R., and Harlow, G.E. (1987) The natural occurence of hydroxide in olivine. Physics and Chemistry of Minerals, 14, 461–472.

Paterson, M.S. (1982) The determination of hydroxyl by infrared absorption in quartz, silicate glasses and similar materials. Bulletin de Minéralogie, 105, 20–29.

Rossman, G.R., Rauch, F., Livi, R., Tombrello, T.A., Shi, C.R., and Zhou, Z.Y. (1988) Nuclear reaction analysis of hydrogen in almandine, pyrope and spessartite garnets. Neues Jahrbuch für Mineralogie Monatshefte, 172–178.

Skogby, H., and Rossman, G.R. (1989) OH in pyroxenes: An experimental study of incorporation mechanisms and stability. American Mineralogist, 74, 1059–1069.

Veblen, D.R., and Bish, D.L. (1988) TEM and X-ray study of orthopyroxene megacrysts: Microstructures and crystal chemistry. American Mineralogist, 73, 677–691.

Veblen, D.R., and Buseck, P.R. (1981) Hydrous pyriboles and sheet silicates in pyroxenes and uralites: Intergrown microstructures and reaction mechanisms. American Mineralogist, 66, 1107–1134.

Wilkins, R.W.T., and Sabine, W. (1973) Water content of some nominally anhydrous silicates. American Mineralogist, 58, 508–516.

Manuscript Received August 14, 1989
Manuscript Accepted April 19, 1989

Appendix 4

Incorporation of hydroxyl in upper-mantle clinopyroxenes.

by

J. R. Smyth, D. R. Bell and G. R. Rossman

Nature **351**, 732-735.

Incorporation of hydroxyl in upper-mantle clinopyroxenes

J. R. Smyth*, D. R. Bell† & G. R. Rossman†

* Department of Geological Sciences, University of Colorado, Boulder, Colorado 80309-0250, USA
† Division of Geological and Planetary Sciences, California Institute of Technology, Pasadena, California 91125, USA

WATER (and hydroxyl, OH) plays an important part in determining the properties of minerals and melts in the Earth's upper mantle. The main hydroxyl-bearing phases found in rocks from the upper mantle, phlogopite and amphibole, are not believed to exist in significant quantities at depth. Some of the less abundant phases found in these rocks contain small amounts of hydrous components[1–3], but do not constitute an important reservoir for water. Traces of hydroxyl have been found in common mantle phases[4–6], but not at concentrations high enough to account for the amount of water thought to be present at depth. An exception

TABLE 1 Electron microprobe analyses of eclogite clinopyroxenes in wt %

Sample	SBB-1	SBB-5H	SBB-7P	SBB-14	SBB-20	SBB-46	SBB-104	SDC-1	SDC-2	SRV-4	XM-37	HRV-147
SiO_2	57.14	55.11	55.06	55.05	55.09	55.81	55.31	55.60	55.71	54.59	56.10	56.25
TiO_2	0.37	0.08	0.06	0.14	0.11	0.28	0.22	0.17	0.17	0.09	0.38	0.30
Al_2O_3	19.08	7.24	2.61	0.31	5.93	10.40	6.27	17.73	17.58	1.25	14.10	14.28
Cr_2O_3	0.03	0.08	3.35	1.82	0.09	0.80	0.03	0.05	0.04	0.08	0.15	0.07
FeO	2.46	3.31	1.74	2.27	4.32	2.44	4.07	1.28	1.27	3.11	2.54	1.98
MnO	0.03	0.03	0.08	0.09	0.04	0.02	0.04	0.01	0.01	0.05	0.02	0.03
MgO	4.14	12.39	15.72	17.46	12.59	10.19	12.72	5.99	6.00	17.11	7.72	8.15
CaO	7.70	17.56	18.93	21.72	17.90	14.53	17.06	10.32	10.37	23.23	11.86	12.75
Na_2O	9.12	4.40	2.85	1.31	4.07	5.78	4.29	8.90	8.90	0.66	6.99	6.76
K_2O	0.05	0.00	0.00	0.00	0.00	0.10	0.00	0.00	0.00	0.07	0.29	0.25
P_2O_5	0.00	0.00	0.00	0.00	0.00	0.00	0.00	0.00	0.00	0.00	0.00	n.d
Total	100.12	100.20	100.40	100.17	100.14	100.35	100.01	100.05	100.05	100.24	100.15	100.82
Atoms per 6 oxygens												
Si	1.971	1.973	1.981	1.995	1.986	1.971	1.988	1.933	1.937	1.981	1.966	1.957
Ti	0.010	0.002	0.002	0.004	0.003	0.007	0.006	0.004	0.004	0.003	0.010	0.002
Al	0.776	0.306	0.111	0.013	0.252	0.433	0.266	0.727	0.720	0.054	0.582	0.585
Cr	0.001	0.002	0.095	0.052	0.003	0.022	0.001	0.001	0.001	0.002	0.004	0.008
Fe	0.071	0.099	0.052	0.069	0.130	0.072	0.122	0.037	0.037	0.094	0.074	0.058
Mn	0.001	0.001	0.002	0.003	0.001	0.001	0.001	0.000	0.000	0.002	0.001	0.001
Mg	0.213	0.661	0.843	0.943	0.677	0.537	0.682	0.311	0.311	0.926	0.403	0.423
Ca	0.285	0.674	0.730	0.843	0.691	0.550	0.657	0.385	0.386	0.903	0.445	0.475
Na	0.610	0.305	0.199	0.092	0.284	0.396	0.299	0.600	0.600	0.046	0.475	0.456
K	0.002	0.000	0.000	0.000	0.000	0.005	0.000	0.000	0.000	0.003	0.013	0.011
P	0.000	0.000	0.000	0.000	0.000	0.000	0.000	0.000	0.000	0.000	0.000	0.000
Total	3.938	4.024	4.014	4.015	4.027	3.994	4.022	3.998	3.998	4.014	3.974	3.975
Vacancy	0.062	−0.024	−0.014	−0.015	−0.027	0.006	−0.022	0.002	0.002	−0.014	0.026	0.025

is suggested by a report[7] that the pyroxene (omphacite) in an eclogite nodule from the Roberts Victor kimberlite pipe contains up to 1,000 p.p.m. OH. Here we show that some of this hydroxyl is associated with cation vacancies in sodic clinopyroxene, and that these pyroxenes may be an important reservoir for hydrous components in the upper mantle.

To constrain the hydroxyl contents of minerals in the eclogite suite of rocks, we have measured infrared absorption spectra of a representative suite of clinopyroxenes covering the range of compositions found in mantle eclogite. The aims of this study were to see if hydroxyl is associated with the M2 cation vacancy previously noted in some of the pyroxenes[8], and to see if the hydroxyl content can help to constrain the origin and evolution of these rocks.

Pyroxene samples were selected from the well documented suite of mantle eclogites from South African kimberlites[9-11]. Samples were selected to span the range of pyroxene compositions observed in mantle eclogites, and to have inclusion-free and fracture-free areas of at least 150 μm in their shortest dimension. Eleven samples were selected for the study. Samples denoted SBB are from the Bobbejaan mine; samples denoted SDC are from the Dan-Carl mine (both at Bellsbank); and samples SRV-4, XM-37 and HRV-147 are from the Roberts Victor Mine near Boshof, Orange Free State, South Africa.

Samples SDC-1 and 2 are from corundum-bearing grospydites, sample SBB-1 is from a kyanite eclogite, whereas the rest are from bimineralic eclogites, except for SBB-14 which is a chromium diopside megacryst. Sample HRV-147 is from an inhomogeneous, kyanite-bearing eclogite described by Hatton[12] and used by Skogby *et al.*[8]. All samples were analysed with the electron microprobe. Pyroxene analyses are presented in Table 1 together with atoms per formula unit (12 oxygens). Samples SDC-1 and 2 and SBB-1 are rich in jadeite (Jd), whereas sample SRV-4 is low in sodium and contains no jadeite in the endmember calculation. Samples SBB-1 and 46, SDC-1 and 2, SRV-4, XM-37 and HRV-147 all contain measurable K_2O. Samples SBB-1 and 46, SDC-1 and 2, XM-37 and HRV-147 all contain a normative calcium-Eskola ($Ca_{0.5}AlSi_2O_6$, CaEs) component, implying some M2 vacancy, with SBB-1 having almost 12 mol % of this endmember.

Infrared spectra at room temperature were obtained with a Nicolet 60SX Fourier Transform infrared spectrometer at a resolution of 2 cm^{-1}. Polished, self-supporting sample plates were mounted over pinhole apertures to define the viewing area through the sample. Viewing areas were 100–200 μm diameter. Pyroxene crystals were oriented using an X-ray precession camera, and (010) parallel facets were cut and polished. For each crystal the α- and γ-polarized spectra were measured in the X and Z principal vibration directions, respectively, in the

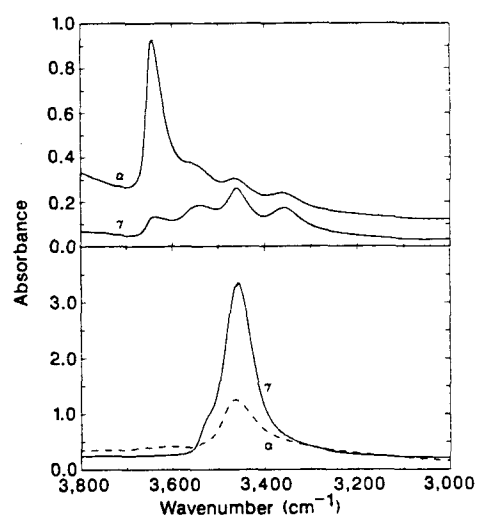

FIG. 1 Two representative infrared spectra in the range 3,000–3,800 cm^{-1}. *a*, Calcic sample (diopside) SRV-4 ($Di_{85}Hd_6Ac_5CaTs_3$). *b*, sodic sample (omphacite) SBB-1 ($Jd_{56}Di_{20}Hd_8CaEs_{12}$). The strong γ-polarized absorption band at 3,470 cm^{-1} correlates with the M2 vacancy concentration calculated from electron microprobe analysis.

region 3,000–3,800 cm^{-1} using a $LiIO_3$ crystal polarizer. (The X direction is approximately aligned with the crystallographic a-axis and Z is inclined ~40° from the c-axis.)

The spectra differed markedly for different compositions with a strong γ-polarized absorption band at 3,470 cm^{-1} appearing in jadeite-rich compositions and a strong α-polarized band at 3,620 cm^{-1} in the diopside-rich (Di-rich) compositions. Two representative spectra, one from a calcic sample SRV-4 of composition $Di_{85}Hd_6Ac_5CaTs_3$ (Hd is hedenbergite, Ac acmite, CaTs calcium-Tschermaks) and another from a sodic sample, $Jd_{59}Di_{20}Hd_8CaEs_{12}$, are plotted in Fig. 3. The relative intensities of the α absorption bands at 3,470 and 3,620 cm^{-1}, and the γ band at 3,470 cm^{-1} were calculated in absorbance units per mm and are listed in Table 2. From a calibration of infrared absorbance against OH content, we estimate the OH content of sample SBB-1 to be 1,840 p.p.m. by weight. The OH contents of the other samples are reported in Table 2.

Clinopyroxenes from mantle eclogites have complex compositions. The samples of this suite may contain more than 5 mol % of eight different endmembers. In addition to jadeite, diopside and hedenbergite, kosmochlor, acmite, Ca-Tschermaks and Ca-Eskola are important constituents. Also, six of the samples contain measurable potassium, of which five also contain a normative CaEs component calculated from the proportion of vacancies (4.00 minus total cations). McCormick[8] has confirmed the presence of vacancies in M2 using X-ray crystal structure refinement and analytical transmission electron microscopy. She also reported the absence of multiple-chain defects in sample SBB-1 using high-resolution transmission electron microscopy.

The infrared spectra of these clinopyroxenes are also complex. In particular, the strong γ-polarized absorption feature at 3,470 cm^{-1} is very strong in sample SBB-1, whereas it is very weak relative to the α-polarized feature at 3,620 cm^{-1} in SRV-4 (Fig. 1). These differences are correlated with composition. Figure 2 is a plot of the intensity of the γ-3,470 feature against the cation deficiency per six oxygens. The 'negative' cation deficiencies of some samples may result from the effect of ferric iron on the vacancy calculation. If samples with positive cation deficiency also contain ferric iron, the calculated cation deficiency would be underestimated. The correlation in Fig. 2 indicates that the cation vacancy at M2 controls the incorporation of the hydroxyl responsible for the dominant 3,470-cm^{-1} band.

Despite the compositional complexities, no clinopyroxenes from these rocks have been reported with space groups other than $C2/c$, consistent with their high temperatures of equilibration. In this space group, the O2 site, bonded to one tetrahedral cation, one M1 site and one M2 site, is under-bonded according

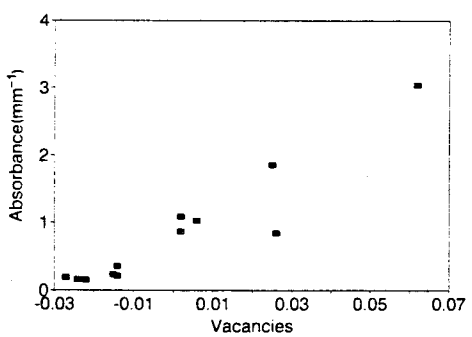

FIG. 2 Plot of absorbance normalized to 1 mm of the γ-polarized absorption peak at 3,470 cm^{-1} against the number of vacancies per 6.0 oxygens (calculated as 4.0 minus the total number of cations per six oxygens) in clinopyroxenes from mantle eclogites. In our calculations we have assumed that all iron is ferrous; a negative number may thus indicate the presence of some ferric iron.

TABLE 2 Absorbance per mm of mantle eclogite clinopyroxenes

Sample	α-polarized 3,620 cm^{-1}	α-polarized 3,470 cm^{-1}	γ-polarized 3,470 cm^{-1}	Total	OH (p.p.m.)*
SBB-1	0.068	0.844	3.040	3.95	1840
SBB-5H	0.530	0.040	0.154	0.72	335
SBB-7P	0.611	0.308	0.353	1.27	595
SBB-14	0.120	0.384	0.230	0.73	340
SBB-20	0.400	0.170	0.184	0.75	350
SBB-46	0.138	0.357	1.020	1.52	710
SBB-104	0.290	0.100	0.148	0.54	250
SDC-1	0.675	0.500	1.080	2.26	1055
SDC-2	0.400	0.280	0.865	1.55	725
SRV-4	0.693	0.093	0.207	0.99	460
XM-37	0.025	0.324	0.841	1.19	555
HRV-147	0.124	0.596	1.853	2.57	1200

* Concentrations in p.p.m. by weight are determined by assuming the summed OH band intensity is proportional to OH content. The reported[7] OH content of HRV-147 was used as a standard.

to its Pauling bond strength, and has the lowest electrostatic site potential in the jadeite structure[13]. If we assume that the proton in these vacancy-bearing pyroxenes is associated with the O2 oxygen and that its bond is parallel to the γ-polarization direction, the O–H bond would extend roughly towards the M2 cation site. This is the same orientation Beran[14] proposed for the OH group that produces the 3,600-cm^{-1} band in the diopside spectrum.

Experimental studies have demonstrated that vacancies exist in pyroxene at the pressures and temperatures at which eclogite is stable[15]. The correlation of hydroxyl content with vacancy concentration in the pyroxene suggests that both components existed in the pyroxene under mantle conditions. Clinopyroxenes are stable constituents of most model mantle compositions to pressures of 12 GPa, so hydroxyl-bearing pyroxenes may be important constituents of the mantle in the depth region of 30–400 km.

If the observed hydroxyl was indeed present in the mantle, then the finding of substantial hydroxyl concentrations associated with M2 cation vacancies is pertinent to understanding the geochemistry content of mantle processes. With an estimated maximum hydroxyl content of 1,840 p.p.m., these are the most hydrous pyroxenes yet observed, and indicate that sodic clinopyroxenes may be an important host for hydroxyl in the upper mantle. Electron microprobe analyses indicate that about one-third of our eclogite sample suite from Bellsbank and more than half of our suite from Roberts Victor contain a considerable concentration of M2 cation vacancies (up to ~9% in some samples). For the entire suite from both of the localities, the vacancy-bearing pyroxenes are 5–10 times as abundant as all other nominally hydrous phases (phlogopite and amphibole), so that the hydrous pyroxenes seem to contain well over half of the total hydrogen in the sample suite.

Compositions of pyroxenes reconstructed from exsolved garnet and kyanite indicate that precursor, near-solidus pyroxene may have contained up to 18% vacant M2 sites[11]. This is supported by thermodynamic calculations[15] based on experimental studies, which indicate that high temperatures favour the occurrence of high concentrations of vacancies in clinopyroxenes within the eclogite stability field. Extrapolating the curve in Fig. 2, we would estimate that the precursor pyroxene contained as much as 4,000 p.p.m. OH. Although the amphibole and ubiquitous phlogopite in the eclogite xenoliths are generally believed to derive from metasomatism by infiltrating kimberlitic fluids[16], re-equilibration of pyroxenes during cooling from their crystallization temperature to their observed equilibration conditions (~1,050 to 1,250 °C in the 3–5 GPa range)[9,10] could evolve sufficient hydroxyl to account for much of that observed in the secondary hydrous phases in these rocks. Re-equilibration

could also result in a small amount of partial melt at depths of about 100 km. □

Received 10 January; accepted 13 May 1991.

1. Beran, A. & Goetzinger, M. A. *Miner. Petrol.* **36**, 41–49 (1987).
2. Navon, O., Hutcheon, I., Rossman, G. R. & Wasserburg, G. J. *Lunar planet. Sci.* **19**, 827–828 (1988).
3. Rossman, G. R. & Smyth, J. R. *Am. Miner.* **75**, 775–780 (1990).
4. Miller, G. H., Rossman, G. R. & Harlow, G. E. *Phys. Chem. Miner.* **14**, 461–472 (1987).
5. Aines, R. D. & Rossman, G. R. *Geology* **12**, 720–723 (1984).
6. Bell, D. R. & Rossman, G. R. *Trans. Am. geophys. Un.* **71**, 523 (1990).
7. Skogby, H., Bell, D. R. & Rossman, G. R. *Am. Miner.* **75**, 764–774 (1990).
8. McCormick, T. C. *Am. Miner.* **71**, 1434–1440 (1986).
9. Smyth, J. R. & Caporuscio, F. A. in *Kimberlites II: The Mantle and Crust–Mantle Relationships* (ed. Kornprobst, J.) 121–132 (Elsevier, Amsterdam, 1984).
10. Caporuscio, F. A. & Smyth, J. R. *Contrib. Miner. Petrol.* **105**, 550–561 (1990).
11. Smyth, J. R., McCormick, T. C. & Caporuscio, F. A. *Kimberlites II: The Mantle and Crust–Mantle Relationships* (ed. Kornprobst, J.) 111–120 (Elsevier, Amsterdam, 1984).
12. Hatton, C. J. thesis, Univ. Cape Town (1978).
13. Smyth, J. R. *Geochim. cosmochim. Acta* **53**, 1101–1110 (1989).
14. Beran, A. *Tschermaks Min. Petrol. Mitt.* **23**, 79–85 (1976).
15. Gasparik, T. *Am. Miner.* **71**, 686–693 (1986).
16. Taylor, L. A. & Neal, C. R. *J. Geol.* **97**, 551–567 (1989).

ACKNOWLEDGEMENTS. We thank J. J. Gurney and J. B. Hawthorne for samples and T. McCormick for helpful discussions. This study was funded in part by the NSF.

Appendix 5

The hydroxide component in synthetic pyrope.

by

C. A. Geiger, K. Langer, D. R. Bell, G. R. Rossman and B. Winkler

The American Mineralogist **76**, 49-59.

American Mineralogist, Volume 76, pages 49–59, 1991

The hydroxide component in synthetic pyrope

CHARLES A. GEIGER,* KLAUS LANGER
Institut für Mineralogie und Kristallographie, Technische Universität Berlin, Ernst-Reuter-Platz 1, D-1000 Berlin 12, Germany
DAVID R. BELL, GEORGE R. ROSSMAN
Division of Geological and Planetary Sciences, California Institute of Technology, Pasadena, California 91125, U.S.A.
BJÖRN WINKLER**
Technische Universität Berlin, Ernst-Reuter-Platz 1, D-1000 Berlin 12, Germany

ABSTRACT

A series of pyrope single crystals up to 2 mm in size was synthesized over a range of hydrothermal pressures of 20.0 to 50.0 kbar and temperatures of 800 to 1200 °C using different starting materials (oxides, glass, gel) and fluid fluxes (H_2O, NaOH, HCl). The crystals were characterized by optical, SEM, microprobe, and X-ray techniques. Single crystal Fourier-transform infrared (FTIR) spectroscopy was used to measure the incorporated structural OH^-. Spectra measured in the region of 4000–3000 cm^{-1} wavenumbers were different for all samples grown from oxides or glass vs. those grown from the gel at temperatures less than 1000 °C. In spectra obtained at room temperature the former are characterized by a single OH^- stretching vibration at 3629 cm^{-1}, full widths at half-height (FWHH) = 60 cm^{-1}, which is present regardless of the synthesis conditions (P,T or fluid flux). At 78 K, the single band splits into two narrow bands of FWHH of 11 cm^{-1} each. The unit-cell dimension of pyrope increases up to 0.004 Å with the incorporation of OH^-. The best interpretation of these data is that OH^- defects are introduced into the pyrope structure as a hydrogarnet component where $(O_4H_4)^{4-} = SiO_4^{4-}$, i.e., by the substitution $Si^{4+} + 4O^{2-} = {}^{[4]}\square + 4OH^-$. The amount of OH^- substitution into pyrope ranges from 0.02 to 0.07 wt% expressed as H_2O. The infrared (IR) spectra of pyropes grown from a gel starting material, at temperatures less than 1000 °C, display four band spectra, which indicate that OH^- substitution is not governed solely by the hydrogarnet substitution. Natural pyrope-rich garnets generally have lower OH^- concentrations and more complicated IR spectra than the synthetic pyrope crystals grown from oxides. This is assumed to be caused by crystal chemistry differences and probably different mechanisms of OH^- incorporation.

INTRODUCTION

Pyrope garnet, $Mg_3Al_2Si_3O_{12}$, is only stable at elevated pressures and is nominally an anhydrous phase of cubic structure, with space group $Ia3d$. Rigorous understanding of the crystallochemical properties of pyrope is not only of mineralogical interest, but also has an important bearing on petrological and geophysical processes. It has been shown that both synthetic end-member pyropes (Ackermann et al., 1983; Begley and Sclar, 1984; Geiger et al., 1989b) and natural pyrope-rich garnets (Aines and Rossman, 1984a, 1984b) contain small amounts of structural OH^- often loosely referred to as water. Pyrope-rich garnets constitute a portion of the earth's mantle and therefore, the bulk H_2O content in the earth's interior is partly a function of H_2O held in garnet. Petrologic processes involving, for example, metasomatism and melting could be influenced by garnet containing OH^-. The presence of OH^- could also affect the physical properties of garnet and, hence, the rheological properties of the mantle.

There are several outstanding questions regarding the presence of OH^- in synthetic pyrope and natural pyrope-rich garnets.

1. Where are the OH^- groups bound in the pyrope structure? It is frequently assumed that the OH^- is substituted as the classic hydrogarnet substitution, where $(H_4O_4)^{4-} = SiO_4^{4-}$, but this has not yet been demonstrated. Substitutional mechanisms other than the hydrogarnet substitution are possible and have been proposed in the case of hydrogrossular garnet (Basso et al., 1984), but have yet to be proven for pyrope.

2. What are the limits of OH^- substitution in synthetic pyrope and how is the concentration influenced by growth conditions and external variables, i.e., P, T, f_{H_2O}?

3. How do the OH^- contents and substitutional mech-

* Present address: Bayerisches Forschungsinstitut für Experimentelle Geochemie und Geophysik, Universität Bayreuth, Postfach 10 12 51, 8580 Bayreuth, Germany.
** Present address: Department of Earth Sciences, University of Cambridge, Cambridge, CB2 3EQ, U.K.

0003–004X/91/0102–0049$02.00

anisms of synthetic pyrope compare to those of natural pyrope and to those of other synthetic garnets (i.e., grossular and almandine)?

The principal analytical technique used to detect and measure the OH^- contents in nominally anhydrous silicates is infrared (IR) spectroscopy, as recently reviewed by Rossman (1988). Unfortunately, this method does not give direct and exact structural information on the location of the protons. The OH^- contents in natural or synthetic pyrope are too low (Ackermann et al., 1983; Aines and Rossman, 1984b) to be detected by present X-ray, neutron diffraction, or H^+-NMR techniques, and therefore direct structural information on the positions of the H^+ is lacking. However, recent developments in Fourier-transform IR (FTIR) spectroscopy permit more accurate and higher resolution measurements to be made on small single crystals. This allows previous uncertainties and discrepancies in the literature to be resolved and new structural inferences regarding the location of the OH^- groups and their concentrations to be made.

Previous work

Ackermann et al. (1983) were the first to show that small amounts of OH^- could be found in hydrothermally prepared synthetic pyrope single crystals. They presented IR spectra obtained on a microscope IR device using an interference filter monochromator, where the accuracy and resolution are not as good as is presently possible with the new FTIR spectrometers. In addition, most of their spectra were dominated by a broad band resulting from molecular H_2O held in tiny fluid inclusions, which masked the weaker OH^- band. They detected a single OH^- stretching vibration located at 3600 cm^{-1}. They estimated that the absolute OH^- in their pyrope samples was in the range of 0.05 wt% expressed as H_2O.

Aines and Rossman (1984a, 1984b) made a systematic study of OH^- in natural pyralspite garnets from a variety of geologic environments. They measured the IR spectra using a conventional grating spectrometer on optically clear crystals using small apertures on 1 mm or thicker platelets at both room and liquid N_2 temperatures. They detected OH^- in nearly all of the pyropic garnets studied, including those of mantle origin. In contrast to the work of Ackermann et al. (1983), they proposed that two OH^- stretching bands located at approximately 3660 and 3560 cm^{-1} were characteristic of pyrope-rich garnets. They estimated that the H_2O content of their pyrope samples ranged from 0.0 up to 0.26 wt% H_2O, and they suggested that this range was a result of different intrinsic H_2O fugacities in the mantle source region where the garnets grew or equilibrated.

On the basis of these two studies, there are differences between natural and synthetic pyrope garnets as to both the number and positions of the OH^- stretching bands. It was argued that the OH^- bands observed in the synthetic pyrope garnets may be a result of included solid phases (Aines and Rossman, 1984b). A primary aim of this study is to make further measurements, using micro-FTIR techniques, of synthetic pyrope so that differences between natural and synthetic pyropes can be understood. In particular, we hope to address the general questions listed above and the following specific questions. (1) How many IR active OH^- stretching bands are present in the spectra of synthetic pyrope containing small amounts of OH^-, and are the experimental spectroscopic observations in agreement with the theoretical predictions based on site group calculations? (2) What are the positions of these bands and do they change as a function of composition or P and T of synthesis? (3) Do the OH^- contents of synthetic pyropes represent equilibrium values incorporated at P, T and f_{H_2O} during growth? (4) Are the OH^- contents a function of the P and T of synthesis?

Experimental methods

Synthesis

Synthetic pyrope single crystals were grown using three different starting materials: an oxide mixture, a glass, and gels. The oxide mixture was prepared by grinding an intimate mixture of MgO (99.999%, Ventron, Alfa Product), SiO_2 (99.99%, Koch-Light Laboratories) and Al_2O_3 (99.9999%, Koch-Light Laboratories) powders of stoichiometric pyrope composition under H_2O in an agate mortar for about 2 h. The oxides were fired at 1000 °C for several hours and then stored in a desiccator prior to weighing. The glass of pyrope composition was prepared by melting a similarly prepared oxide mixture at 1620 °C in platinum crucibles and quenching it in H_2O (Geiger et al., 1987). The pyrope gel used in Berlin was the same as that used in the study of Ackermann et al. (1983). Syntheses at Pasadena were conducted solely with the gel technique. The gel was provided by P. J. Wyllie (Sekine et al., 1981).

Pyrope single crystals were grown hydrothermally in a piston-cylinder device in Au or Pt capsules with outer dimensions of 3.5 mm diameter and 5 mm long or 5.5 mm diameter and 10 mm long, and placed in a 26-mm-diameter salt-based high pressure assembly described in Cemič et al. (1990). Experiments above 25 and below 31 kbar were made in an 18 mm assembly consisting of an outer salt sleeve with inner parts fabricated from salt or boron nitride. Syntheses at Cal Tech were conducted using Au capsules and a half-inch NaCl-based furnace assembly. For syntheses above 30 kbar a 0.5 in. assembly, similar to the type I cell of Massonne and Schreyer (1986), was used at Bochum University, except that the capsule was situated vertically below the thermocouple. We estimate that the temperatures are accurate to ±10 °C and the nominal pressures differ by no more than 1 kbar from the true pressures. Several experiments were also made using 1N NaOH and dilute HCl as the fluid flux together with the oxide mix. The ratio of solids to fluid varied slightly, but was normally between 4 and 6 to 1, by weight. A couple of syntheses were also made using an oxide mixture containing 10 wt% excess SiO_2.

The experimental conditions varied from 800 to 1200

TABLE 1. Synthesis conditions of the pyropes used in this study

Sample	Pressure (kbar)	Temperature (°C)	Duration (h)	Starting material	Fluid	Fluid/solid ratio (g)
P-5	23.9	1000	24	oxides	H_2O	0.008/0.031
P-7	23.9	1000	48	glass	H_2O	0.008/0.037
P-8	23.9	1000	24	gel	H_2O	0.007/0.037
P-13	22.9	1100	20	oxides	H_2O	0.009/0.034
P-18	25.8	1000	16	oxides	H_2O	—
P-27	20.0	900	20	gel	H_2O	0.0004/0.030
P-29	24.0	950	36	oxides	H_2O	0.026/0.162
P-44	22.0	1025	18	oxides	HCl	0.008/0.0399
P-51	24.0	1000	19	oxides + silica	H_2O	0.025/0.150
P-54	40.0	1000	18	oxides	H_2O	0.022/0.150
P-57	45.0	1000	3	oxides	H_2O	0.008/0.043
P-69	50.0	800	24	gel	H_2O	0.007/0.025
P-77	35.0	1000	2.5	oxides + silica	H_2O	0.008/0.033
P-90	30.0	900	48	oxides	H_2O	0.007/0.036
P-94	30.0	1000	50	oxides	NaOH	0.006/0.041
DB-31	20.0	1000	100	gel	H_2O	—
DB-30	25.0	1000	100	gel	H_2O	—

Note: The samples from the P series were made in Berlin and those from DB in Pasadena.

°C and from 20 to 50 kbar. The durations of the experiments were from several hours up to 4 d. Upon opening, the capsules were always examined for a liquid to ensure that a fluid phase was present during crystal growth. Capsules that had leaked or did not show the presence of a fluid were discarded. Table 1 lists the synthesis conditions of the crystals used in this study.

Characterization and FTIR spectroscopy

The experimental products were examined by optical microscope, X-ray powder diffraction, electron microprobe, and SEM techniques. Routine X-ray measurements using smear mounts on glass slides were undertaken to detect additional phases coexisting with the pyrope crystals in most of the syntheses. Powder refinements were also made on several crushed and ground pyrope single crystals. Data were collected from 10° to 100° 2θ using Cu$K\alpha_1$ radiation on a Stoe diffractometer. Powdered Si from the U.S. National Bureau of Standards was used as an internal standard. The spectra were fit assuming lorenzian squared line shapes and refined using a least-squares program.

Analyses (WDS) using a Cameca microprobe were made on representative crystals, mostly the same ones used in the FTIR measurements. Synthetic oxides (MgO and Al_2O_3) and natural wollastonite for Si were used as standards. Several line scans across the crystals were made to check for chemical zonation, otherwise random spot analyses were made. The beam size was 2–10 μm in diameter with an accelerating voltage of 15 kV and a beam current of 20 nA measured with a Faraday cup. The data correction program employed was supplied by Cameca and entitled PAP (Pouchoux and Pichoire).

For the IR measurements, pyrope crystals were selected from a given synthesis that were generally the largest and most euhedral and contained the least amount of solid inclusions. The single crystals were embedded in epoxy and ground and polished on both sides to obtain crystal platelets with thicknesses ranging from approximately 50 up to 700 μm, with most between 100 and 250 μm (Fig. 1). These single crystal mounts were used for microscopic examination and also for the microscopic FTIR measurements. This method of preparation allowed us to examine the crystals optically for both solid and liquid inclusions and to make IR measurements across crystals of known and constant thickness without spectral interference from epoxy or glass.

The IR measurements were made on two different spectrometers. The device used at Caltech was a Nicolet 60SX FTIR spectrometer, and the measurements were made at a resolution of 2 to 4 cm^{-1} using an InSb detector. The experimental arrangement consists of attaching circular apertures of various sizes (approximately 50–150 μm in diameter) directly onto the ground and polished crystals held in the epoxy mounts and, after careful alignment in the IR beam, measuring generally between 1000 and 2000 spectra. Measurements made at 78 K were made on this spectrometer using a home-made liquid N_2 cell. The second spectrometer employed was a Bruker FTIR 66 model equipped with a microscope. A variety of measuring sizes were used ranging from 50 × 50 to 10 × 10 μm at a resolution of 2 to 4 cm^{-1} using a HgCdTe detector. 15 × or 36 × objectives were used. The background measurement in the latter was made in air and in the former within the spectrometer using air that had been dried and purged of CO_2.

RESULTS

Product materials

A variety of synthetic pyrope single crystals was grown. Crystal sizes ranged from 0.05 to 2 mm. The crystals were typically subhedral to euhedral with forms {110} or {110} and {211} present. The largest single crystals were grown at pressures in excess of 20 kbar (Table 1) from the oxide mixture. They frequently nucleated along the walls of the

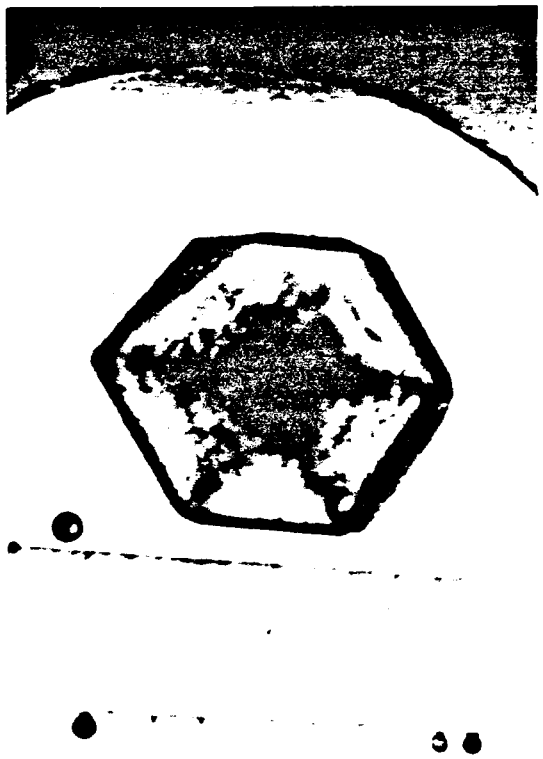

Fig. 1. Plane light photograph showing a typical mount used for optical microscopic examination and the FTIR measurements. The top crystal is pyrope and the bottom a quartz platelet oriented parallel to the c-axis. Note the inclusion pattern in the pyrope crystal. The crystal is approximately 1.3 mm across from corner to corner.

capsule. In many syntheses using oxides the capsule contained large pyrope crystals, surrounded by a finer-grained matrix consisting of a complex variety of other phases (i.e., enstatite, forsterite, chlorite, etc.) within the system MgO-Al_2O_3-SiO_2-H_2O. These additional phases were highly variable in abundance and modal proportions, and their occurrence depended upon the pressure and temperature conditions and duration of the syntheses. They were more prevalent at the lower temperatures. Pyrope crystals could not be grown from the oxide mixture at temperatures less than 900 °C. For syntheses at lower temperature the gel and glass were employed. Pyrope crystals grown from the glass and gel were typically smaller in size than those grown from oxide mix, but these starting materials resulted in more complete yields of pyrope. The largest euhedral single crystals produced were grown around 1000 ± 50 °C at 25 ± 5 kbar. SEM photographs of pyrope single crystals grown from the three different starting materials are shown in Figure 2.

Table 2. Unit-cell dimensions of synthetic pyrope

a_o (Å)	Pressure (kbar)	Temperature (°C)	Synthesis conditions
11.4540 (5)-*R*	30	1350–1400	dry from glass[1]
11.454 (1)	30	1400	dry from glass[2]
11.457 (1)-*R*	37	1000	hydrothermal[3]
11.456 (1)	36	1300	hydrothermal[4]
11.4568 (3)	25	1000	hydrothermal[5]
11.464 (1)-*R*	25	1000	hydrothermal[6]
11.457 (1)-*R*	40	1300	dry from glass[7]
11.459 (1)	30	1370	dry from glass[8]
11.459 (1)	unspecified		oxides[9]
11.456 (2)	30	1300	hydrothermal[10]
11.4579 (3)	25	1000	hydrothermal[11]
11.457 (1)-*R*	25	1000	hydrothermal[12]
11.458 (1)-*R*	45.0	1000	hydrothermal (P-57)[13]
11.458 (1)-*R*	50.0	800	hydrothermal (P-69)[13]
11.457 (1)-*R*	23.9	1000	hydrothermal (P-8)[13]
11.457 (1)-*R*	40.0	1000	hydrothermal (P-54)[13]

[1] Haselton and Westrum (1980).
[2] Geiger et al. (1987).
[3] Akaogi and Akimoto (1977).
[4] Hazen and Finger (1978).
[5] Ackermann et al. (1983).
[6] Schreyer and Seifert (1969).
[7] Newton et al. (1977).
[8] Wood (1988).
[9] Skinner (1956).
[10] Meagher (1975).
[11] Frentrup (1980).
[12] Cahay et al. (1981).
[13] This work, *R*—least-squares refinement.

Pyrope crystals often contained both solid and liquid inclusions less than 10 μm in size, the former especially in those synthesized from oxides. The solid inclusions generally could not be identified because of their small grain size. Olivine and quartz were detected in several pyrope crystals during microprobe analysis. The inclusions were concentrated in the cores, whereas the rims were mostly clear and almost free of inclusions. Inclusion patterns of the type shown in Figure 1 are sometimes, but not always present. These inclusions and the zonation of the OH^- contents in some samples (see below) made estimation of the refractive indices difficult. Therefore the refractive indices were not used as a measure of the OH^- contents (Ackermann et al., 1983).

The X-ray measurements and refinements, together with data available in the literature (Table 2), show that there is a slight increase in the cell dimension (a_o) of pyrope grown hydrothermally compared to polycrystalline pyrope synthesized anhydrously from a glass (Geiger et al., 1988). The stoichiometries of representative pyrope crystals determined from electron microprobe analyses are listed in Table 3. Crystals synthesized at lower pressure (i.e., <30 kbar) generally display garnet stoichiometries, within the errors of the analyses, but those synthesized at higher pressure (>40 kbar) were generally slightly alumina deficient and magnesia enriched relative to pure pyrope. Alumina-deficient synthetic pyropes were also noted by Charlu et al. (1975). If a majorite component ($Mg_4Si_4O_{12}$) were responsible for this effect, the silica would also be elevated to the same extent as the magnesia con-

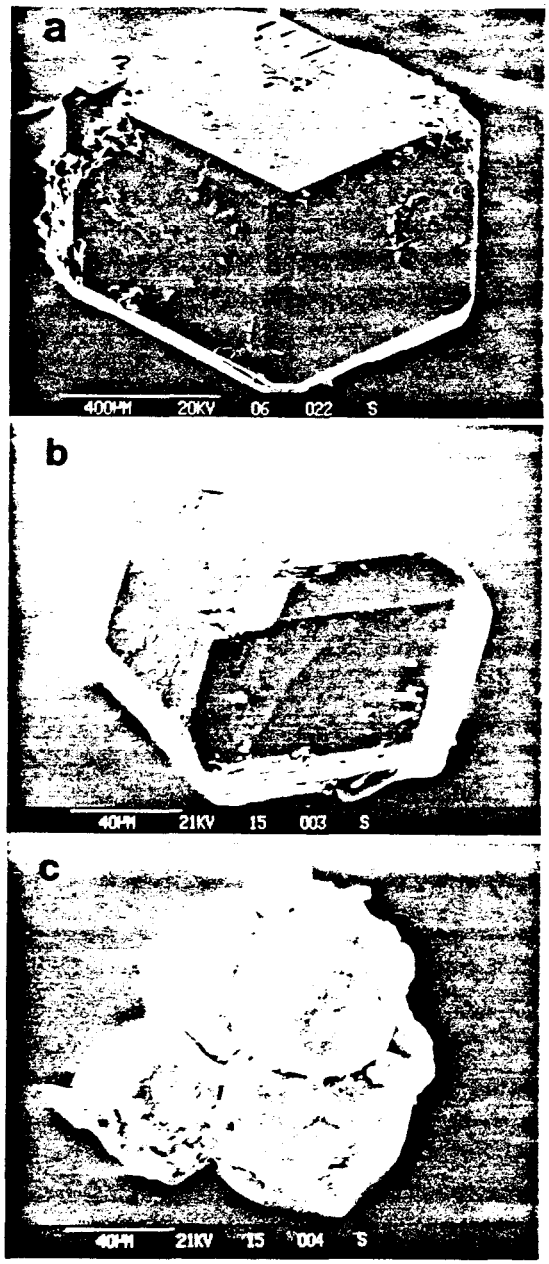

Fig. 2. SEM photographs of representative pyrope single crystals grown from (a) an oxide mixture (P-5), (b) a glass (P-7), and (c) a gel (P-8). All three syntheses were made at 1000 °C and 22.9 kbar, using equal proportions of solids and H_2O. The scales are shown in the lower left.

←

tents. Systematic variation (i.e., zonation) in the stoichiometries was not observed in core to rim traverses.

The IR spectra taken on optically clear parts of the crystals showed no variation in the number of bands or their position in all of the pyropes grown from oxides. In the room-temperature measurements only a single asymmetric OH^- stretching vibration was observed. The position of this band was 3629 $cm^{-1} \pm 2$ cm^{-1} regardless of the pressure and temperature of synthesis and composition of the fluid flux (i.e., 1 N NaOH, HCl, or H_2O) employed. Figure 3 shows a FTIR spectrum obtained on a large pyrope single crystal grown at 900 °C and 30 kbar. Also shown for comparison is the IR spectrum of a pyrope crystal grown in dilute HCl (Fig. 4). The spectra shown in Figures 3 and 4 were taken using measuring spots of 20 and 100 µm respectively. The bottom spectrum in Figure 4 is corrected for the H_2O held in very small fluid inclusions. To do this, a spectrum was first obtained from a thin film of H_2O squeezed between two glass slides. The H_2O spectrum was then subtracted from the pyrope spectrum. The OH^- band shapes in both spectra are slightly asymmetric with full widths at half-height (FWHH) of 60 $cm^{-1} \pm 5$ cm^{-1}. Both spectra agree with the St-1 spectrum presented by Ackermann et al. (1983), except for the band position, 3600 cm^{-1}, which was less certain in the latter case. In many spectra a broad absorption band centered at approximately 3425 cm^{-1} was observed (Fig. 4). The intensity of this band was greater in those regions where more fluid inclusions could be observed (Ackermann et al., 1983). This band varied greatly in intensity and sometimes dwarfed the OH^- stretching vibration. In Figure 3 it is not present.

Measurements made at 78 K showed the presence of two narrow (FWHH = 11 cm^{-1}) absorption bands with peak positions at 3638 cm^{-1} and 3614 cm^{-1}. Figure 5 is a comparison of the room-temperature and 78 K spectra of the same pyrope crystal. The slight corrugation present in the spectra is related to interference effects. The intensity ratio of the two bands is about 3.3 to 1.

In contrast to the single crystals grown from oxides, those pyrope crystals synthesized from the gel, at temperatures lower than 1000 °C, display a four band spectrum with narrow bands at 3665, 3651, 3641, and 3618

Table 3. Electron microprobe analyses of representative pyrope single crystals

Sample/ crystal no.	Average stoichiometry	Standard deviation Mg	Al	Si	Number of points
P-54/1	$Mg_{3.09}Al_{1.93}Si_{3.01}O_{12}$	0.03	0.01	0.02	15
P-13/1	$Mg_{3.00}Al_{2.00}Si_{3.00}O_{12}$	0.01	0.01	0.01	10
P-29/1	$Mg_{2.99}Al_{1.97}Si_{3.04}O_{12}$	0.02	0.01	0.01	6
P-18/1	$Mg_{2.99}Al_{1.99}Si_{3.02}O_{12}$	0.03	0.01	0.01	25
P-57/1	$Mg_{3.09}Al_{1.93}Si_{3.01}O_{12}$	0.05	0.02	0.02	11
P-44/1	$Mg_{3.01}Al_{1.97}Si_{3.02}O_{12}$	0.02	0.01	0.01	8
P-77/1	$Mg_{3.01}Al_{1.94}Si_{3.04}O_{12}$	0.03	0.02	0.08	5
DB-31	$Mg_{3.02}Al_{2.00}Si_{2.99}O_{12}$	—	—	—	3

Note: All analyses normalized to 12 O atoms.

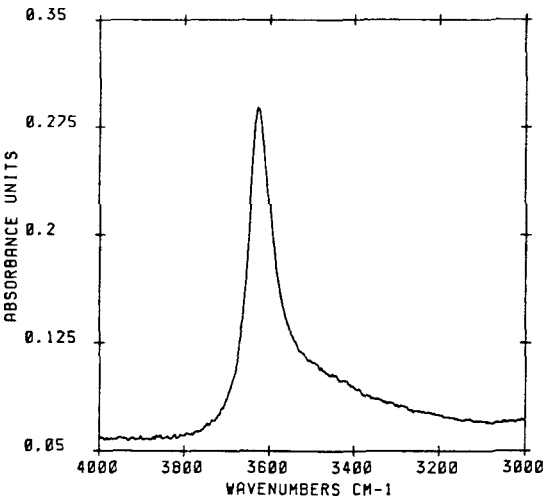

Fig. 3. FTIR microscope spectrum of a pyrope (P-90a) at 298 K with a single band at 3629 cm^{-1}. The crystal is 324 μm thick and the measurement was made at a resolution of 4 cm^{-1} with a measuring diameter of 20 μm.

and a shoulder at 3604 cm^{-1}, with respective FWHH of 12, 6, 11, 10, and 10 cm^{-1} estimated by eye (Fig. 6). This spectrum was not observed in any pyrope crystals grown from oxides or glass. Crystals grown from gel at 1000 °C gave variable results. Crystals grown at Berlin gave the four band spectrum, whereas crystals grown at Pasadena gave the single band pattern. One major difference between the two syntheses was the time the experiments were held at T and P (Table 1).

Variations in the absorbance values of the 3629 cm^{-1}

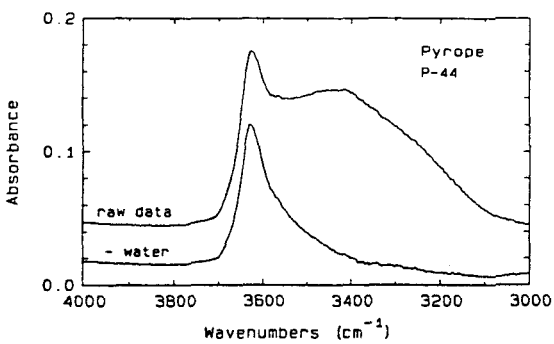

Fig. 4. IR spectra of a pyrope single crystal (P-44) grown in dilute HCl. The top spectrum is the actual measured spectrum which shows a broad H_2O band around 3425 cm^{-1}, and the OH^- stretching band due to structurally incorporated OH^- groups at 3629 cm^{-1}. The bottom spectrum shows the single OH^- stretching band after the broad H_2O band has been subtracted. The crystal is 341 μm thick and the measurements were made on the Nicolet spectrometer using an aperture of 100 μm at a resolution of 4 cm^{-1}.

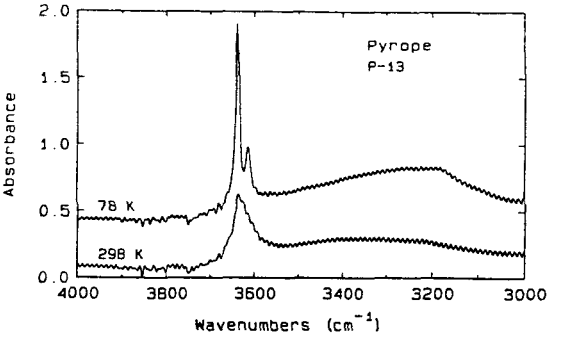

Fig. 5. Comparison of the IR spectrum of pyrope (P-13) at 78 K (above) and at room temperature (below). The crystal is 272 μm thick; the measurements were made using an aperture of 160 μm at a resolution of 4 cm^{-1}. The high frequency oscillations are due to interference fringes.

band indicate that the OH^- content in the crystals changes as a function of pressure and temperature of synthesis. However, we have not been able to establish a simple systematic variation of the OH^- content as a function of pressure and temperature of synthesis. Complications are related to two factors. First, the OH^- content depends upon the starting material used in the synthesis. The OH^- content is higher in pyrope grown from a glass or gel compared to pyrope grown from oxides. In the garnets grown from gel the amount of OH^- is roughly four to five times higher than those grown from oxides at T, P conditions around 1000 °C and 23 kbar. Huckenholz and Fehr (1982) have observed that in synthetic hydrogrossular garnets the hydrogarnet component decreases at a given temperature, with different starting materials, decreasing from glass to oxide to hydroxide mix to condensed gel to (anhydrous) grossular. They also noted that the initially formed composition could not be reequilibrated at high temperatures in short experimental durations. Second, IR profiles measured across our samples show that the OH^- content is sometimes, but not always, greatest in the core and decreases toward the rim (Fig. 7). The above discrepancies among the different starting materials and lack of systematic correlations between P and T and OH^- content indicate that there are problems in obtaining equilibrium products.

To test the proposal of Begley and Sclar (1985) that OH^- containing pyropes are unstable at 1-atm and lose OH^- with time, we measured the IR spectrum of P-51 on the same rim location 1 yr after the first measurements. We observed absolutely no change in the intensity of the single OH^- stretching vibration.

Discussion

Crystal growth

The synthesis work and optical and SEM studies suggest that pyrope growth is a complex process. Crystal size is governed by the nature of the starting material, with

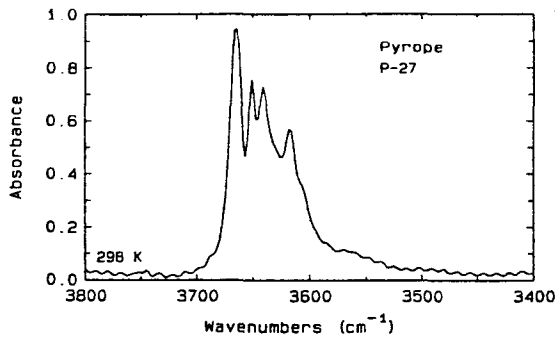

Fig. 6. IR spectrum of pyrope P-27 synthesized from a gel and normalized to 1 mm thickness. The measurement was made on the Nicolet spectrometer. The four bands are located at 3665, 3651, 3641, and 3618 cm^{-1}, with a shoulder at 3604 cm^{-1}.

the larger crystals being produced from oxides, which should be the least reactive starting material compared to either the glass or gel. When glass or gel starting materials are employed, a large number of pyrope crystals nucleate sooner and grow faster than pyrope crystals grown from oxides. The crystals produced are also more homogeneous as demonstrated by the higher abundance of solid phase inclusions in the single crystals grown from oxides. Temperature, pressure, and experimental duration are also factors in crystal growth rates and product sizes, but no simple relationship could be found in the experiments made here. Nucleation effects are also surely important, but poorly understood at the present time. Crystal growth probably occurs relatively rapidly immediately after nucleation and then proceeds more slowly toward the rims. This is consistent with both the higher concentration of inclusions and OH^- found in the cores (Figs. 1 and 7), compared to the clear rims. The crystals

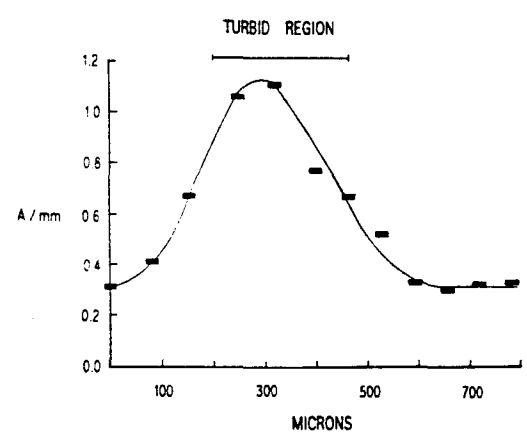

Fig. 7. A plot of the absorbances per millimeter of the OH^- stretching band measured across a single crystal of 800 μm width (DB-31) from rim to rim.

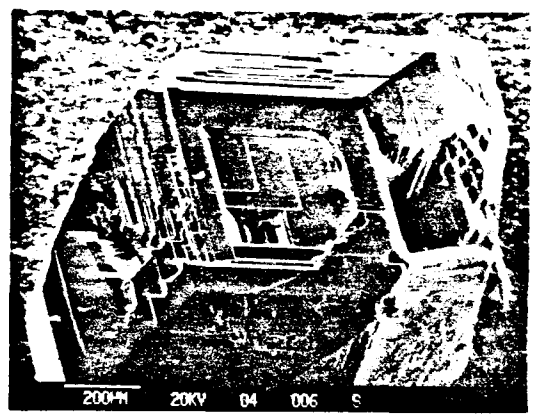

Fig. 8. SEM photograph showing growth steps on a euhedral pyrope single crystal (P-90) synthesized hydrothermally at 900 °C and 30 kbar for 48 h. The top crystal face grew alongside the wall of the capsule. The scale is at the bottom left.

grown from glass also contain more tiny fluid inclusions compared to the oxide-grown crystals.

It appears that pyrope growth from oxides occurs slowly in concentric step layering as opposed to a sector growth process. The SEM photo of the single crystal shown in Figure 8 displays growth zoning steps which are suggestive of an isotropically outwardly growing crystal.

FTIR spectroscopy and location of the OH^- groups

The IR spectroscopic data obtained for pyrope crystals grown from oxides, which show the single sharp IR band at 3629 cm^{-1}, are best interpreted as indicating that the OH^- is indeed incorporated in the classic hydrogarnet substitution, where a cluster of $(O_4H_4)^{4-}$ replaces a SiO_4^{4-} tetrahedral group of point symmetry $\bar{4}$. The room temperature IR measurements made on completely clear and inclusion-free parts of the crystals display the same spectra regardless of the P and T of synthesis and the composition of the fluid phase (H_2O, NaOH, or HCl). There is no change in the position of the single OH^- band. The possibility that submicroscopic inclusions could be responsible for this band at 3629 cm^{-1} was given careful thought. However, we were unable to match the IR spectra of pyrope single crystals grown from oxides with those of known hydrous phases in the system MgO-Al_2O_3-SiO_2-H_2O. Furthermore, the intensity of the OH^- band does not increase in regions of the crystals with dense concentrations of observable inclusions. These observations suggest that the OH^- is structurally bound in pyrope and the IR spectra are not related to submicroscopic inclusions or alteration products. Figure 9 shows the IR spectrum taken on polycrystalline pyrope synthesized dry from a glass (Haselton and Westrum, 1980). No absorption bands are present in the OH^- stretching region; the spectrum is featureless except for the presence of interference effects. Therefore the OH^- band is not a surface related effect made during grinding and polishing of the crystals. This

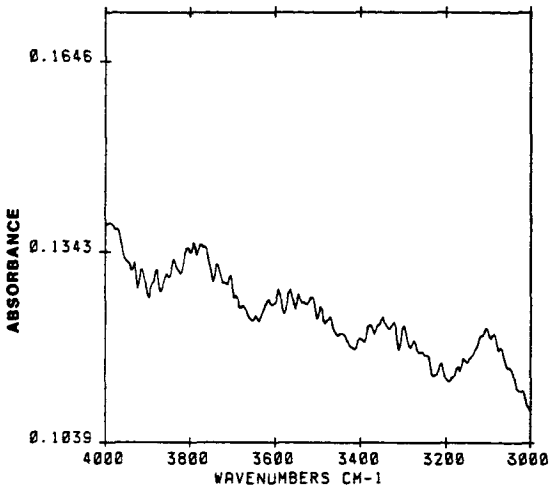

Fig. 9. IR spectrum taken on polycrystalline pyrope synthesized dry from a glass. No OH^- bands are present. Measurements were made on a polycrystalline chip of 75 μm thickness, prepared for spectroscopy in the same way as the synthetic OH-bearing pyrope crystals, at a resolution of 8 cm^{-1} using a microscope spectrometer with 1500 total scans.

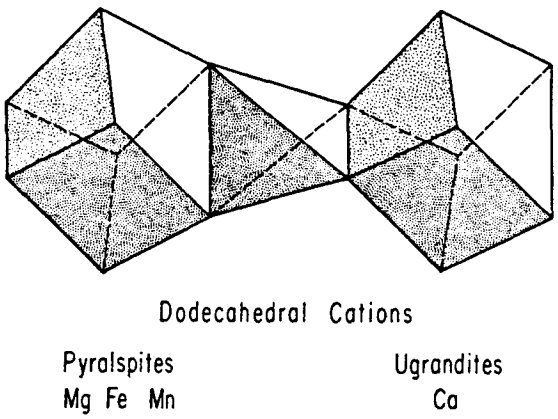

Fig. 10. Polyhedral diagram of part of the garnet structure showing two dodecahedral sites that share edges with a single tetrahedral site, which in the case of the hydrogarnet substitution consists of $(O_4H_4)^{4-}$ (reproduced from Aines and Rossman, 1984b).

further proves that the 3629 cm^{-1} band is not some other feature of the spectrum of pyrope such as an overtone of a Si-O motion.

The low-temperature IR measurements show two distinct OH^- stretching bands (Geiger et al., 1989b). The room temperature spectra display an asymmetry that suggests the possible presence of two overlapping bands which might separate at the lower temperatures. Harmon et al. (1982) calculated the number of IR active bands that are present in tetrahedral, T_d, clusters of the type H_4X_4, where X = Cl, F, or O. They predict that under D_{2d} or S_4 symmetry a T_2 band should split into B_2 + E (D_{2d}) or B + E (S_4) and one should observe two bands in the OH^- stretching region. S_4 is the symmetry of the tetrahedral site in the aluminosilicate garnets (Menzer, 1926; Meagher, 1980) and in hydrogrossular (Cohen-Addad et al., 1967) as determined from X-ray and neutron diffraction studies. The suggestion that a single absorption band is characteristic of the hydrogarnet substitution in pyrope (Ackermann et al., 1983) is only true at room temperature conditions. The apparent single band spectrum at room temperatures demonstrates the need for making low-temperature measurements in these types of studies. Typical spectra of natural pyrope garnets observed by Aines and Rossman (1984b) show two bands in the OH^- region at approximately 3660 and 3560 cm^{-1}. The difference in frequency and relative intensities of the bands between natural and synthetic samples suggests that the mode of OH^- substitution differs in these two types of samples, although this interpretation is complicated by the chemical complexity of natural pyrope samples.

The narrow widths (FWHH) of the two bands observed at 78 K reflect, in part, the absence of different nearest or next-nearest neighbor interactions that are present in the natural garnets. The effect of adding additional components in natural garnets is not only to shift the positions of the OH^- bands, but also to increase their widths (see Aines and Rossman, 1984b). This has been demonstrated in IR studies of the lattice vibrations of natural and synthetic garnets (Moore et al., 1971; Geiger et al., 1989c), which show vibrational coupling between the tetrahedral and dodecahedral sites in garnet (see Fig. 10).

The IR spectrum of synthetic hydrogrossular $[Ca_3Al_2(O_4H_4)_3]$ displays a single asymmetric OH^- band at room temperature that splits at 4 K into two major components at 3680 and 3590 cm^{-1} (Cohen-Addad et al., 1967). At 10 K only one band is observable (Harmon et al., 1982). In the latter study the hydrogarnet substitution was verified by neutron diffraction and H^+-NMR methods.

Room temperature FTIR spectra from single crystals of hydrothermally prepared synthetic almandine ($Fe_3Al_2Si_3O_{12}$) also display two OH^- stretching bands. At 78 K their positions are 3617 and 3595 cm^{-1}, with FWHH of 11 and 9 cm^{-1} respectively. The spectrum is similar in appearance to the 78 K pyrope spectrum (Geiger et al., 1989a). The energy difference between the two bands is the same within experimental error, namely 24 cm^{-1} for pyrope and 22 cm^{-1} for almandine but is much smaller than the value of 90 cm^{-1} observed for hydrogrossular. However, the relative intensities of the two bands appear to be different: 4.8 to 1 in almandine and 3.3 to 1 in pyrope. It is difficult to make definitive statements regarding the locations of the H^+ atoms, but Cohen-Addad et al. (1967) measured an O-H length of 0.93 to 0.95 Å from low-temperature neutron diffraction data. The structures of pyrope and almandine are the most similar

of the aluminosilicate garnets, and therefore it should be expected that their IR spectra should be similar. However, it is not clear why the room temperature spectrum of almandine displays two IR active OH^- stretching bands. One explanation may lie in the low atomic displacement factors which have been observed in single crystal X-ray studies of synthetic almandine relative to pyrope and grossular (Armbruster et al., unpublished data). Thermal and/or positional atomic disorder in pyrope and grossular may act to blur the double band spectra at room temperature.

It is difficult to interpret the four band spectrum observed in certain pyrope crystals crystallized from gel. No band is present at 3629 cm^{-1} and nothing similar was observed in pyrope crystals grown from the oxides. It is possible that submicroscopic hydrous inclusions could be responsible for the additional bands or that the mode of OH^- incorporation is different in these pyrope crystals. It is possible that OH^- incorporation is faster in pyrope grown from gel and additional substitutions such as $^{[6]}Al^{3+} + 3O^{2-} = {}^{[6]}\square + 3OH^-$, $^{[8]}Mg^{2+} + 4OH^- = {}^{[8]}\square + 2OH^-$, $^{[6]}Al^{3+} + O^{2-} = {}^{[6]}Mg^{2+} + OH^-$ or $^{[4]}Si^{4+} + O^{2-} = {}^{[4]}Al^{3+} + OH^-$ may play a role in introducing very small amounts of OH^- in the pyrope structure.

Estimates of OH^- concentrations

The absolute concentrations of OH^- in pyrope can, in principle, be measured using Beer's Law

$$A = \epsilon \cdot t \cdot c \qquad (1)$$

where A is defined as the absorbance and can be measured directly from the spectrum, ϵ is the molar absorptivity of OH^- and is dependent upon the material measured, t is thickness in cm, and c is the concentration in mole l^{-1}. The problem in using Equation 1 for H_2O determination arises from the necessity to know ϵ. It is necessary to obtain independent estimates of the absolute H_2O contents using other techniques (e.g., Rossman et al., 1988) that can then be used to calibrate the IR spectrum. We can estimate the OH^- contents in the synthetic pyropes using the value of ϵ, which is known for OH^- bearing natural grossulars (Rossman and Aines, in preparation). Assuming that ϵ is the same for pyrope and grossular, we calculate that the pyrope in Figure 3 contains 0.05 wt% H_2O. In general, the H_2O contents range from 0.02 to 0.07 wt% for pyrope crystals grown from oxides.

The OH^- contents can also vary considerably within a single crystal. Figure 7 shows an IR traverse from rim to rim, through the core, of a 800 μm pyrope crystal, DB-31, grown in the continual presence of H_2O. The absorbance varies by a factor of almost four from the rim compared to a turbid region located toward the center of the crystal. This bell-shaped profile is consistent with the idea that rapid pyrope nucleation and growth occurred initially and incorporated nonequilibrium amounts of structural OH^-, followed by slower crystal growth and incorporation of less OH^- probably approaching equilibrium concentrations near the edges or rim of the crystal. The OH^- contents appear to level off toward the edges of the crystal. This profile also indicates that the kinetics of the exchange $(O_4H_4)^{4-} = SiO_4^{4-}$ in garnet crystals is very slow even at elevated temperatures (i.e., >1000 °C).

A single OH^- stretching vibration was also observed in pyrope single crystals which were grown in the presence of excess silica (P-51 and P-77). The hydrogarnet component at the rims of single crystals grown from oxides is likely to be a stable equilibrium component fixed at P and T and governed by the relation

$$Mg_3Al_2(SiO_4)_3 + 2x\,H_2O = Mg_3Al_2(SiO_4)_{3-x}[(OH)_4]_x + xSiO_2 \qquad (2)$$

Hydrothermally grown pyrope crystals cannot be stoichiometric, $Mg_3Al_2(SiO_4)_3$, however anhydrous pyrope can be synthesized from anhydrous glass precursors. Work is in progress wherein we are attempting to determine the OH^- contents on a number of crystals grown over a wide range of P and T and f_{H_2O} through careful IR profiling analyses, but ultimately equilibrium will need to be demonstrated by reversal experiments. Moreover, Equilibrium 2 is dependent upon the activity of SiO_2 and this should be buffered during pyrope growth.

The amount of OH^- that can be held in pyrope is much less than in grossular, which forms a complete solid solution with hydrogrossular (Flint et al., 1941; Huckenholz and Fehr, 1982). The low OH^- contents in pyrope may be dictated by the "intrinsic instability" of the structure as discussed by Lager et al. (1989). The amount of inflation of a_o for OH^- containing pyrope is very small ranging from about 0.002 to 0.004 Å (Table 2). Begley and Sclar (1985) reported a much larger increase in a_o (≈0.2 Å), which was not reproduced in these measurements. The smallest a_o value of 11.454 Å was obtained on pyrope synthesized dry from a glass and contains no structural OH^- (see Fig. 9—however see data of Newton et al., 1977 and Wood, 1988). The cell dimension data for pyrope are, therefore, also consistent with a small hydrogarnet substitution. Care must be placed in quantitative interpretation of the unit-cell data because of possible zonation in the crystals and the possible presence of a majorite component in the higher pressure syntheses.

The low absolute amounts of OH^- may be controlled crystallochemically by the edge-sharing structural arrangement between the tetrahedral sites and dodecahedral sites as shown in Figure 10. In strictly anhydrous pyrope the dodecahedral site is too large for the small Mg cation, as evidenced by the large displacement factor (i.e., B = 0.789) which has been observed for Mg in X-ray diffraction experiments (Novak and Gibbs, 1971). Addition of a hydrogarnet component into pyrope forces the dodecahedral site to expand and this is not structurally or energetically favorable in comparison with grossular as argued by Zabinski (1966). Lager et al. (1989) have used distance-least-squares modeling to simulate the effect of the $(O_4H_4)^{4-} = (SiO_4)^{4-}$ substitution on the garnet structure. These calculations indicate that the substitu-

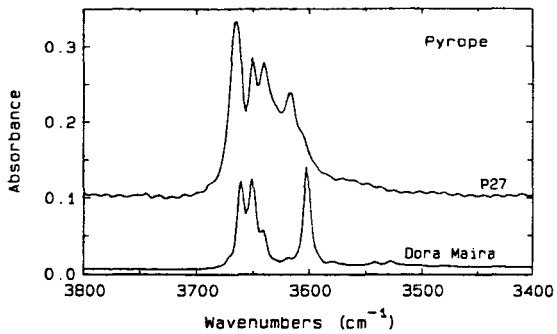

Fig. 11. IR spectra of pyrope P-27 (above) grown from gel compared to the spectrum of the Dora Maira pyrope (below—Rossman et al., 1989). Both spectra are normalized to 1 mm thickness (see text for band energies).

tion may be controlled by the relative lengths of shared and unshared octahedral-dodecahedral bond lengths and that in pyrope a large degree of the hydrogarnet substitution will lead to a structurally and energetically unfavorable situation. Based on a simple size consideration of the dodecahedral cation, it can be expected that the amount of hydrogarnet component will decrease in the series grossular, spessartine, almandine, and finally pyrope (i.e., decreasing size of the divalent cation) at a given pressure, temperature, and f_{H_2O}.

Applications to natural pyrope garnets

A desirable goal for further study would be to measure quantitatively the OH^- contents of natural pyrope crystals and to make inferences regarding the values of f_{H_2O} during garnet growth. If the substitution of OH^- in natural pyrope is as in hydrogarnet, then the prospect for such measurements is favorable because it is likely that the measured OH^- contents are those recording mantle equilibration conditions and not reequilibration conditions attained during rapid ascent to the Earth's surface. This view is justified by the stable OH^- profiles observed in our synthetic crystals. OH^- is not unstable and easily lost from the pyrope structure as proposed by Begley and Sclar (1985).

Rossman et al. (1989) have recently measured the IR spectrum of a nearly end-member pyrope found in the high pressure coesite-bearing metapelites of the Dora Maira Massif of the Alps. The characteristic IR spectrum of this pyrope is radically different from either the spectra of natural pyrope-rich garnets of mantle origin or synthetic pyrope grown from oxides, but it is similar to the spectra shown in Figure 6. It is a four band pattern with sharp narrow bands located at 3662, 3651, 3641, and 3602 cm^{-1}, with FWHH of 3.9, 5.7, 5.3, and 3.7 cm^{-1} respectively (Fig. 11). The highest energy bands in both differ by only 4 cm^{-1}, which is slightly greater than the uncertainty, while the three lower energy bands have analogous counterparts in the pyrope crystals grown from gel. It is probable that the OH^- held in the Dora Maira pyrope and the synthetic pyrope with four bands is located in several different structural sites. The absolute OH^- contents, however, are at least an order of magnitude lower in the Dora Maira pyrope (0.0032 to 0.00016 wt%) than the ones studied by Aines and Rossman (1984a) and also in our synthetics.

Bell and Rossman (in preparation) have also measured the IR spectra on a large number of mantle-derived pyrope crystals taken from South African kimberlites which show more complicated spectroscopic features than those published earlier (Aines and Rossman, 1984a). The same is also true for natural grossular garnets, where many different IR spectra have been observed (Rossman and Aines, in preparation). It is clear that OH^- incorporation into natural garnets is a more complicated structural process than in the chemically simple end-member garnets.

Acknowledgments

We would like to thank H. Reuff for skillful preparation of the sample mounts. D. Ackermand at Christian Albrechts University, Kiel and F. Galbert at Zelmi of the Technische Universität Berlin helped in the microprobing. H. Newesely generously assisted in making the SEM photos at the Free University in Berlin. Some of the high pressure syntheses were done at the Ruhr University through the courtesy of W. Schreyer and H.J. Massonne. We also thank P.J. Wyllie for access to the high pressure facility at Caltech. C.R. Ross II made some of the initial X-ray refinements. We gratefully acknowledge financial support by the Deutsche Forschungsgemeinschaft, Bonn–Bad Godesberg under grant La 324/25, and the National Science Foundation (USA) grant EAR-8618200. Gerlind Siebeker carefully typed the final version of the manuscript.

References cited

Ackermann, L., Cemič, L., and Langer, K. (1983) Hydrogarnet substitution in pyrope: A possible location for "water" in the mantle. Earth and Planetary Science Letters, 62, 208–214.

Aines, R.D., and Rossman, G.R. (1984a) Water content of mantle garnets. Geology, 12, 720–723.

——— (1984b) The hydrous component in garnets: Pyralspite. American Mineralogist, 69, 1116–1126.

Akaogi, M., and Akimoto, S. (1977) Pyroxene-garnet solid solution equilibria in the systems $Mg_4Si_4O_{12}$-$Mg_3Al_2Si_3O_{12}$ and $Fe_4Si_4O_{12}$-$Fe_3Al_2Si_3O_{12}$ at high pressures and temperatures. Physics of the Earth and Planetary Interiours, 15, 90–106.

Basso, R., Cimmino, F., and Messiga, B. (1984) Crystal chemistry of hydrogarnets from three different microstructural sites of a basaltic metarodingite from the Voltri Massif (Western Ligura, Italy). Neues Jahrbuch für Mineralogie Abhandlung, 3, 246–258.

Begley, A.L., and Sclar, C.B. (1984) Experimental evidence for the existence of hydropyrope. Eos, 65, 1091.

——— (1985) High-pressure hydrothermal synthesis of hydrogen-bearing pyrope garnet. 2nd International Symposium on hydrothermal reactions, Program and Abstracts, 36.

Cahay, R., Tarte, P., and Fransolet, A.-M. (1981) Interprétation du spectre infrarouge de variétés isotopiques de pyropes synthétiques. Bulletin de Minéralogie, 104, 193–200.

Cemič, L., Geiger, C.A., Hoyer, H., Koch-Müller, M., and Langer, K. (1990) Piston-cylinder techniques: Pressure and temperature calibration of a pyrophyllite-based assembly by means of DTA measurements, a salt-based assembly, and a cold sealing sample encapsulation method. Neues Jahrbuch für Mineralogie Monatshefte, 2, 49–64.

Charlu, T.V., Newton, R.C., and Kleppa, O.J. (1975) Enthalpies of formation at 970 K of compounds in the system MgO-Al_2O_3-SiO_2 from high temperature solution calorimetry. Geochimica et Cosmochimica Acta, 39, 1487–1497.

Cohen-Addad, C., Ducros, P., and Bertaut, E.F. (1967) Etude de la substitution du groupement SiO_4 par $(OH)_4$ dans les composes $Al_2Ca_3(OH)_{12}$ et $Al_2Ca_3(SiO_4)_{2.16}(OH)_{3.36}$ de type grenat. Acta Crystallographica, 23, 220–230.

Flint, E.P., McMurdie, H.F., and Wells, L.S. (1941) Hydrothermal and X-ray studies of the garnet-hydrogarnet series and the relationship of the series to hydration products of portland cement. Journal Research National Bureau of Standards, 82, 213–219.

Frentrup, K.-R. (1980) Absorptionsspektren von synthetischen Silikatgranaten und Granatmischkristallen und ihre Anwendung zur spektroskopischen 3d-Ionenanalyse in Granaten, 216 p. Ph.D. dissertation, University of Bonn.

Geiger, C.A., Newton, R.C., and Kleppa, O.J. (1987) Enthalpy of mixing of synthetic almandine-grossular and almandine-pyrope garnets from high-temperature solution calorimetry. Geochimica et Cosmochimica Acta, 51, 1755–1763.

Geiger, C.A., Langer, K., Winkler, B., and Cemič, L. (1988) The synthesis, characterization and physical properties of end-member garnets in the system $(Fe,Mg,Ca,Mn)_3Al_2(SiO_4)_3$. In H. Vollstädt, Ed., High pressure geosciences and material synthesis, p. 193–198, Akademie-Verlag, Berlin.

Geiger, C.A., Lager, G.A., Amthauer, G., Richardson, J.F., and Armbruster, T. (1989a) Almandine garnet: Synthesis, structure, and Mössbauer and NIR spectroscopy (abs). 12th European Crystallographic Meeting, Moscow USSR, 2, 6.

Geiger, C.A., Langer, K., Bell, D.R., and Rossman, G.R. (1989b) Realbau of pyrope single crystals grown hydrothermally (abs.). International Conference Crystal structure, microstructure and properties of minerals and ceramic materials, Bochum University, FRG, 55–56.

Geiger, C.A., Winkler, B., and Langer, K. (1989c) Infrared spectra of synthetic almandine-grossular and almandine-pyrope garnet solid-solutions: Evidence for equivalent site behaviour. Mineralogical Magazine, 53, 231–237.

Harmon, K.M., Gabriele, J.M., Nuttall, A.S. (1982) Hydrogen bonding in the tetrahedral $O_4H_4^{4-}$ cluster in hydrogrossular. Journal of Molecular Structure, 82, 213–219.

Haselton, H.T., and Westrum, E.F. (1980) Low temperature heat capacities of pyrope, grossular, and $pyrope_{60}$ $grossular_{40}$. Geochimica et Cosmochimica Acta, 44, 701–709.

Hazen, R.M., and Finger, L.W. (1978) Crystal structures and compressibilities of pyrope and grossular to 60 kbar. American Mineralogist, 63, 277–303.

Huckenholz, H.G., and Fehr, K.T. (1982) Stability relationships of grossular + quartz + wollastonite + anorthite II. The effect of grandite-hydrograndite solid solution. Neues Jahrbuch für Mineralogie Abhandlung, 145, 1–33.

Lager, G.A., Armbruster, T., Rotella, F.J., and Rossman, G.R. (1989) The OH substitution in garnets: X-ray and neutron diffraction, infrared and geometric modelling studies. American Mineralogist, 74, 840–851.

Massonne, H.-J., and Schreyer, W. (1986) High-pressure syntheses and X-ray properties of white micas in the system K_2O-MgO-Al_2O_3-SiO_2-H_2O. Neues Jahrbuch für Mineralogie Abhandlung, 153, 177–215.

Meagher, E.P. (1975) The crystal structures of pyrope and grossularite at elevated temperatures. American Mineralogist, 60, 218–228.

——— (1980) Silicate garnets. Mineralogical Society of America Reviews in Mineralogy, 11, 25–66.

Menzer, G. (1926) Die Kristallstrukture von Granat. Zeitschrift für Kristallographie, 63, 157–158.

Moore, R.K., White, W.B., and Long, T.V. (1971) Vibrational spectra of the common silicates: I. The garnets. American Mineralogist, 56, 54–71.

Newton, R.C., Charlu, T.V., and Kleppa, O.J. (1977) Thermochemistry of high pressure garnets and clinopyroxenes in the system CaO-MgO-Al_2O_3-SiO_2. Geochimica et Cosmochimica Acta, 41, 369–377.

Novak, G.A., and Gibbs, G.V. (1971) The crystal chemistry of the silicate garnets. American Mineralogist, 56, 791–825.

Rossman, G.R. (1988) Vibrational spectroscopy of hydrous components. Mineralogical Society of America Reviews in Mineralogy, 18, 193–204.

Rossman, G.R., Rauch, F., Livi, R., Tombrello, T.A., Shi, C.R., and Zhou, Z.Y. (1988) Nuclear reaction analysis of hydrogen in almandine, pyrope, and spessartine garnets. Neues Jahrbuch für Mineralogie Monatshefte, 4, 172–178.

Rossman, G.R., Beran, A., and Langer, K. (1989) The hydrous component of pyrope from the Dora Maira Massif, Western Alps. European Journal of Mineralogy, 1, 151–154.

Schreyer, W., and Seifert, F. (1969) High-pressure phases in the system MgO-Al_2O_3-SiO_2-H_2O. American Journal of Science, 267-A, 407–443.

Sekine, T., Wyllie, P.J., and Baker, D.R. (1981) Phase relationships at 30 kbar for quartz eclogite composition in CaO-MgO-Al_2O_3-SiO_2-H_2O with implications for subduction zone magmas. American Mineralogist, 66, 938–950.

Skinner, B.J. (1956) Physical properties of end-members of the garnet group. American Mineralogist, 41, 428–436.

Wood, B.J. (1988) Activity measurements and excess entropy-volume relationships for pyrope-grossular garnets. Journal of Geology, 96, 721–729.

Zabinski, W. (1966) Hydrogarnets. Polska Akademia Nauk, Oddzial Krakowie, Komisja Nauk Mineralogicznych, Prace Mineralogiczne, 3, 1–69.

Manuscript received October 9, 1989
Manuscript accepted November 7, 1990

Appendix 6

Water in the mantle: OH in garnets from southern African kimberlites

by

D. R. Bell and G. R. Rossman

Geological Society of America Abstracts with Programs **20**, A367

G. S. A. Annual Meeting, Denver, 1988.

WATER IN THE UPPER MANTLE ; STRUCTURAL OH IN GARNETS FROM SOUTHERN AFRICAN KIMBERLITES.

BELL, David R. and ROSSMAN, G.R., Div. Geol. Planet. Sci., Caltech, Pasadena, CA 91125

In order to characterize the concentrations and chemical speciation of hydrous volatile components in the Earth's upper mantle, we have used Fourier-Transform infrared spectroscopy to determine relative concentrations of structurally-bound OH in southern African mantle garnets from peridotites, eclogites and megacrysts. Garnets were extracted from well characterized xenolith suites in kimberlites erupted both on and off the Archean Kaapvaal craton, and the OH absorption was measured in the 3600 cm^{-1} region on gem-quality, microscopically inclusion-free fragments.

Cr-poor garnet megacrysts (discrete nodules) have the greatest OH absorptions of all garnets examined (equivalent to about .02 wt. %). OH absorbance and Mg/(Mg+Fe) ratio are inversely correlated for individual megacryst suites. In addition, garnet megacrysts from the micaceous (group II) Lace kimberlite are more OH-rich than compositionally similar megacrysts from four "basaltic" (group I) kimberlites. Since water is probably incompatible in early crystallizing megacryst phases, we suggest that the garnet OH contents reflect increasing water content of the differentiating parental megacryst magmas. Garnets from high-temperature, deformed lherzolites of the Premier and Jagersfontein kimberlites are more hydrous than their coarse-granular, "depleted" counterparts. Off-craton lherzolite garnets are similar in overall OH content to the on-craton samples. Compositionally diverse garnets from Roberts Victor eclogites and a diamondiferous eclogite from the Lace Mine, are generally extremely poor in OH.

Southern African mantle garnets display OH contents that are well correlated with their petrogenetic origins, suggesting that many may be unmodified during the eruptive process. Mantle olivines, pyroxenes, kyanites and zircons from these kimberlites also contain structural OH and our preliminary studies have revealed a variability in inter-mineral OH partitioning. Application of this phenomenon to quantitative estimation of upper mantle hydrous volatile activity requires careful delineation of crystal-chemical and external (P_{H2O}, P_{H2}) controls, which we are currently investigating.

Appendix 7

The OH content of "anhydrous" minerals in mantle eclogites.

by

D. R. Bell and G. R. Rossman

Eos, Transactions, American Geophysical Union **71**, 523.

A. G. U. Spring Meeting, Baltimore, 1990

Hydroxyl in "Anhydrous" Minerals From Eclogite Xenoliths

David R Bell and George R Rossman (Division of Geological and Planetary Sciences, Caltech, Pasadena, CA 91125)

As part of a comprehensive study of OH in high pressure "anhydrous" minerals, we analyzed by infrared spectroscopy suites of eclogitic garnets from kimberlites in southern Africa and diatremes on the Colorado Plateau. In addition, OH in coexisting minerals was analyzed in samples from southern Africa. Large differences in the OH concentrations of the garnets were observed. Kimberlite-hosted garnets erupted through the Archean craton of southern Africa ("on-craton") commonly contain extremely low amounts (<5 ppm as H_2O) of hydroxyl. Where greater amounts are measured (up to 100 ppm H_2O) the OH absorption bands are linked to the presence of minute inclusions of unknown composition. Garnets from graphite- and diamond- bearing eclogites, as well as one diamond-inclusion garnet, have low OH contents comparable to other "on-craton" garnets. Hydroxyl in most "off-craton" garnets is bound in the garnet structure at concentrations typically greater than in "on-craton" samples. Southern African "off-craton" garnets contain 30 - 120 ppm H_2O; Colorado Plateau samples are notably more hydrous with 80 -700 ppm H_2O. Differences in OH content may be due to a combination of pressure and water activity effects. In contrast to the garnets, kyanites from "on-craton" type1 eclogites contain the most OH. All kyanites exhibit IR spectra very similar to those previously published for mantle kyanite. For the water budget of the stoichiometrically anhydrous minerals in eclogite, omphacitic pyroxene is probably the most important phase (up to ~600 ppm H_2O), although rutile (modally subordinate) may be more hydrous (700 ppm H_2O). Orthopyroxene is moderately hydrous (200-300 ppm H_2O) whereas corundum and spinel are extremely OH-poor. Typical eclogite xenoliths may thus contain several hundred ppm H_2O bound in stoichiometrically anhydrous phases. In the common phlogopite- and amphibole-poor varieties of eclogite, this OH is an important fraction of the total water content.

Appendix 8

Hydroxyl in mantle minerals.

by

D. R. Bell, G. R. Rossman and P. D. Ihinger

Eos, Transactions, American Geophysical Union **72**, 537.

A. G. U. Fall Meeting, San Francisco, 1991

Hydroxyl in upper mantle minerals

David R Bell, George R Rossman and Phillip D Ihinger (Div. of Geological and Planetary Sciences, Caltech, Pasadena, CA 91125)

In order to evaluate the importance of nominally anhydrous minerals as a reservoir of mantle water, we used infrared (IR) spectroscopy to determine the structural hydroxyl (OH) contents of common minerals of upper mantle origin. Mineral-specific calibrations of the IR technique for quantitative analysis of hydroxyl (OH) were developed for garnet, clinopyroxene and orthopyroxene using carefully cleaned megacryst and lherzolite mineral samples, vacuum extraction of H and manometry. The new and previously published calibrations were applied to IR spectra of olivine, orthopyroxene, clinopyroxene, garnet and accessory minerals from mantle xenoliths to yield quantitative estimates of their structural OH contents.

Of the common nominally anhydrous minerals in peridotites, diopsidic clinopyroxene contains the greatest OH concentrations (100-500 ppm H_2O by weight). The highest clinopyroxene OH contents occur in a Cr-rich megacryst and in eclogitic omphacites. Orthopyroxene contains 50-450 ppm H_2O and is probably the most important reservoir of H in "anhydrous" peridotites. Most olivines and peridotite garnets contain less than 30 ppm H_2O. However, olivine and garnet megacrysts with concentrations in excess of 100 ppm H_2O, as well as OH-rich zircons, appear to reflect unusually hydrous environments. Peridotite water contents estimated from coexisting nominally anhydrous minerals range from 25 ppm in a spinel lherzolite from British Columbia to 200 ppm in coarse garnet peridotites from South Africa.

Concentrations of OH in the common "anhydrous" minerals suggest that these phases are petrologically significant hosts for upper mantle water, and may account for the water budget of the depleted upper mantle (MORB source region). Nominally anhydrous, OH-bearing minerals also provide a mechanism for the transport of water into deep regions of the mantle at subduction zones.

Appendix 9

The isotopic composition of hydrogen in nominally anhydrous mantle minerals

by

P. D. Ihinger and D. R. Bell

Eos, Transactions, American Geophysical Union **72**, 537.

A. G. U. Fall Meeting, San Francisco, 1991

Isotopic Composition of Hydrogen in Nominally Anhydrous Mantle Minerals.

Phillip D Ihinger and David R Bell (Division of Geological and Planetary Sciences, 170-25, Caltech, Pasadena, CA 91125)

The variations in abundance and isotopic composition of H in the mantle place important constraints on the nature of the earth's water cycle. Recent attention has focused on nominally anhydrous minerals as a reservoir of mantle H. In this study we report the isotopic composition of H bound structurally as OH in garnet, orthopyroxene (opx) and clinopyroxene (cpx) of mantle origin.

Samples for analysis were selected on the basis of their structural OH contents, as determined by infrared (IR) spectroscopy, and their ability to yield the large volumes of pure and crack-free material mandated by the low H concentrations (50-300 ppm H_2O by weight). This required unusually large kimberlite-hosted megacrysts of cpx and garnet. Opx was separated from a large spinel-lherzolite xenolith. For the megacrysts, contamination by hydrous phases was minimized by preparation of large plates of gem-quality mineral (2-10 mm across) for microscopic examination under dark-field illumination. All natural surfaces and visible imperfections were removed. Purity is believed to be >99.95%. H was extracted from sample aliquots of 200 to 3000 mg under vacuum by heating in an induction furnace and was largely released as H_2. Samples were not melted, and their dehydrogenation was verified by IR analysis after extraction.

δD_{SMOW} values are mostly in the range -100 to -130 ‰. These contrast with prevailing estimates of mantle δD of -80 ‰ from basalts[1] and -60 to -80 ‰ from phlogopite in xenoliths[2], but are similar to δD of some mantle amphiboles[2,3]. While the possible effects of near-surface exchange processes on the isotopic compositions need to be evaluated, these results suggest systematic heterogeneity in mantle δD, as was inferred from some basalt studies[4,5] and the possible existence of an isotopically distinct reservoir of H in nominally anhydrous minerals.

Refs: 1. Kyser & O'Neil (1984) GCA **48**, 2123. 2. Boettcher & O'Neil (1980) Amer. J. Sci. **280A**, 594. 3. Kuroda *et al.* (1975) CMP **52**, 315. 4. Poreda (1985) EPSL **73**, 244. 5. Poreda *et al.* 1986 EPSL **78**, 1.

Appendix 10

Data Tables

10.1 Compositions and OH contents of garnets from Garnet Ridge, Arizona.

10.2 Compositions and OH contents of mantle kyanites.

10.3 Integrated absorbances and OH contents of mantle zircons.

Appendix 10.1 Garnet Ridge garnets

Sample	Na2O	MgO	Al2O3	SiO2	CaO	TiO2	Cr2O3	MnO	FeO*	P2O5	TOTAL	H2O (ppm)
GRR1134-C1	0.0335	19.25	21.76	40.84	4.44	0.0969	2.15	0.49	9.41	0.0165	98.49	144
GRR1134-C2	0.0373	19.57	22.46	41.41	4.41	0.1626	1.49	0.42	8.94	0.0151	98.93	0
GRR1134-C3	0.0342	19.15	20.86	41.05	5.12	0.1163	3.80	0.50	8.92	0.0454	99.59	130
GRR1134-C4	0.0337	19.51	21.43	40.87	4.76	0.1635	2.32	0.45	9.07	0.0169	98.63	131
GRR1134-C5	0.0412	17.70	20.41	40.04	4.22	0.1273	3.13	0.38	10.76	0.0225	96.83	104
GRR1134-C6	0.0277	18.79	21.22	41.30	5.03	0.0787	3.28	0.51	9.75	0.0166	100.00	56
GRR1134-C7	n.a.	n.a.	n.a.	n.a.	n.a.	n.a.	n.a.	n.a.	n.a.	n.a.	n.a.	113
GRR1134-C9	0.0496	20.34	23.66	41.82	3.69	0.1561	0.05	0.35	9.06	0.0420	99.21	41
GRR1134-C10	0.0209	19.85	23.71	41.90	4.05	0.0485	0.10	0.40	10.07	0.0168	100.16	60
GRR1134-C11	0.0339	15.32	22.88	40.66	4.57	0.1017	0.04	0.42	16.06	0.0360	100.12	109
GRR1134-C12	0.0272	18.92	23.55	41.79	4.02	0.0571	0.19	0.37	11.15	0.0370	100.11	98
GRR1134-C13	0.0148	17.38	23.55	41.68	7.04	0.0381	0.09	0.35	10.18	0.0304	100.35	0
GRR1134-C14	0.0302	19.98	21.58	41.39	4.74	0.1192	3.07	0.47	8.49	0.0212	99.89	111
GRR1134-C15	0.0426	10.89	22.43	40.02	10.16	0.1229	0.04	0.34	15.32	0.0374	99.41	233
GRR1134-C16	0.0071	16.33	23.42	41.65	9.86	0.0161	0.20	0.27	8.48	0.0134	100.24	22
GRR1134-C17	0.0414	19.07	19.73	41.30	4.84	0.1065	5.31	0.53	8.85	0.0256	99.81	79
GRR1134-C18	0.0470	18.55	23.42	41.82	4.59	0.1734	0.16	0.32	11.00	0.0564	100.15	129
GRR1134-C19	0.0249	14.73	23.14	41.17	9.15	0.0898	0.09	0.36	11.10	0.0303	99.89	107
GRR1134-C20	0.0341	19.75	23.54	42.24	4.04	0.1471	0.18	0.38	10.16	0.0254	100.50	136
GRR1134-DB1	0.0177	8.22	22.03	39.11	8.61	0.0482	0.05	0.52	22.31	0.0230	100.94	67
GRR1134-DB2	0.0284	19.59	21.69	41.81	4.88	0.1302	2.95	0.49	8.97	0.0160	100.55	126
GRR1134-DB3	0.0081	19.69	21.48	42.05	5.64	0.0086	3.34	0.37	7.96	0.0013	100.56	0
GRR1134-DB4	0.0294	19.08	23.48	42.13	5.04	0.1756	0.44	0.36	10.13	0.0289	100.89	14
GRR1134-DB5	0.0406	20.02	22.45	42.04	4.54	0.1941	1.81	0.41	9.00	0.0174	100.52	157
GRR1134-DB6	0.0216	19.24	22.77	41.69	5.04	0.1281	1.56	0.43	9.70	0.0106	100.60	101
GRR1134-DB7	0.0243	20.48	22.51	42.12	4.24	0.0821	2.30	0.45	8.39	0.0177	100.61	76
GRR1134-DB8	0.0058	11.37	22.62	39.49	2.33	0.0203	0.00	2.69	22.81	0.0276	101.38	7
GRR1134-DB9	0.0558	10.26	22.74	39.78	7.57	0.0753	0.04	0.42	20.11	0.0771	101.11	100
GRR1134-DB10	0.0301	15.30	23.32	40.82	3.13	0.0242	0.09	0.39	18.23	0.0615	101.40	25
GRR1134-DB11	0.0140	12.54	22.94	40.33	7.53	0.0362	0.06	0.35	17.10	0.0182	100.93	42
GRR1134-DB12	0.0343	17.74	23.37	41.41	3.09	0.0774	0.21	0.42	14.59	0.0265	100.95	58
GRR1134-DB13	0.0193	19.60	23.81	41.98	3.90	0.0540	0.19	0.26	10.90	0.0241	100.73	51
GRR1134-DB14	0.0254	12.12	22.58	40.28	7.61	0.0977	0.09	0.52	17.48	0.0148	100.82	35
GRR1134-DB15	0.0408	19.32	22.11	41.80	4.68	0.2207	2.06	0.45	9.65	0.0181	100.34	109
GRR1134-DB16	0.0137	15.92	22.66	40.96	4.92	0.0902	0.75	0.44	15.23	0.0104	101.00	144
GRR1134-DB17	0.0126	15.72	22.69	40.73	3.93	0.0308	0.75	0.47	16.59	0.0267	100.94	85
GRR1134-DB18	0.0146	19.03	22.53	41.58	5.20	0.0606	1.76	0.47	9.62	0.0085	100.27	22
GRR1134-DB19	0.0404	20.46	22.13	41.95	4.15	0.1212	2.38	0.44	8.55	0.0291	100.26	91
GRR1134-DB20	0.0518	20.17	22.09	41.81	4.56	0.2887	2.24	0.42	8.80	0.0193	100.45	169
GRR1134-DB21	0.0249	19.38	21.57	41.40	5.06	0.1052	3.14	0.50	9.09	0.0104	100.31	87
GRR1134-DB22	0.0300	13.76	21.24	40.64	7.56	0.2221	1.55	0.55	14.99	0.0112	100.57	289
GRR1134-DB23	0.0394	13.39	21.26	40.05	4.38	0.1354	1.61	0.63	19.61	0.0506	101.18	111
GRR1134-DB24	0.0219	6.31	20.94	38.60	5.91	0.1033	0.07	2.44	27.43	0.0459	101.88	330
GRR1134-DB25	0.0232	17.05	21.97	40.98	5.10	0.1212	1.48	0.58	13.11	0.0138	100.44	164
GRR1134-DB26	0.0131	7.16	21.84	38.02	1.73	0.0083	0.00	0.74	31.58	0.0118	101.10	8
GRR1134-DB27	0.0428	17.85	23.01	41.44	3.83	0.1450	0.43	0.36	13.72	0.0291	100.85	96
GRR1134-DB28	0.0139	16.18	23.05	40.90	4.17	0.0197	0.06	0.46	15.57	0.0274	100.45	40
GRR1134-DB29	0.0364	18.97	23.24	41.64	3.81	0.1026	0.13	0.36	12.02	0.0216	100.34	109
GRR1134-DB30	0.0266	20.60	22.74	42.09	4.26	0.1250	1.21	0.43	8.38	0.0189	99.88	125
GRR1134-DB31	0.0414	8.42	21.83	39.18	6.65	0.1321	0.03	0.52	24.13	0.0239	100.95	85
GRR1134-DB32	0.0094	7.58	21.81	38.56	1.39	0.0073	0.02	7.47	24.82	0.0523	101.72	12
GRR1134-DB33	0.0396	17.49	22.90	41.65	4.28	0.1947	0.37	0.40	13.36	0.0110	100.69	90
GRR1134-DB34	0.0283	16.34	23.09	41.10	4.21	0.0621	0.25	0.43	15.35	0.0317	100.89	76
GRR1134-DB35	0.0024	9.22	22.28	39.16	2.40	0.0102	0.01	1.72	26.85	0.0174	101.67	4
GRR1134-DB36	0.0086	20.36	20.75	42.05	4.29	0.0068	4.31	0.50	7.94	0.0101	100.22	16
GRR1134-DB37	0.0176	19.57	22.46	42.03	5.15	0.1080	1.76	0.41	9.01	0.0102	100.53	75
GRR1134-DB38	0.0244	18.69	18.81	41.30	6.17	0.0577	6.60	0.50	8.02	0.0372	100.21	53
GRR1134-DB39	0.0060	19.51	22.32	42.20	5.37	0.0344	2.20	0.40	8.39	0.0014	100.42	3
GRR1134-DB40	0.0291	19.40	22.70	42.11	4.45	0.1439	1.39	0.46	9.94	0.0147	100.64	86
GRR1134-DB41	0.0124	19.30	22.33	42.15	5.26	0.0837	2.02	0.44	9.04	0.0078	100.66	96
GRR1134-DB42	0.0344	19.79	22.07	42.04	4.39	0.1163	2.36	0.47	9.46	0.0205	100.76	69
GRR1134-DB43	0.0209	19.98	22.26	42.16	4.66	0.0760	2.33	0.48	8.83	0.0185	100.80	132
GRR1134-DB44	0.0308	19.79	22.21	42.05	4.77	0.1892	2.10	0.43	8.98	0.0092	100.56	96

Sample	Na	Mg	Al	Si	Ca'	Ti	V	Cr	Mn	Fe3+	Ni	P	O	Total Cat	Charge Def	H2O(ppm)
JAG-14	0.00008	0.00157	1.985	1.006	0.00012	0.00080	0.00010	0.00204	0.00001	0.00289	0.00001	0.00017	5	2.9988	0.0019	-
BBM-2	0.00029	0.00065	1.970	1.010	0.00017	0.00055	0.00099	0.00864	0.00001	0.00588	0.00005	0.00004	5	2.9973	0.0015	-
BBM-1	0.00006	0.00058	1.962	1.009	0.00002	0.00060	0.00092	0.01899	0.00004	0.00569	0.00001	0.00004	5	2.9976	0.0008	-
BBM-18	0.00007	0.00073	1.983	1.007	0.00009	0.00053	0.00039	0.00302	0	0.00226	0.00004	0.00005	5	2.9975	0.0010	77
BBB-4	0.00031	0.00033	1.993	1.002	0.00020	0.00009	0.00022	0.00047	0	0.00294	0.00003	0.00006	5	3.0003	0.0012	-
BBB-5	0.00006	0.00027	1.982	1.010	0.00009	0.00019	0.00024	0.00053	0.00002	0.00308	0.00000	0.00004	5	2.9969	0.0005	72
RVC-7	0.00011	0.00378	1.978	1.007	0.00010	0.00250	0.00028	0.00275	0.00005	0.00297	0.00007	0.00003	5	2.9983	0.0042	-
RFT-1	0.00008	0.00074	1.987	1.005	0.00008	0.00060	0.00009	0.00137	0.00001	0.00326	0.00001	0.00006	5	2.9983	0.0010	59
RFT-2	0.00045	0.00092	1.985	1.006	0.00037	0.00066	0.00009	0.00118	0	0.00339	0.00000	0.00019	5	2.9986	0.0022	96
FSM-15	0.00014	0.00219	1.986	1.004	0.00006	0.00129	0.00019	0.00090	0	0.00367	0.00004	0.00007	5	2.9989	0.0026	222
LTL-3	0.00008	0.00185	1.984	1.007	0.00008	0.00148	0.00022	0.00067	0.00001	0.00261	0.00005	0.00013	5	2.9977	0.0021	200
JAG-14	0.00004	0.00363	1.984	1.004	0.00004	0.00220	0.00027	0.00292	0	0.0026	0.00002	0.00010	5	2.9992	0.0038	163
HRV-147	0.00005	0.00286	1.985	1.004	0.00003	0.00180	0.00015	0.00118	0	0.00364	0.00006	0.00004	5	2.9991	0.0031	-
GRR-6/18/81	0.00005	0.00306	1.987	1.001	0.00005	0.00239	0.00022	0.00061	0.00001	0.00481	0.00003	0.00008	5	2.9996	0.0033	144
LOV-1	0.00008	0.00079	1.975	1.009	0.00011	0.00037	0.00007	0.00144	0	0.00975	0.00000	0.00011	5	2.9967	0.0011	85
GRR-1126	0.00005	0.00240	1.977	1.009	0.00010	0.00193	0.00020	0.00106	0.00002	0.00552	0.00000	0.00013	5	2.9971	0.0026	55
173/33/K106/17	0.00007	0.00234	1.980	1.008	0.00002	0.00171	0.00014	0.00055	0.00002	0.00573	0.00002	0.00025	5	2.9982	0.0025	-
SRV-1	0.00003	0.00163	1.989	1.004	0.00006	0.00081	0.00004	0.00138	0.00002	0.00254	0.00000	0.00014	5	2.9990	0.0018	92
RVC-32	0.00003	0.00127	1.997	0.995	0.00005	0.00094	0.00020	0.00145	0.00002	0.00522	0.00000	0.00009	5	3.0015	0.0014	57
A1 Kyanite std	0.00031	0.00108	1.991	1.000	0.00004	0.00012	0.00028	0.00041	0.00002	0.0031	0.00001	0.00211	5	2.9988	0.0018	-
KY20 std	0.00035	0.00064	1.994	1.000	0.00002	0.00014	0.00040	0.00042	0.00002	0.00324	0.00004	0.00122	5	3.0005	0.0014	-

Appendix 10.2 Compositions and OH contents of mantle kyanites

Appendix 10.3 OH in mantle zircons

Sample	∫A //c	∫A perp c	∫A total	ppm H2O
KLV-33 rim	31.6	13.4	58.4	61
KLV33.c3	24.3	13.8	51.9	54
KLV33.c2	24.1	13.6	51.3	53
KLV33.c1	24.1	14.6	53.3	55
173/44/K8/9	21.9	12.8	47.5	49
175/37/K5/5	24.2	23.4	71.0	74
173/33/k3/383.1	15.1	8.5	32.1	33
KLV-22	22.0	11.1	44.2	46
ROM177.Z1	12.6	8.7	29.9	31
ROM181.Z1	11.7	7.7	27.2	28
ROM181.Z2	12.7	9.9	32.5	34
ROM121.Z010	9.1	8.9	26.9	28